2014

Characterization of a Utica Shale Reflector Package using Well Log Data and Amplitude Variation with Offset Analysis

Andrei Butterfield
Wright State University

Characterization of a Utica Shale Reflector Package Using Well Log Data and Amplitude Variation with Offset Analysis

A thesis submitted in partial fulfillment of
the requirements for the degree of
Master of Science

By

ANDREI BUTTERFIELD

B.S., University of Mary Washington, 2011

2014

Wright State University

WRIGHT STATE UNIVERSITY

GRADUATE SCHOOL

April 12, 2014

I HEREBY RECOMMEND THAT THE THESIS PREPARED UNDER MY SUPERVISION BY Andrei Butterfield ENTITLED Characterization of a Utica Shale Reflector Package Using Well Log Data and Amplitude Variation with Offset Analysis BE ACCEPTED IN PARTIAL FULFILLMENT OF THE REQUIREMENTS FOR THE DEGREE OF Master of Science.

_____
Doyle Watts, Ph.D. Thesis Director

_____
David Dominic, Ph.D. Department Chair

Committee on Final

Examination

_____
Ernest Hauser, Ph.D.

_____
Doyle Watts, Ph.D.

_____
David Dominic, Ph.D.

_____
Robert E. W. Fyffe, Ph.D.
Vice President for Research and
Dean of the Graduate School

ABSTRACT

Butterfield, Andrei, M.S., Department of Earth and Environmental Sciences, Wright State University, 2014. Characterization of a Utica Shale Reflector Package Using Well Log Data and Amplitude Variation with Offset Analysis

Using well logs and AVO gradient analysis, I identify and characterize a package of reflectors associated with the Utica Shale from vibroseis data collected by Wright State University at the Gabor Gas Storage field near Canton, Ohio. I also correlate TOC measurements from wells to densities and velocities at the same depths. On the seismic data, I interpret prominent reflections from the top and bottom of the Utica Shale and an intra-Utica reflector of varying frequency content associated with a velocity/density low in well log data. I investigate the possibility that the lateral variation in frequency content and change in wavelet character of these reflections is influenced by velocity gradients, termed Wolf Ramps. A Matlab software script was written in order to approximate this behavior using synthetic wavelets, and the resulting model matched well with the seismic data. Additionally, I note a possible reverse fault within the Utica that could create fracture porosity and a migration pathway. To model the AVO response, an AVA volume was created from prestack data and reflection coefficients up to 30 degrees of incidence were calculated using the two-term Aki-Richards approximation. Large negative normal incidence reflection coefficients attenuated at higher angles of incidence (Class IV anomalies) were observed at the top of Utica reflector, a response consistent with a change from silica-rich nonsource shale to black source shale. Large positive normal incidence reflection coefficients decreasing at higher angles of incidence (Class I anomalies) were noted at the bottom of Utica reflector, consistent with a shift from low impedance source shale to higher impedance calcareous shale.

To perform forward modeling, I used geophysical well logs and NS-EW vibroseis line data. Using Hampson Russell commercial software, acoustic impedance and reflectivity were computed from sonic and density logs. An average wavelet at the Utica two-way travel time was extracted using Promax software and convolved with the reflectivity to create a synthetic seismogram for each well. Lastly, the Utica Shale and underlying formations were correlated in Petrel software using well logs in the vicinity of the seismic lines. The results of the correlation allowed me to make connections between the depositional processes that led to the formation of the Ohio Utica from the New York Utica, for which outcrops and a large number of well logs are available.

TABLE OF CONTENTS

TABLE OF FIGURES

I. INTRODUCTION

I.1 Motivation of Study

NS-EW vibroseis seismic reflection lines collected by Wright State University at the Dominion East Ohio Gabor Gas Storage Field show reflections attributed to the middle-Ordovician Utica Shale, a recent target for oil and gas exploration. The Utica is thick and multiple reflectors are likely associated with its top and bottom. Reflections within the formation are noted as well. We seek to assign top of Utica (TOU) and bottom of Utica (BOU) reflectors and make as many correlations as are possible at the seismic scale between the reflectors and known stratigraphic units. Due to the presence of Ordovician-Silurian outcrops New York, the members of the Utica are well mapped in that state. Though depositionally possible, these members of the Utica have not been correlated between NY and Ohio. Despite the fact that for this thesis only Ohio well logs in the vicinity of the gas storage field were analyzed, it is still hoped to determine the degree to which New York stratigraphic terms correspond to Ohio stratigraphic terms.

To characterize the reflector package itself, we use geophysical well log data in conjunction with the vibroseis seismic reflection lines. In many well logs, we note a low-density and low-velocity zone towards the middle of the Utica interval on density and DT logs. We attempt to explain this low-density zone (LDZ) in terms of lithology and organic matter. We also seek to determine

if the LDZ appears in our seismic data, or if tuning obfuscates it. There is also a positive phase (peak) reflector in the middle of the Utica on our seismic volume that spans a portion of the low density zone. This peak is laterally inconsistent in terms of frequency content and intermittent multiples. We seek to determine whether this is a result of stratigraphy, a result of a double Wolf Ramp (gradient) source of reflections, or some combination of the two. Additionally, we possess an AVA-processed data set that can be used for AVO analysis. Applied to shale on shale interfaces, AVO crossplots and type curves can be used in an attempt to identify source rocks and estimate mineralogy, kerogen content and anisotropy when calibrated to a modeled well log or pseudolog. However, we do not have a well log located on our seismic line (well tie), making AVO crossplot calibration impossible, or shear wave logs, making the calculation of the full elastic tensor and in turn the anisotropy parameters and Vp/Vs impossible. However, sufficient data exists from well logs in the region to allow us to forward model the seismic response over the vicinity and our AVA volume is robust enough that AVO anomalies can be analyzed at the upper non-source on source shale interface and the lower source on non-source shale or limestone interface.

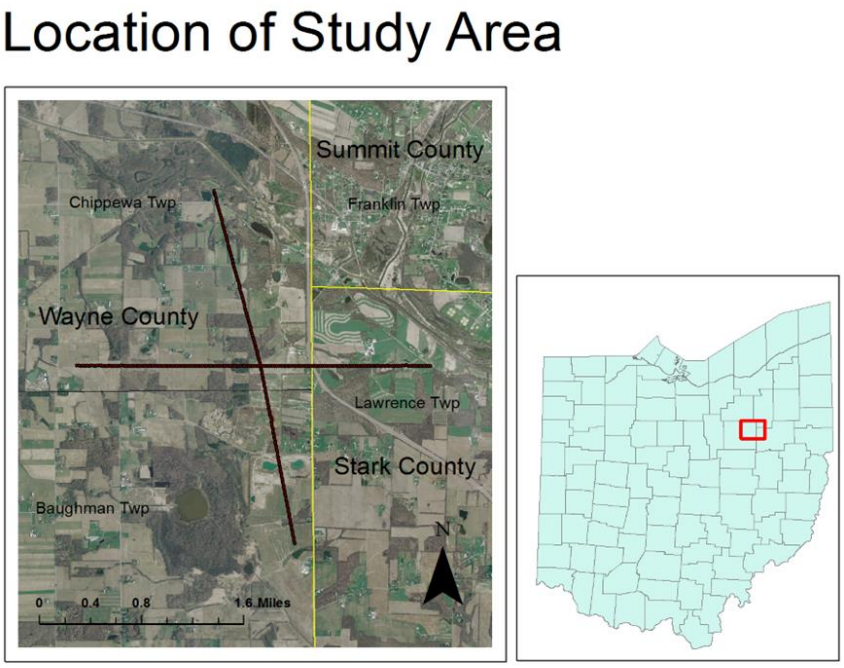

Figure 1: Vibroseis Seismic Survey Geometry and Location with County Boundaries

I.2 Shale Petrophysics

Shales are sedimentary rocks composed chiefly of groups of clay minerals such as illite, kaolinate smectite (Carcione 2001) that pack in flat, horizontal sheets, with orthoclase and quartz grains of silt to sand size interspersed within the clay matrix (Kuila 2010). This flat, layered bedding at the mineralogical level is what gives shales their fissility and inherent anisotropy, and the presence of alkali earth metals in interstitial spaces leads to incompressibility. If the shale was deposited during conditions of explosive plant growth or proliferation of marine organisms such as plankton or algae, it can contain a large amount of TOC (total organic carbon) and have utility as a source shale. A shale considered to be organic rich will have a TOC ranging between 1-20 wt% (Chopra 2012). An organic-rich source rock usually contains >3%-4% TOC (Loseth 2011). The hydrocarbon in a shale largely resides in kerogen, an amorphous high molecular weight semisolid that is subject to liquefaction at increasing temperature and pressure (Carcione 2001).

Kerogen inclusions are dispersed in the clay matrix in large aspect ratio spaces oriented parallel to bedding. Besides the kerogen itself, oil, natural gas and formation water may be found ab- and adsorbed to clay particles, in low aspect ratio pores and, in mature shales, within high aspect ratio bedding-parallel microcracks (Vernik 1991, Sayers 2012) that create secondary porosity by connecting to pores. These cracks derive from the conversion of kerogen to lower molecular weight hydrocarbons (Sayers 2012). Kerogen and other forms of hydrocarbon in the source rock can be linked to the depositional environment of the organic matter based on the vertical dispersion of organic matter and the thickness of beds (Passey 1990).

Shale anisotropy yields seismic velocities far higher parallel to bedding than orthogonal at both the seismic and ultrasonic scale (Kuila 2010). Thus, shales are often modelled as viscoelastic transversely isotropic (VTI) media (Carcione 1998), due to the orientation of bedding, kerogen inclusions, and microcracks perpendicular to the direction of propagation of a normal incident p-wave originating from the surface. In addition to viscoelasticity (time-dependent rate of strain), mature source shales also display plastic deformation due to increased compliance by way of the transformation of kerogen to oil through catagenesis. This further increases viscoelasticity and leads to increased dissipation and attenuation of seismic waves (Carcione 2001) that must be accounted for when modelling or selecting a seismic wavelength to use when surveying source shales.

Shale anisotropy is often characterized through the three anisotropy parameters ε, γ and δ corresponding to p-wave, s-wave and Thomson's anellipticty parameter, respectively (Kuila 2010, Sayers 2005, Sayers 2012, Vernik 1992). Determining these parameters requires simplifying assumptions or the calculation of the full elastic tensor in all directions. ε and γ can be modified by the presence of silt or spherical carbonate grains, microcracks, and low and high aspect ratio cracks (Sayers 2012). Silt and carbonates will decrease ε and γ through replacing

anisotropic clay minerals with larger, isotropic grains and disrupting the alignment of anisotropic clay minerals. These inclusions also increase Young's moduli and decrease Poisson's ratio, thus enhancing the fracability of the shale (Schuelke 2011). Interestingly, carbonates such as limestone and dolomite contribute to enhancing brittleness only up to a volume fraction of about 0.4. Above this, the component minerals form carbonate interlayers that act as fracturing boundaries (Wang 2012). The inclusion of high or low aspect ratio kerogen within the clay matrix increases ε and γ by adding an additional anisotropic body to the already anisotropic clay. These bodies decrease Young's moduli and decrease Poisson's ratio up to 0.6 volume fraction kerogen. This decreases fracability but of course increases TOC, resulting in a sort of trade-off. The presence of low and high aspect ratio cracks aligned with clay mineral orientation add discontinuities to the shale and decrease seismic wave velocity more in the vertical direction than the horizontal. The resulting effect on Young's modulus and Poisson's ratio is less clear cut than the other two cases. Even though we lack the means to directly quantify anisotropy within the Utica shale in the study, the understanding of how anisotropy parameters might vary laterally within the Utica could help explain some of the complex reflections seen in our seismograms. The Vp/Vs ratio is another widely used measure of anisotropy that was beyond the scope of this analysis to quantify.

I.3 AVO

Amplitude variation with Offset Analysis is a classic seismic attribute that has been used to great effect to find traditional gas/oil reservoirs since 1989 (Isaacson 1999) through hunting for bright, dim and flat spots associated with the traditional sandstone reservoir progression of brine to oil to gas under a structural trap, and other scenarios. Only since the late 1990's has AVO been applied to hydrocarbon source rocks. This application hinges on the fact that kerogen

inclusions found in source shales decrease the acoustic impedance of the interval and enhance intrinsic velocity anisotropy (Kuila 2010). As the angle of incidence of a propagating seismic wave in a shale increases, the acoustic impedance increases concomitantly, due to shale minerals packing more densely along their bedding, allowing for faster transfer of p-wave energy between shale particles and thus faster Vp. This petrophysical quirk is the foundation of the AVO response seen in shales, and the recent incorporation of this attribute into the seismic interpretation workflow of unconventional plays.

In a pair of seminal papers, Carcione et al. (1998) and Carcione (2001) modelled the AVO effects of a variety of interfaces involving shale source rocks. The interface modelled was a limestone overlying a black shale interface with the shale exhibiting higher impedance than the limestone, the PP reflection coefficient was positive and reached its maximum at different points depending on the quality factor Q, a measurement of the damping (oscillatory dissipation) of the shale. This factor, along with ε, γ and δ are used to model and describe the dissipation encountered due to viscoelastic shale behavior (Carcione 1998). Even though complex oscillations of the reflection coefficient were observed, they only occurred at angles exceeding the 30* valid maximum predictable by the Shuey approximation, indicating that attenuating forces do not dominate at lower incidence angles. In 2001, Carcione expanded upon this work by modelling the PP and other reflection coefficients when varying layer thickness and kerogen content in a chalk-on-shale-on-sandstone with the shale as the only anisotropic layer. This model was based off the Kimmeridge Shale in the North Sea (Carcione 2001). Through this modelling, he showed how reflection coefficients in shale interfaces analogous to that modelled decrease at near to moderate incidence angles (up to 30 degrees) and then begin to oscillate as the two competing forces of anelastic attenuation and velocity increase with bedding at higher incidence angles interfere with one another. Expanding on

Carcione, it can be concluded that a nonsource shale on source shale interface will display a class IV AVO response at the top of the interface as the large negative reflection coefficient at normal incidence is attenuated by the velocity increase towards the direction of bedding at higher incidence angles, and a class I response at the bottom interface where the impedance contrast between kerogen-rich source and the underlying nonsource rock is at its highest at normal and near incidence angles (Chopra 2012). At greater angles, the aforementioned velocity increase in the direction of bedding will decrease the impedance contrast between the nonsource and source shales. The minimum amount of TOC required to precipitate this AVO behavior in shale-shale interfaces has been estimated at 3-4% (Loseth 2011, Chopra 2012).

The AVO analysis of source rocks is simplified in some ways to that of conventional plays due to the fact that there is limited opportunity for fluid substitution. Shales, though capable of having relatively high porosity, do not have sufficient permeability as to allow for full saturation with brine and natural gas to the degree that would occur in a reservoir sand and be able to greatly alter Poisson's ratio through varying pore fluid fill. In a conventional AVO analysis, brine, oil and gas sands would shift the R_0 and G into different quadrants of a cross plot, and require careful calibration with a background trend (Castagna 1997, Avseth 2005) to distinguish between the different saturating constituents of the sand. In source shales, we see amplitude variation with offset effects driven primarily by kerogen content and anisotropic variation between and within the shales, instead of fluid fill.

I.4 Utica

The Utica shale is a middle Ordovician calcareous shale facies that underlies much of eastern North America. It is a current target of hydraulic fracturing and horizontal drilling as far north as Quebec, Canada (Eaton 2010). It is diachronous and was initially was co-deposited with the Trenton limestone on different regions of the foreland basin created during an early phase of the Taconian orogeny. This orogeny was largely responsible for the creation of the Appalachian Mountains and was active between the mid to late Ordovician (Ettensohn 1994). It is postulated that the organic-rich muds that were lithified to form the lutites of the Utica were deposited in a dysoxic to anoxic foredeep on the cratonward side of the basin (Baird 2002). Distal deposition with respect to the orogeny (Ettensohn 1994) resulted in a filtering of clastic sediments that, in conjunction with regional transgression, contributed to giving the Utica its black shale character. In Ohio, the Utica becomes decreasingly calcareous and increasingly siliciclastic from its base. The organic content is high for the area, ranging from 1.5% to 3.5% (OGS 2012) and is likely contained in kerogen inclusions. These factors all lead in general to lower p-wave velocity and density toward the top of the Utica. In Ohio, the Trenton and Utica are younger and dip upwardly to the west. There are no outcrops containing Utica strata in Ohio, and so the members and surrounding groups and formations chronologically adjacent to the Utica are not well mapped in this area. Utica outcrops are found and have been studied extensively in the Mohawk Valley region of New York (Baird 2002). Studying these outcrops has elucidated the mapping of many members and smaller formations within the Trenton and Utica, as well as the tectonic and eustatic processes that led to the formation, filling and shaping of the foreland basin.

In New York, the Trenton Limestone and Utica Shale are separate towards center of the basin and interfingered towards the basin margin.

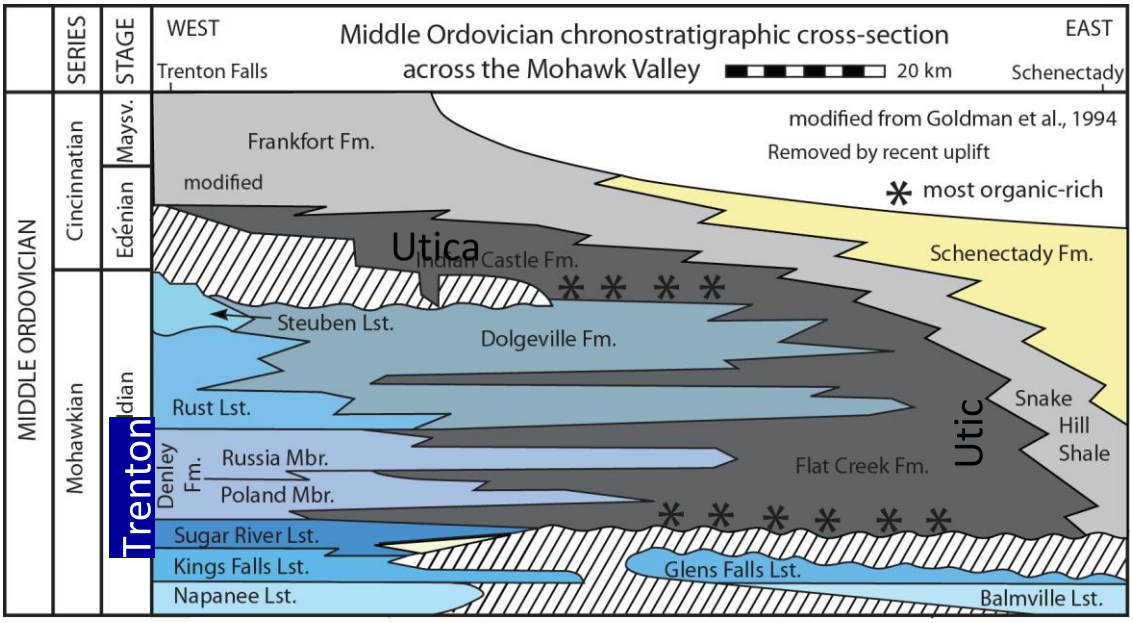

Figure 2: Middle Ordovician Chronostratigraphic Cross Section from New York

It is important to note the Dolgeville formation that separates the lower and upper Utica. The Thruway Disconformity is sometimes found between the upper Indian Castle (upper Utica) Formation and the Dolgeville, the deposition of which is attributed to density flows composed of interbedded tabular ribbon limestones and dark gray shales (Brett and Baird 2002). The Dolgeville pinches out between the New York and Ohio regions of the Utica Formation, but the presence of carbonate turbidites within the Utica could by analog be possible in Ohio, and would have the potential to greatly alter the seismic response. Along similar lines, there exists an E-W dipping fault system in New York that occurred simultaneously as depositional thickening of the Utica into grabens towards the west. The faults are thought to have stymied the flow of siliciclastics from the Taconic mountains towards the east (Talk 2. Finish citation). On our seismic sections, we note a fault within the Utica that may be related to a similar pattern of

syndepositional faulting. In between the Flat Creek (lower Utica) and the Trenton is the interregional Knox unconformity, which marks the drowning and corrosion of marginal carbonates during a long period of nondeposition, followed by the deposition of basinal shale. Baird and Brett (2002) suggest that this unconformity extends elsewhere into the basin, such as into Ohio and potentially to the midcontinent.

In Ohio, the Utica and Trenton are less subdivided than in New York. The Utica underlies the Cincinnati group, a thick upper Ordovician set of shales, and overlies the Point Pleasant formation. This formation is broadly interpreted as a marl and is only mappable to the far eastern and western margins of the basin. Towards the center of the basin, it is replaced by deep/shallow marine shales that extend into the Trenton. The Trenton is divided into three members: the Lexington, Logana and Curdsvillle. All three members become increasingly tight and calcareous. The Curdsville is the first stratum without a substantial shale matrix, as seen through its >17,000 ft/s p-wave velocity. I propose that the units comprising the Utica in New York and Ohio and the unconformities between them likely correlate across the extent of the sedimentary basin. The geologic processes that support this scenario are centered on the formation of regional and intraregional unconformities as a combination of tectonics and eustasy (Ettensohn 1994).

I.5 Previous Work

The body of work investigated for this thesis comprised shale petrophysical studies, shale and conventional AVO and AVO case studies, and geology and stratigraphy studies of the Utica Shale, primarily in the Mohawk Valley region of New York State. No studies investigating AVO behavior in Ohio's Utica shale have been published thus far.

Avseth (2005) summarized the geologic sceneries likely to yield successful AVO R_0 vs G crossplots. The study targeted conventional sandstones, but considered shales as necessary for defining a background trend with which to compare anomalous deviations from the crossplot. Carcione (1998) laid the groundwork for shale AVO by deriving equations that accounted for inherent dissipation and attenuation mechanisms in shales. He utilized these to model how different reflection coefficients and phase angles vary with offset. Carcione (2001) expanded his models to incorporate more realistic shale properties such as mineralogy and fluid content. These refinements were applied to a model consisting of an orthorhombic source shale embedded between two isotropic half spaces: a chalk and a sandstone. From this model, P, S, and PS reflection coefficients were calculated with varying layer thickness and kerogen content. Castagna (1997) laid out a practical methodology for AVO workflows by describing how the Shuey approximation may be used to rapidly approximate reflection coefficients at varying incidence angles. He showed how varying sand lithologies and fluid fills can shift points of an R_0 vs G crossplot to different quadrants of the crossplot. These deviations correspond with the four known AVO anomalies. Chopra et al. (2012) summarized the characteristics of a shale formation likely to result it in being successfully developed. They expanded Carcione's (2001) shale AVO modelling to reservoir on nonreservoir shale facies. Lastly, they surveyed modern techniques for shale reservoir characterization, in terms of both azimuthal variations in velocity and impedance, as well as seismic waveform classification. Isaacson & Neff (1999) applied AVO cross plotting to gas fields in the Hammerfest basin of the North Sea. The lithologies they analyzed were complex mixtures of gas sands and shales. Though they did not investigate any shale reservoir rocks, they well illustrated how variations in shale lithologies and fluid fill can be modelled with AVO cross plotting. Loseth et al. (2011) of Statoil linked Vp/Vs and AVO behavior with high TOC values. They also applied Carcione's seminal modelling to describe the expected

AVO anomalies at different source shale interfaces. Kuila et al. (2010) conducted a highly quantitative examination of stress and velocity anisotropy in shales. In it, they used a triaxial load frame to apply azimuthally varying stresses to shale samples and measured P and S velocities in different directions. Additionally, they laid out detailed petrophysical explanations for the increase of velocities parallel to bedding and the concomitant decrease in anisotropy and Vp/Vs. Lucier et al. (2011) used Vp/Vs crossplots created from sonic log data to characterized variable gas saturation in Louisiana's Haynesville shale. They compared how a thermally overmature shale prone to natural gas generation like the Haynesville differs from a less mature shale in the oil window, such as the Bakken. Ozdemir et al. (2008) applied the breakout technique of multicomponent seismic inversion to a North Sea dataset. They created attribute sections of acoustic impedance, bulk modulus and volume of shale. Neural net modelling was used to create the shale volume sections. Passey et al. (1990) released a paper on the delta log R technique, a quantitative measurement that compares sonic and resistivity logs to determine the TOC present. They established the in immature (kerogen-rich) source rocks, deviation of the sonic log is indicative of hydrocarbon. In mature (oil and gas-rich) source rocks, deviation of the resistivity log shows the replacement of formation water by oil and gas. Measured curve deviations may be calibrated to level of maturity, which in turn is used to directly predict %TOC. Sayers (2005) of Schlumberger modeled clay petrophysics at the mineralogical scale, and stated that shale elastic behavior can be better described by the degree of alignment and level of organization of clay platelets within a shale than by the mineralogy itself. He referred to the regions of particle alignment as domains, and proved how the tensor describing a shale can be fully represented by the coefficients W200 and W400. In 2012, he expanded this work to calculate how the Young's modulus and Poisson's ratio of shales vary with different levels of particle alignment. He also described the accompanying effects on the anisotropy parameters ε,

γ and δ. Schuelke (2012) of Devon Energy modeled and described how seismic velocities in shales vary with respect to fracture orientation and direction of maximum horizontal stress in 3D space. He noted that velocities parallel to fractures are faster those of waves propagating perpendicular to fractures and that velocities parallel to the direction of maximum horizontal stress will also be faster than those in the direction of minimum horizontal stress. Treadgold et al. (2011) interpreted an azimuthal 3D survey of the Eagle Ford shale, and noted small to no reflection events between the upper and lower members of the Eagle Ford. The boundary region displays a gradient of acoustic impedance caused by upwardly decreasing TOC and porosity. Vernik and Nur (1991) used ultrasonic waves to measure the effects of kerogen inclusions, microcracks and temperature on p and s-wave velocities. They found a positive correlation between these three properties and lowered velocities in shales. Wang and Carr (2012) conducted a study in the Marcellus that deployed advanced logs such as pulsed neutron spectroscopy to directly determine mineralogy, differentiate lithofacies at the borehole and determine TOC content. From these data, they conducted several different types of neural net modeling to try and extrapolate between borehole and regional lithofacies. Yoon and Farfour (2012) described the limits of the AVO technique in situations of thin bed tuning, and related the arising complications to offset and problematically low ratios of layer thickness to wavelength. The particular region where they found AVO difficult was in a clastic channel fill deposit in Alberta, Canada. They applied spectral composition the track horizons and elicit details that were not possible through well logs and AVO. Zadeh et al. (2011) conducted a review study that drew together the most prolific techniques for analyzing source shale composition and organic content. In their list, they included Passey's delta log R technique, the LMR parameters, and advanced inversion (ExMax) algorithms that are capable of operating with missing data. Zhu et al. (2011) laid out how different shale mineralogies (chiefly varying amounts of quartz, clay, TOC

and calcite) affect impedance and AVO response. They noted that in clay-rich source rocks, calcite was correlated with high TOC and low Vp/Vs, while large amounts of clay or quartz grains show higher impedance and Vp/Vs and lower TOC.

Ettensohn (1994) described the general sedimentary sequence seen in foreland basins as caused by tectonic loading. Specifically, the steps of peripheral bulge formation, loading and unloading lead to a sequence of an unconformity overlain by transgressive carbonates or shallow marine sands, then basinal shales, then flysch overlain by marginal-marine clastics and redbeds. He also explains how bulge migration can lead to basement faulting in the Appalachian basin. Brett and Baird (2002) laid out New York stratigraphic correlations of Utica and Trenton members based on outcrops and detailed the depositional processes and history of the Dolgeville turbidite facies that bisects the Utica. In a separate paper, Baird and Brett (2002) exhaustively described how graptolite and K-Bentonite correlation was used in the Mohawk Valley to describe the Trenton-Utica succession. He also notes a drowning disconformity between the Trenton and Utica and proposes it may extend all the way to the midcontinent.

II. METHODS

M.1 Seismic Data Collection and Processing

In January 2011, two 2D seismic lines were collected by Wright State University with the help of Precision Geophysical and Dominion East Ohio. The lines were oriented N-S and E-W roughly perpendicular to one another, and were collected using a vibroseis source. The intersection of the lines was located at the intersection of Stark, Summit and Wayne counties. The N-S line had 185 seismic recording stations and the E-W line had 178 stations, with an 82.5 foot interval between stations. Each station had a six geophone array with an individual geophone spacing of 15 feet. The geophone frequency was 10 Hz. Two pilot sweeps were collected at 8-128 Hz per vibration point without move-up by one vibroseis truck, with a 12 second listening time. The first sweep was conducted in order to compact loose soil to enhance ground-base plate coupling for the second sweep. Data were recorded at 1 ms with a 3-205 Hz recording filter by using Precision Geophysical's Aram Aries system. The acquisition parameters are found in the appendix **A.1**.

The seismic lines were professionally processed by Tom McGovern of Seismic Earth Resources Technology in Denver, Colorado. The result of his workflow was pre-stacked and post-stacked migrated data along with the velocities, provided below. The 15-75 Hz E-W seismic line

was also processed to produce an AVA volume. To construct the AVA volume used for AVO gradient and crossplot analysis in this study, Radon transform filtering was applied to normal moveout (NMO) corrected common depth point gathers processed to preserve amplitude. The gathers were transformed to amplitude vs angle of incidence gathers to examine potential AVO effects. The acquisition parameters described in **M.1** were adapted from Bey (2012). A portion of the AVA volume is reproduced below. In it, we see the variation of reflection coefficients at increasing angle of incidence for each CDP.

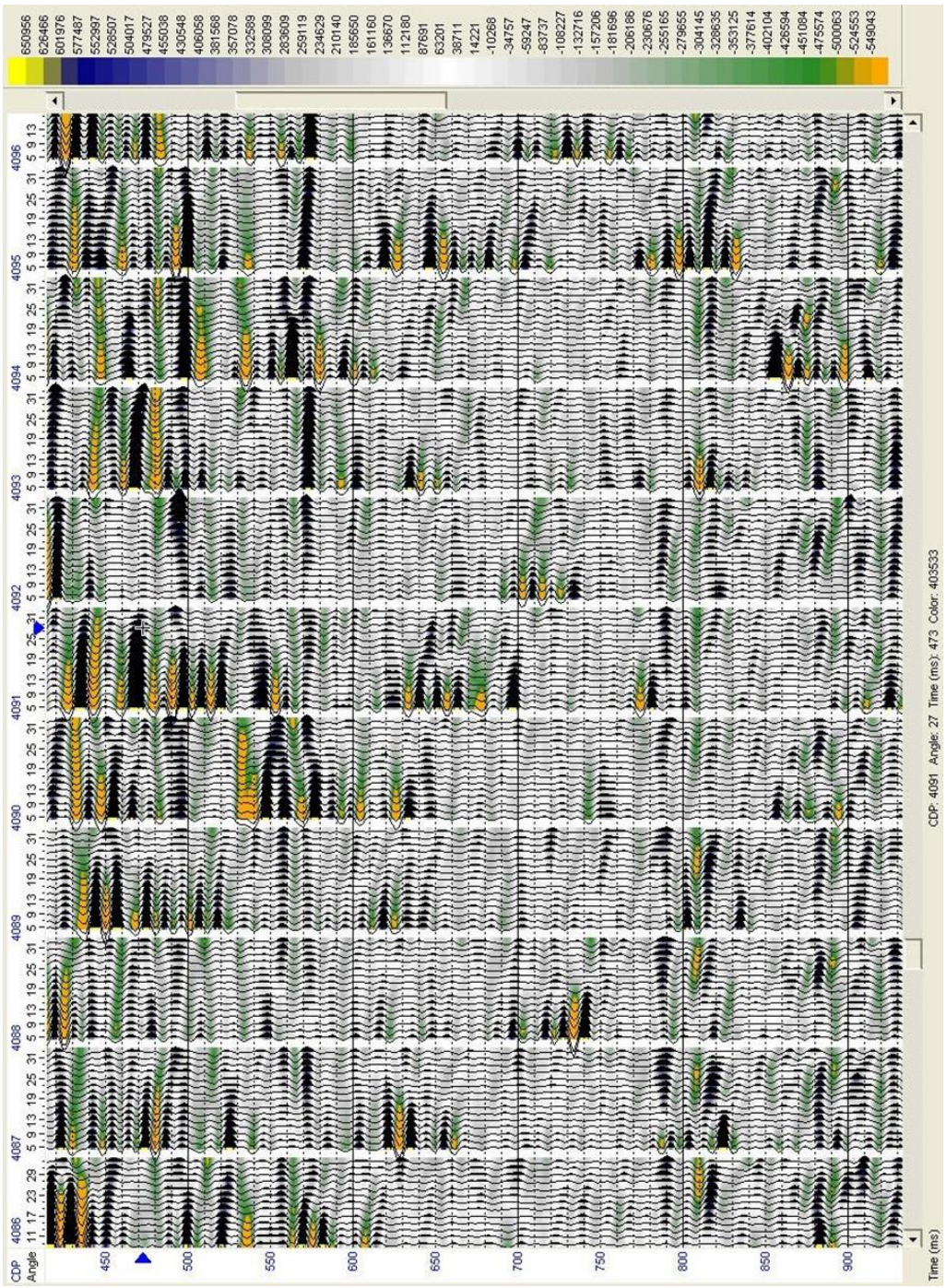

Figure 3: Excerpt from AVA Gather, E-W Line

M.2 Well Log Selection, Digitization and Mapping

To find wells in the study area that might be used for forward modeling, a query was sent to the Ohio Geological Survey to search for wells logs with DT and bulk density measurements that

penetrate the Utica formation. These wells were provided to us on CD in the form of .tif files. From the CD, nine well logs were selected for digitization. The two main criteria used to pick them were proximity to the seismic line and even geographic distribution around the line. Three of the wells were picked because they had full pyrolysis data available. Neuralog was used to digitize the wells, and the resulting .las files were imported into Hampson-Russell. ArcMap 10 was used to plot the wells and seismic line. The coordinate system used for mapping was Ohio State Plane (feet). To input well locations into ArcMap, an excel spreadsheet with Easting and Northing (X and Y coordinates respectively) was created, and the Ohio SPCS values were entered. In the ArcMap environment containing the seismic data, a layer referencing the well coordinate values was added. This enabled the program to display the well log and seismic lines at the same time.

M.3 FORWARD MODELLING

In preparation for modeling the seismic response, all available curves for nine digitized well logs were imported into the Hampson-Russell software package as .las files. The minimum amount of curves imported for all wells were density, velocity, and gamma ray, but some wells also came with resistivity, caliper, neutron porosity, and others. The well logs were all investigated to determine the regional extent of the low density/low velocity zone seen in wells closest to the seismic lines and for other anomalous signals. Next, reflectivity was convolved with the source wavelet extracted from the seismic lines to produce synthetics for all nine wells. This was done in order to determine if the complex reflections from the Utica on the seismic data could be attributed to variations and/or anomalies in density, velocity, or other petrophysical parameters similar to those seen in local wells. Previous modelling by Bey 2012 had used an average wavelet over the entire two-way travel time of the section. This wavelet was

determined to be too high frequency to provide optimal bed resolution over the Utica interval. To remedy this, the derived average wavelet function of Promax was used to extract the source wavelet between 700-800 ms, a TWT window encompassing the Utica. The input parameters were:

Phase output option: Zero

SELECT Primary derive gate header word: CDP bin number

SPECIFY derive gate parameters: 1:0.0:700-800

Apply a taper to the derive gate: Yes

Taper type: Hanning

Trace length for the average wavelet trace: 100

Time on output trace representing time zero: Center

Write wavelet trace to disk dataset? Yes

Next, the results of the convolutional modeling for each well log were used in the picking of preliminary stratigraphic horizons corresponding to the Utica Shale and underlying Trenton Limestone. The Promax-extracted wavelet is reproduced below. It must be noted that the wavelet, while very close to zero-phase, is slightly phase shifted in the positive direction.

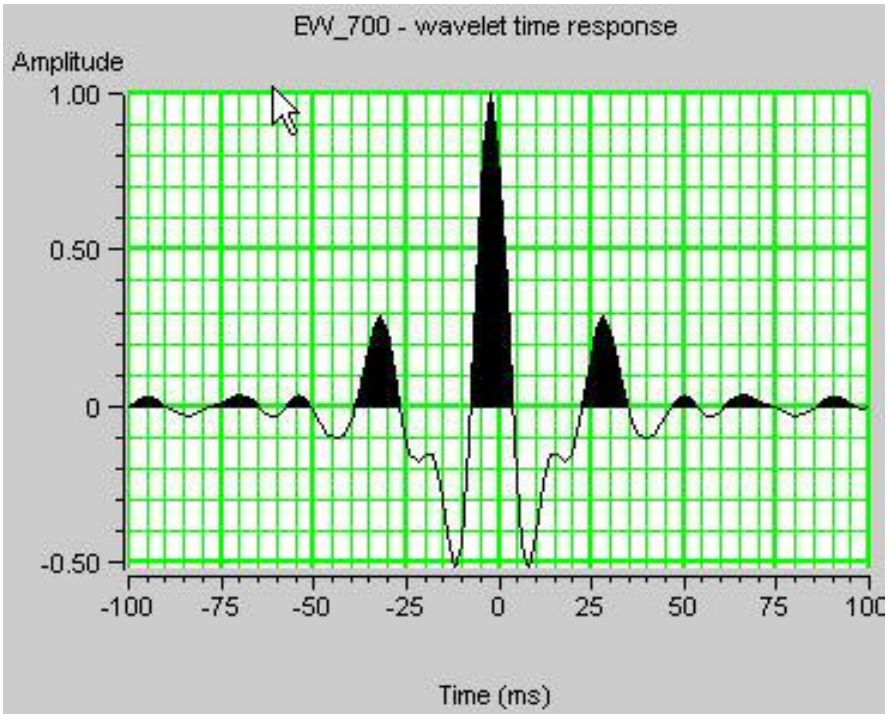

Figure 4: Source Wavelet from the E-W Seismic Line Extracted Between 700-800ms

M.4 AVO Gradient and Crossplot Analysis

Using Hampson-Russell, an intercept vs gradient analysis was performed on the E-W AVA volume. AVO modelling was performed without the application of a rolling angle super gather, and sample input parameters for one CDP were:

Input Volume: AG_NR_RG_LINE_B (Input Data is Angle Gather)

CDP at: 4136

Angle from: 5 to: 30

Velocity information: Time-Velocity Table

Apply 500ms smoothing on velocity

Minimum Acceptable Correlation: 0.1000

Minimum Acceptable Fold:3

Type of Analysis: A/B (Two Term Aki-Richards)

Stabilizing Method: Robust

To select portions of the reflector for AVO, a series of CDP's corresponding to regions of large, bright amplitudes at the top of Utica and bottom of Utica reflectors was selected from the stacked migrated CDP section. At the TOU, CDPs 4250-4290 and 4085-4100 were combed for anomalies between 745 to 748 ms and 736-744 ms, respectively. The former amplitude anomaly corresponded to a bright spot, and the latter, a dim spot. At the BOU, there was little amplitude variation between CDPs and so a region of constant amplitude at CDPs 4131-4175 and between 774-782 ms was selected for gradient analysis. Gradient analysis at the BOU interface was less straightforward, due to ambiguity at the interface itself. The Utica-Point Pleasant interface appears as a dim peak within a deep trough on well log data. On the EW seismic line, no peak whatsoever appears. Thus, AVO anomalies at the BOU interface could in actuality arise from any of the thin beds aggregating to form the trough at the base of the Utica. The amplitude anomaly for each CDP (if any) was captured via screenshot with Snagit6 and stored in a folder corresponding to each reflector. The contents of each folder were then catalogued and the number of each type of anomaly or lack of anomaly was recorded and tallied. The strongest anomalies are included in the results section of this thesis.

An normal incidence reflectivity vs AVO gradient crossplot deconstructs the Shuey approximation and plots the resulting pairs of values over a specified time interval to simultaneously look at all anomalies present. To create an R0 vs G crossplot, a two-way travel time window of 720-830 ms was used. This window fully encompasses the Utica Shale and Point Pleasant Shale.

From the resulting crossplot, a background trend was established. The crossplot was then divided into four quadrants, each corresponding to a different AVO anomaly. Any coherent deviations from the background trend into different quadrants were noted.

M.5 Well Log Total Organic Carbon Analysis

TOC and other pyrolysis data were available for many wells in Ohio, courtesy of the Ohio Geological Survey and a variety of companies. Data were provided to us by the Survey in a spreadsheet, which was queried to determine which wells were in the study area and penetrated the Utica and/or Point Pleasant. The list of useable wells was further narrowed down to those hundred odd provided to us on CD by the survey. Three of these wells were within 60 miles, which was used as a de facto proximity cutoff. Once the well logs had been digitized and imported into Hampson-Russell, P-wave velocity was extracted from the logs' .las files into an excel spreadsheet. Next, pyrolysis information from the top of the Utica through the Curdsville, as well as depth information for where each sample were taken were added to the spreadsheet. P-wave velocity and TOC were crossplotted separately for each well, and different symbology was used for each formation. This was done in order to determine if there was a correlation between TOC, velocity and depth in the wells, and more pertinently, the shape assumed by p-wave and density curves at instances of high TOC. Ideally, patterns seen in the wells with TOC data might also be seen in wells closer to the seismic line, where they could be incorporated into their well synthetics, allowing for the comparison of synthetic reflections arising from or involving high TOC with real reflections on our seismograms.

M.6 Well Correlation

The Utica Shale, Point Pleasant Shale, and the Trenton Limestone members that are known in Ohio as the Logana, Trenton/Lexington, and Curdsville were correlated in a NE-SW

section using Petrel. Nine wells were used to make the Petrel span, and formation tops were picked using a type log created by Ron Riley of the Ohio Geological survey in conjunction with well number 34151251020000, the closest well to our seismic lines. Formation tops for this well were also picked by Ron Riley. To import the logs into Petrel, a spreadsheet was created with the Northing and Easting values for each well in Ohio State Plane North, as well as the top and bottom logged depths. This was input as the well headers, which allowed gamma ray, density and DT curves for the nine wells to be properly tracked in three dimensions.

To correlate the wells, the gamma ray high corresponding to the top of the Utica was used as a datum. All wells were snapped to this datum, and TOU was picked first for wells closest to well number 34151251020000, which was used as a well template. The top of the Curdsville was picked next, as it is associated with a large and rapid drop in dT and rise in density associated with a shift from calcareous shale to limestone. The other Trenton members and the Point Pleasant Shale were picked next, and were tracked without too much problem up to well number 34075252750000, the far southeastern-most well. In this well, the Point Pleasant was not discernable from the surrounding shale, possibly because the lateral extent of the formation had been reached. My pick for the underlying Trenton/Lexington hinged upon the position of the Point Pleasant, and thus was also not picked for well number 34075252750000.

M.7 Wolf Ramp Modeling

Through forward modeling, we were able to see the mid-Utica reflector, but its complex variations in frequency content and wavelet character were not observed in any well synthetics. Furthermore, we noticed that reflections were not arriving directly at sharp reflectivity contrasts as would be expected in convolutional modeling, despite the source wavelet being extremely close to zero-phase. After examining the well log

impedance curve we arrived at the conclusion that the delayed arrival of reflections in the mid-upper Utica may be caused by a gradual drop and increase in velocity and density logs. This low density zone (LDZ) leads to gradational acoustic impedance and can no longer be accurately described through convolutional well synthetics. To model these effects, we created a Matlab script to recursively calculate systems of partial differential equations that describe the complex reflection coefficients arising from linear velocity gradients in transition layers after Justice and Zuba (1986), Gomez and Ravazzoli (2011) and Liner and Bodmann (2010). These velocity gradients are termed Wolf Ramps after Alfred Wolf (1937). A wedge-shaped constant velocity model approximating acoustic impedance gradients was used. Depth velocity pairs (Z,V) of (0ft, 12000 ft/s), (100 ft, 11000 ft/s) and (200 ft, 13000 ft/s) were the inputs to the model. These velocities were characteristic of the Utica Shale at the depth of the transition zone and were extracted from the p-wave log of well number 34169250100000. The velocities were very close to those in other wells in the upper Utica that showed the evidence of the LDZ. The model was applied to the Promax-extracted source wavelet to determine the form of the reflection and investigate the fit of the resulting wavelet to the seismic data. A fast Fourier transform was performed on the amplitude-time domain modeled response to convert to the amplitude-frequency domain. The resulting complex reflection coefficients calculated by the model were multiplied by the source wavelet to produce a filtered source wavelet approximating the wavelet distortion and shifts in phase and frequency caused by velocity gradients

(Justice and Zuba 1986). The Matlab script for the algorithm describing the four-layer double velocity transition zone model is reproduced in the appendix.

III. RESULTS AND DISCUSSION

R.1 Seismic and Geological Interpretations, E-W Line

On the E-W CDP gather, we identify three prominent reflectors associated with the Utica Shale and highlight the Top of Utica reflector in green, the Bottom of Utica reflector in red, and the Trenton Limestone in cyan. The latter reflector marks the location of an unconformity (disconformity) between basinal Utica shale and subtidal platform Trenton carbonate (Brett and Baird 2002). The reflector in the middle of the Utica is not highlighted but is the only major event between the TOU and BOU. The TOU reflector is a large negative amplitude event that spans the entire section. This trough arises from the marked decrease in acoustic impedance crossing from nonsource Cincinnati Group shale into source rock Utica Shale. The TOU reflector is a clean, fully developed event that, being sufficiently far away from the Trenton, is free from tuning effects and side lobe interference associated with the underlying bed. We note a region of bright, strong amplitudes between CDPs 4250 and 4290 at 746ms TWT. We interpret them as either arising from a heightened impedance contrast due to kerogen inclusions aligned with bedding in in the upper Utica as is typical in source rock shales (Vernik 1991), or a shift from more brittle to more ductile shale. We use this high amplitude region as a target for AVO gradient analysis (See **R.7** AVO). In contrast, we note a narrow portion of the reflector with anomalously dim amplitudes between CDPs 4085 and 4100 at 740ms that we also target for

AVO for the sake of contrast. The reflector at the top of the Utica Shale is fully realized in the convolutional modeling of well logs up to 40 miles away from the seismic line.

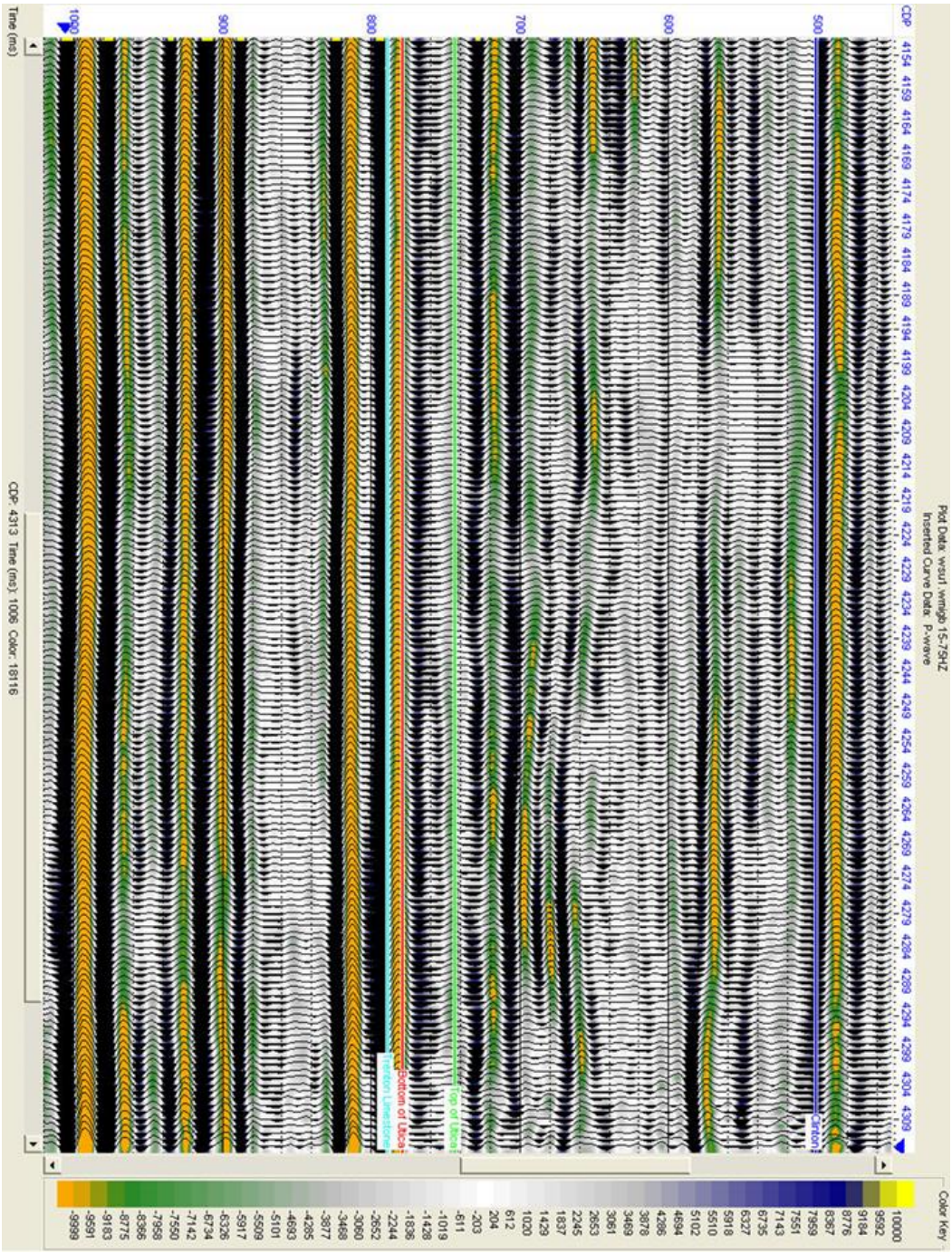

Figure 5: E-W Line Migrated CDP Stack

The second reflector we identify is intra-Utica, and displays tuning effects in terms of frequency content, phase shifts, variable amplitudes, and wavelet splitting. These effects are inconsistent across the line and are most pronounced between around CDP 4210 to 4320. In our convolutional modeling of the two well logs nearest to the seismic line (34169250100000 and 34151251020000), we observe the reflector, albeit without the aforementioned variation in wavelet character. This indicates that the variations in p-wave velocity and bulk density that give rise to the typically sharp contrasts in acoustic impedance that are the basis for well synthetics were not at work in tuning the intra-Utica reflector. Moreover, the synthetic reflections were not occurring at two-way travel times that corresponded with the reflectivity spikes that are convolved with acoustic impedance to create a standard synthetic reflection. However, we did note a gradational decrease and subsequent increase in acoustic impedance beginning at a depth corresponding to the top of the LDZ within the upper Utica. This impedance transition zone is similar in practice to the velocity gradients observed in CO_2 transition layers by Gomez and Ravazzoli (2011) and modeled permafrost zones by Justice and Zuba (1985). Reflections from transition zones have been noted since first being described by Alfred Wolf (1937). Using Matlab, we simplified the largest transition zone seen in the intra-Utica reflector to a simple wedge and produced a synthetic reflection that closely matched what is seen in the seismogram (see **R.5** for interpretation of the model). We must introduce a caveat to this explanation. Model input velocity-depth pairs were taken from a well about five miles away from the seismic line. Therefore, despite waveforms of the vibroseis data and the well synthetics being identical, the velocity gradient hypothesis proposed cannot be strictly verified without well control. Another possible explanation is that a formation analogous to Middle-Late Ordovician Dolgeville Formation described by Brett and Baird (2002), in New York's Mohawk Valley region. The Dolgeville is located between the Upper Indian Castle Shale (upper Utica in

Ohio) and Lower Indian Castle Shale (lower Utica in Ohio). It is a thin, turbidically-deposited sequence of rhythmically interbedded dark gray shale and calcisiltic ribbon limestones (Baird and Brett 2002). Even though the Dolgeville only occurs on a narrow band on the Mohawk Valley region, a similar turbidite facies could by analog be found in Ohio. In theory, the chaotic nature of turbidite deposition could result in the complex wavelets and variable TWT seen on the seismic section as the sediment that would lithify to form the Dolgeville slumped down the slope of the Trenton platform. In well logs there is no prominent increase in density or velocity that could help in the picking of such a bed and attributing the peak on the synthetic seismogram to any real specific lithological change. Thus, the intra-Utica reflector cannot be tied to a lithology without observing a core.

The third reflector is located at about 780 ms TWT. Amplitudes across the section are very uniform, more so than the mid-Utica or TOU reflectors, and do not vary appreciably in peak amplitude or phase. Since the next major reflection event on both seismic lines is interpreted as the Trenton Limestone basinwide, we know that the wavelet around 780 ms must be a combination of the signal from the lower Utica and the three beds under it and above the Trenton. These are the Point Pleasant Shale, Trenton/Lexington, Logana, and Curdsville (all Trenton Limestone members). In well logs from the study area, these formations have characteristic variations in the velocity, density and gamma ray curves that make them readily identifiable at depths matching the TWT of 780 ms. These strata are not resolvable on the seismic data, indicating that they are below the tuning thickness and likely constructively interfering to create the single aggregated trough on the seismogram. Also likely is some interference from the large side lobes of the typical Trenton Limestone wavelet. This may destructively interfere with wavelets returned from the thin-bedded formations above the Trenton. Specifically, reflections returned from this region are of low frequency, indicating that

the Trenton's side lobes may be obscuring the high frequencies of the wavelet. In terms of lithology, the thin beds that aggregate to from the trough above the Trenton are all increasingly carbonate-rich lutites that show gradational bed boundaries before unconformably changing to the Trenton limestone. Despite the grading lithologies, reflectivity spikes are different enough in AI to return separate reflections between beds in well synthetics (see **R.3**). Most notable is the boundary between the Point Pleasant and the Utica, which appears as a small trough.

R.2 Seismic and Geological Interpretations, N-S Line

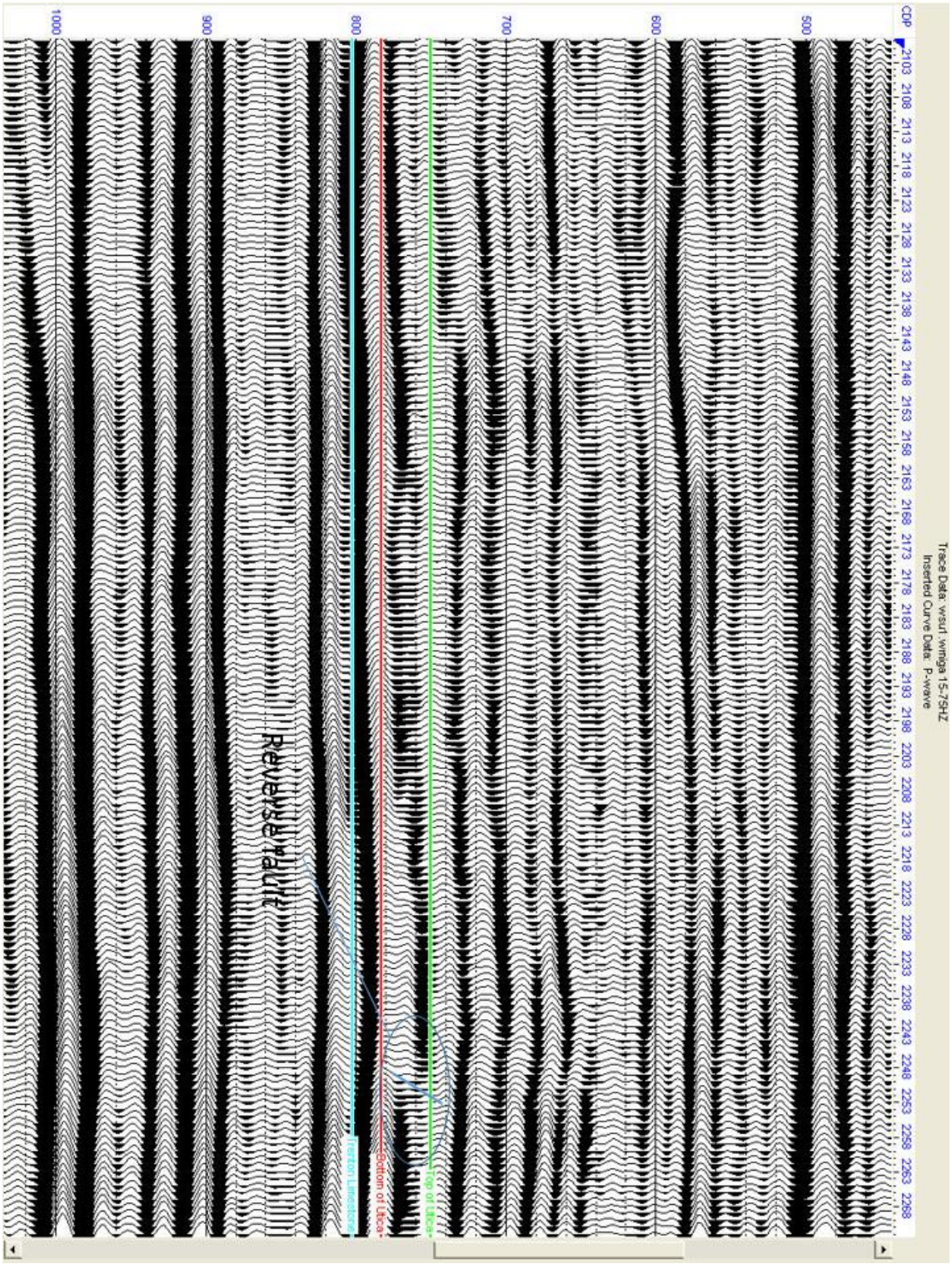

Figure 6: N-S Line Migrated CDP Stack

The N-S seismic section shows the same three prominent reflectors at identical TWT times as on the E-W section. The "layer cake" stratigraphy of the Utica-Trenton succession in Ohio is evident on both seismic lines. We do however see some structure at further offsets. Most notable is a discontinuity centered over CDP 2250 and around TWT 785 ms that we interpret as a reverse fault. Similar lineaments have been identified in the Middle and Upper Ordovician strata of New York, and it is noted that the foreland basin during the deposition of the Trenton and Utica is extensively faulted (Smith and Leone 2013). These faults are thought to be caused by submarine movement creating scarps, or synthetic in nature and resultant of flexural and eustatic changes during the Taconic orogeny (Brett and Baird 2002). The reverse fault identified on our section disrupts the continuity of the mid-Utica reflector, and is "pulled up" between CDPs 2220 and 2250 into an anticlinal shape. We note the same effect in the next four reflectors towards the surface. This could be attributed to deposition during faulting or post-faulting that caused later sedimentation to occur on a convex surface, until the deposition of the thick Queenston Shale flattened out the shape of the bed and marked a return to the layer cake stratigraphy often characteristic of Paleozoic Ohio strata. Below the reverse fault, we note that the Trenton Limestone reflector is continuous and uninterrupted by faulting. This is indicative of a decollement at the location of the unconformity above the Trenton. It is possible that further faulting is invisible due to sideswipe, leading to the flattening and distortion of other faults that would otherwise be visualized on a 3D seismic section.

R.3 Well Log Analysis

The nine wells evaluated for this study showed varying amounts of similarity in synthetic reflections to the actual reflections in the seismic sections. Convolutional modeling most

matched the seismic in wells closest to seismic lines. The most prominent feature seen within the Utica is the LDZ. It varies in character between well logs. For instance, in well 34169250100000, the LDZ shows within it a decreased velocity spike at about 5080 feet. In the nearby well 34151251020000, no such sharp decrease exists. The LDZ could only be observed close to the seismic line, supporting the hypothesis that a region of closely interspersed kerogen inclusions and accompanying microcracks (Vernik 1991) could be leading the anomalous signal, its extent would not likely be widespread. Indeed, AVO analysis only shows class IV anomalies over a limited number of CDPs.

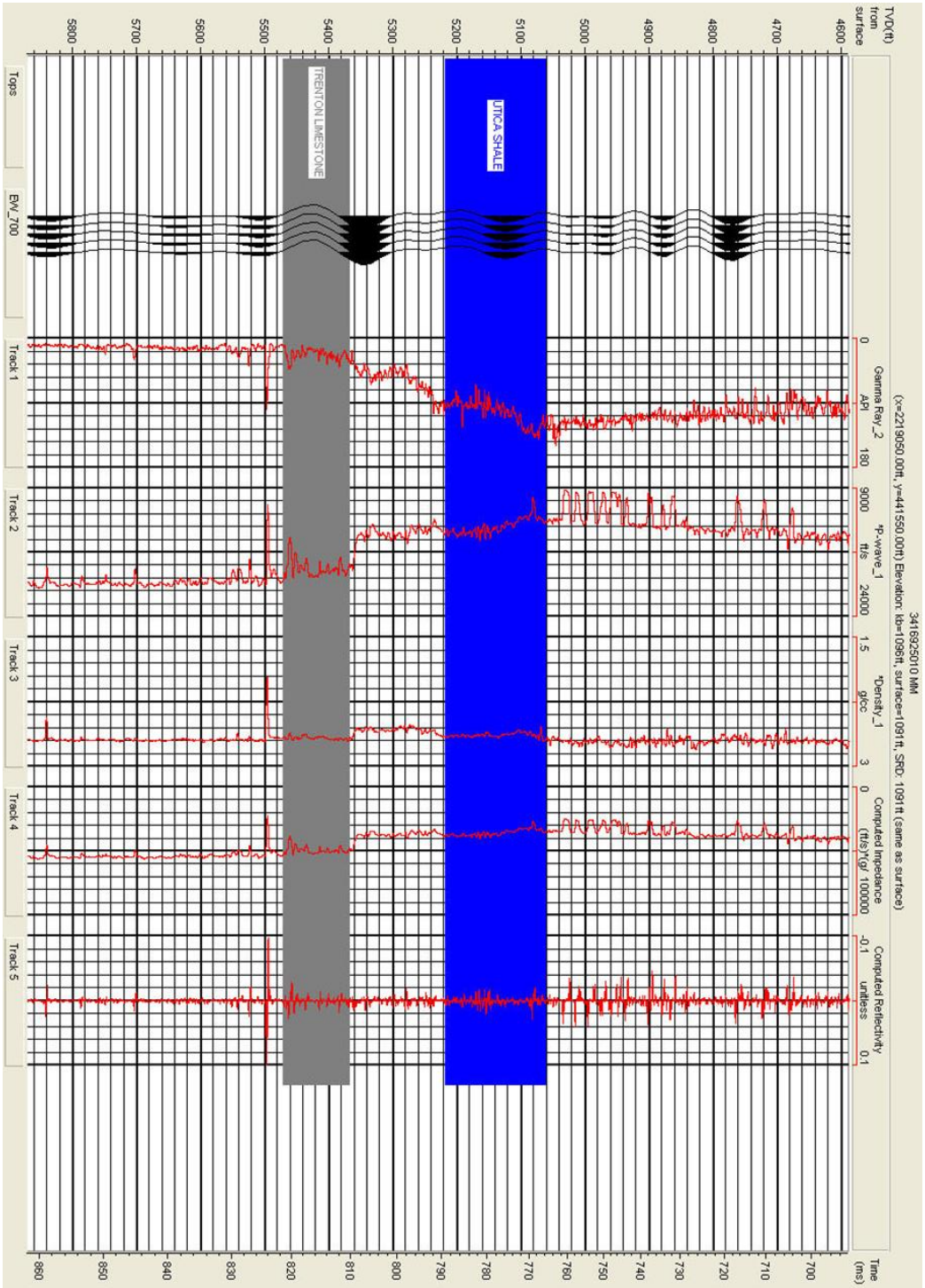

Figure 7: Logged Parameters and Synthetic Seismogram of the Closest Well to the Seismic Lines

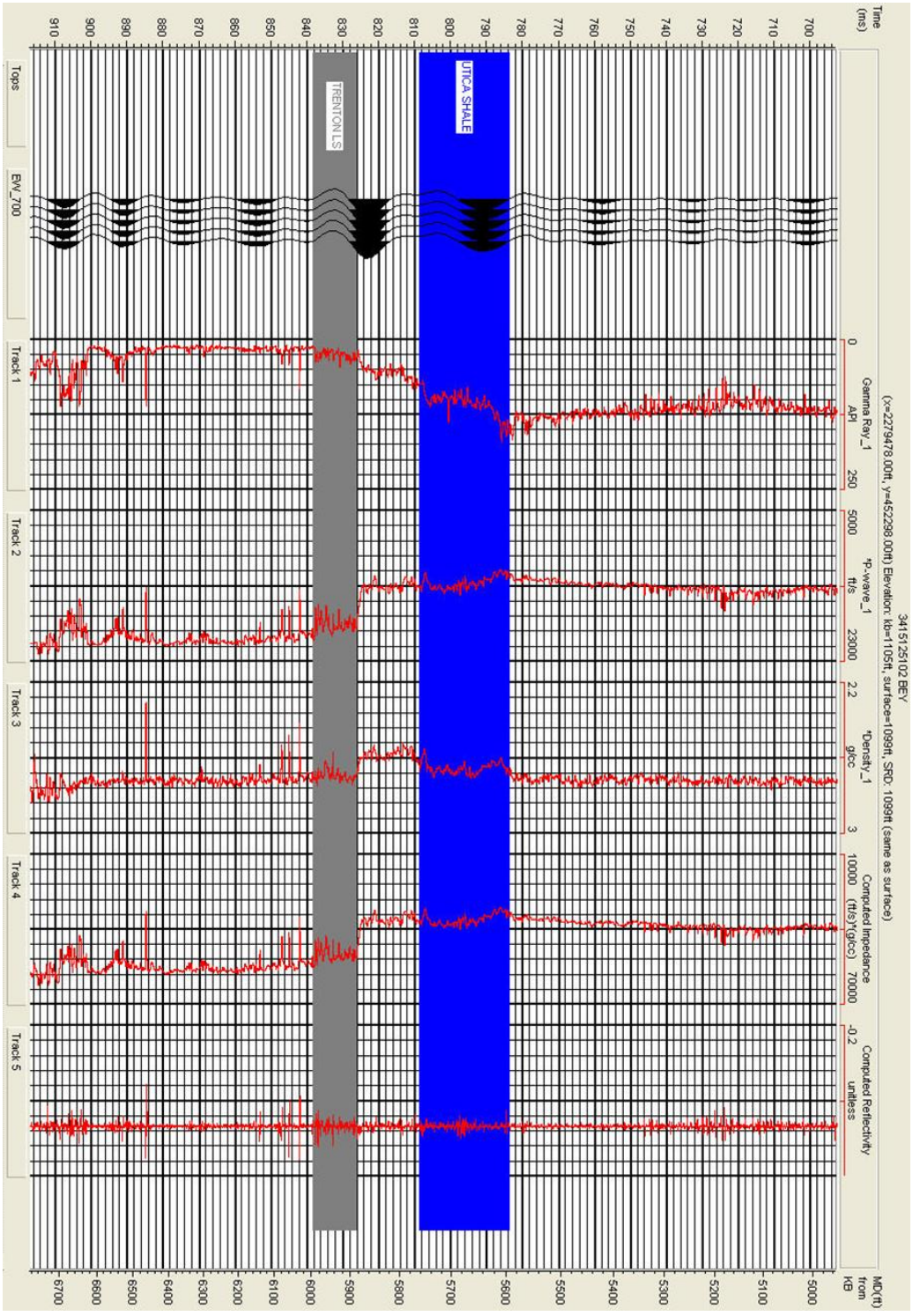

Figure 8: Logged Parameters and Synthetic Seismogram of the Second-Closest Well to the Seismic Lines

The succession beginning at the TOU becomes increasingly calcareous until the Curdsville is reached. These lithologic changes are seen most prominently in P-wave and

gamma ray logs, with the gamma ray signal decreasing gradually and the p-wave velocity increasing gradually. Depositionally, this would have corresponded to the drowning and corrosion of the Trenton limestone located on the peripheral bulge at the side of the basin, and subsequent deposition of the shaly succession that culminated with the Utica Shale and Cincinnati group. The gross lithologies of the Utica Shale and Trenton are identified on the two well logs closest to the seismic line as well as the wells that contained TOC data. Identification of the formations and members in between the Utica and Trenton are seen in the well log fence diagrams of **R.6**. The remainder of the wells are found in the appendix section.

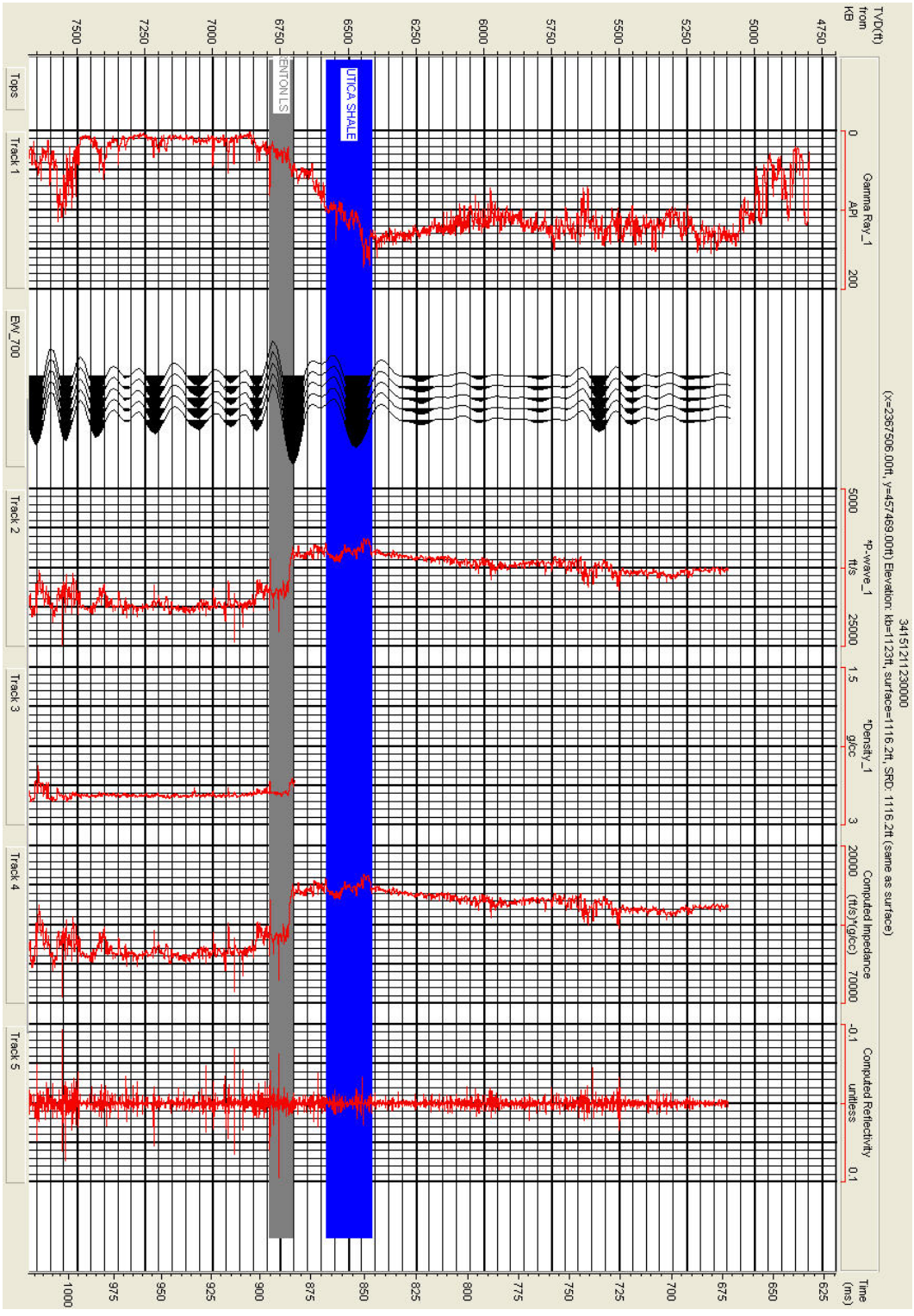

Figure 9: Eastern Well Log with Convolutional Modeling and Core-Derived TOC Data

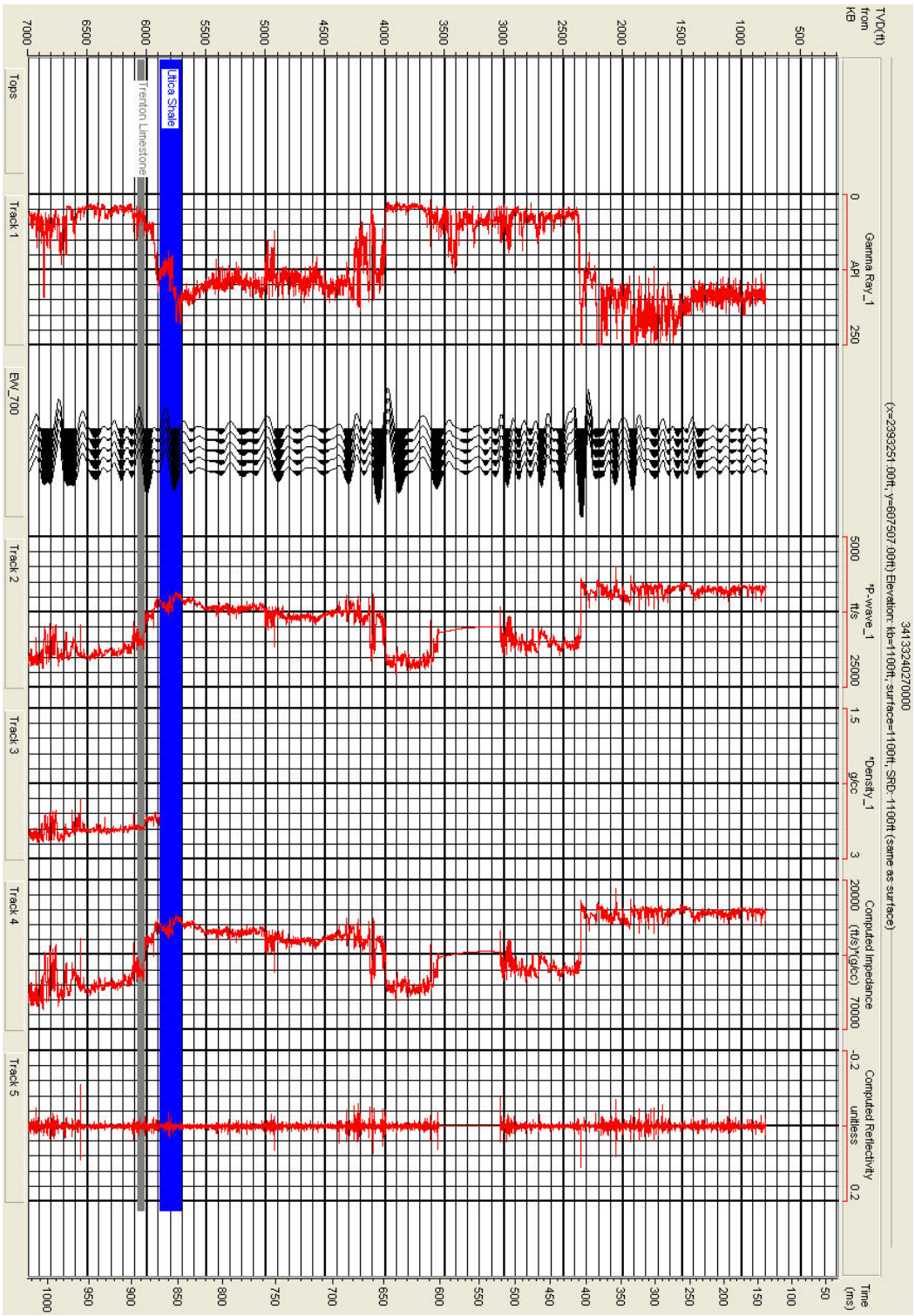

Figure 10: Northeastern Well Log with Convolutional Modeling and Core-Derived TOC Data

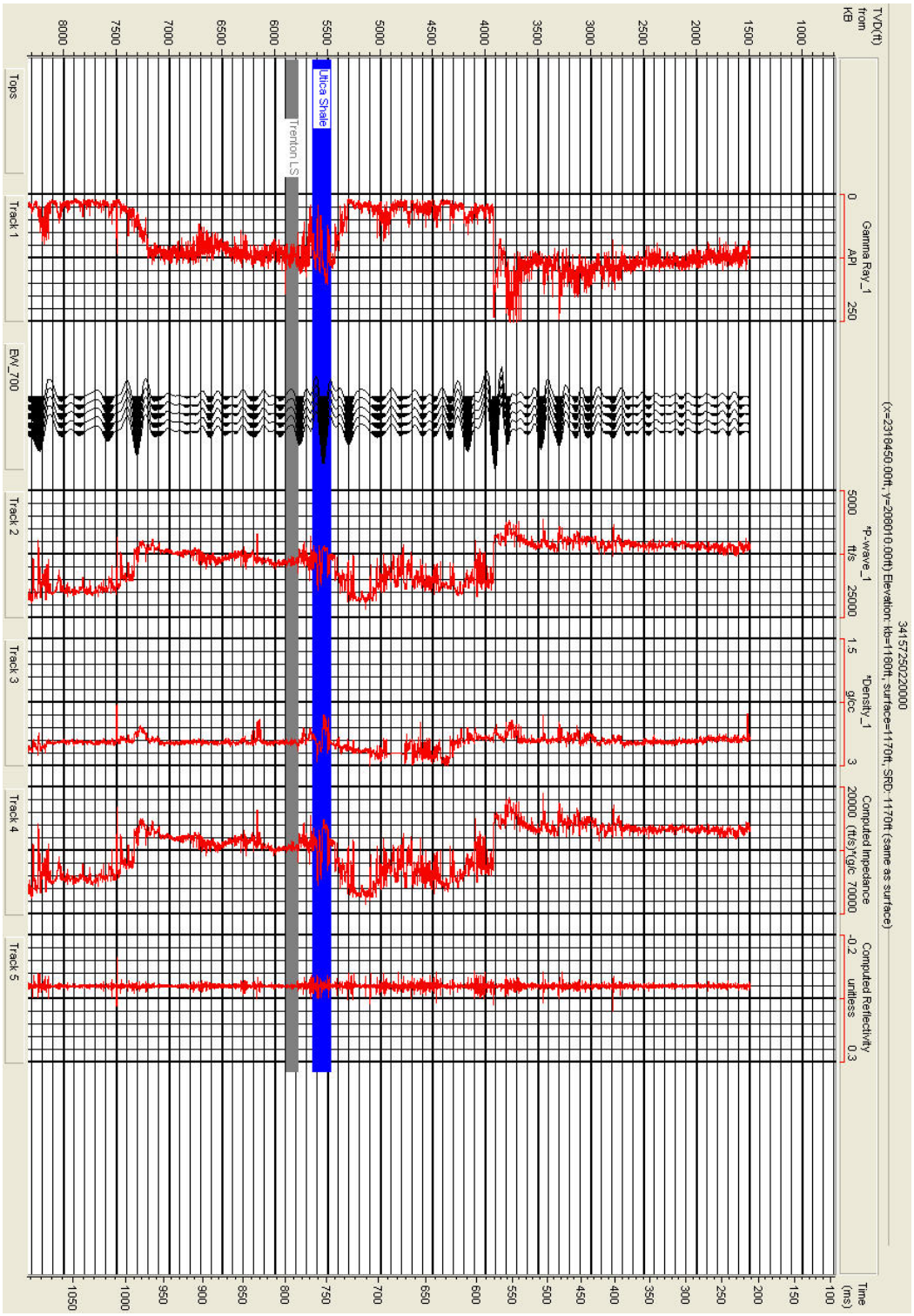

Figure 11: Southeastern Well Log with Convolutional Modeling and Core-Derived TOC Data

R.4 Well Log Pyrolysis Data Analysis

According to TOC measurements taken from cores, the Utica, Point Pleasant, Trenton/Lexington and Logana are source rocks with TOC between 2-3.5%. If we assume that they are all clay-rich strata, their increasing calcite content can been correlated with increased TOC (Zhu et al 2011). Within the Appalachian basin, highest TOC is seen towards the cratonward margin, where transgressive shales onlap shallow marine carbonates (Smith and Leone 2013), with highest TOC values located nearest to unconformities. There are not enough wells in the study area with TOC in order to be able to spatially map thickness versus TOC and thus infer proximity to a basin margin. However, the correlation between TOC and unconformities appear to hold true in the Ohio Utica-Trenton succession, with the Utica displaying TOC values between 1-2%, while the underlying Point Pleasant, Logana and Trenton/ Lexington that are located closer to the major unconformity above the Trenton displaying TOC of 2-3.5%.

When crossplotted with velocity, the well logs for which there is TOC data available show dips in Vp that are associated with high TOC at different depths. The characteristic shape of the curve at high TOC was applied to wells close to the Cardinal line to look for patterns. We note that decreases in velocity in the area are correlated with high TOC in places, and that high TOC may be responsible for some of the dips in velocity and density for the closest wells to the seismic line that were used in the convolutional modeling.

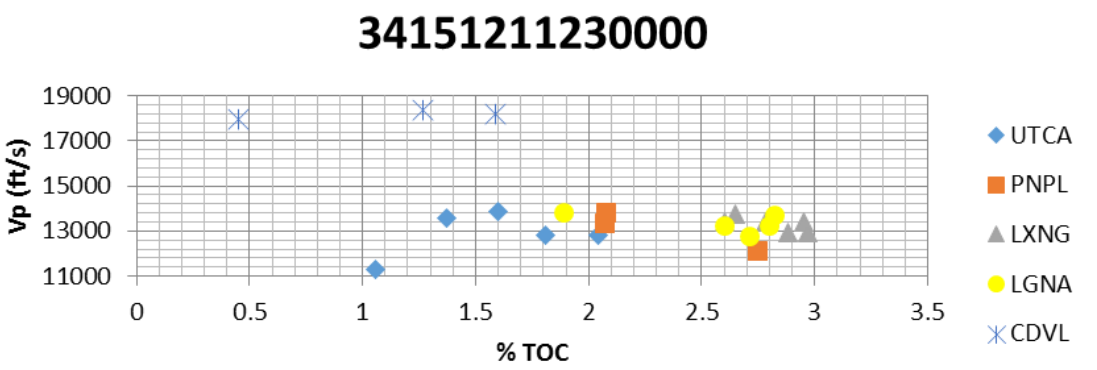

Figure 12: Velocity vs Total Organic Content for Six Intervals, First Well

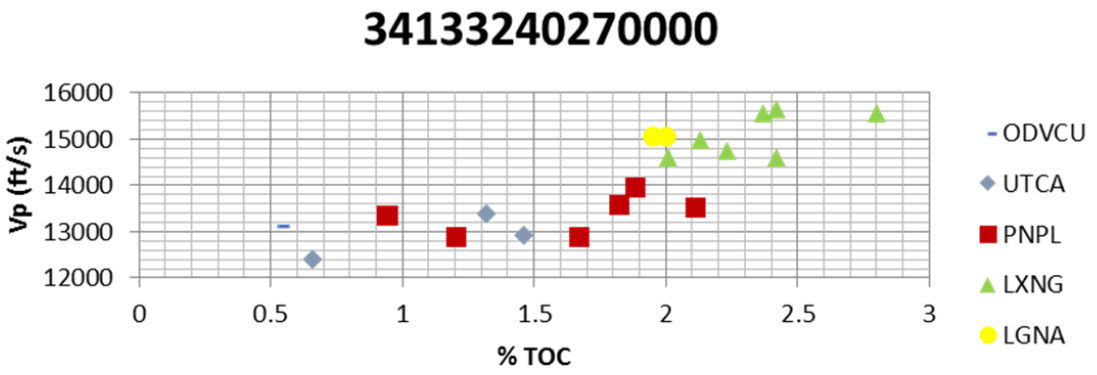

Figure 13: Velocity vs Total Organic Content for 5 Intervals, Second Well

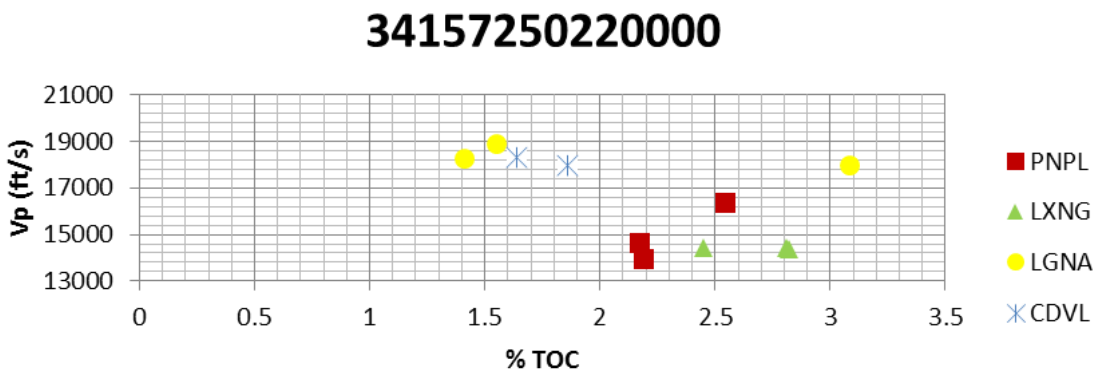

Figure 14: Velocity vs Total Organic Content for 4 Intervals, Third Well

The other main control on Vp besides TOC and lithology is induration due to depth, and indeed the regions where Vp kept increasing at greater TOC values were at greater depths. Within the Utica, there were not enough TOC measurements over the three wells to definitively link decreased velocity with increased TOC. We do however we do note a set of points in well 34151211230000 that showed Vp decreasing with increased TOC. The low Vp in the one data point that has less TOC than the other samples could be attributed to a very ductile and "soft" shale sample with anomalously high clay content. This would lead to a marked decrease in AI similar to that which would occur at a very high %TOC. Despite the lack of TOC data strictly within the Utica as opposed to one of the underlying shaly carbonates, Vp vs TOC crossplotting illustrates how variable TOC is throughout the Utica Shale and indicates that the effects of TOC on velocity may exceed the effects of depth in certain places.

R.5 Wolf Ramp Model Interpretation

The wavelet calculated through transition zone-based modeling showed similarities to the complex wavelet seen in the reflector in the middle of the Utica. The same intermittent reflection splitting that causes a double peak is present, and amplitudes in these regions are decreased compared to those of reflections from the non-gradational interfaces above and below the transition zone. The diminished amplitudes can be seen in the two figures below, and concur with the findings of Justice and Zuba (1985) that the amplitude of a transition zone reflector will change by equal to or greater than ½ ln (v1/Vo) if V1 <V0, as we see in the upper

transition zone of the model where we have set V0= 12000 ft/s, and V1=11000 ft/s.

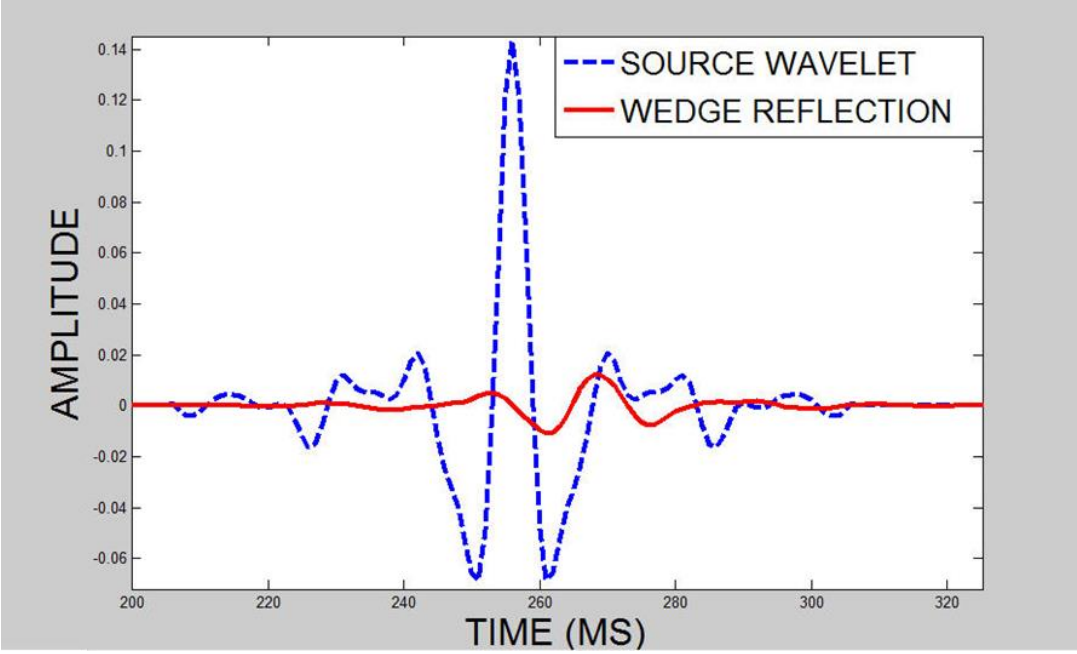

Figure 15: Modeled Velocity Transition Zone Reflections

Reflections from transition zones display marked intrinsic frequency dependence that results in their mathematical description as complex functions (Liner and Bodmann, 2010). We certainly observe frequency effects in the intra-Utica reflector, and use the FFT to visualize them. The FFT allows us to examine the wedge model reflections in the frequency domain and view exactly what band of frequencies are attenuated. This attenuation is best seen in the filter coefficients that are extracted from the model. The frequencies that are diminished most are those centered around 60 and 120 Hz, with partial attenuation of the 70-120 Hz band. Multiplication of the source wavelet with the filter coefficients produces a diminishing of the signal that is apparent in terms of wavelet broadening, peak splitting and decreased amplitude in the time domain due to frequency loss of the transition zone reflection. Since phase angle is a scaled up version of frequency, frequency loss also results in a phase shift, as can be seen in the source wavelet vs the wedge reflection. In practice, these effects, in conjunction with a possible

change in short-term deposition such as a carbonate turbidite layer resembling the Dolgevile, are impossible to disentangle without well control. Either a reflectivity gradient, a change in deposition, or reflectivity gradient caused by a change in deposition could produce the complexity observed in the mid-Utica reflector.

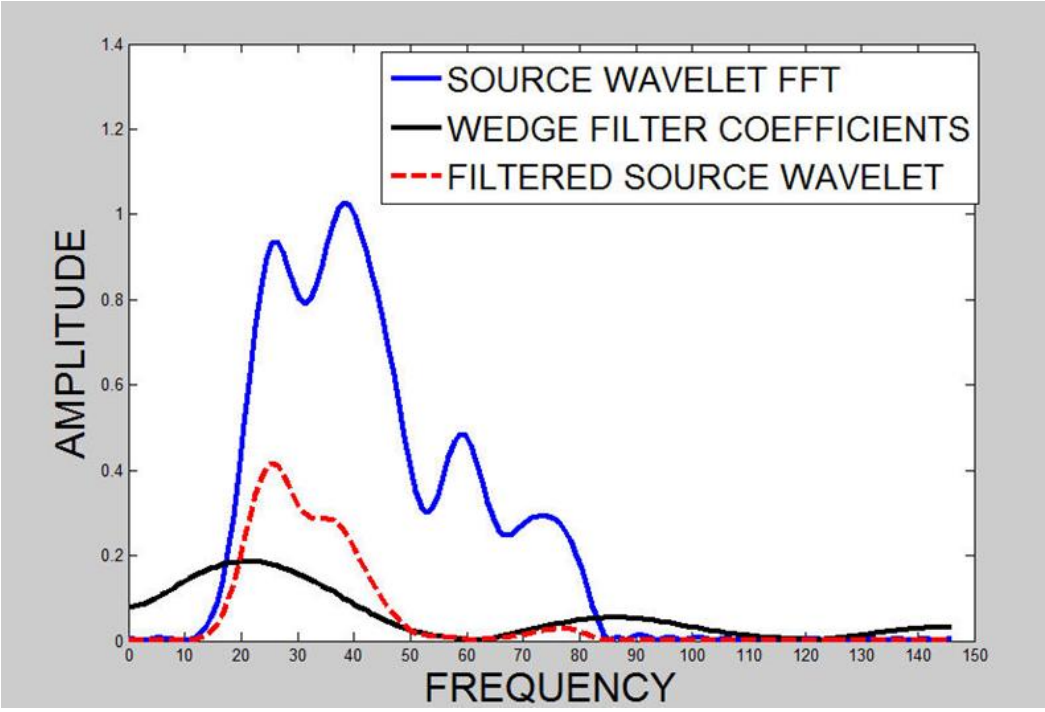

Figure 16: Frequency-Dependent Effects of the Velocity Transition Zone

R.6 Well Log Correlation and Regional Stratigraphy

A NE-SW section spanning nine well logs over an A-A' distance of about 80 miles was used to correlate the top of Utica down to the top of the Curdsville throughout the study area.

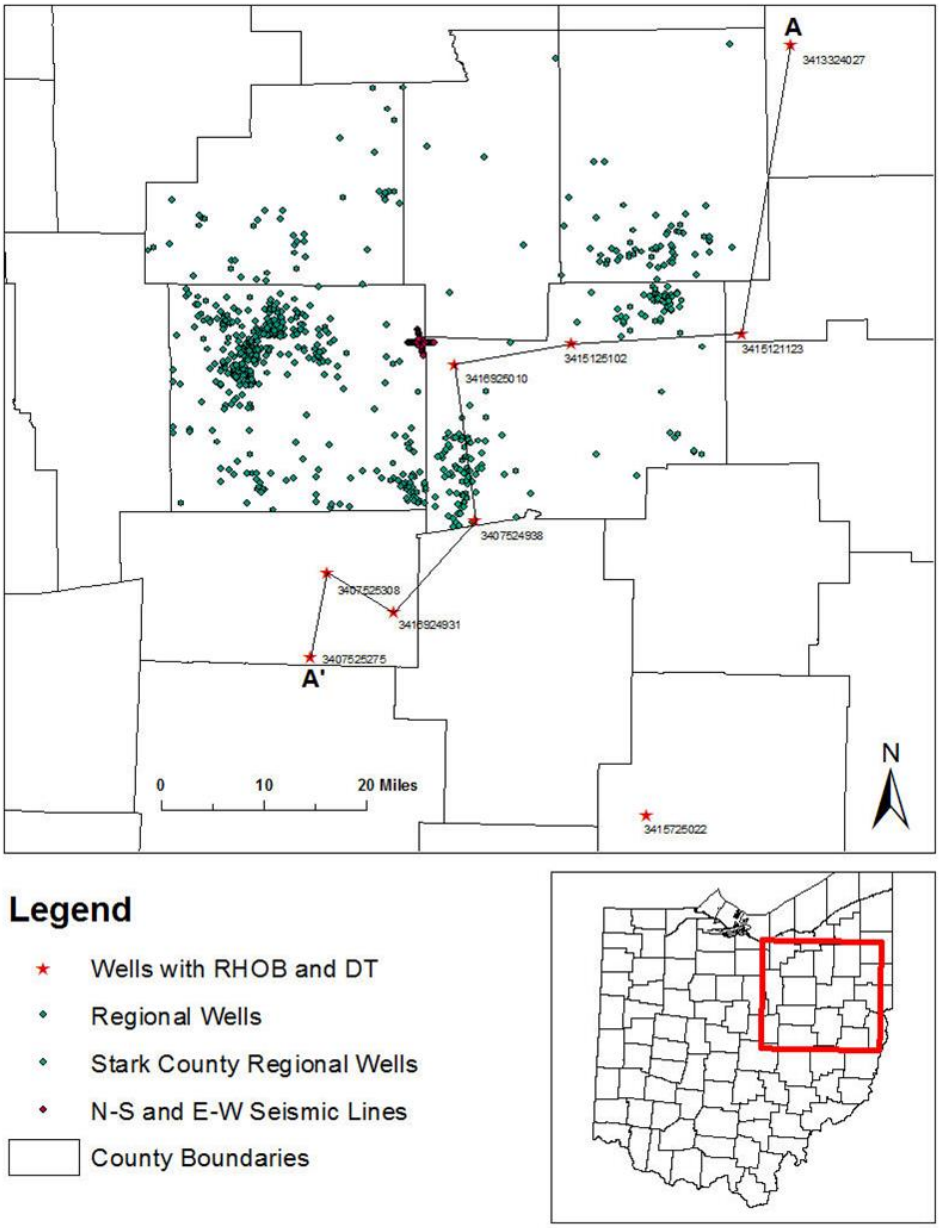

Figure 17: NE-SW Well Log Correlation in the Study Area Used to Create a Petrel Cross Section

A

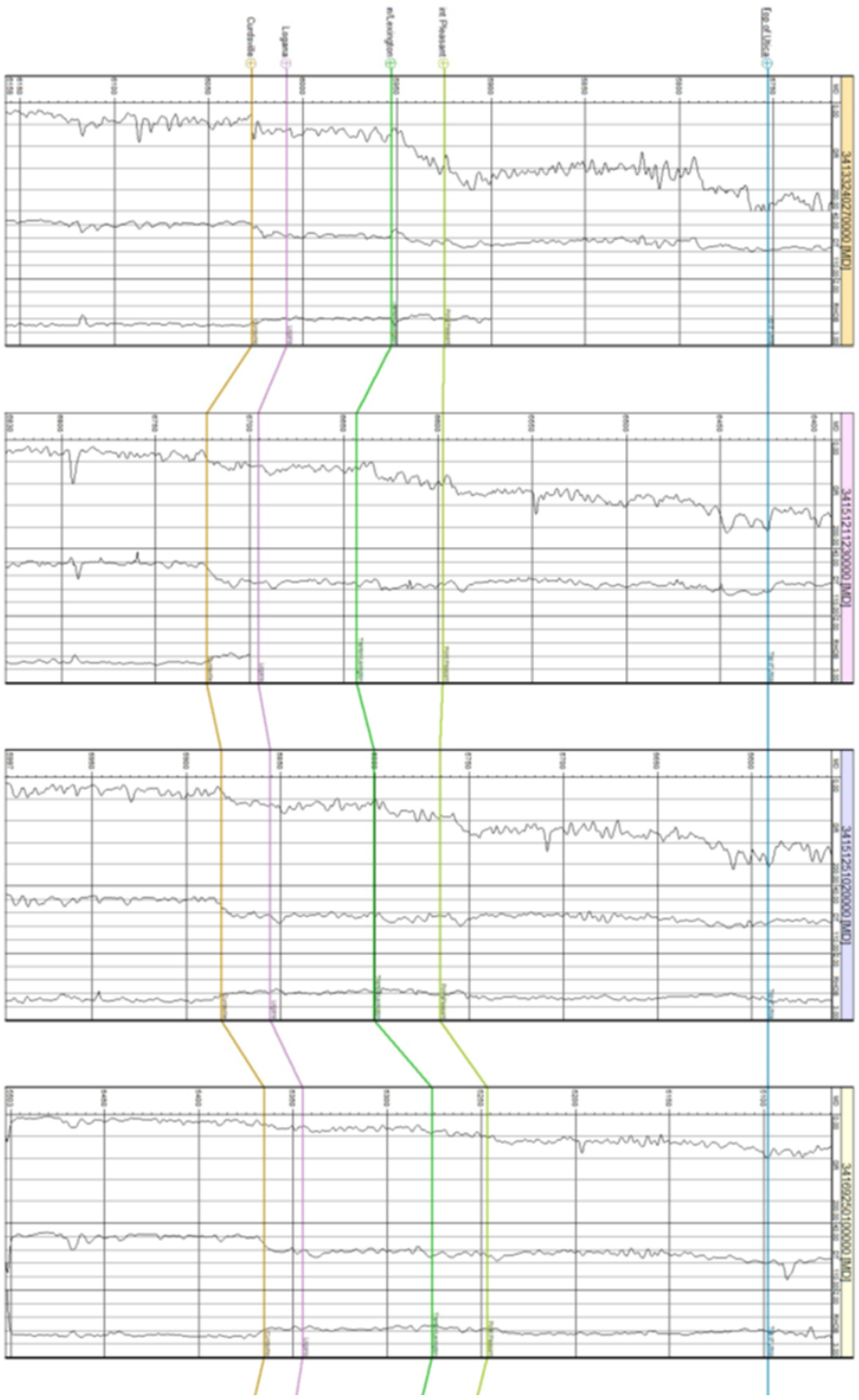

Figure 18: Well Log Correlation of the Utica-Trenton Succession in NE Ohio

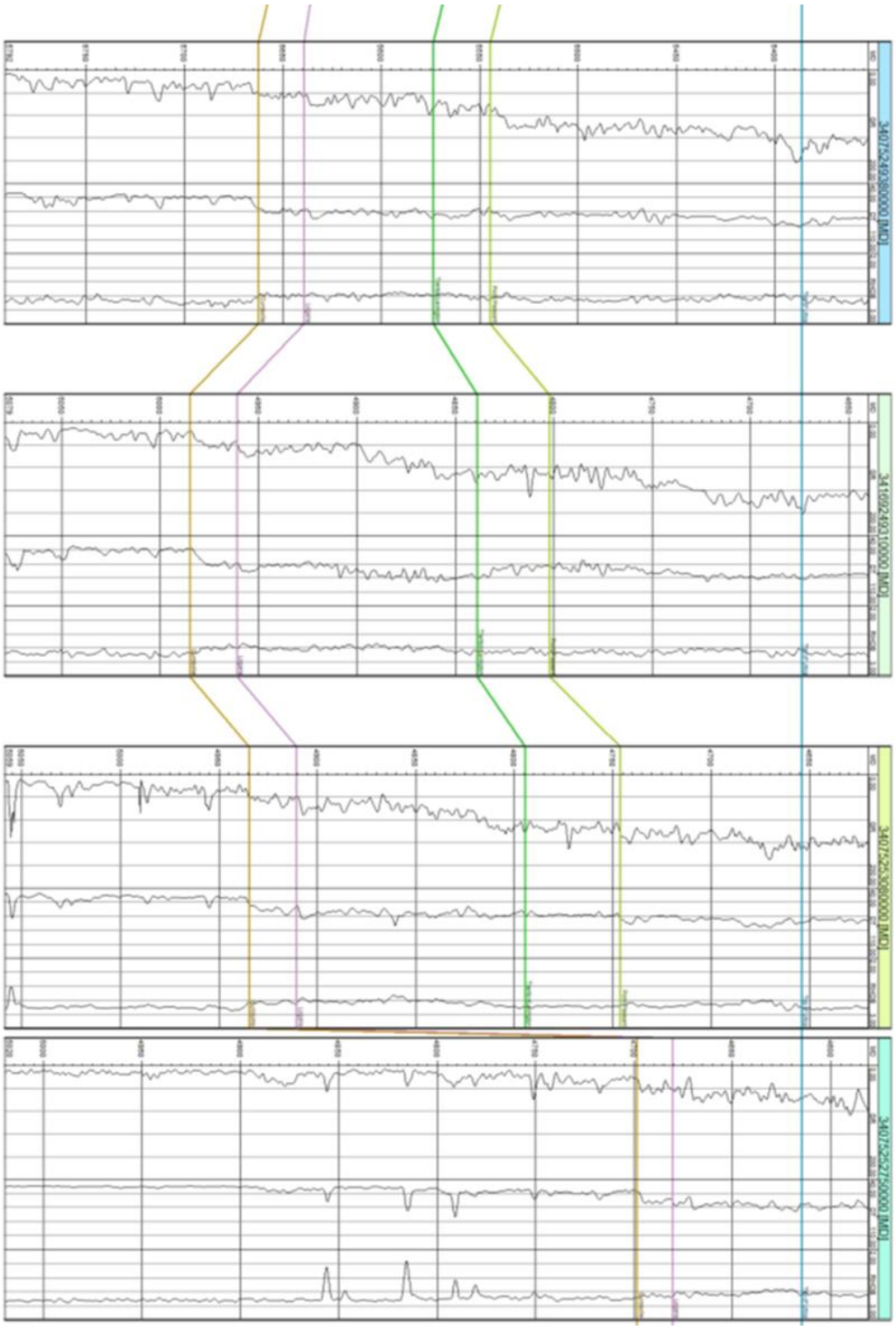

A

The cross section was successful in answering a number of questions that were posed at the beginning of this study. The well section allowed us estimate the regional dip of the Utica. In addition, it allowed us to track the depth and thickness of the Utica itself as well as the underlying Point Pleasant Shale and upper Trenton Limestone members, which are themselves viable downhole targets for oil and gas exploration. Lastly, the stratigraphic correlation enabled us to make direct though speculative connections between the Ohio Utica and the analog New York Utica, allowing us infer that the depositional changes and depositional interruptions active in New York during the middle Ordovician were also active in Ohio. For instance, the circumstances that led to the formation of the Thruway and Knox unconformities that are seen in New York may also apply in Ohio, though they would have transpired during a later and more cratonward stage of the Taconic Orogeny. Since we possess DT and RHOB logs for all of the logs used in the section, we were able to correlate carbonate-rich beds that do not show a strong diagnostic gamma ray signature.

The Utica in the study area is observed to shallow to the west-northwest. It is relatively thick in the vicinity of our seismic line, indicating that this portion of the Utica may be a graben, as described by Baird and Brett (2002). Well number 341511230000 marks the deepest position of the Utica within the cross section and in conjunction with the much shallower well number 341511230000 provides evidence that the depositional plane is upwardly tilted W-NW. The underlying Point Pleasant Shale is much thinner than the Utica and does not display any evidence of horst or graben stratigraphy, despite being part of the same shaly succession as the Utica. In well logs, the Point Pleasant shows decreasing gamma ray counts corresponding with increased calcite content, putting it in the compositional range of a calcareous or argillaceous shale. Below the Point Pleasant, the Trenton/ Lexington and Logana continue to decrease in percent clay, as seen through the gamma ray reading of half or less than half of the counts seen

at the top of the Utica, a stratigraphic gamma ray high that was used as a datum for correlating the well logs. On the textural spectrum ranging from mudstone to limestone at either end, this puts them in the region of a marl. While decreasing in gamma ray, they remain relatively constant in DT and RHOB, indicating that the expected increase in p-wave velocity and density and accompanying increase in carbonate character may be attenuated by relatively high TOC values. The Curdsville itself is where the density and Vp rapidly increase, and has the lowest gamma ray signature of all beds correlated, putting it in the region of an argillaceous limestone. Below the Curdsville reflector, we see a large, narrow gamma ray peak on some well logs that is attributed to K-bentonites and is diagnostic of the base of the Utica-Trenton succession. On the well cross section, it is worth noting just how thin the Point Pleasant and Logana are, and leaves no surprise that they aggregate into the single peak seen on the seismogram.

In terms of similarities to western and west-central New York stratigraphy, we note that the Upper Utica appears to correlate with the Indian Castle Shale, and the Lower Utica correlates with the Flat Creek Formation. The Indian Castle and Flat Creek have been variously defined by different authors as either separate formations or a members of the Utica (Baird and Brett 2002). The turbidically-deposited Dolgeville that separates the Indian Castle and the Flat Creek is confined to the western and west-central Mohawk Valley, a rather narrow region. By analog, if the intra-Utica peak seen in our seismic data is being caused by similar calcisiltic turbidites, it is quite possible that we would not see it in well logs located five or more miles away. Correlation of Ohio's Trenton/Lexington, Logana, and Curdsville to the New York Trenton members known in order of increasing depth as the Rust, Russia and Poland cannot be done definitively within the scope of this study as this would require the correlation of wells over several state lines. However, some similarities do exist. In New York, the submembers of the Rust and Russia members are described as consisting of parasequences of wackestone,

packstone, and grainstone (Brett and Baird 2002). The presence of clay in this succession would definitely lead to a marked gamma ray signature. Indeed, in Ohio, the Trenton/Lexington, Logana and Curdsville show a gamma ray log response that is illustrative of some clay content, and could in turn indicate a similar shallowing-upward cycle of submembers as that which is seen in the western and west-central New York stratigraphy. As far as unconformities, the corrosional Thruway Unconformity is clearly confined to the Mohawk Valley. However, the disconformity that stratigraphically separates the Trenton and Utica clearly exists in Ohio as well as New York. As previously stated in **I.3**, Baird and Brett (2002) themselves ask where this post-Trenton unconformity might occur in the Cincinnati Arch region and elsewhere towards the midcontinent. In our seismic data, we note this same unconformity. Even though different cycles of basin expansion were probably active since its formation at a later time and at a different portion of the basin, similar large-scale processes may have been active. Specifically, the flexural depression from the orogeny that led to deepening and cessation of carbonate input into the foreland basin and subsequent anoxic conditions, corrosion and drowning of the unconformity followed by the deposit of marine Utica Shale may also be a valid explanation for the unconformity between the Trenton and Utica that is seen in Ohio.

R.7 AVO

AVO gradient and crossplot analyses were variously performed between 700-800 ms TWT, a time interval encompassing the Utica. The AVO response up to 30 degrees incidence angle was taken at the TOU interface and BOU interfaces. The quality of anomalies was quite variable, especially at higher angles, and some of the stronger anomalies between around 0-15 degrees became difficult to interpret over 15 degrees due to overlapping interference from other reflections that resembled what would be seen in a non-NMO corrected common receiver

gather. This may be due to the fact that the angle gather used for AVO gradient analysis appears to only directly "hard" measure offsets up to 15 degrees, and rely on the Shuey approximation to determine reflection coefficients beyond. This would be appropriate for conventional AVO type curve analysis, which involves calculating the reflection coefficient of a shale-on-isotropic sandstone reservoir interface, with anisotropy occurring only in the top layer. Creating an angle gather for the purpose of measuring AVO in a shale-on-shale interface, however, may entail special processing with respect to anisotropy in order to prevent bleed through from other nearby reflections at large incidence angles. Even perfectly processed, the many powerful anisotropy effects seen in shales can make it difficult to observe and interpret "clean" anomalies. Difficulty interpreting AVO anomalies in regions of complex geology with many competing lithologic factors was noted by Isaacson and Neff (1999) when looking at shale-on-sandstone reservoirs. They observed that lithologies other than sand and shale make the establishment and calibration of a background trend difficult. In our seismic data, we observe calcisiltic rocks and limestones, which would prove to be equally difficult and require well log AVO modeling and careful calibration of crossplots. In a scaled Poisson's ratio vs normal incidence reflectivity crossplot taken over the TWT of the entire Utica, however, we do note what appears to be a rough shale background trend.

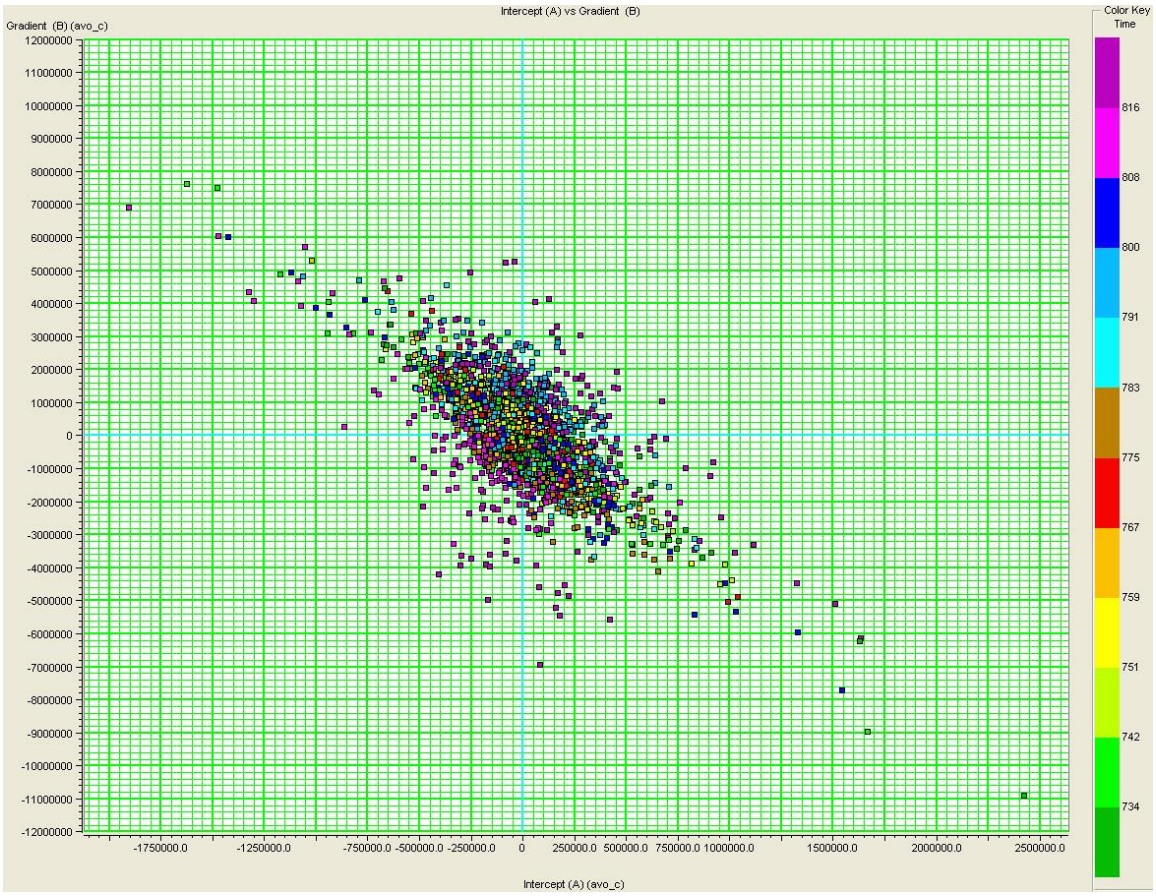

Figure 19: Poisson Reflectivity vs Normal Incidence Reflectivity Crossplot 700-800 ms

However, the changes in Poisson's ratio that cause deviations into different regions of the crossplot are most easily applied to changes in in fluid fill in sands. For instance, saturation by natural gas will shift Poisson's ratio for sands to about 0.1, down from the brine saturated value of 0.4. This is a consequence of the incompressibility of water leading to little resistance to change in volume in cases of brine saturation, versus the increased compressibility that results from gas saturation. In shales, anisotropy appears to be a far greater control upon Poisson's ratio than fluid fill, with theoretical values ranging from 0 to 0.5 for stress applied parallel to bedding and strain measured along the same plane, to between 0.25-0.38 for stress applied perpendicular to bedding and strain measured parallel to bedding (Sayers 2012). These

modeled values are representative of different levels of clay platelet disorder as characterized by the coefficients W200 and W400. The inclusion of varying amounts of carbonate grains such as what is seen in the Utica-Trenton succession would serve disrupt platelet orientation and lead to unpredictable Poisson's ratios that would affect the G value that represents the scaled Poisson's ratio change in a way that would require very careful calibration to unravel.

Gradient analysis is slightly more straightforward than crossplot analysis in that we do not need to directly calibrate to variations in Poisson's ratio. Some other anisotropic effects that could lead to difficulty in defining the type of AVO anomaly include variations in the elastic moduli at different angles of applied stress that lead to different values of Thompson's anisotropy parameters, and variations in brittleness, characterized by high Young's modulus and low Poisson's ratio, versus ductility, characterized by the opposite. In selecting the regions to perform AVO, the E-W CDP gather was used. Since a CDP gather approximates zero-offset, anisotropic effects cannot exert their influence to the degree that is seen in the AVA gather. Thus, the brightening and dimming of amplitudes at the Cincinnati Group-Utica Shale interface is limited to variations in TOC content and brittleness/ductility. Despite the obvious complexity in performing AVO in shales, we were able to observe 17 class IV anomalies over the 40 CDPs that comprised the "bright" region of the TOU reflector, compared with five class IV out of the 15 CDPs in the "dim" region. The TOC in source rocks necessary to precipitate a class IV has been estimated at 3-4% (Chopra 2012), indicating that portion of the reflector between CDPs 4250-4290 may be kerogen-rich compared to other segments. A sample Class IV anomaly is seen in **Figure 20** and the remainder are located in the appendix. We also note the presence of other types of anomalies, indicating rapidly varying lithology and/or spatial distribution of organic matter above and below the Utica and highlighting some regions as more viable targets for exploration than others. One example of a promising class IV anomaly occurring at the TOU

interface at CDP 4256 is presented below. The Class IV event occurs at 746 ms TWT, and shows a strong R^2 value of 0.79.

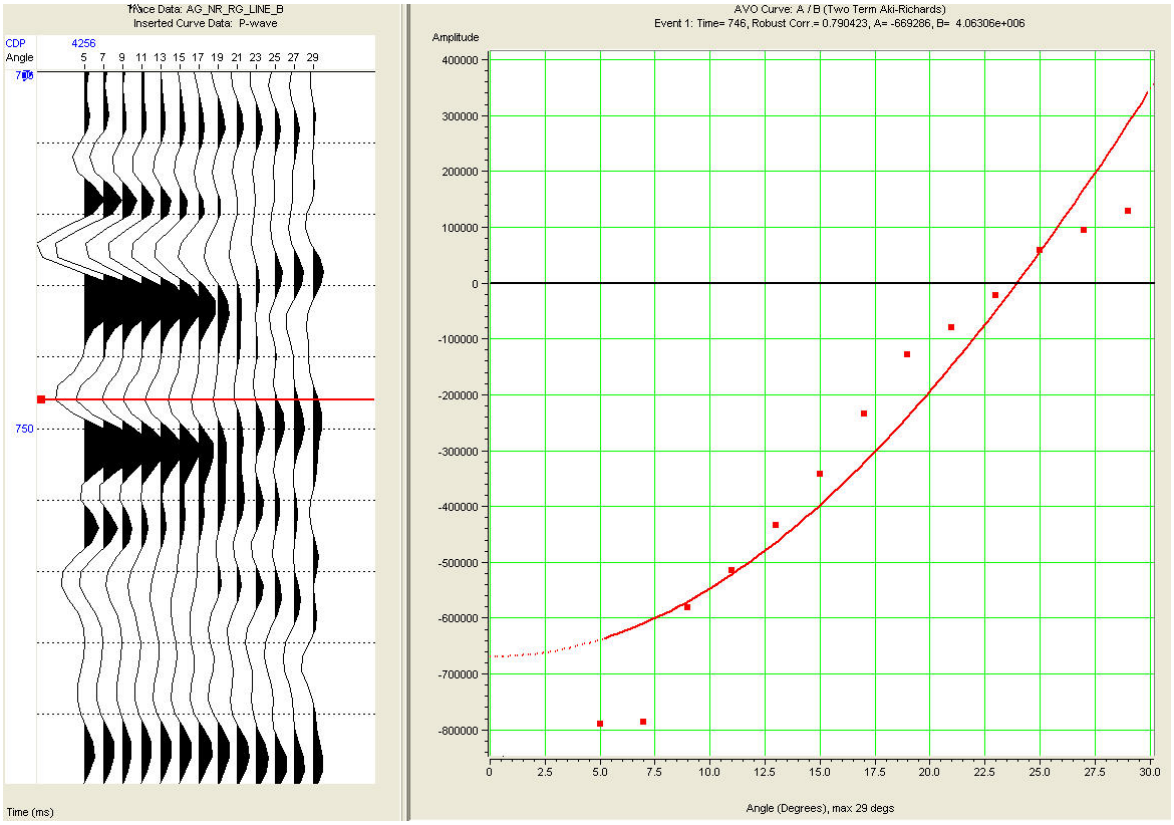

Figure 20: Sample Class IV AVO Anomaly Observed at the Top of the Utica Interface

The anomaly is rather clean, and we note that bleed-through from other reflections only occurs at the highest incidence angles of beyond 22.5 degrees. This appears to lead to a polarity reversal far earlier in terms of incidence angle than where oscillation in the reflection coefficient is noted to begin to occur by Carcione (1998). An idealized class IV anomaly in nonsource on source shale as described by Loseth et al. (2011) exhibits a strong negative amplitude that dims towards 30 degrees incidence, but does not change polarity.

AVO gradient analysis conducted at the BOU interface showed much variation in anomaly type. The anomalies were mostly type I, however several of type II, III and even IV were noted. This was to be expected, since the BOU interface on the seismic data is the combined

signal from multiple thin beds, all with varying amounts of TOC. The presence of class I anomalies is consistent with a move from source to nonsource shale. The observation of this response at the BOU indicates that there are likely regions of appreciable TOC distributed throughout the vertical extent of the Utica and that there are regions of the Point Pleasant, Trenton/Lexington, and Logana that show little TOC. One example of a Class I anomaly found at the BOU interface is shown below. This anomaly occurs at CDP 4136 and shows the expected polarity reversal at higher angles of incidence for a class I (Castagna 1997).

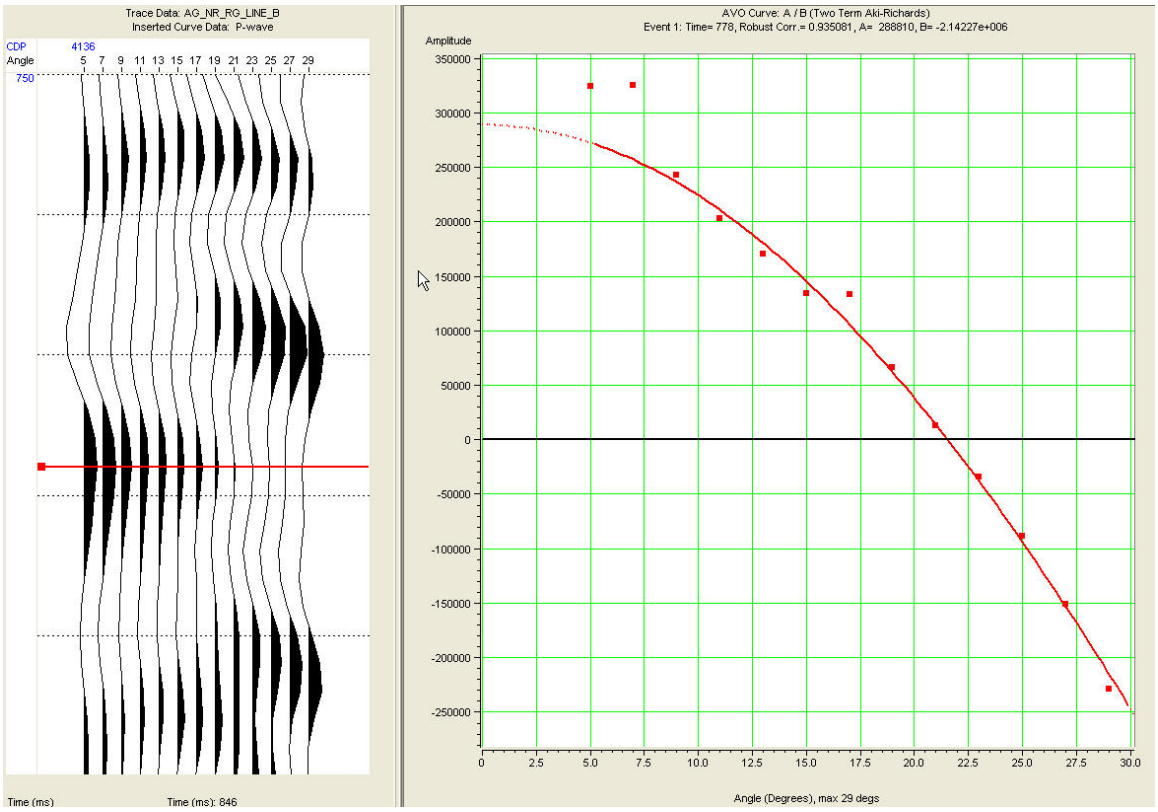

Figure 21: Sample Class I AVO Anomaly Observed at the Bottom of the Utica Interface

The R^2 value at this anomaly is high at 0.93. The time slice was taken at 778 ms, a TWT encompassed by the aggregate negative reflection event that contains the BOU interface. All told, there were 14 class I anomalies found at the BOU interface. Class II, III and IV anomalies within the BOU time window indicate the presence of appreciable amounts of TOC below the

Utica, but to keep within the scope of this study I focused on TOC/kerogen related AVO effects only within the Utica.

The ideal place to perform source on nonsource AVO would have been the peak between the Utica and underlying higher impedance Point Pleasant to see which regions exhibited a class IV AVO response and thus determine where high TOC/kerogen is found in the upper Point Pleasant and, in a second order fashion, what portions of the bottom of the Utica contain low TOC. Unfortunately, since the Point Pleasant is below the tuning thickness, its location must be approximated by performing AVO on a time interval encompassing the full trough itself in hopes of detecting anomalies from this interval. Another possibility would be to look at the underlying shale on Trenton Limestone interface, though doing this would elucidate little due to the fact that we would still see Class I and other anomalies that do not indicate a source shale. All told, the TOU interface was a better and more illustrative target for AVO than the BOU interface due to the uncertainties and complications arising from bed boundaries below the tuning thickness.

V. CONCLUSIONS

Each component of this study was successful in answering the questions posed at the beginning of the thesis. The seismic interpretation, total organic carbon analysis, and velocity gradient modeling led to a broader understanding of the package of reflectors associated with the Utica Shale in the study area. In particular, the variations in frequency, wavelet character and phase are likely due to velocity gradient effects, localized stratigraphic changes within the Utica similar to the Dolgeville carbonate turbidite interval The well log correlation served to explore the connection between Ohio stratigraphy in the Utica Shale-Trenton Limestone succession and the broader Appalachian basin stratigraphy, particularly in the Mohawk Valley region of New York. Well log analysis and AVO gradient analysis led to the conclusion that the low density zone seen in well logs up to 20 miles away from the seismic lines are likely due to kerogen inclusions and the source shale character of the upper Utica. The amplitude effects in the same region that are visible in the migrated CDP seismic sections appear to come from a lithologically-driven shift from more brittle Cincinnati Group shale to more ductile Utica Shale. Likely contributing to this effect is the presence of kerogen and other forms of hydrocarbon subject to liquefaction.

Structure was found within the Utica in the form of a reverse fault visible on the N-S seismic line. This fault may be due in part to the generation of hydrocarbons. The growth

anticlines above the fault are likely due to syndepositional faulting, and the accumulation of sediment atop the fault. Visible below the fault is an apparent detachment and sliding surface known as a decollement. The fault could have been better imaged with another seismic line, and it is possible that sideswipe effects are obscuring more faults in the nearby strata. A 3D seismic survey would be the best solution, and would negate all ambiguity as to the presence and position of faults. It must be noted again that only the Utica Shale and the Curdsville Limestone appear on the seismic section. Though the bed boundary between the Utica and Point Pleasant is visible in convolutional modeling, the Point Pleasant, Trenton/Lexington, and Logana are below the tuning thickness and thus are not identifiable on the seismic section.

Future work on the dataset or in the study area could benefit most from the availability of different types and more numerous well logs. A shear wave log would allow for the quantification of shale anisotropy, which is the most influential factor in shale AVO behavior. With shear wave data, anisotropy measurements such Vp/Vs and Thompson's parameters ε, γ and δ could be calculated. These allow for the comparison of shale plays anywhere in the world to one another, since certain values of the petrophysical parameters may be associated with increased or decreased fracability, level of TOC typically found at a particular value of anisotropy, and other considerations that ultimately may help decide whether or not to produce the interval.

Though we possess well control in the form of a well within 10 miles of the seismic line, direct lithological interpretation can only be achieved through having a well located on the seismic line and core data. However, the well we had was close enough that the approximations made are accurate assuming that there is no drastic change in lithology between the well and the line. A well on the line would also have allowed us to perform AVO modeling to determine the expected variation of the reflection coefficient at incidence angle and see how it compares

to the AVO effects seen on the angle gather that was created from the E-W seismic data. An angle gather of the N-S line would have had similar utility. AVO analysis could be have further refined through performing a gradient analysis on the interface between the calcareous shale of the Utica-Point Pleasant and the Curdsville Limestone. Carcione (2001) modeled a similar interface, and the results of the gradient analysis would lend themselves nicely for comparison and corroboration with his work.

Lastly, the geological observations made in this thesis assume that the Utica Shale is correlatable between Ohio and New York. In order to verify this and apply the depositional processes and designations of members and formations of the New York Utica to the Ohio Utica, well logs must be correlated between Ohio and the Mohawk Valley region of New York. The logs to do so could be obtained from the geological surveys of each state.

IV. REFERENCES

Avseth, P. (2005). AVO responses; the good, the bad and the evil. *Geo Expro, 2*(5-6; 5-6), 22.

Avseth, P., Draege, A., van Wijngaarden, A., Johansen, T. A., & Jorstad, A. (2008). Shale rock physics and implications for AVO analysis; a north sea demonstration. *Leading Edge [Tulsa, OK], 27*(6; 6), 788-797. doi:10.1190/1.2944164

Baird, G. C., & Brett, C. E. (2002). Indian castle shale; late synorogenic siliciclastic succession in an evolving middle to late ordovician foreland basin, eastern new york state. *Physics and Chemistry of the Earth, 27*(1-3; 1-3), 203-230. Retrieved from http://ezproxy.libraries.wright.edu:2048/login?url=http://search.ebscohost.com/login.aspx?direct=true&db=geh&AN=2003-015587&site=ehost-live; http://www.elsevier.com/wps/find/journaldescription.cws_home/413/descriptionscription

Bey, S. M. (2012). Reservoir Characterization and Seismic Expression of the Clinton Interval over Dominion's Gabor Gas Storage Field in North-East Ohio. A thesis submitted in partial fulfillment of the requirements for the degree of Master of Science. *Wright State University,* 1-100.

Brett, C. E., & Baird, G. C. (2002). Revised stratigraphy of the trenton group in its type area, central new york state; sedimentology and tectonics of a middle ordovician shelf-to-basin succession. *Physics and Chemistry of the Earth, 27*(1-3; 1-3), 231-263. Retrieved from http://ezproxy.libraries.wright.edu:2048/login?url=http://search.ebscohost.com/login.aspx?direct=true&db=geh&AN=2003-015588&site=ehost-live; http://www.elsevier.com/wps/find/journaldescription.cws_home/413/descriptionscription

Brevik, I., Ahmadi, G. R., Hatteland, T., & Rojas, M. A. (2007). Documentation and quantification of velocity anisotropy in shales using wireline log measurements. *Leading Edge [Tulsa, OK], 26*(3; 3), 272-277. doi:10.1190/1.2715048

Carcione, J. M. (2001). AVO effects of a hydrocarbon source-rock layer. *Geophysics, 66*(2; 2), 419-427. doi:10.1190/1.1444933

Carcione, J. M., Helle, H. B., & Zhao, T. (1998). Effects of attenuation and anisotropy on reflection amplitude versus offset. *Geophysics, 63*(5; 5), 1652-1658. doi:10.1190/1.1444461

Castagna, J. P., & Swan, H. W. (1997). Principles of AVO crossplotting. *Leading Edge [Tulsa, OK], 16*(4; 4), 337-342. doi:10.1190/1.1437626

Chopra, S., Ritesh, S. K., Keay, J., & Marfurt, K. J. (2012). Shale gas reservoir characterization workflows. *SEG Las Vegas 2012 Annual Meeting,* Las Vegas. 1-5.

Curtis, J. B. (2002). Fractured shale-gas systems. *AAPG Bulletin, 86*(11; 11), 1921-1938. doi:10.1306/61EEDDBE-173E-11D7-8645000102C1865D

Eaton, S. R. (2010). Utica emerges in quebec; shale play extends to canada. *AAPG Explorer, 31*(1; 1), 10.

Ettensohn, F. R. (1994). Tectonic control on formation and cyclicity of major appalachian unconformities and associated stratigraphic sequences. *Concepts in Sedimentology and Paleontology, 4*, 217-242. Retrieved from http://ezproxy.libraries.wright.edu:2048/login?url=http://search.ebscohost.com/login.aspx?direct=true&db=geh&AN=1995-065721&site=ehost-live

Fleet, A. J. [., & Boldy, S. A. R. [. (1999). *Petroleum geology of northwest europe; proceedings of the 5th conference*. United Kingdom: The Geological Society of London: London, United Kingdom.

Foster, D. J., Keys, R. G., & Lane, F. D. (2010). Interpretation of AVO anomalies. *Geophysics, 75*(5; 5), 75A3-75a13. doi:10.1190/1.3467825

Gomez, J. L., & Ravazzoli, C. L. (2012). Reflection characteristics of linear carbon dioxide transition layers. *Geophysics, 77*(3; 3), D75-d83. doi:10.1190/geo2011-0428.1

Hassan, Z., E., Rezaee, R., & Kemper, M. (2011). Quantitative analysis of seismic response to total organic content and thermal maturity in shale gas plays. *APPEA Journal, 51*

Isaacson, E. S., & Neff, D. B. (1999). A, B AVO cross plotting and its application in greenland and the barents sea. *Petroleum Geology of Northwest Europe: Proceedings of the ...Conference, 5*, 1289-1298.

Jingye, L., & Dvorkin, J. (2012). Effects of fluid changes on seismic reflections; predicting amplitudes at gas reservoir directly from amplitudes at wet reservoir. *Geophysics, 77*(4; 4), D129-d140. doi:10.1190/geo2011-0331.1

Justice, J. H., & Zuba, C. (1986). Transition zone reflections and permafrost analysis. *Geophysics, 51*(5; 5), 1075-1086. doi:10.1190/1.1442163

Kuila, U., Dewhurst, D. N., Siggins, A. F., & Raven, M. D. (2011). Stress anisotropy and velocity anisotropy in low porosity shale. *Tectonophysics, 503*(1-2; 1-2), 34-44. doi:10.1016/j.tecto.2010.09.023

Liner, C. L., Bodmann, B. G. (2010). The Wolf ramp: Reflection characteristics of a transition layer. *Geophysics, 75*(5; 5), A31-A35.

Loseth, H., Wensaas, L., Gading, M., Duffaut, K., & Springer, M. (2011). Can hydrocarbon source rocks be identified on seismic data? *Geology [Boulder], 39*(12; 12), 1167-1170. doi:10.1130/G32328.1

Lucier, A. M., Hofmann, R., & Bryndzia, L. T. (2011). Evaluation of variable gas saturation on acoustic log data from the haynesville shale gas play, NW louisiana, USA. *Leading Edge [Tulsa, OK], 30*(3; 3), 300-311. doi:10.1190/1.3567261

Ozdemir, H., Flanagan, K., & Tyler, E. (2010). Lithology and hydrocarbon mapping from multicomponent seismic data. *Geophysical Prospecting, 58*(2; 2), 297-306. doi:10.1111/j.1365-2478.2009.00821.x

Passey, Q. R., Creaney, S., Kulla, J. B., Moretti, F. J., & Stroud, J. D. (1990). A practical model for organic richness from porosity and resistivity logs. *AAPG Bulletin, 74*(12; 12), 1777-1794. doi:10.1306/0C9B25C9-1710-11D7-8645000102C1865D

Sayers, C. M. (2005). Seismic anisotropy of shales. *Geophysical Prospecting, 53*(5; 5), 667-676.

Sayers, C. M. (2013). The effect of anisotropy on the young's moduli and poisson's ratios of shales. *Geophysical Prospecting, 61*(2), 416-426.

Schuelke, J. S. (2011). Overview of seismic attribute analysis in shale plays. *Papers Presented at the Gulf Coast Section, Society of Economic Paleontologists and Mineralogists Foundation Annual Bob F.Perkins Research Conference, 31*, 806-827.

Smith, T. (2013). Ordovician utica shale. *AAPG Pittsburgh Annual Meeting,*

Smith, T., & Leone, J. (2013). Utica and marcellus potential in new york state. *AAPG Pittsburgh Annual Meeting,*

Treadgold, G., Campbell, B., McLain, B., Sinclair, S., & Nicklin, D. (2011). Eagle ford shale prospecting with 3D seismic data within a tectonic and depositional system framework. *Leading Edge [Tulsa, OK], 30*(1; 1), 48-53. doi:10.1190/1.3535432

Vernik, L., & Nur, A. (1992). Ultrasonic velocity and anisotropy of hydrocarbon source rocks. *Geophysics, 57*(5; 5), 727-735. doi:10.1190/1.1443286

Wang, G., & Carr, T. R. (2012). Methodology of organic-rich shale lithofacies identification and prediction; a case study from marcellus shale in the appalachian basin. *Computers & Geosciences, 49*, 151-163. doi:10.1016/j.cageo.2012.07.011

Wolf, A. (1937). The reflection of elastic waves from transition layers of variable velocity. *Geophysics, 2*(4; 4), 357-363. doi:10.1190/1.1438104

Yoon, W. J., & Farfour, M. (2012). Spectral decomposition aids AVO analysis in reservoir characterization; a case study of blackfoot field, alberta, canada. *Computers & Geosciences, 46*, 60-65. doi:10.1016/j.cageo.2012.04.012

Zhu, Y., Liu, E., Martinez, A., Payne, M. A., & Harris, C. E. (2011). Understanding geophysical responses of shale-gas plays. *Leading Edge [Tulsa, OK], 30*(3; 3), 332-338. doi:10.1190/1.3567265

VI. APPENDIX

A.1 Vibroseis Line Parameters

@1 Client/Line information; Maximum number of characters in a line is 17 WRIGHT STATE UNIVERSITY WSU PART B 2001-2178 CHIPPEWA TWP. WAYNE CO. OHIO @2 General Information; Maximum number of characters in a line is 65 MIGRATION LOW FREQUENCY @3 Processing Sequence; Maximum number of characters in a line is 65 1 Demultiplex/Reformat 2 Shot / Trace Edits 3 Geometry and Survey Information Header Application 4 System Filter Dephase Low Cut 3 Hz. High Cut 205 Hz. PreAmp Gain 30 Db Sample 1 ms. Applied During Cross-Correlation 5 Geophone De-Phase 10 Hz. / 1 Ms. 6 Spherical Divergence Gain Recovery 7 Offset Limitation to +/-10000 Ft. 8 Surface Consistent Deconvolution: Design Gate for both Source and Receiver Operator length= 128 ms. Pre-Whitening= 3.0 % Single Window: 0 ft. open: 225 msec. closed: 1500 msec. 6820 ft. open: 750 msec. closed: 1500 msec. 10000 ft. open: 1000 msec. closed: 1500 msec. 9 Spherical Divergence Gain Recovery 10 Sort into Common Midpoint Gathers 2-D Pseudo Swath Line 11 Datum Corrections Refraction Based Datum: 1000 feet Vel (W) 4000 feet/sec. Vel (SW) 10000 feet/sec. Vel (COR) 10000 feet/sec. 12 Zero-Phase Spectral Balancing: 5 - 40 Hz. 13 Velocity Analysis - 2 Passes Analysis Every 1/3 Mile 14 NMO Corrections Application Every 1/3 Mile 15

Muting: First Arrival Stretch 16 Filtering: Zero Phase Operator Length 512 msec. Low 5 Hz. High 40 Hz. Start 0 ms. End 2000 ms. 17 Trace Balance Four(4) Window Overlapping Function 18 Surface Consistent Statics: Gate: 200 - 1000 msec. 19 CDP Trim Statics: Gate: 200 - 1000 msec. Maximum Shift 4 msec. 20 Common Depth Point Stack: 89 fold 21 FX Deconvolution/Filter 22 Full Wave Equation Migration @4 Recording Information; Maximum number of characters in a line is 65 SHOT BY: Precision Geophysical Date: 02-04-2011 ACQUIRED FOR: Wright State University INSTRUMENTS SOURCE GEOPHONES TYPE: Aram Aries INTERVAL: 82.5 ft. INTERVAL: 82.5 ft. FORMAT: SEG-Y ARRAY: 1 Vibs/ 75 Ft. ARRAY: inline NO.CHANS: 363 TYPE: Vibrator TYPE: 10 Hz. SAMPLE RATE: 1 ms. Sweep Type: 8-128 Hz. NO./GROUP: 06 DATA LENGTH: 04 Sec. Sweep Length 12000 Ms. SPACING: 15.0 ft. FILTERS: 3 / 205 Hz. REEL:wsu1.label1 inpt:wsu1-17.wmig Spread geometry (Variable - 0 * 0 – Variable)

A.2 Velocities

North-South Velocities

cdp=2034 t=0,68,147,241,348,427,519,683,735,854,946,1041,1150,1537,2000 v=8000,8577,9462,10916,12607,12413,13048,13854,14001,14077,13317,14313,15048,16264,17499 cdp=2079 t=0,173,237,322,384,457,550,633,728,856,953,1053,1202,1430,2000 v=8000,9741,9988,11154,11333,11883,12863,14414,14317,14290,14834,15104,16925,17789,17499 cdp=2104 t=0,156,260,332,410,481,564,595,666,742,863,948,1041,1160,1236,1440,1674,2000 v=8000,9605,9979,11967,12434,12444,13600,14567,14905,14780,14908,15364,17207,16847,17220,17131,16927,17499 cdp=2139 t=0,132,232,289,370,443,507,562,612,666,756,856,958,1051,1157,1340,1553,1762,2000

v=8000,9330,10701,12058,12415,12433,13048,13553,14747,14477,14233,14728,15184,
16389,16804,17012,17991,17811,17499 cdp=2154

t=0,156,256,308,358,462,536,621,718,780,861,963,1058,1257,1563,1646,2000

v=8000,9412,10743,11250,11883,11823,12855,14230,13989,13565,14228,14715,15297,
16481,17525,18340,17499 cdp=2174

t=0,142,258,355,460,550,628,676,754,835,956,1039,1179,1259,1551,1760,2000

v=8000,9220,11242,12010,12124,12999,13685,13933,14413,14797,15406,16131,16309,
16482,19151,18632,17499 cdp=2209

t=0,156,249,351,391,469,533,642,692,763,842,965,1029,1164,1409,1561,1750,2000

v=8000,9752,11059,11536,11456,11853,13130,13818,14292,13981,13945,14583,15718,
15833,15769,16405,17666,17499 cdp=2244

t=0,154,232,308,372,455,543,616,683,763,844,951,1053,1221,1349,1487,1760,2000

v=8000,9341,10702,11458,11699,12027,12812,13175,13768,13616,13847,14496,15124,
15076,14723,14480,17385,17499 cdp=2279

t=0,144,239,306,351,472,545,635,680,744,816,960,1074,1174,1349,1499,1677,2000

v=8000,9226,10860,11912,12335,12084,13236,14214,14858,14293,14552,15461,16242,
16226,15354,16052,17409,17499 cdp=2314

t=0,135,230,313,377,476,562,621,685,775,873,979,1060,1172,1347,1430,1674,2000

v=8000,9302,11232,12304,12149,12213,13457,14897,14356,14577,14708,15850,16276,
15665,15632,16641,17792,17499 cdp=2349

t=0,142,173,256,355,450,540,640,690,773,849,972,1039,1164,1276,1473,1686,2000

v=8000,9163,10333,11822,12250,12391,12958,14480,14360,14351,13685,14155,14590,
15531,16003,17060,17637,17499

East-West Velocities

cdp=4034 t=0,151,237,341,422,462,529,645,756,844,946,1048,1150,1359,1551,1743,2000
v=8000,9701,10445,11638,11694,11982,12936,15025,14510,14633,14451,14658,15372,
16163,16719,17276,17499 cdp=4069
t=0,161,258,344,419,465,548,659,730,849,937,1048,1141,1285,1539,1651,2000
v=8000,10000,10766,10920,11780,12030,13021,14381,14427,14339,14736,15490,1618
4,16004,16809,17589,17499 cdp=4104
t=0,156,249,341,405,465,543,647,744,835,958,1029,1141,1259,1368,1542,2000
v=8000,9797,9796,11151,11956,12319,12996,13830,13740,13962,14513,15142,15811,1
5690,15286,16468,17499 cdp=4139
t=0,130,251,346,431,526,645,735,837,941,1043,1138,1257,1366,1451,1758,2000
v=8000,9677,10331,11635,12262,12912,13716,13742,14336,14874,15659,15724,16017,
15859,14810,16866,17499 cdp=4174
t=0,161,260,367,455,540,645,749,830,948,1020,1157,1250,1359,1473,1646,2000
v=8000,9786,11957,12229,12340,13354,13774,14206,14491,15047,15715,15528,16464,
16698,16830,17733,17499 cdp=4209
t=0,125,244,336,455,538,659,740,844,941,1032,1141,1250,1368,1489,1660,2000
v=8000,9466,11263,11724,12043,12664,13938,14328,14586,14832,15405,16206,16174,
16127,16574,17735,17499

cdp=4244 t=0,142,251,351,434,548,652,749,835,937,1020,1157,1257,1352,1470,1644,2000
v=8000,9279,11111,12137,12739,13400,14172,14169,14701,15318,15585,15932,15719,
15857,16091,17090,17499 cdp=4279
t=0,154,251,348,450,543,659,749,858,944,1022,1115,1262,1357,1440,1610,2000
v=8000,9400,10831,12089,12534,14001,15052,13978,14561,15370,16044,16058,15805,
15681,16234,16806,17499 cdp=4314

t=0,151,225,358,446,557,640,749,835,951,1046,1145,1259,1364,1437,1608,2000

v=8000,9220,10283,11623,12783,14186,15529,14483,14247,14781,15223,15333,15648,

15654,16662,17202,17499 cdp=4349

t=0,142,241,348,455,552,647,747,861,967,1065,1138,1243,1361,1475,1655,2000

v=8000,8804,10798,11786,11938,13071,14867,14310,14299,15040,15760,15631,15946,

16164,17069,17597,17499

A.3 Supplemental Well Logs

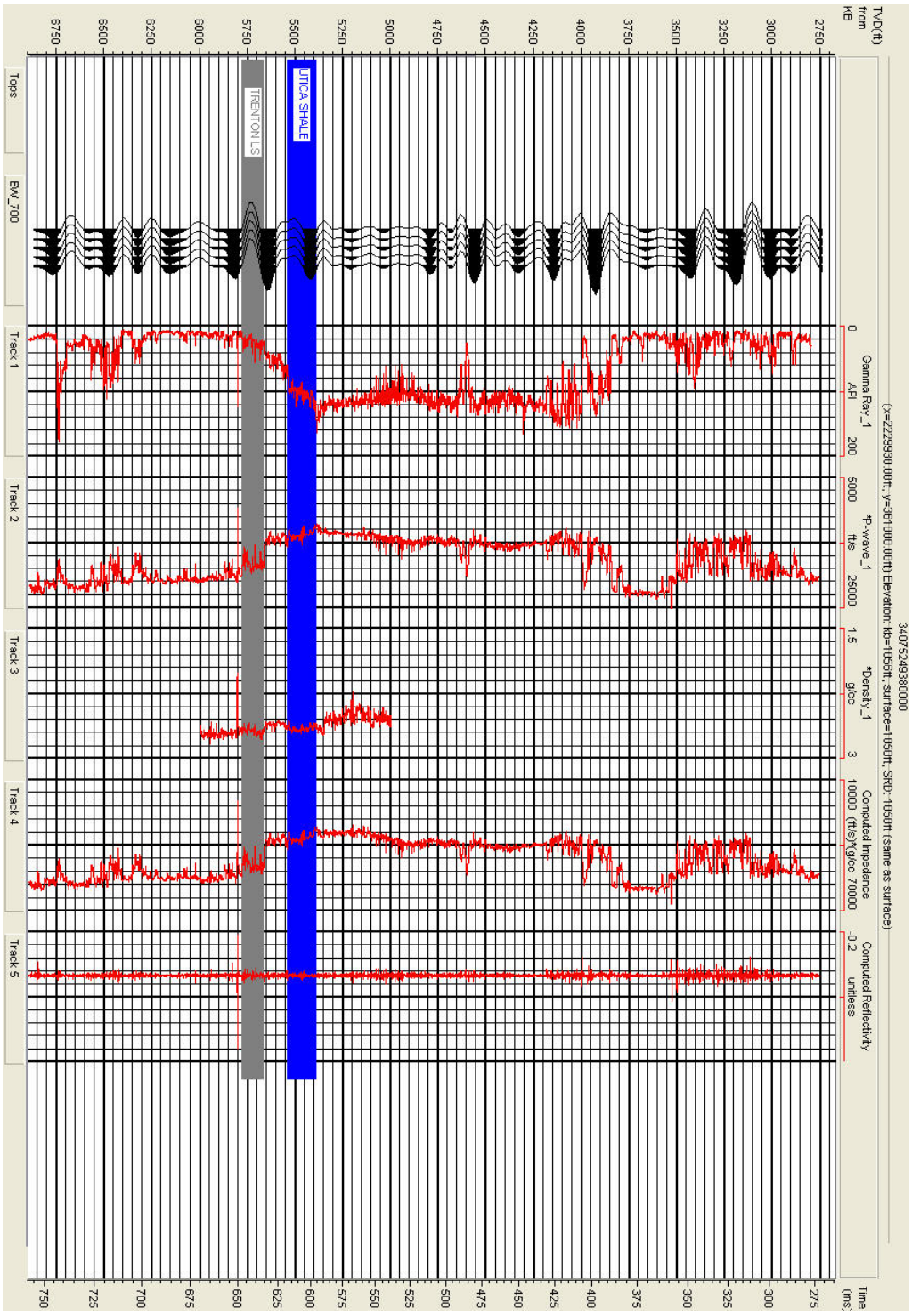

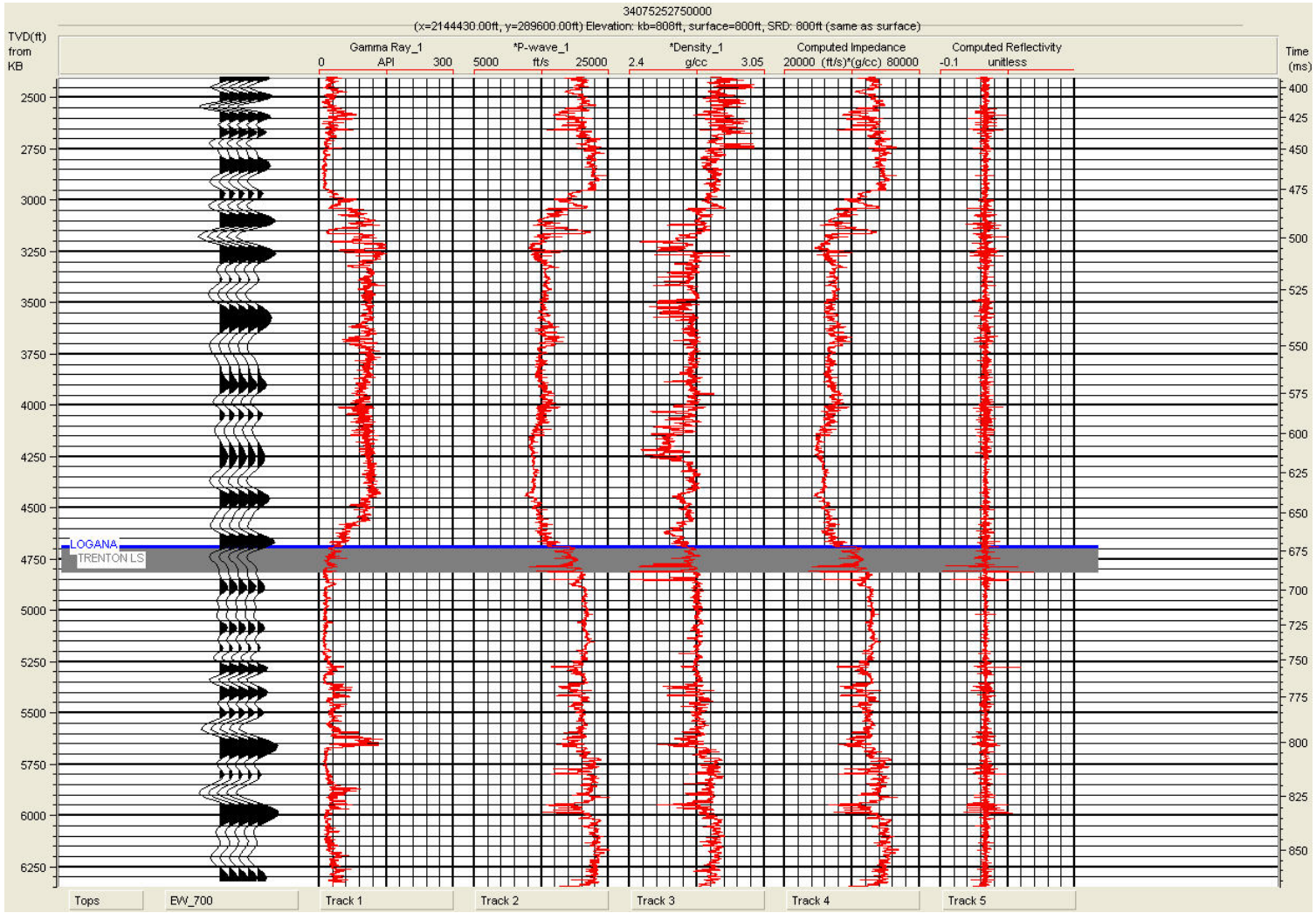
34075252750000
(x=2144430.00ft, y=289600.00ft) Elevation: kb=808ft, surface=800ft, SRD: 800ft (same as surface)
TVD(ft) from KB
Gamma Ray_1
0 API 300
*P-wave_1
5000 ft/s 25000
*Density_1
2.4 g/cc 3.05
Computed Impedance
20000 (ft/s)*(g/cc) 80000
Computed Reflectivity
-0.1 unitless
Time (ms)
2500
2750
3000
3250
3500
3750
4000
4250
4500
4750
5000
5250
5500
5750
6000
6250
400
425
450
475
500
525
550
575
600
625
650
675
700
725
750
775
800
825
850
LOGANA
TRENTON LS
Tops
EW_700
Track 1
Track 2
Track 3
Track 4
Track 5

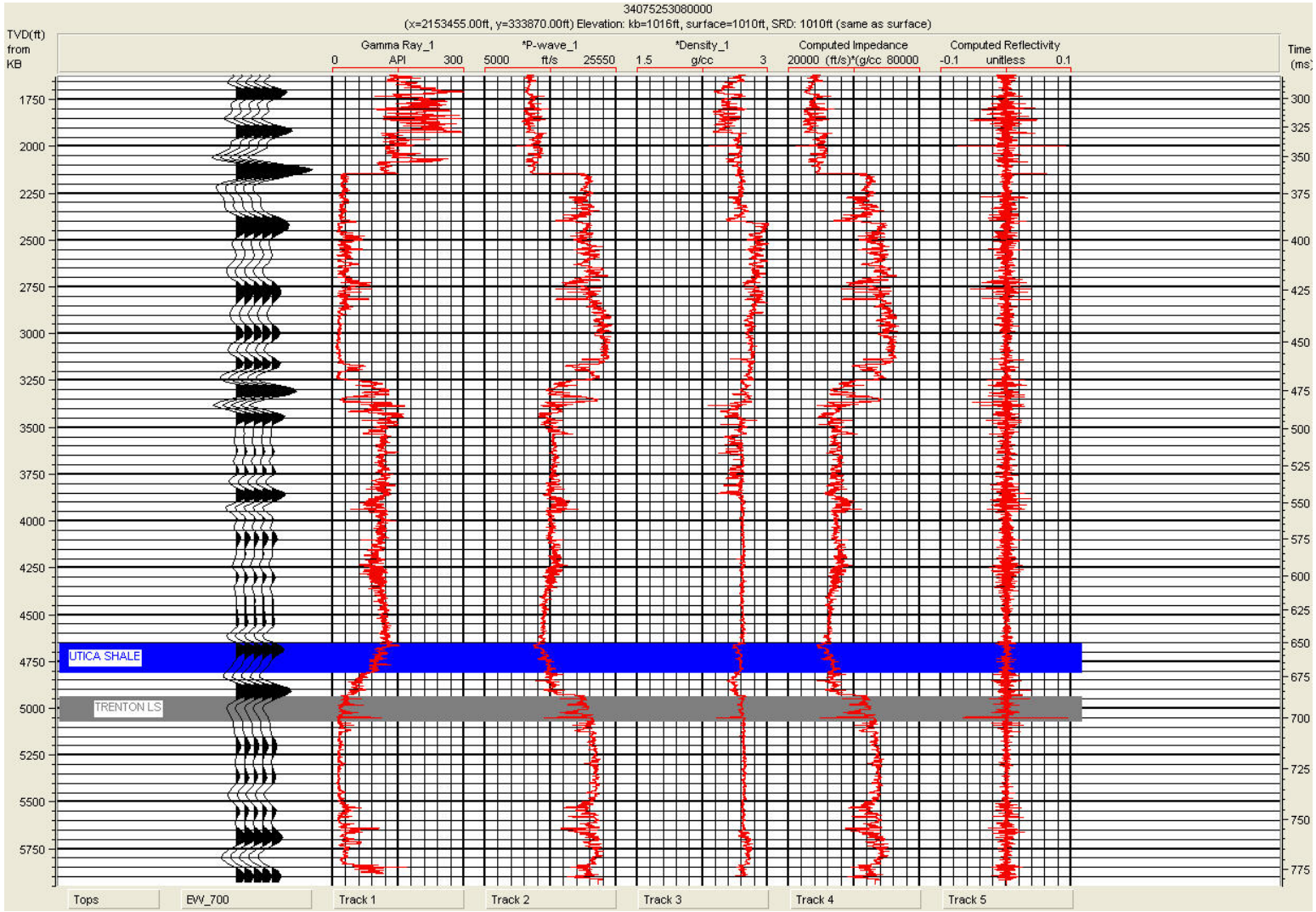
34075253080000
(x=2153455.00ft, y=333870.00ft) Elevation: kb=1016ft, surface=1010ft, SRD: 1010ft (same as surface)
TVD(ft) from KB
Gamma Ray_1
0 API 300
*P-wave_1
5000 ft/s 25550
*Density_1
1.5 g/cc 3
Computed Impedance
20000 (ft/s)*(g/cc 80000
Computed Reflectivity
-0.1 unitless 0.1
Time (ms)
1750
2000
2250
2500
2750
3000
3250
3500
3750
4000
4250
4500
4750
5000
5250
5500
5750
300
325
350
375
400
425
450
475
500
525
550
575
600
625
650
675
700
725
750
775
UTICA SHALE
TRENTON LS
Tops
EW_700
Track 1
Track 2
Track 3
Track 4
Track 5

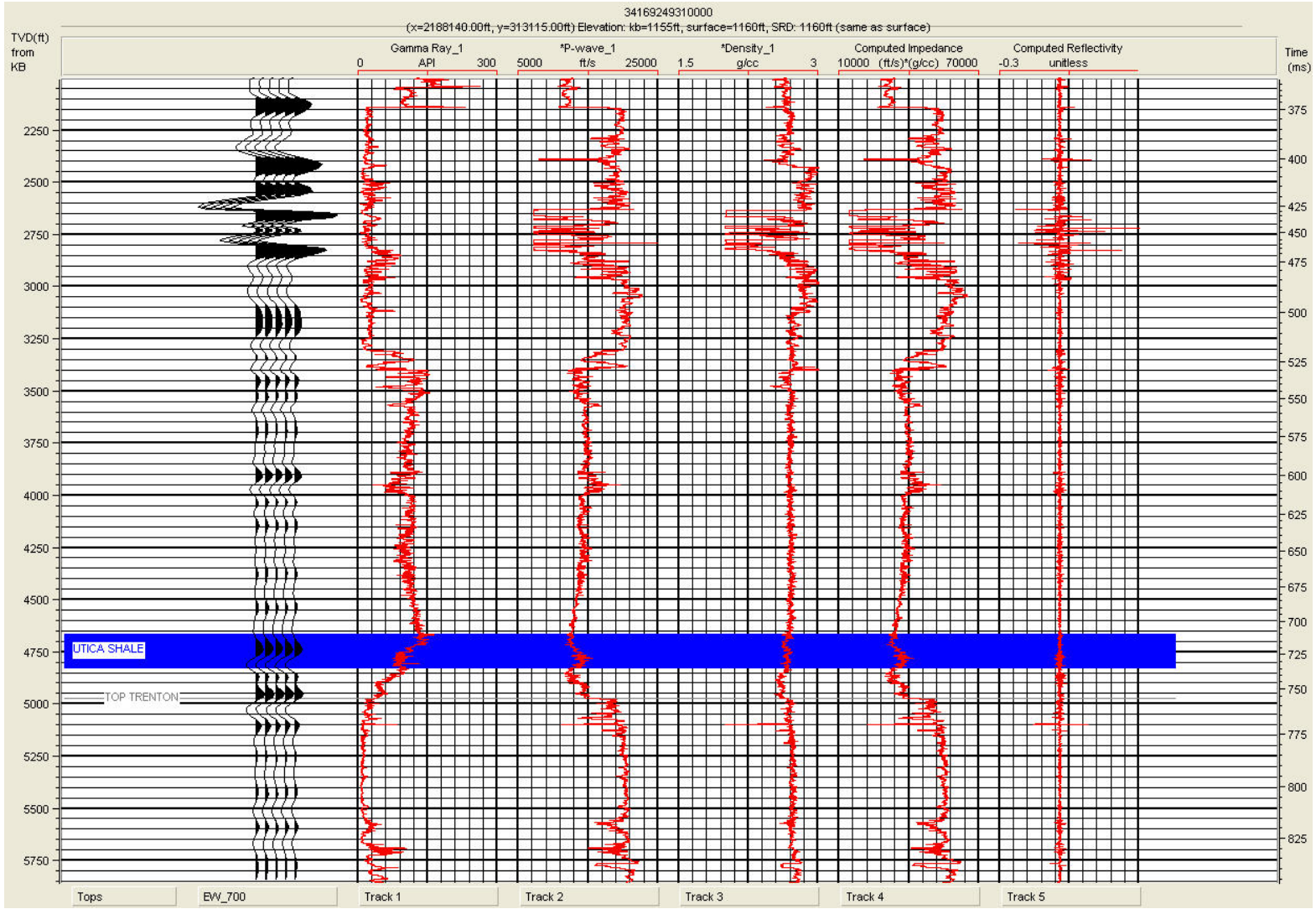
34169249310000
(x=2188140.00ft, y=313115.00ft) Elevation: kb=1155ft, surface=1160ft, SRD: 1160ft (same as surface)
TVD(ft) from KB
Gamma Ray_1
0 API 300
*P-wave_1
5000 ft/s 25000
*Density_1
1.5 g/cc 3
Computed Impedance
10000 (ft/s)*(g/cc) 70000
Computed Reflectivity
-0.3 unitless
Time (ms)
2250
2500
2750
3000
3250
3500
3750
4000
4250
4500
4750
5000
5250
5500
5750
375
400
425
450
475
500
525
550
575
600
625
650
675
700
725
750
775
800
825
UTICA SHALE
TOP TRENTON
Tops
EW_700
Track 1
Track 2
Track 3
Track 4
Track 5

A.4 OGS source rock analysis within the succession of interest

API_WELLNO	ORESAMP_N	TYPE	AB_SAMP_N	AB_SOURCE	B_SAMP_TO	SAMP_DEP	B_SAMP_BA	LITH_UNIT	ORG_CARB	S1_mg	S2_mg	S3_mg	HI	Tmax	OI	PI	PC	CO3	RO	DATE_MOD	COMMENTS	SOURCE
34133240270000.00	4157	samp	53295-2-1	rd labs		5655		ODVCU	0.53	0.24	0.76	0.19	142	430	36	0.24			0.58	27-Nov-12	calculated	Overton
34133240270000.00	4157	samp	1.RAW	rd		5655		ODVCU	0.534	0.24	0.76	0.19	142	430	36	0.24			0.58	30-Jul-12	calculated	Resources
34133240270000.00	4157	samp	53295-2-2	rd labs		5755		UTCA	0.66	0.32	1	0.19	151	430	29	0.24			0.58	27-Nov-12	calculated	Overton
34133240270000.00	4157	samp	2.RAW	rd		5755		UTCA	0.661	0.32	1	0.19	151	430	29	0.24			0.58	30-Jul-12	calculated	Resources
34133240270000.00	4157	samp	53295-2-3	rd labs		5785		UTCA	1.46	1.06	2.47	0.22	169	440	15	0.3			0.76	27-Nov-12	calculated	Overton
34133240270000.00	4157	samp	3.RAW	rd		5785		UTCA	1.46	1.06	2.47	0.22	269	440	15	360			0.76	30-Jul-12	calculated	Resources
34133240270000.00	4157	samp	53295-2-4	rd labs		5815		UTCA	1.32	0.79	2.4	0.28	182	450	21	0.25			0.94	27-Nov-12	calculated	Overton
34133240270000.00	4157	samp	4.RAW	rd		5815		UTCA	1.32	0.79	2.4	0.28	182	450	21	0.25			0.94	30-Jul-12	calculated	Resources
34133240270000.00	4157	samp	53295-2-5	rd labs		5895		PNPL	0.94	0.58	1.48	0.31	157	439	33	0.28			0.742	27-Nov-12	calculated	Overton
34133240270000.00	4157	samp	5.RAW	rd		5895		PNPL	0.943	0.58	1.48	0.31	157	439	33	0.28			0.742	30-Jul-12	calculated	Resources
34133240270000.00	4157	samp	53295-2-6	rd labs		5915		PNPL	1.67	1.4	2.99	0.34	179	443	20	0.32			0.814	27-Nov-12	calculated	Overton
34133240270000.00	4157	samp	6.RAW	rd		5915		PNPL	1.67	1.4	2.99	0.34	179	443	20	0.32			0.814	30-Jul-12	calculated	Resources
34133240270000.00	4157	samp	100908-	GeoMark	5910	5915	5920	PNPL	1.2	1.2	1.8	0.28	150	444	23	0.4			0.83	28-Nov-11	Calculated	Consulting
34133240270000.00	4157	samp	151		5910	5920	5930	PNPL	2.11	1.56	3.49		165.4028			0.308911				18-Dec-12		Chesapeak
34133240270000.00	4157	samp	100908-	GeoMark	5920	5925	5930	PNPL	1.88	1.98	2.89	0.29	154	444	15	0.41			0.83	28-Nov-11	Calculated	Consulting
34133240270000.00	4157	samp	100908-	GeoMark	5930	5935	5940	PNPL	1.82	1.93	2.85	0.25	157	443	14	0.4			0.81	28-Nov-11	Calculated	Consulting
34133240270000.00	4157	samp	152		5940	5945	5950	LXNG	2.42	1.78	3.9		161.157			0.31338				18-Dec-12		Chesapeak
34133240270000.00	4157	samp	100908-	GeoMark	5940	5945	5950	LXNG	2.01	2.31	3.36	0.27	167	443	13	0.41			0.81	28-Nov-11	Calculated	Consulting
34133240270000.00	4157	samp	100908-	GeoMark	5950	5955	5960	LXNG	2.13	2.37	3.51	0.32	165	444	15	0.4			0.83	28-Nov-11	Calculated	Consulting
34133240270000.00	4157	samp	100908-	GeoMark	5960	5965	5970	LXNG	2.23	2.53	3.81	0.37	171	444	17	0.4			0.83	28-Nov-11	Calculated	Consulting
34133240270000.00	4157	samp	153		5970	5975	5980	LXNG	2.8	2.27	4.7		167.8571			0.325682				18-Dec-12		Chesapeak
34133240270000.00	4157	samp	100908-	GeoMark	5970	5975	5980	LXNG	2.37	2.91	4.1	0.32	173	443	14	0.42			0.81	28-Nov-11	Calculated	Consulting
34133240270000.00	4157	samp	100908-	GeoMark	5980	5985	5990	LXNG	2.42	2.92	4.3	0.32	178	443	13	0.4			0.81	28-Nov-11	Calculated	Consulting
34133240270000.00	4157	samp	154		6000	6005	6010	LGNA	2	1.87	3.93		196.5			0.322414				18-Dec-12		Chesapeak
34133240270000.00	4157	samp	100908-	GeoMark	6000	6005	6010	LGNA	1.95	2.16	3.2	0.29	164	448	15	0.4			0.9	28-Nov-11	Calculated	Consulting
3.41512E+13	1990	SAMP	RJRE-110301-001	GeoMark	6430	6445	6460	UTCA	1.06	0.86	1.27	0.41	120	442	39	0.4			0.8	14-Jun-12	Low Temp S2 Shoulder, RO value is calculated (RE-TMAX)	Petroleum Consulting Inc D. Prezbindowski
34151211230000	1990	SAMP	RJRE-110301-002	GeoMark	6460	6475	6490	UTCA	2.04	1.25	2.63	0.35	129	440	17	0.32			0.76	14-Jun-12	Low Temp S2 Shoulder, RO value is calculated (RE-TMAX)	Petroleum Consulting Inc D. Prezbindowski
34151211230000	1990	SAMP	RJRE-110301-003	GeoMark	6490	6505	6520	UTCA	1.81	1.15	2.35	0.53	130	447	29	0.33			0.89	14-Jun-12	Low Temp S2 Shoulder, RO value is calculated (RE-TMAX)	Petroleum Consulting Inc D. Prezbindowski

34151211230000	1990	SAMP	RJRE-110301-004	GeoMark	6520	6535	6550	UTCA	1.6	0.97	1.92	0.46	120	448	29	0.34			0.9	14-Jun-12	Low Temp S2 Shoulder, RO value is calculated (RE-TMAX)	Petroleum Consulting Inc D. Prezbindowski
34151211230000	1990	SAMP	RJRE-110301-005	GeoMark	6550	6565	6580	UTCA	1.37	1.21	1.99	0.29	145	448	21	0.38			0.9	14-Jun-12	Low Temp S2 Shoulder, RO value is calculated (RE-TMAX)	Petroleum Consulting Inc D. Prezbindowski
34151211230000	1990	SAMP	RJRE-110301-006	GeoMark	6580	6595	6610	PNPL	2.07	2.55	4.11	0.33	199	422	16	0.38			0.44	14-Jun-12	Low Temp S2 Shoulder, RO value is calculated (RE-TMAX)	Petroleum Consulting Inc D. Prezbindowski
34151211230000	1990	SAMP	RJRE-110301-007	GeoMark	6610	6615	6620	PNPL	2.08	2.63	5.06	0.37	243	420	18	0.34			0.4	14-Jun-12	Low Temp S2 Shoulder, RO value is calculated (RE-TMAX)	Petroleum Consulting Inc D. Prezbindowski
34151211230000	1990	SAMP	RJRE-110301-008	GeoMark	6620	6625	6630	PNPL	2.75	3.9	4.99	0.34	181	445	12	0.44			0.85	14-Jun-12	Low Temp S2 Shoulder, RO value is calculated (RE-TMAX)	Petroleum Consulting Inc D. Prezbindowski
34151211230000	1990	SAMP	RJRE-110301-009	GeoMark	6640	6645	6650	LXNG	2.95	4.15	4.35	0.35	147	452	12	0.49			0.98	14-Jun-12	Low Temp S2 Shoulder, RO value is calculated (RE-TMAX)	Petroleum Consulting Inc D. Prezbindowski
34151211230000	1990	samp	11-1107-166		6650	6655	6660	LXNG	2.97	3.75	5.08		171.0438			0.424689				18-Dec-12		B. Brulet - Chesapeake Energy
34151211230000	1990	SAMP	RJRE-110301-010	GeoMark	6650	6655	6660	LXNG	2.88	3.89	4.45	0.32	155	451	11	0.47			0.96	14-Jun-12	Low Temp S2 Shoulder, RO value is calculated (RE-TMAX)	Petroleum Consulting Inc D. Prezbindowski
34151211230000	1990	SAMP	RJRE-110301-011	GeoMark	6660	6665	6670	LXNG	2.65	3.35	4.32	0.35	163	452	13	0.44			0.98	14-Jun-12	Low Temp S2 Shoulder, RO value is calculated (RE-TMAX)	Petroleum Consulting Inc D. Prezbindowski
34151211230000	1990	samp	11-1107-167		6670	6675	6680	LXNG	2.78	3.48	4.85		174.4604			0.417767				18-Dec-12		B. Brulet - Chesapeake Energy
34151211230000	1990	SAMP	RJRE-110301-012	GeoMark	6670	6675	6680	LXNG	2.6	3.51	4.02	0.37	155	451	14	0.47			0.96	14-Jun-12	Low Temp S2 Shoulder, RO value is calculated (RE-TMAX)	Petroleum Consulting Inc D. Prezbindowski
34151211230000	1990	SAMP	RJRE-110301-013	GeoMark	6680	6685	6690	LGNA	2.71	3.51	4.4	0.37	162	450	14	0.44			0.94	14-Jun-12	Low Temp S2 Shoulder, RO value is calculated (RE-TMAX)	Petroleum Consulting Inc D. Prezbindowski
34151211230000	1990	samp	11-1107-168		6690	6695	6700	LGNA	2.8	3.57	4.75		169.6429			0.429087				18-Dec-12		B. Brulet - Chesapeake Energy
34151211230000	1990	SAMP	RJRE-110301-014	GeoMark	6690	6695	6700	LGNA	2.6	3.4	3.89	0.35	150	452	13	0.47			0.98	14-Jun-12	Low Temp S2 Shoulder, RO value is calculated (RE-TMAX)	Petroleum Consulting Inc D. Prezbindowski
34151211230000	1990	SAMP	RJRE-110301-015	GeoMark	6700	6705	6710	LGNA	2.82	3.37	4.42	0.35	157	451	12	0.43			0.96	14-Jun-12	Low Temp S2 Shoulder, RO value is calculated (RE-TMAX)	Petroleum Consulting Inc D. Prezbindowski
34151211230000	1990	SAMP	RJRE-110301-016	GeoMark	6710	6715	6720	LGNA	1.89	1.64	1.85	0.34	98	453	18	0.47			0.99	14-Jun-12	Low Temp S2 Shoulder, RO value is calculated (RE-TMAX)	Petroleum Consulting Inc D. Prezbindowski
34151211230000	1990	SAMP	RJRE-110301-017	GeoMark	6720	6725	6730	CDVL	1.59	1.88	2.45	0.32	154	445	20	0.43			0.85	14-Jun-12	Low Temp S2 Shoulder, RO value is calculated (RE-TMAX)	Petroleum Consulting Inc D. Prezbindowski
34151211230000	1990	SAMP	RJRE-110301-018	GeoMark	6730	6735	6740	CDVL	1.27	1.19	2.34	0.31	184	414	24	0.34			0.29	14-Jun-12	Low Temp S2 Shoulder, RO value is calculated (RE-TMAX)	Petroleum Consulting Inc D. Prezbindowski
34151211230000	1990	SAMP	RJRE-110301-019	GeoMark	6750	6755	6760	CDVL	0.45	0.63	1.19	0.3	264	390	67	0.35			-0.14	14-Jun-12	Low Temp S2 Shoulder, RO value is calculated (RE-TMAX)	Petroleum Consulting Inc D. Prezbindowski

34157250220000	4508	samp	RJRE-101103-001	GeoMark	7250	7255	7260	PNPL	2.19	1.7	2.46	0.45	112	456	21	0.41			1.05	28-Nov-11	RO value is Calculated (RE-TMAX)	Petroleum Consulting Inc D. Prezbindowski
34157250220000	4508	samp	RJRE-101103-002	GeoMark	7260	7265	7270	PNPL	2.54	2.07	3.21	0.42	126	457	17	0.39			1.07	28-Nov-11	RO value is Calculated (RE-TMAX)	Petroleum Consulting Inc D. Prezbindowski
34157250220000	4508	samp	RJRE-101103-003	GeoMark	7270	7275	7280	PNPL	2.17	1.51	2.3	0.42	106	457	19	0.4			1.07	28-Nov-11	RO value is Calculated (RE-TMAX)	Petroleum Consulting Inc D. Prezbindowski
34157250220000	4508	samp	RJRE-101103-004	GeoMark	7280	7285	7290	LXNG	2.81	2.24	3.31	0.47	118	459	17	0.4			1.1	28-Nov-11	RO value is Calculated (RE-TMAX)	Petroleum Consulting Inc D. Prezbindowski
34157250220000	4508	samp	RJRE-101103-005	GeoMark	7290	7295	7300	LXNG	2.45	1.78	2.79	0.41	114	460	17	0.39			1.12	28-Nov-11	RO value is Calculated (RE-TMAX)	Petroleum Consulting Inc D. Prezbindowski
34157250220000	4508	samp	RJRE-101103-006	GeoMark	7300	7305	7310	LXNG	2.82	2.43	3.98	0.5	141	458	18	0.38			1.08	28-Nov-11	RO value is Calculated (RE-TMAX)	Petroleum Consulting Inc D. Prezbindowski
34157250220000	4508	samp	RJRE-101103-007	GeoMark	7310	7315	7320	LGNA	3.08	2.65	4.63	0.42	150	458	14	0.36			1.08	28-Nov-11	RO value is Calculated (RE-TMAX)	Petroleum Consulting Inc D. Prezbindowski
34157250220000	4508	samp	RJRE-101103-008	GeoMark	7320	7325	7330	LGNA	1.41	0.86	1.41	0.38	100	456	27	0.38			1.05	28-Nov-11	RO value is Calculated (RE-TMAX)	Petroleum Consulting Inc D. Prezbindowski
3.41573E+13	4508	samp	RJRE-101103-009	GeoMark	7330	7335	7340	LGNA	1.55	0.77	1.24	0.38	80	457	25	0.38			1.07	28-Nov-11	RO value is Calculated (RE-TMAX)	Petroleum Consulting Inc D. Prezbindowski
34157250220000	4508	samp	RJRE-101103-010	GeoMark	7340	7345	7350	CDVL	1.86	0.87	1.71	0.4	92	456	22	0.34			1.05	28-Nov-11	RO value is Calculated (RE-TMAX)	Petroleum Consulting Inc D. Prezbindowski
34157250220000	4508	samp	RJRE-101103-011	GeoMark	7350	7355	7360	CDVL	1.64	0.9	1.52	0.38	93	457	23	0.37			1.07	28-Nov-11	RO value is Calculated (RE-TMAX)	Petroleum Consulting Inc D. Prezbindowski

A.5 Supplemental AVO Type Curves

Gradient Analysis at Top of Utica Reflector between CDPs 4250-4290 over 745-748 ms

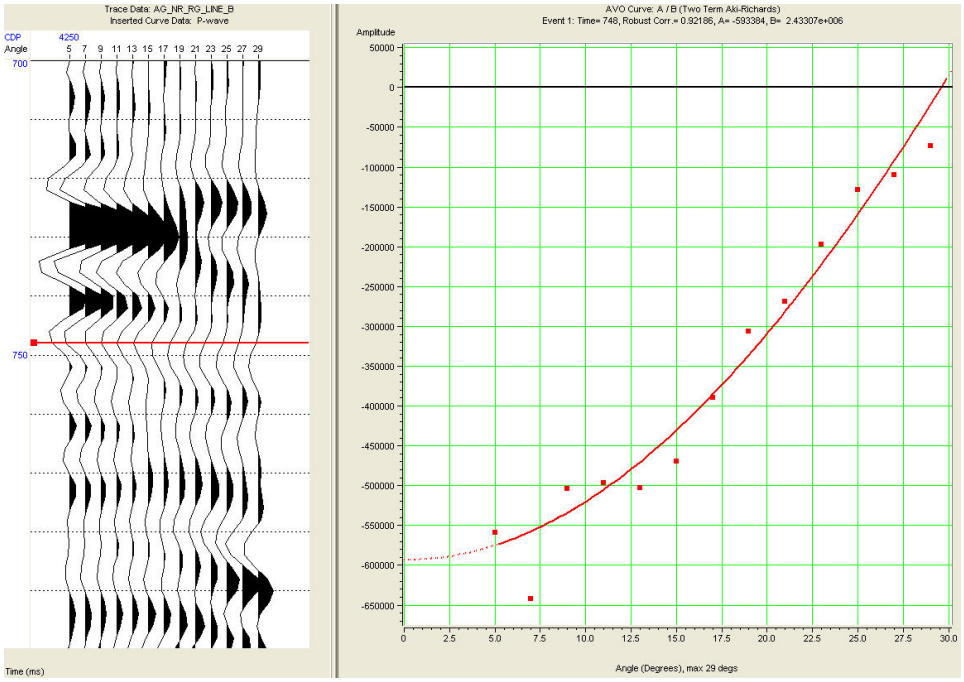

Class IV anomaly at CDP 4250

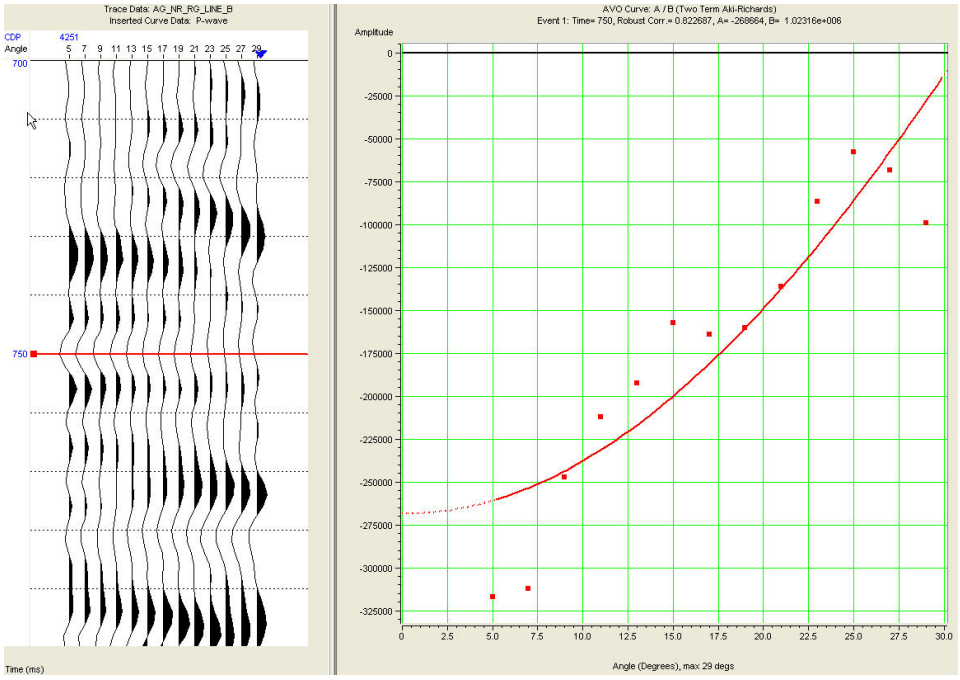

Class IV anomaly at CDP 4251

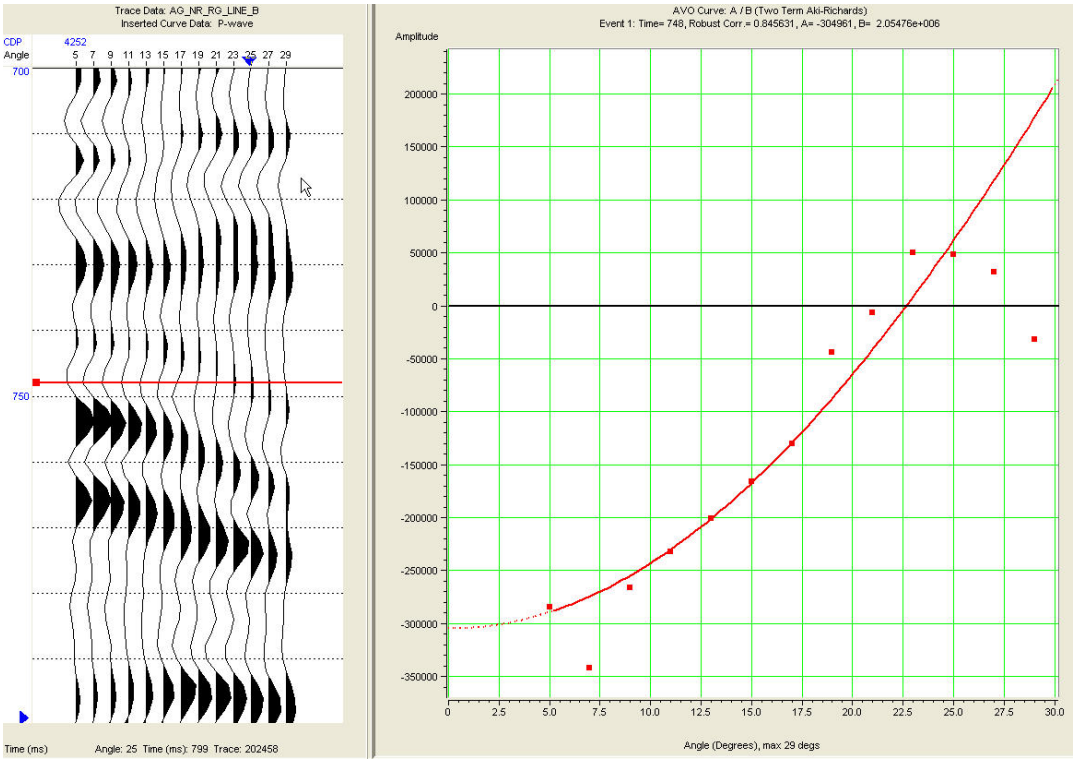

Class IV Anomaly at CDP 4252

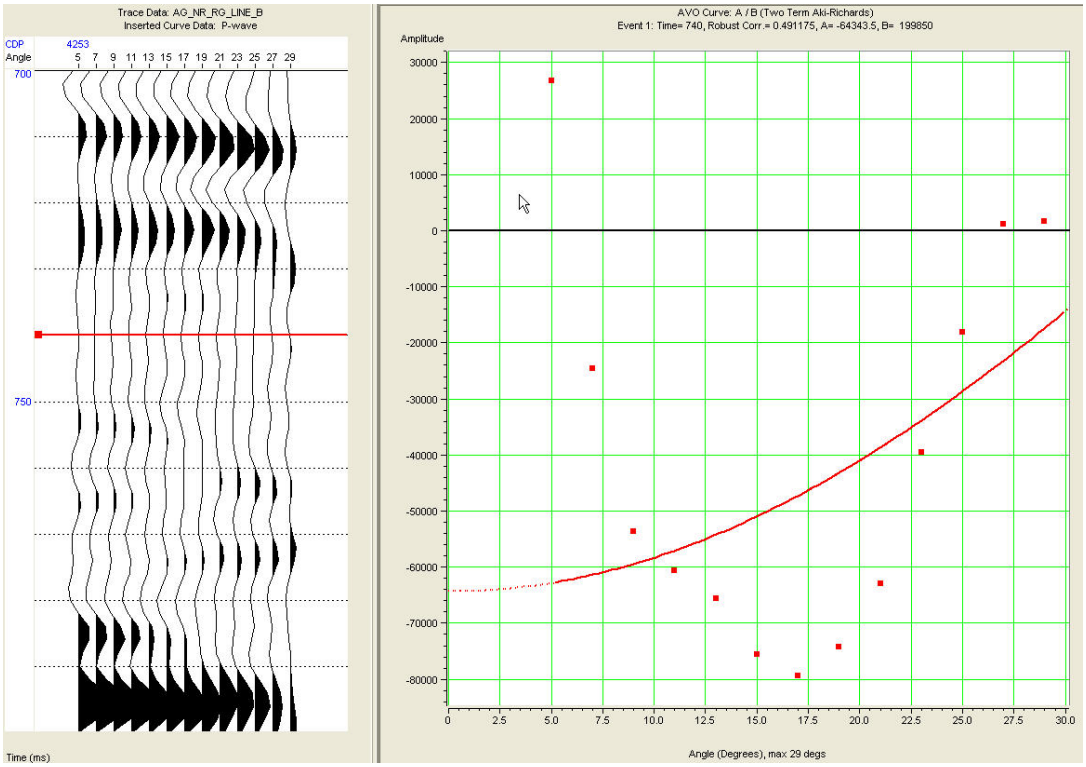

No coherent anomaly at CDP 4253

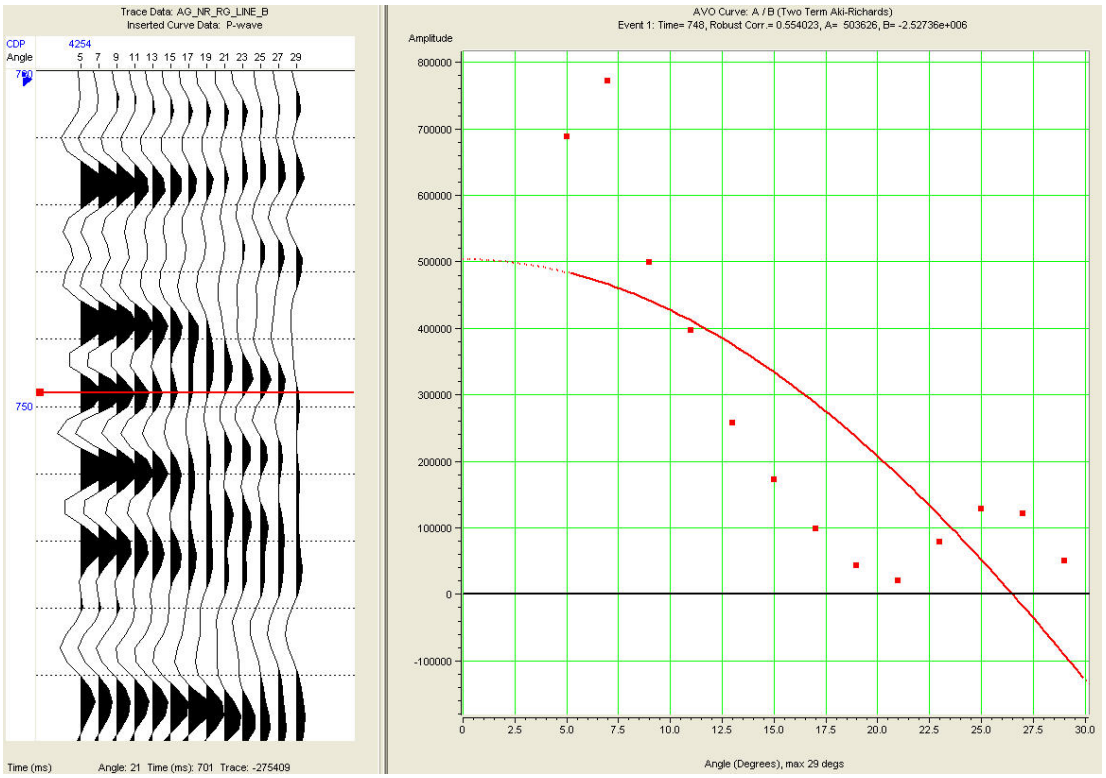

No coherent anomaly at CDP 4254

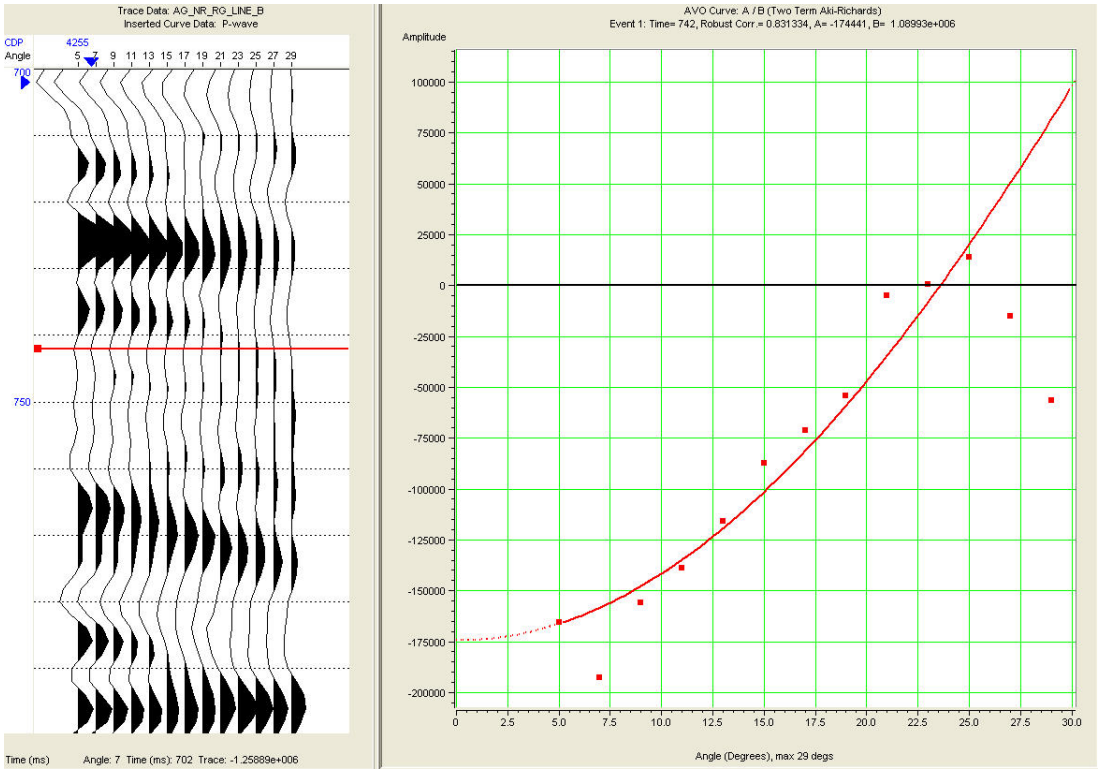

Weak Class IV anomaly at CDP 4255

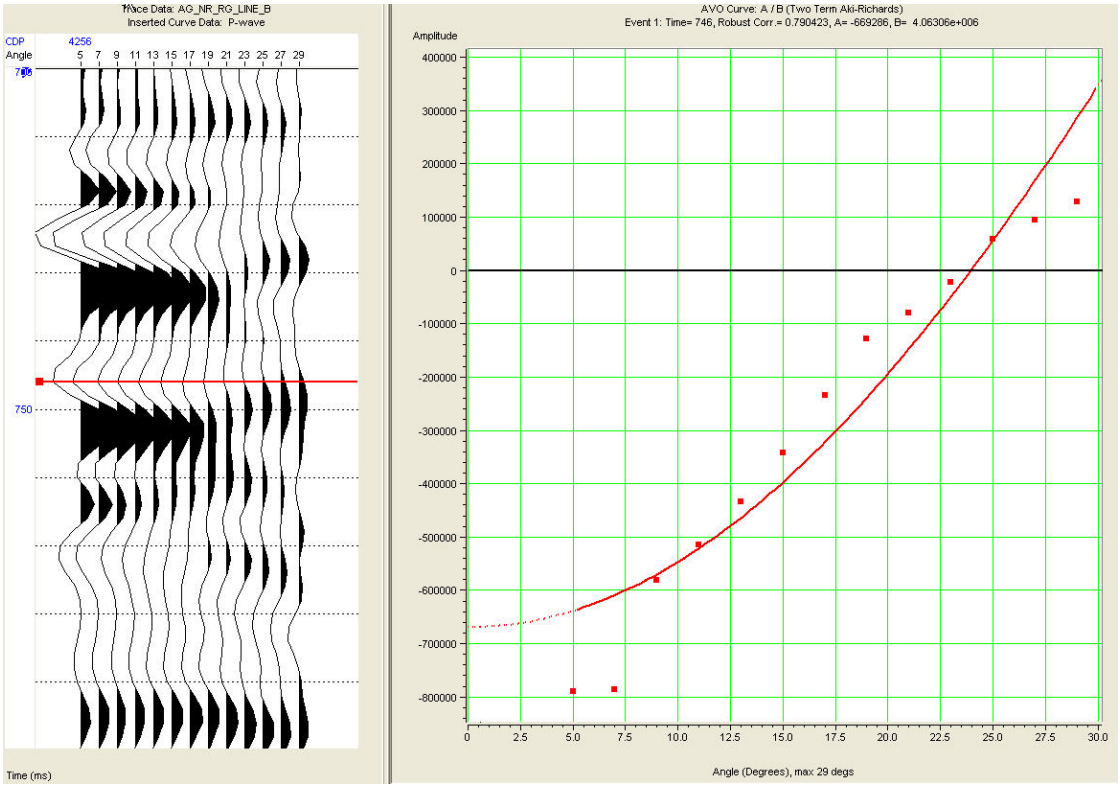

Class IV anomaly at CDP 4256

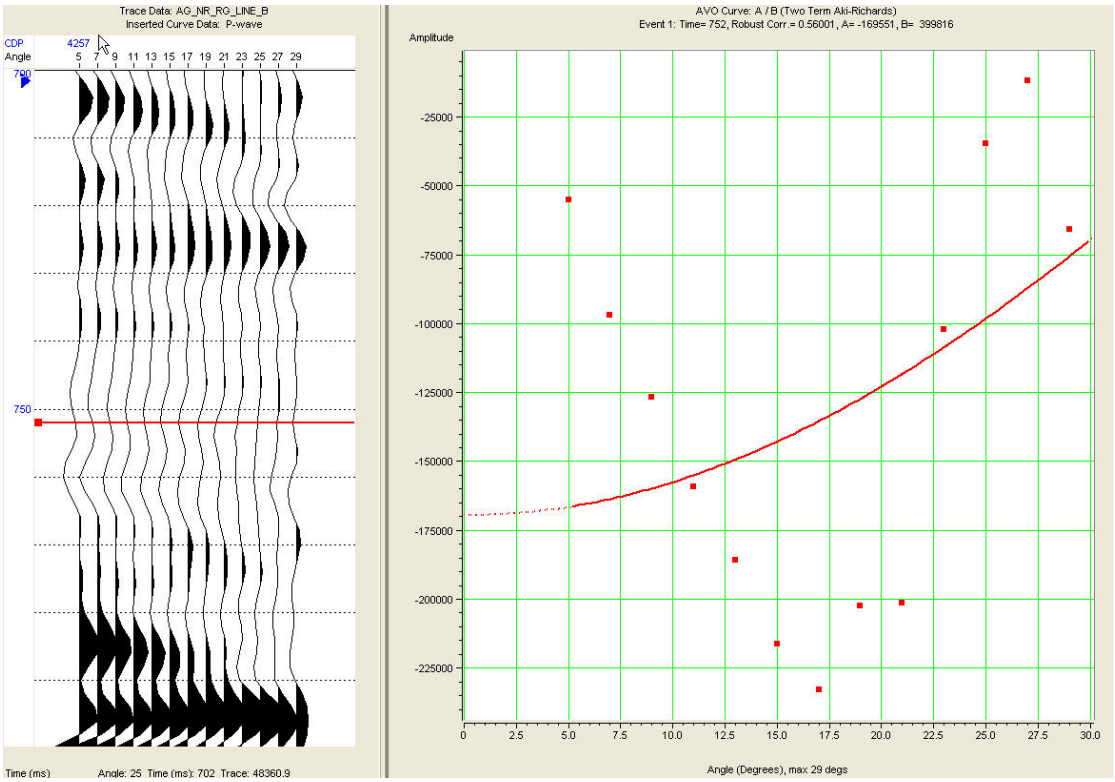

No coherent anomaly at CDP 4257

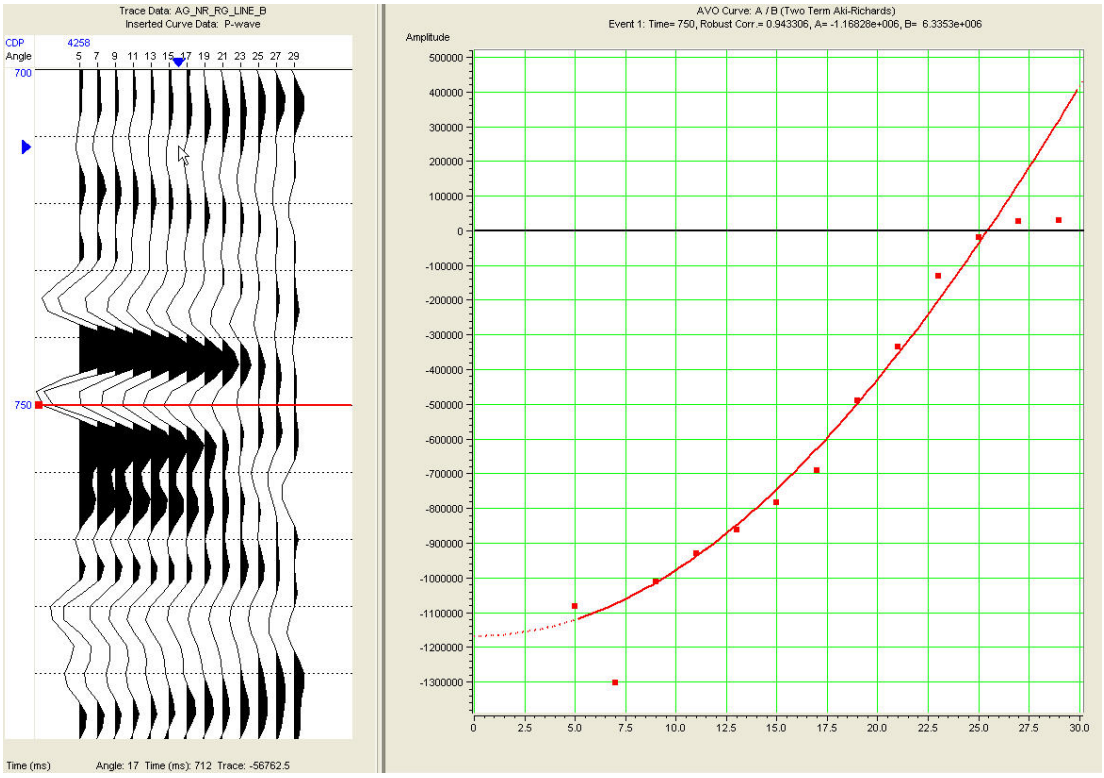

Class IV anomaly at CDP 4258

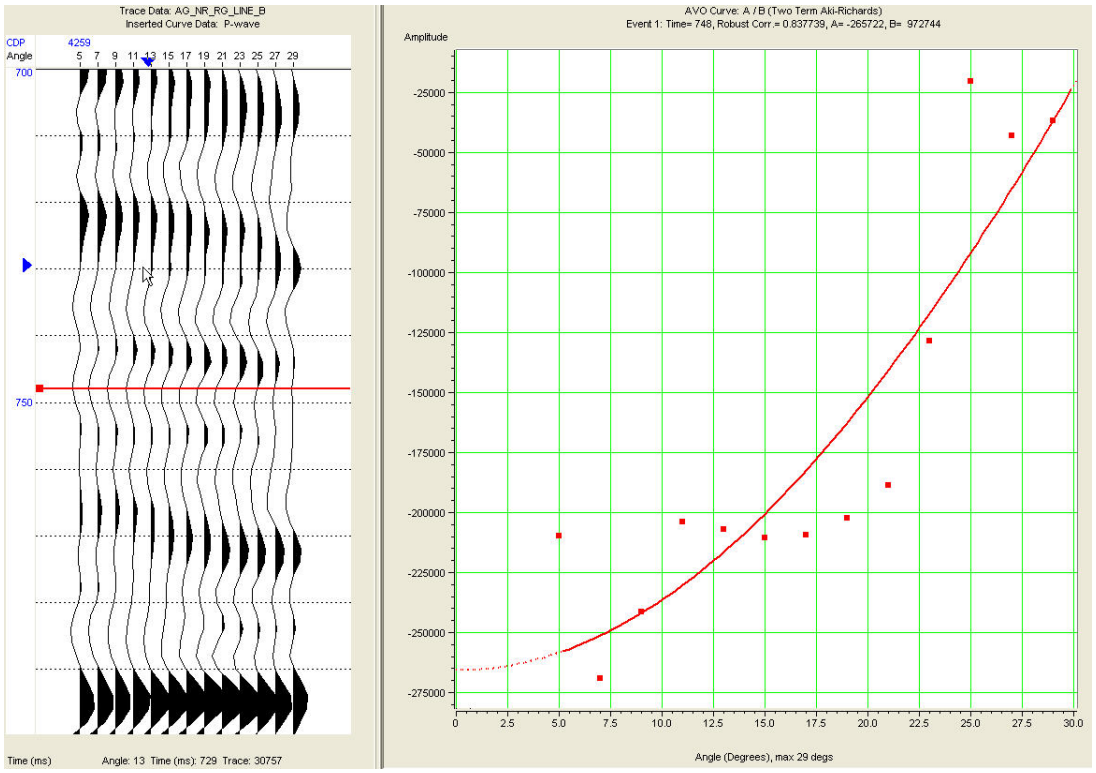

Weak Class IV Anomaly at CDP 4259

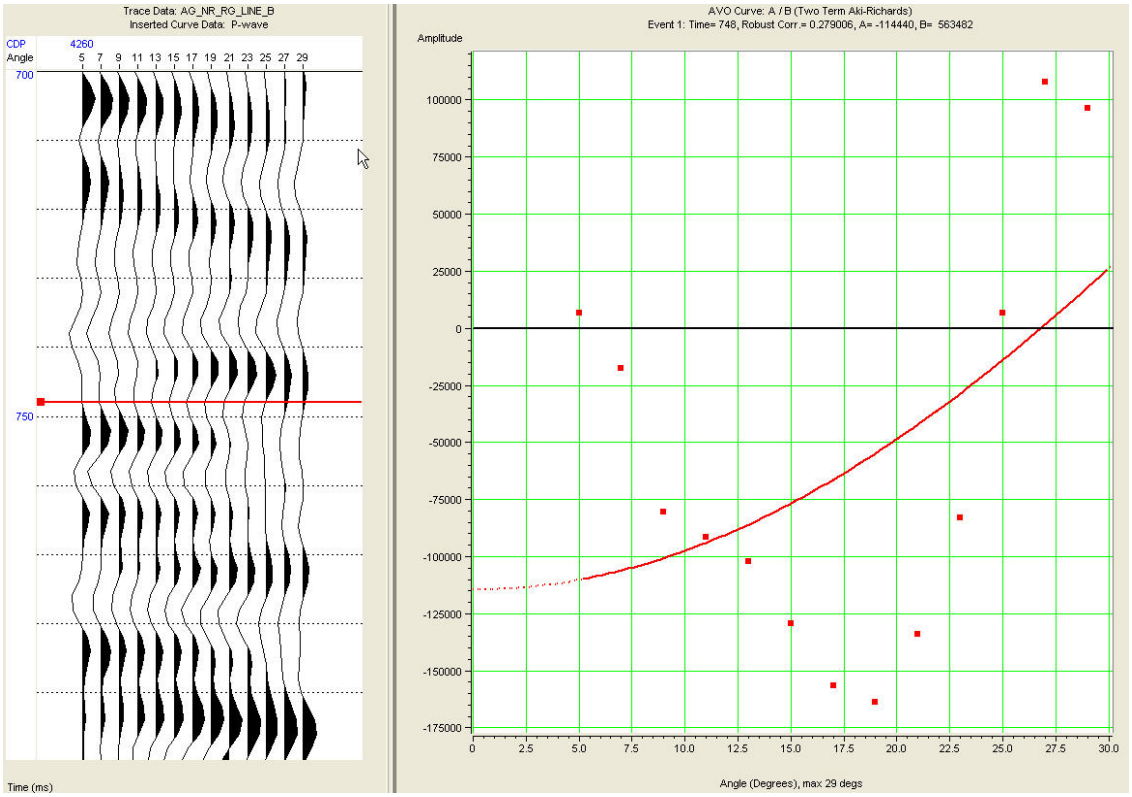

No coherent anomaly at CDP 4260

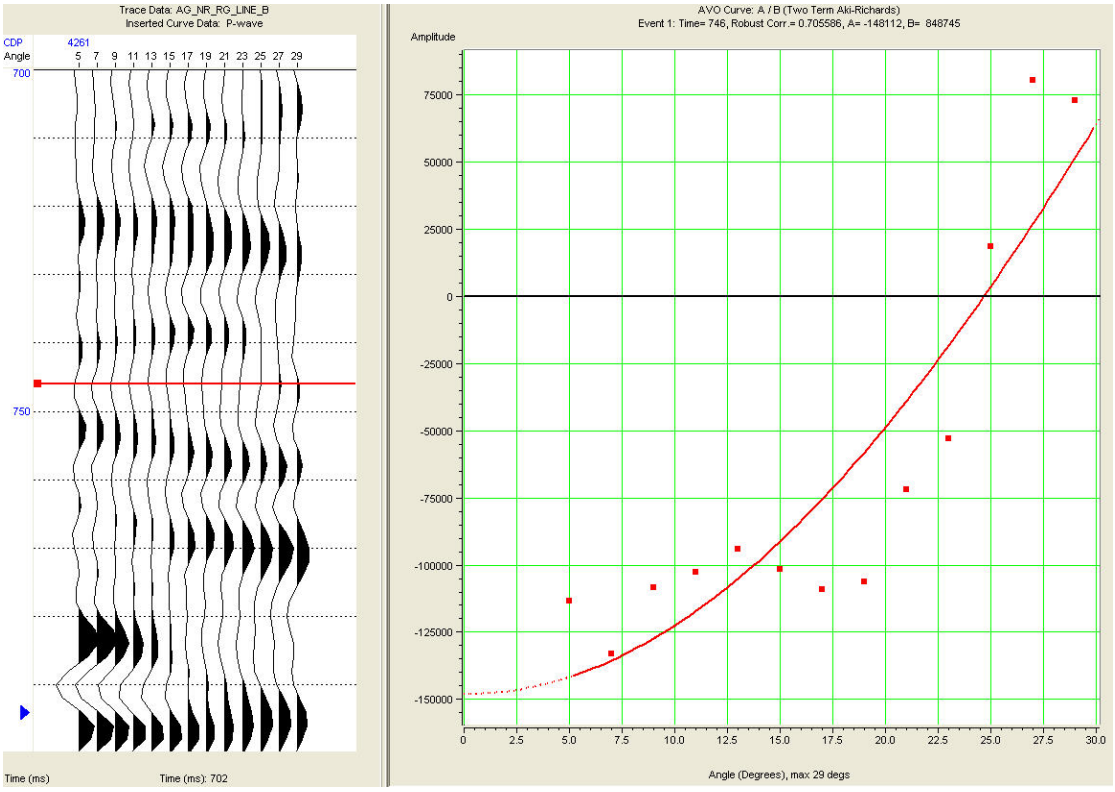

Weak Class IV anomaly at CDP 4261

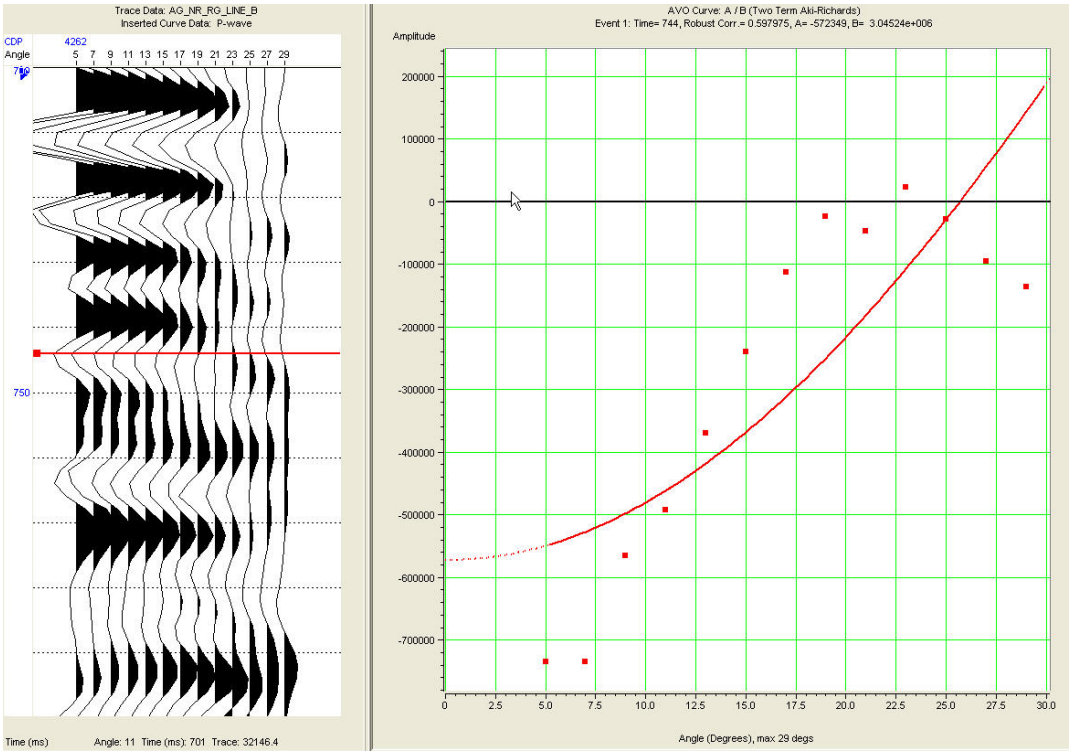

Weak Class IV anomaly at CDP 4262

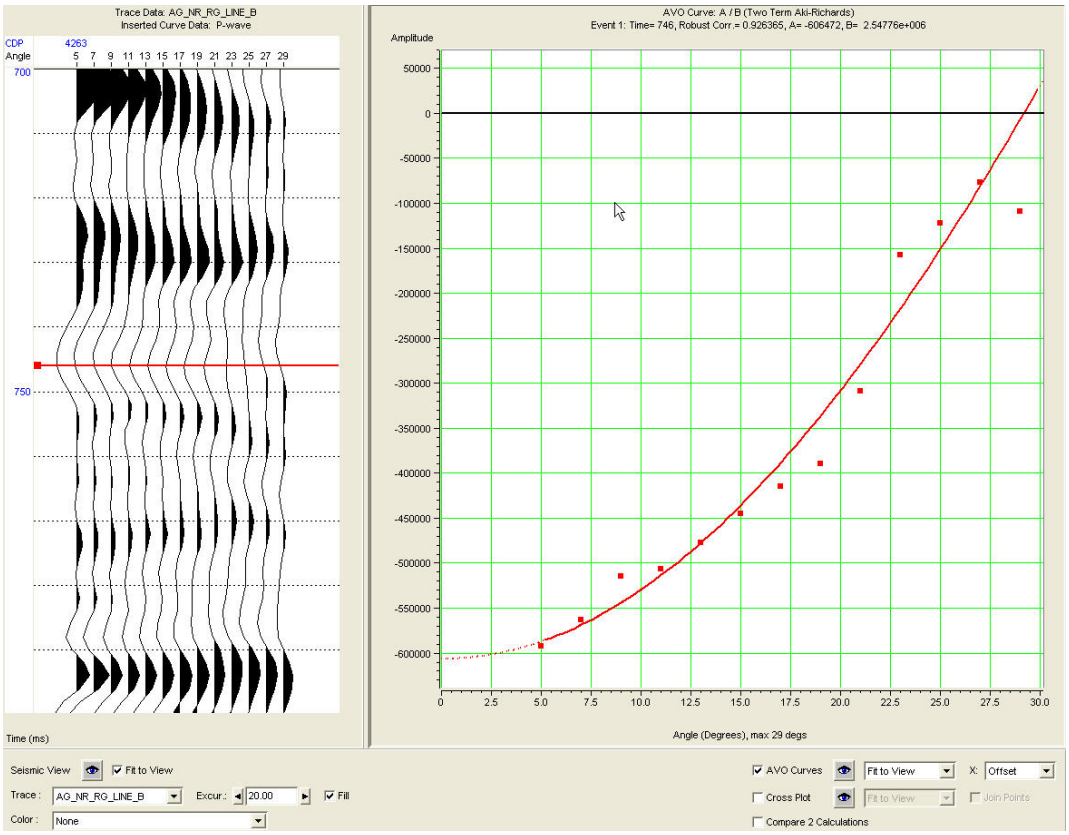

Class IV anomaly at CDP 4263

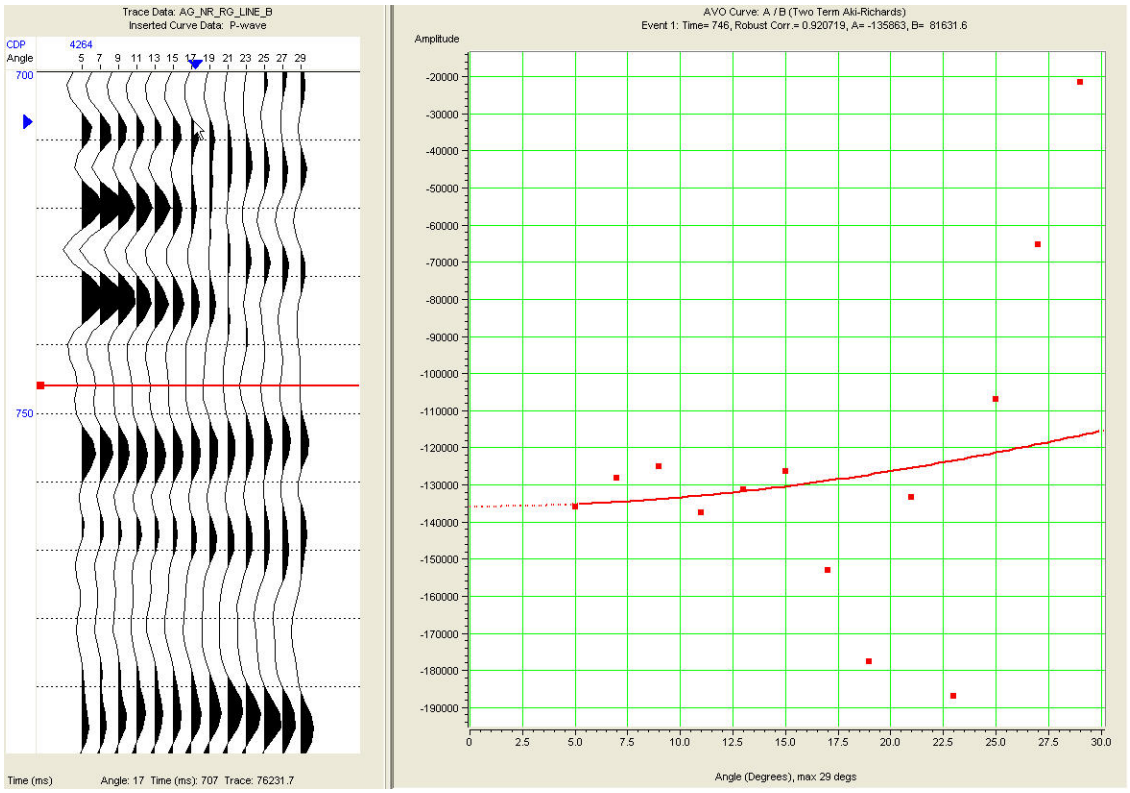

No coherent anomaly at CDP 4264

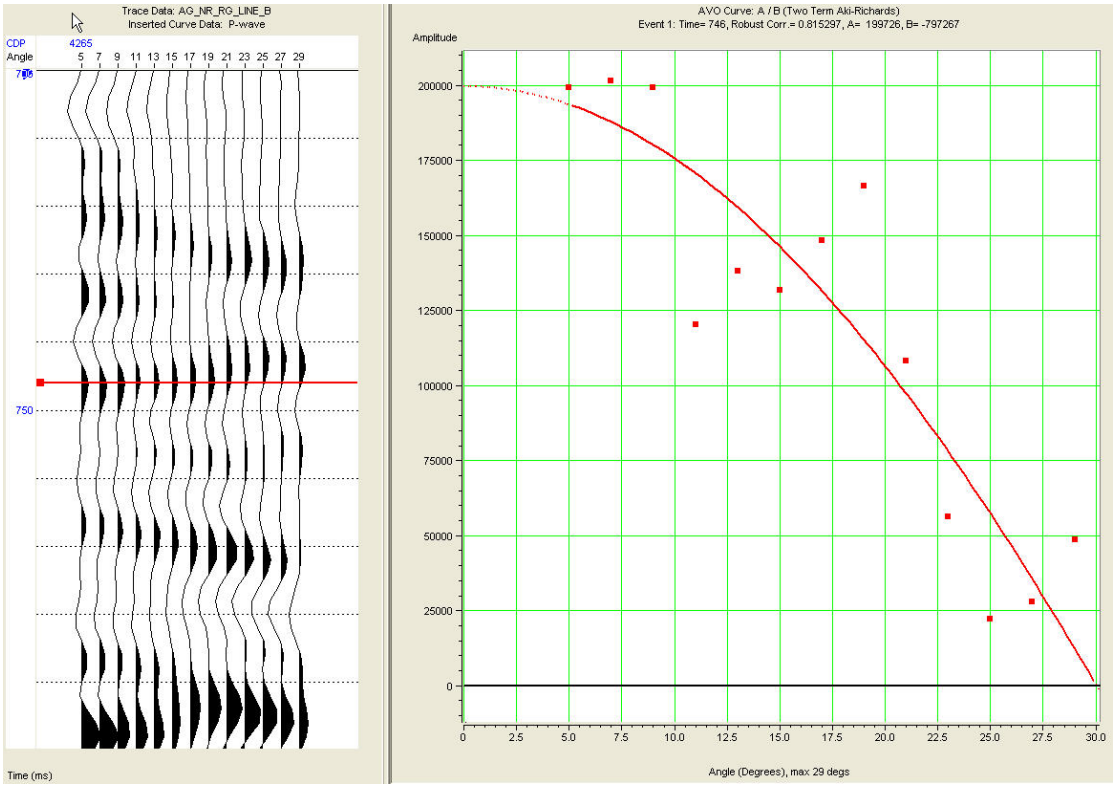

No coherent anomaly at CDP 4265

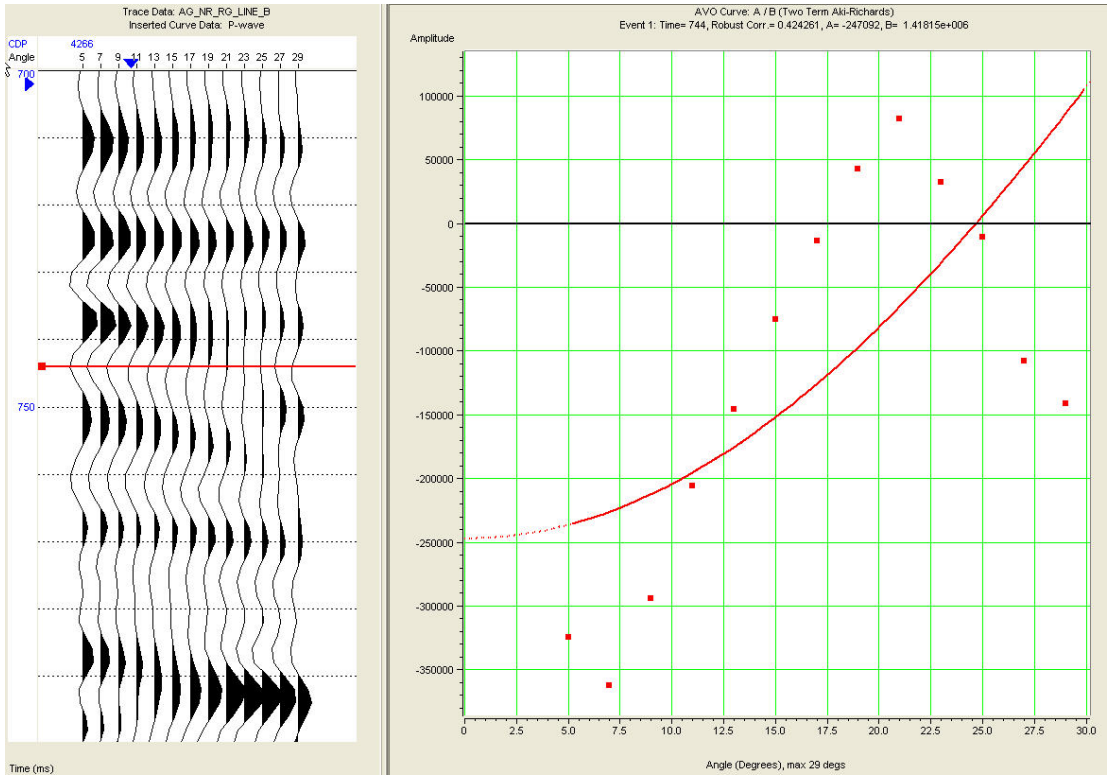

No coherent anomaly at CDP 4266

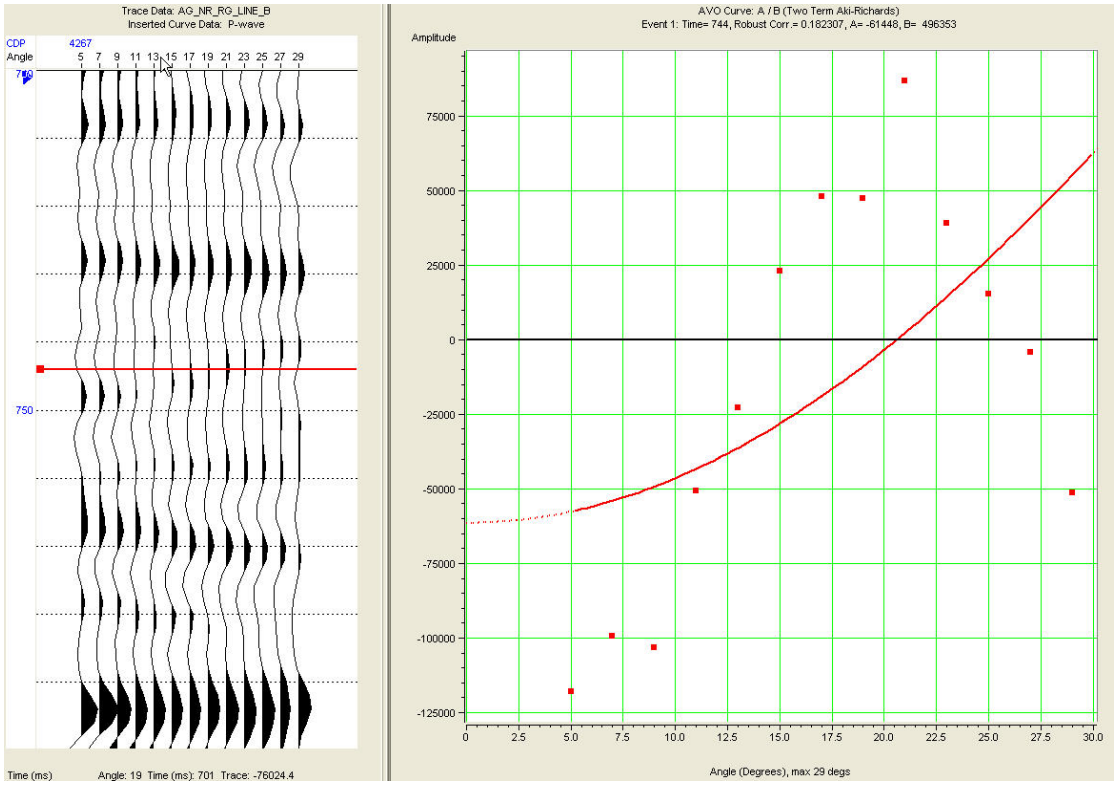

No coherent anomaly at CDP 4267

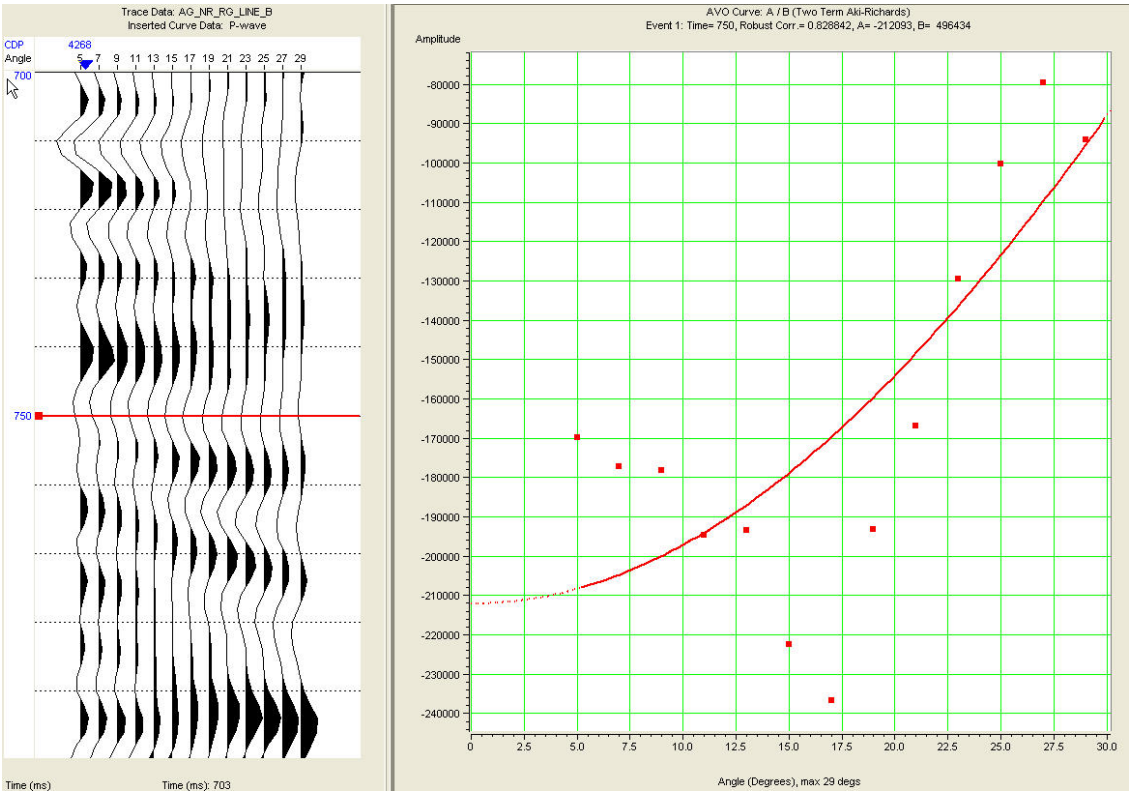

No coherent anomaly at CDP 4268

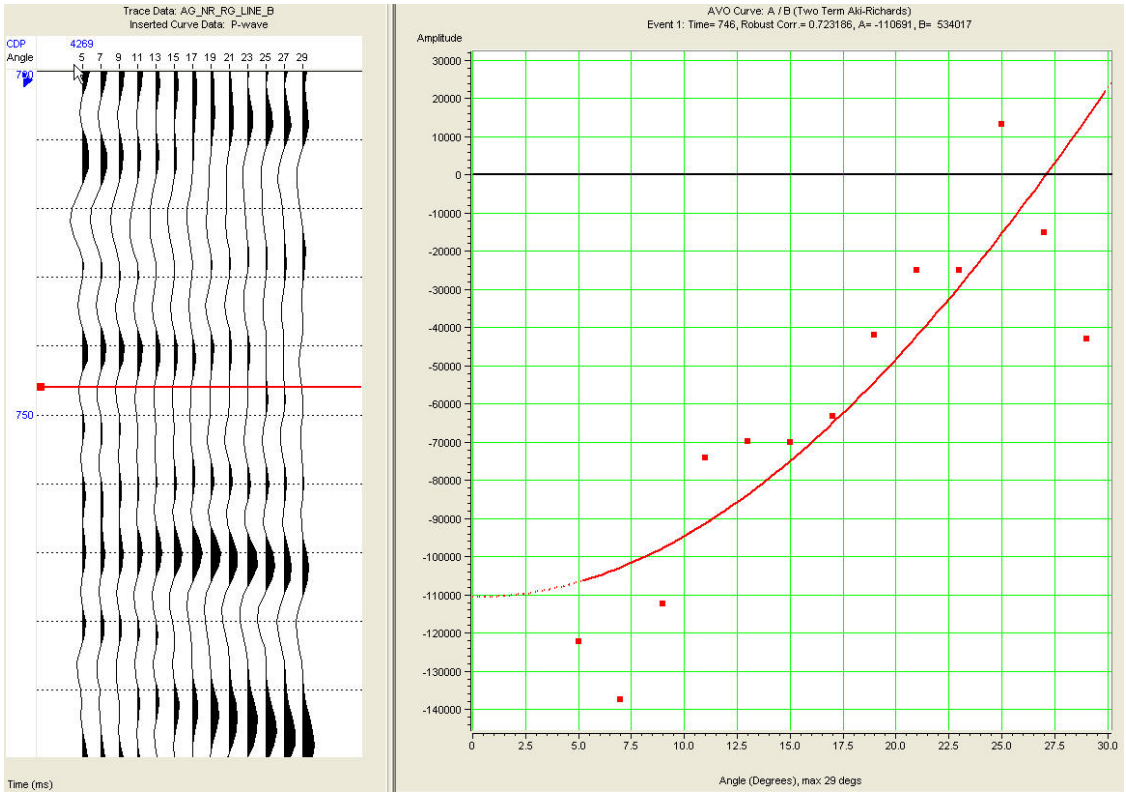

Weak class IV anomaly at CDP 4269

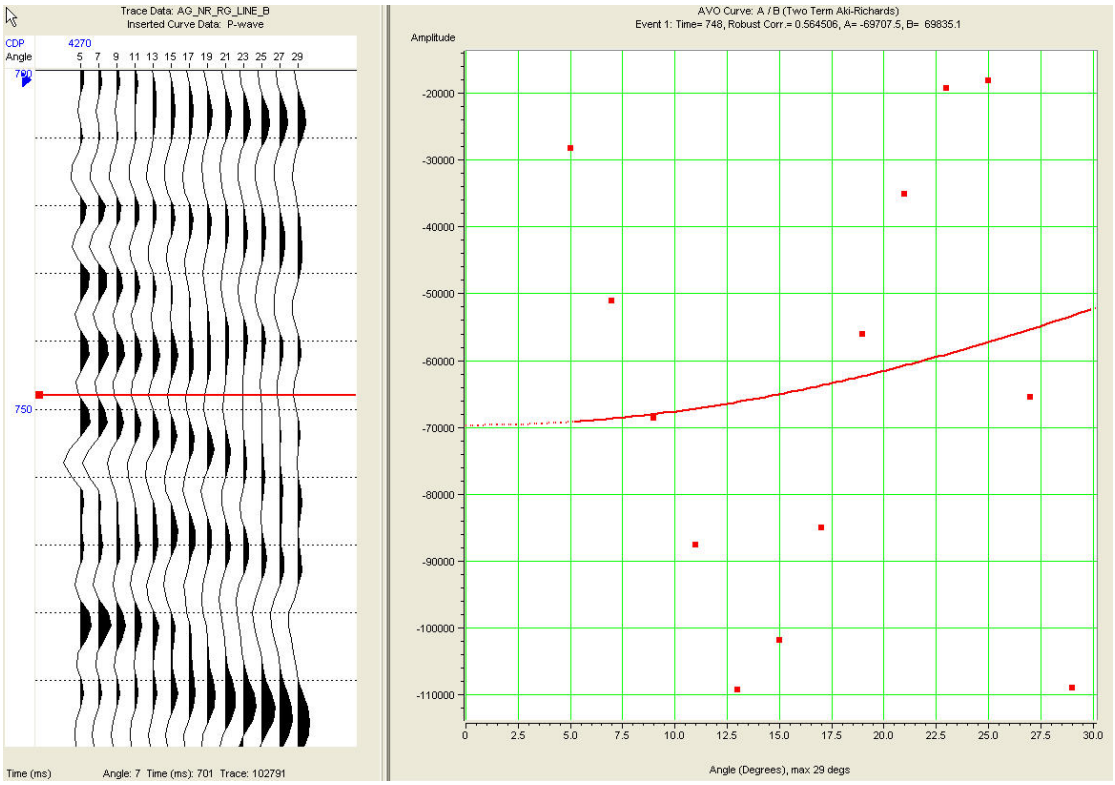

No coherent anomaly at CDP 4270

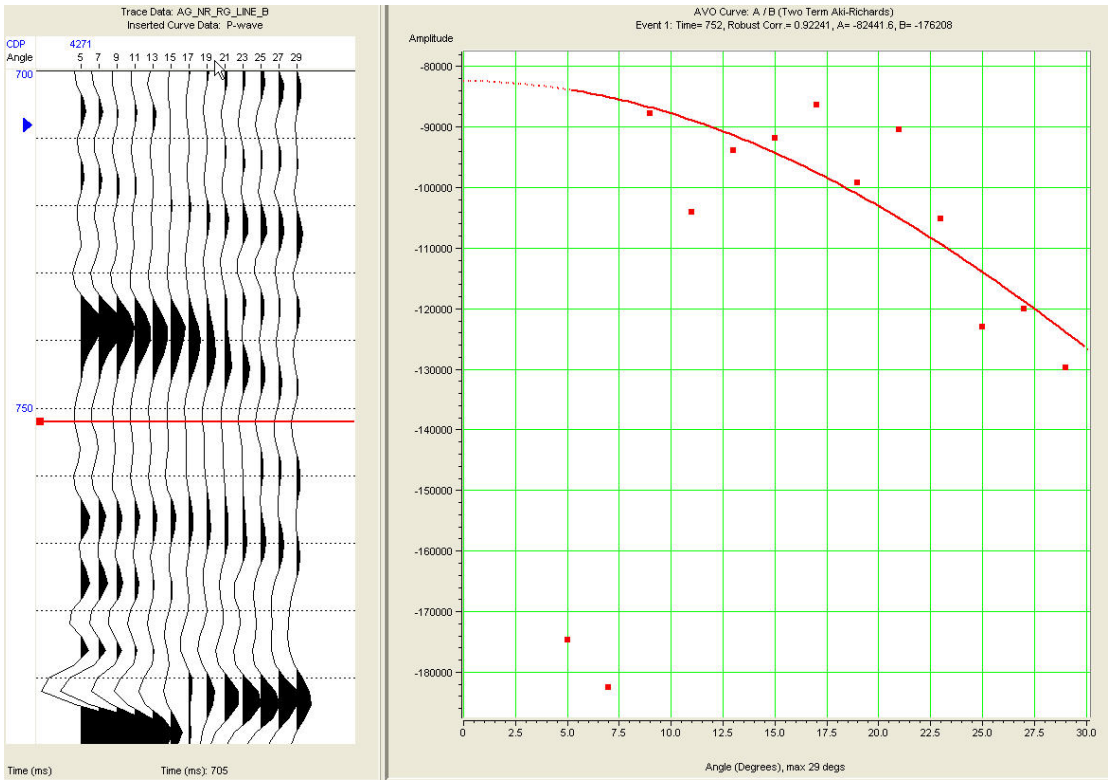

Class IV anomaly at CDP 4271

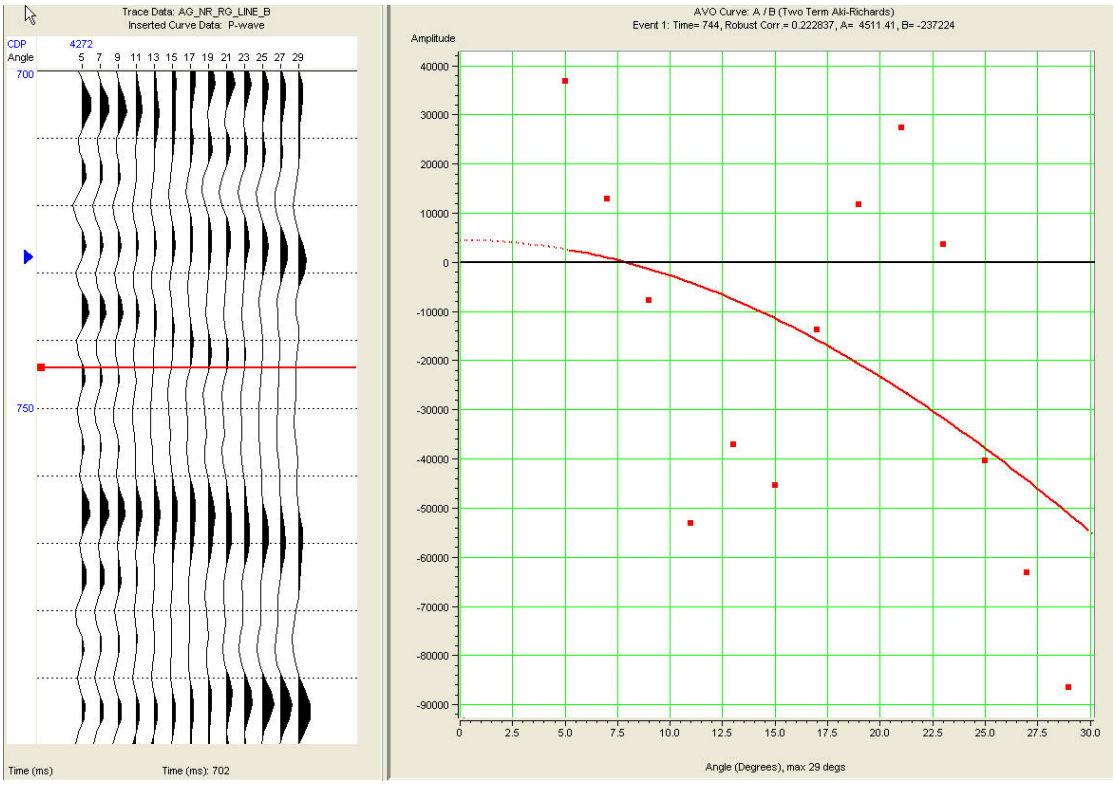

No coherent anomaly at CDP 4272

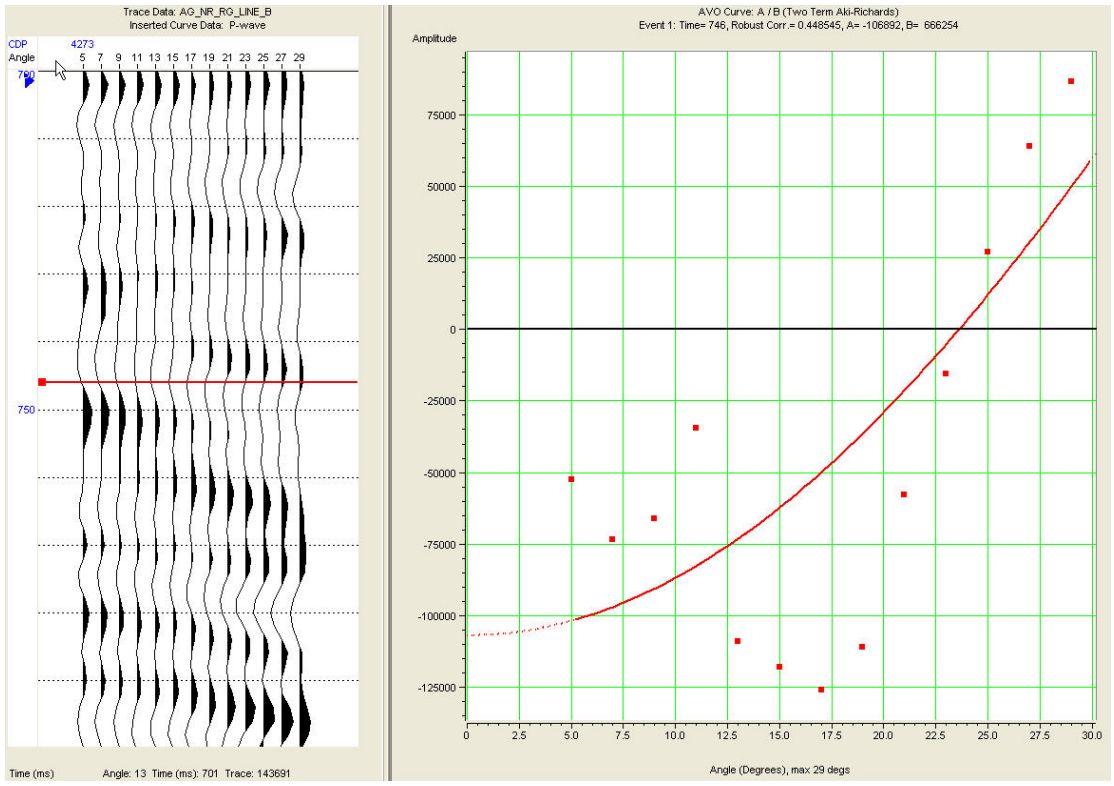

No coherent anomaly at CDP 4273

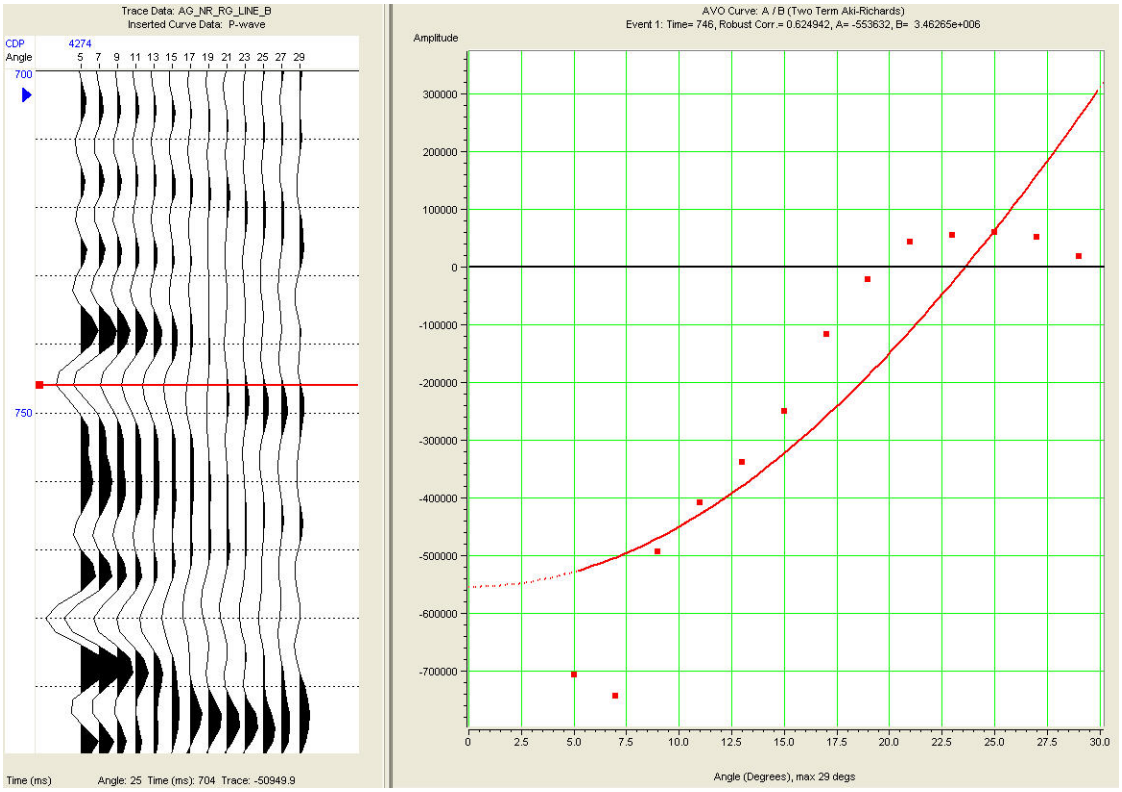

Weak Class IV anomaly at CDP 4274

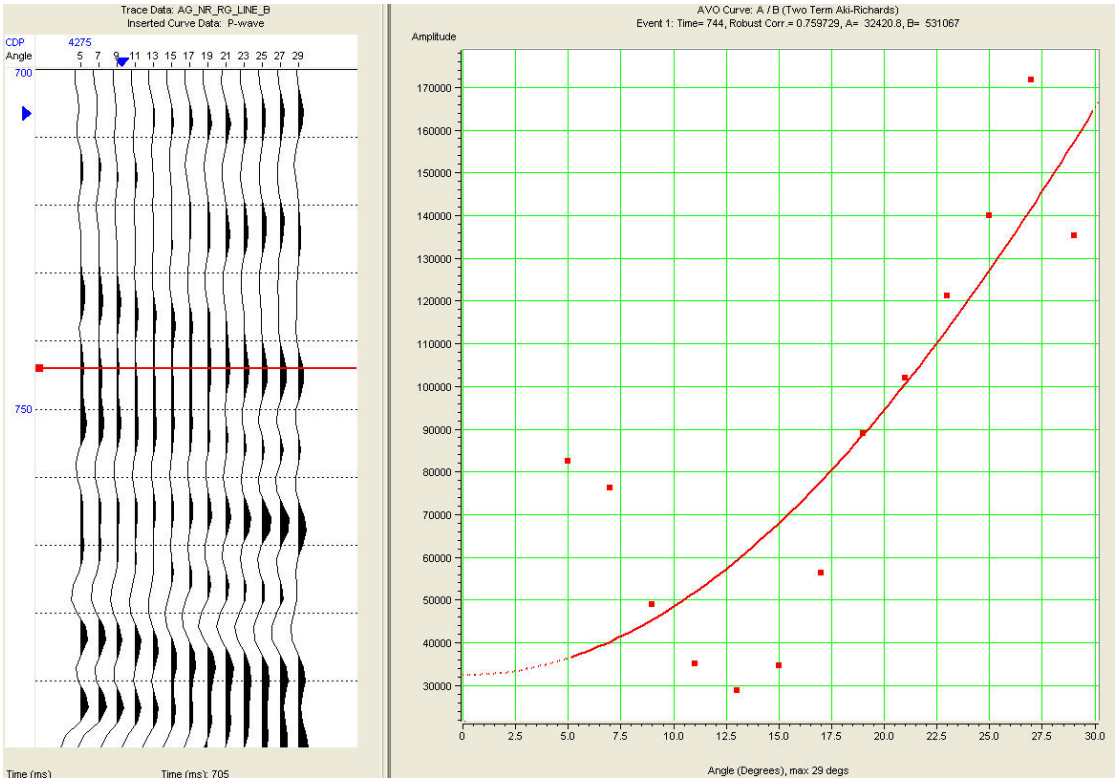

No coherent anomaly at CDP 4275

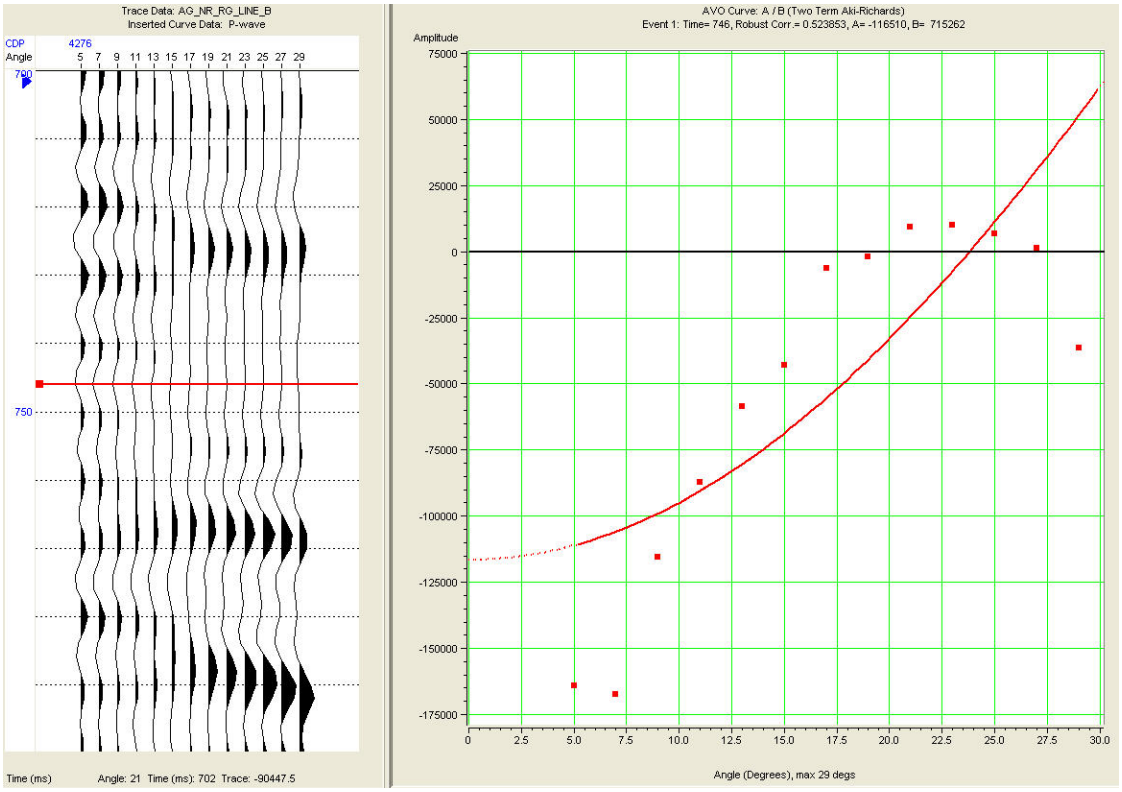

No coherent anomaly at CDP 4276

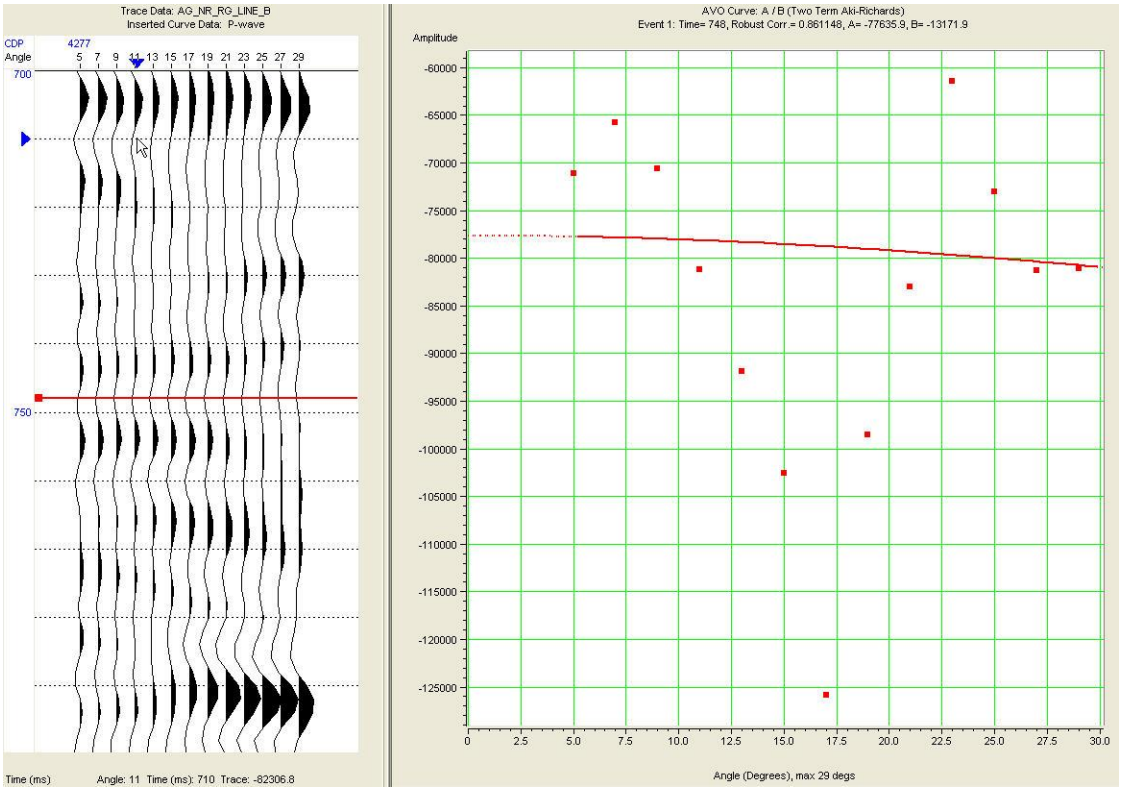

No coherent anomaly at CDP 4277

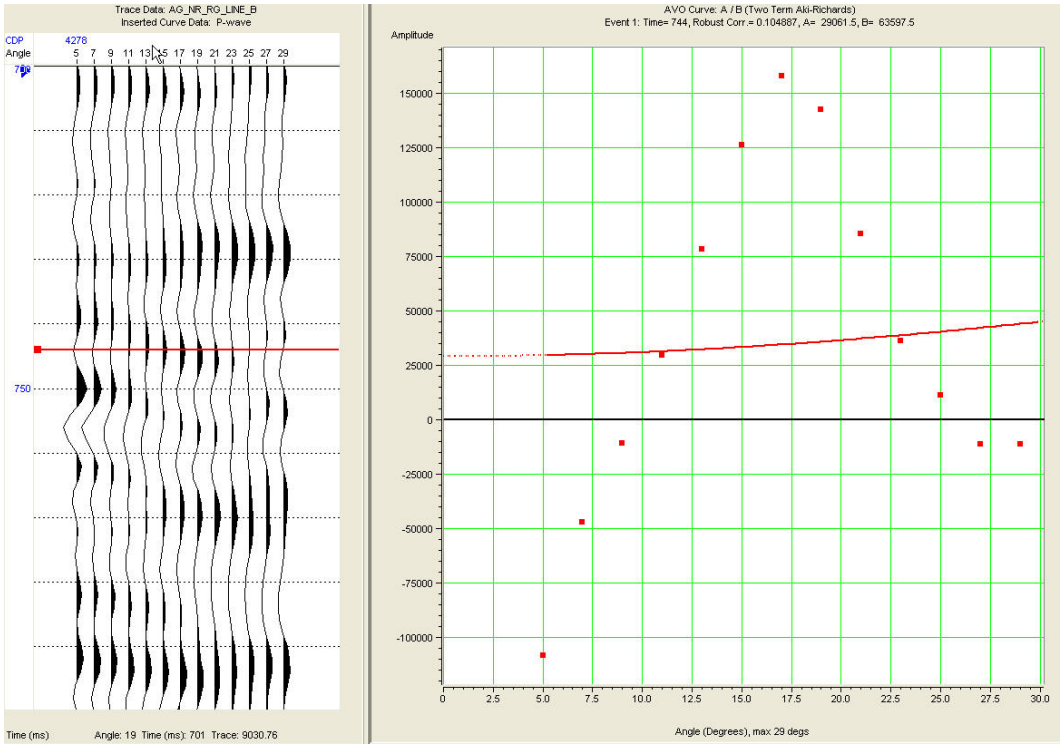

No coherent anomaly at CDP 4278

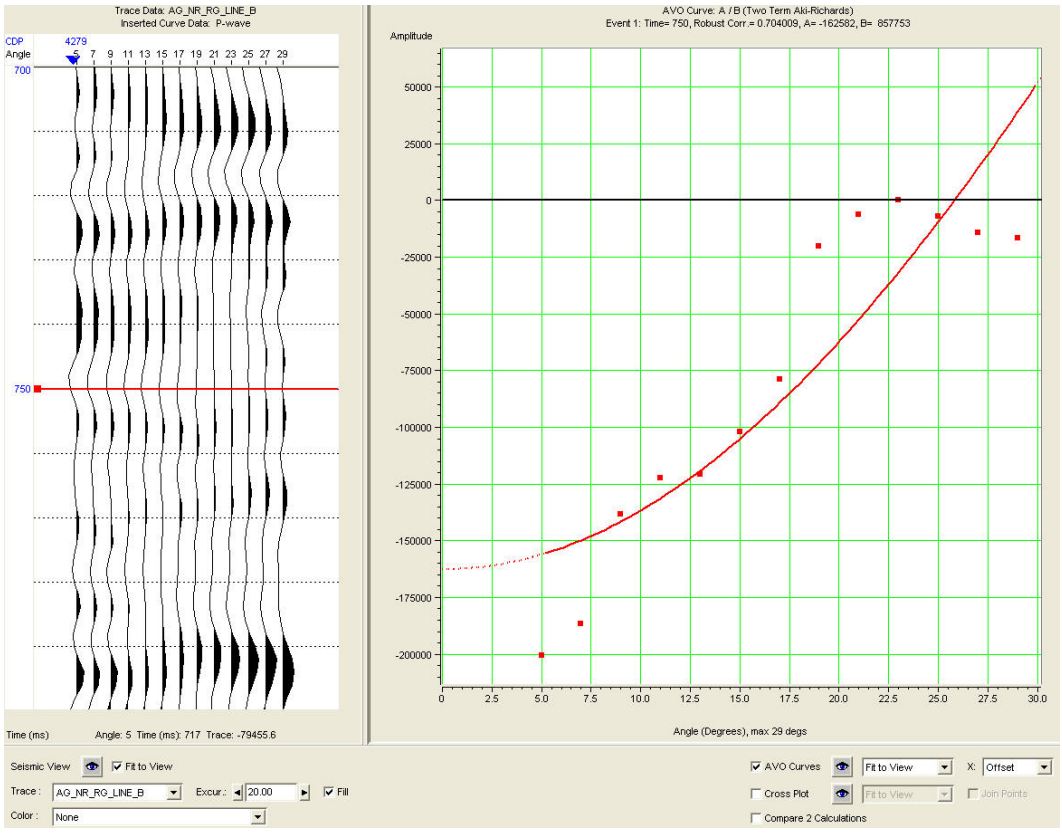

Weak Class IV anomaly at CDP 4279

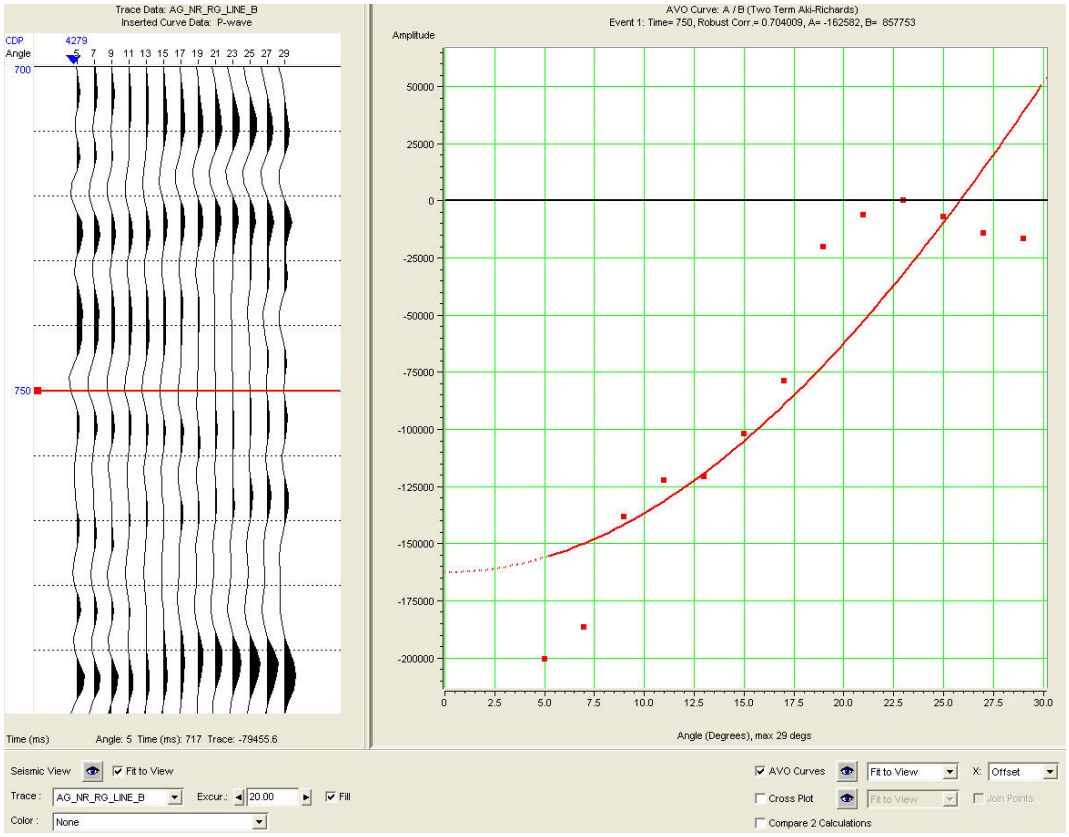

Weak Class IV anomaly at CDP 4280

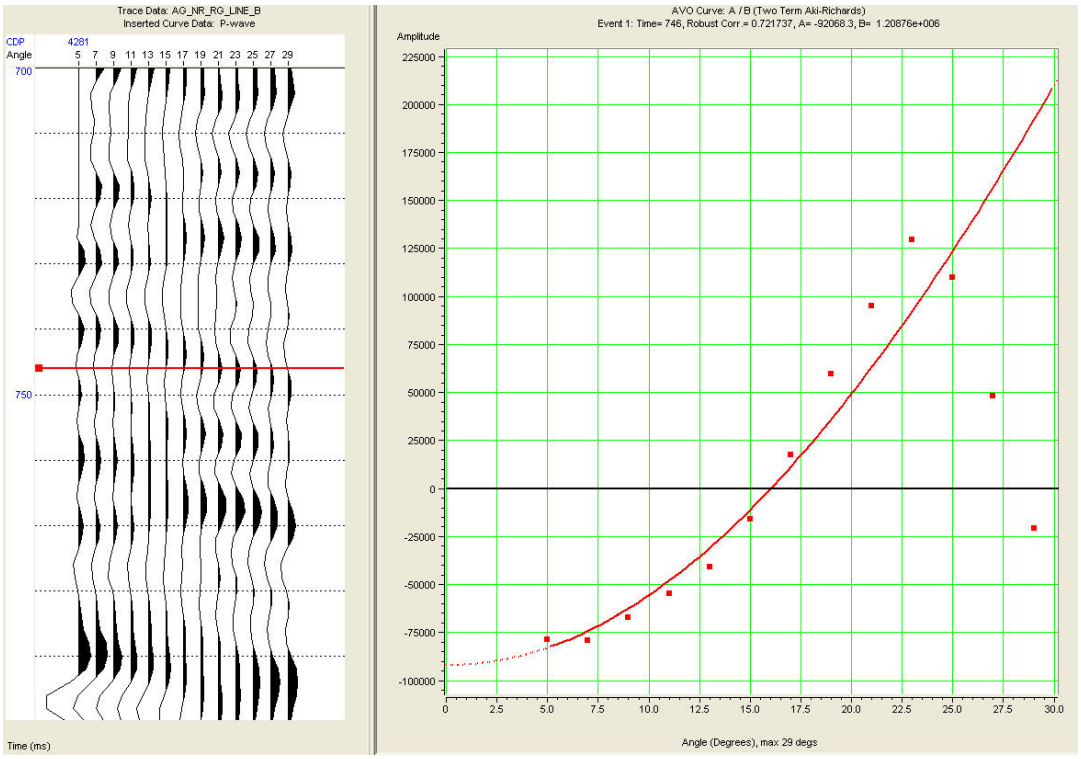

No coherent anomaly at CDP 4281

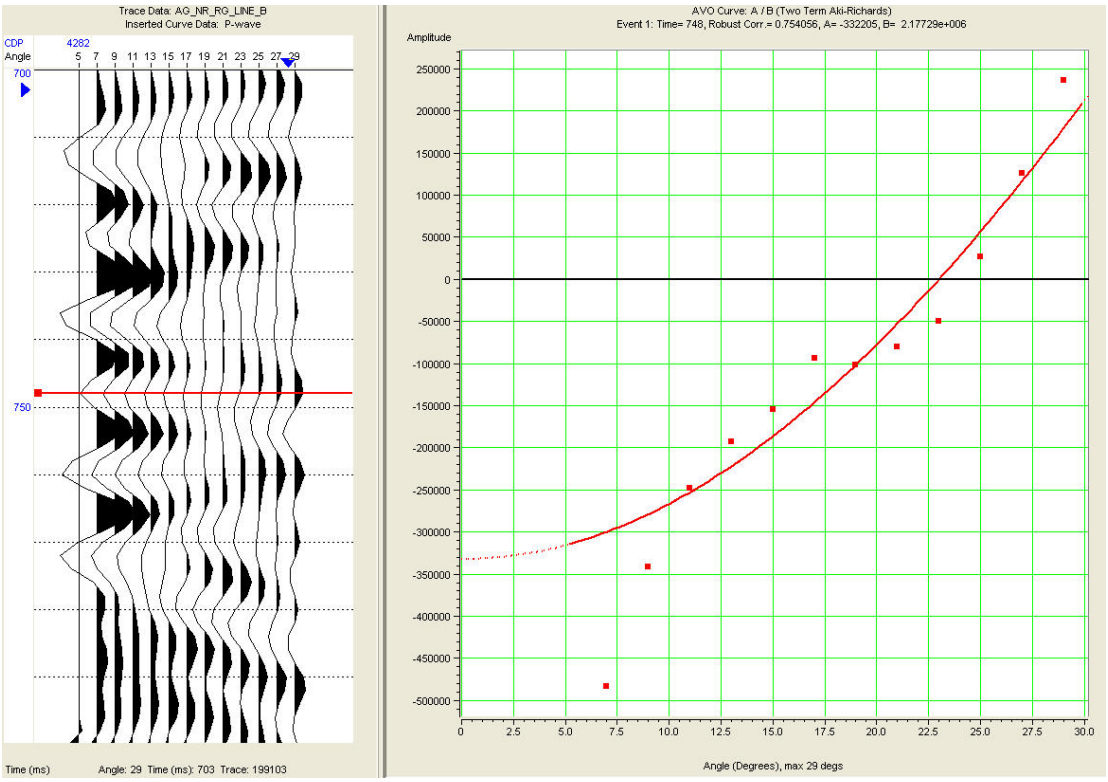

Class IV anomaly at CDP 4282

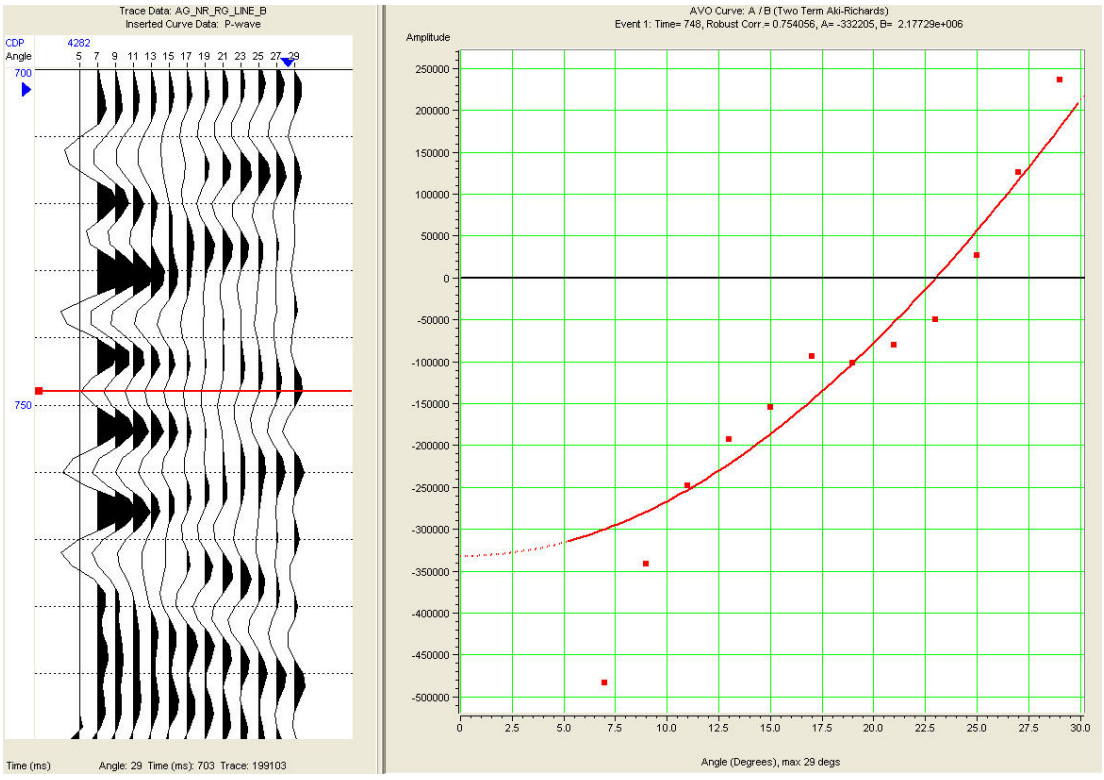

Class IV anomaly at CDP 4283

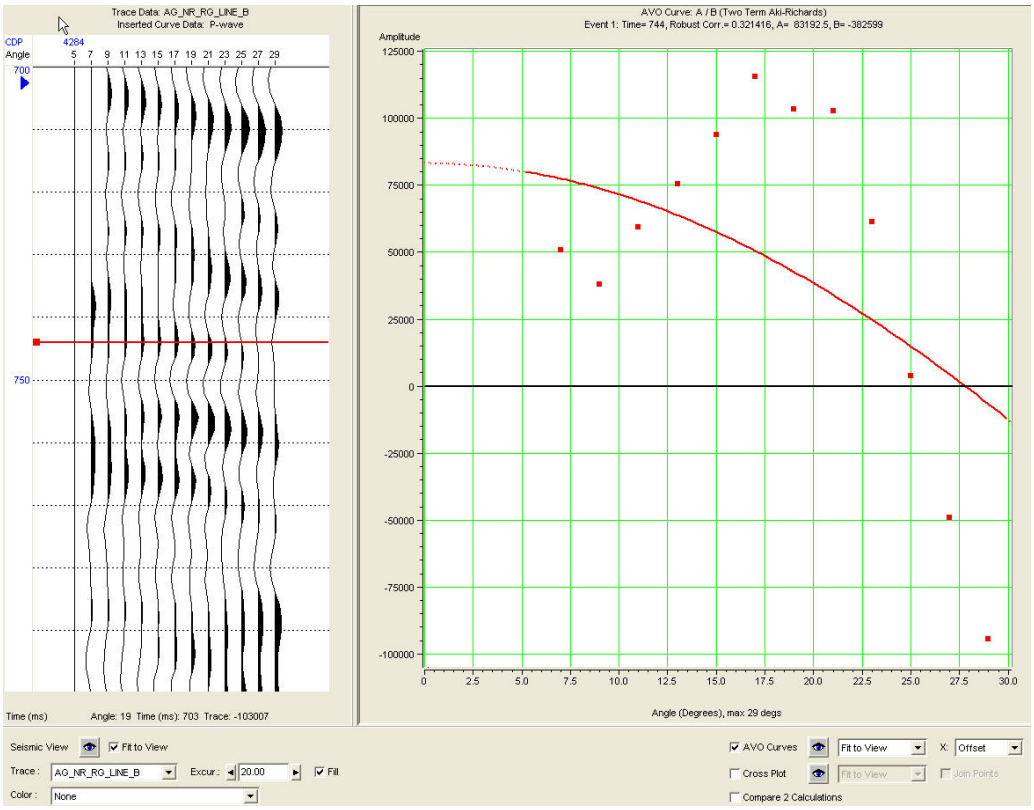

No coherent anomaly at CDP 4284

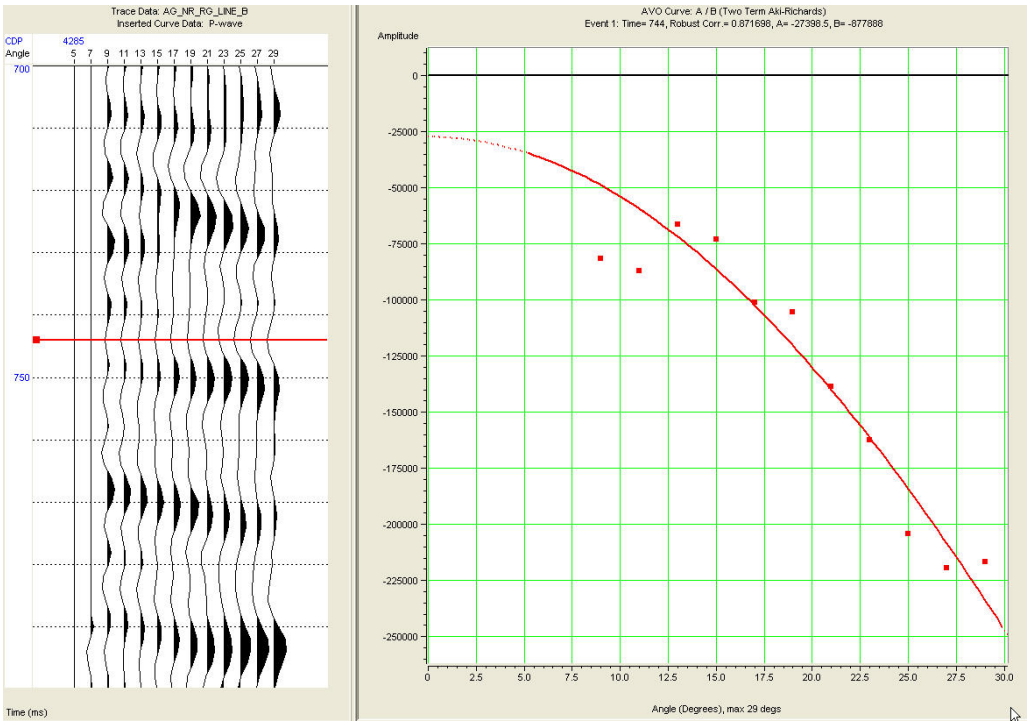

Class III anomaly at CDP 4285

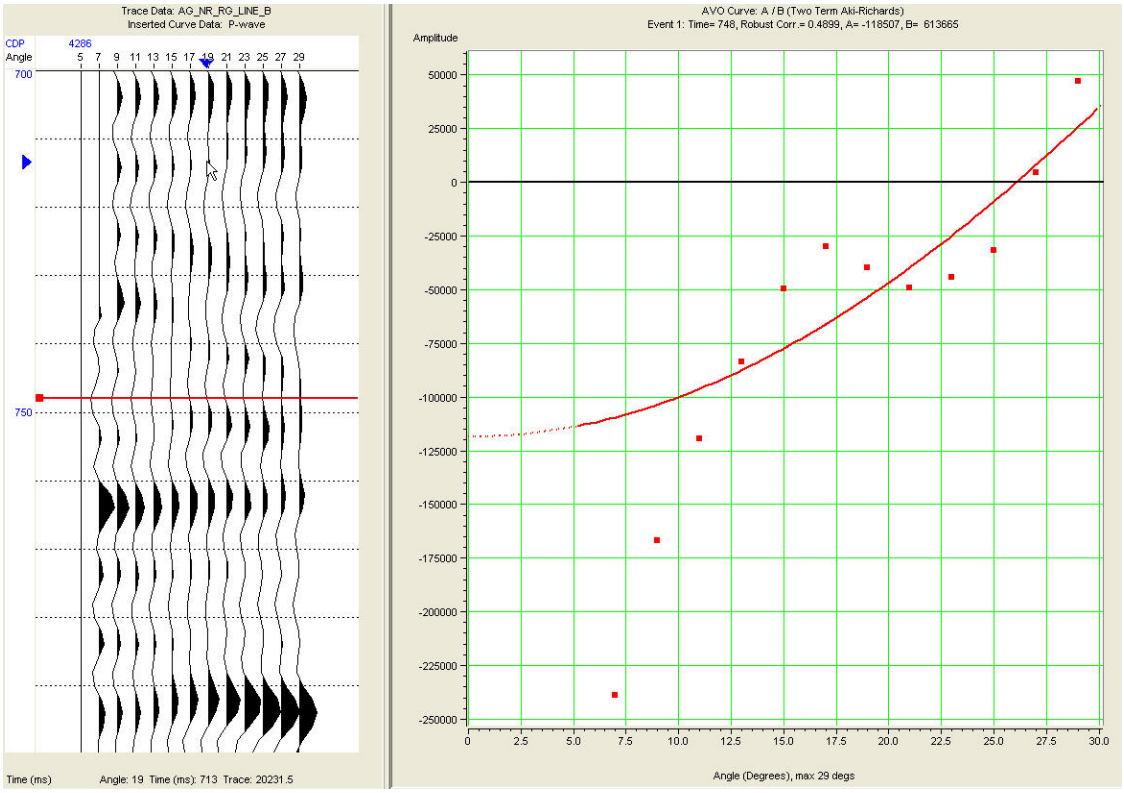

Weak Class IV anomaly at CDP 4286

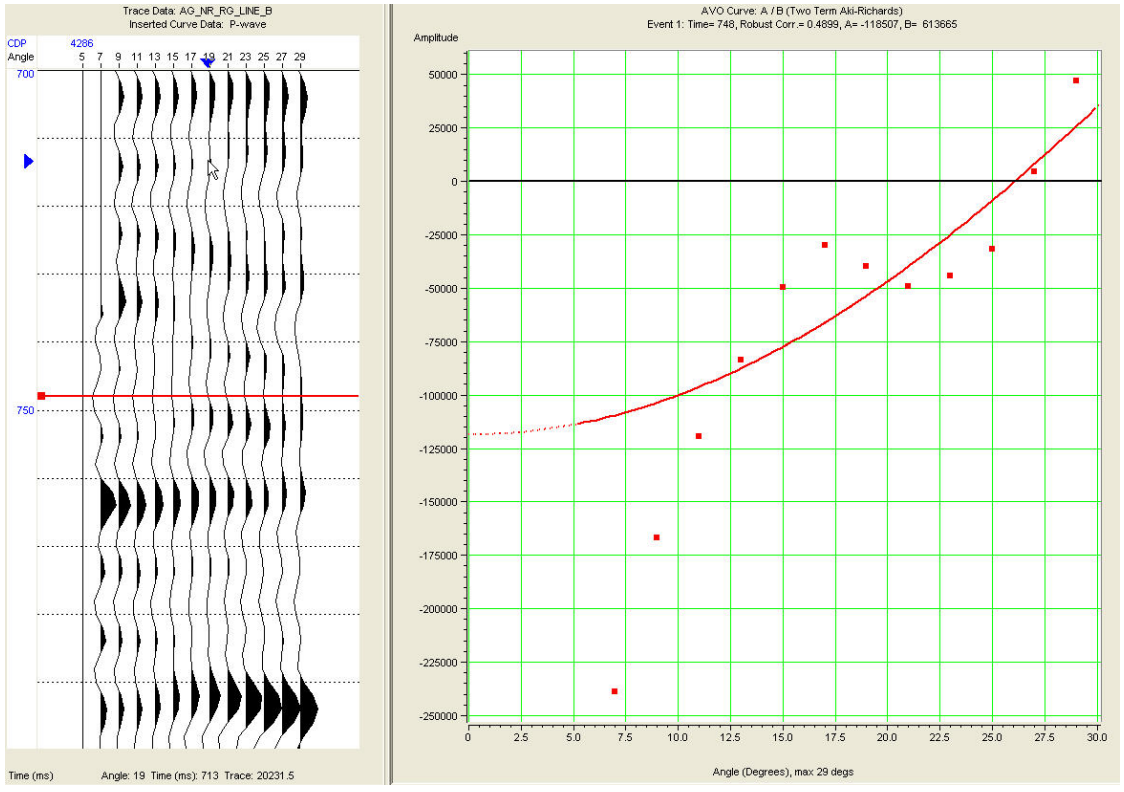

No coherent anomaly at CDP 4287 (low robustness)

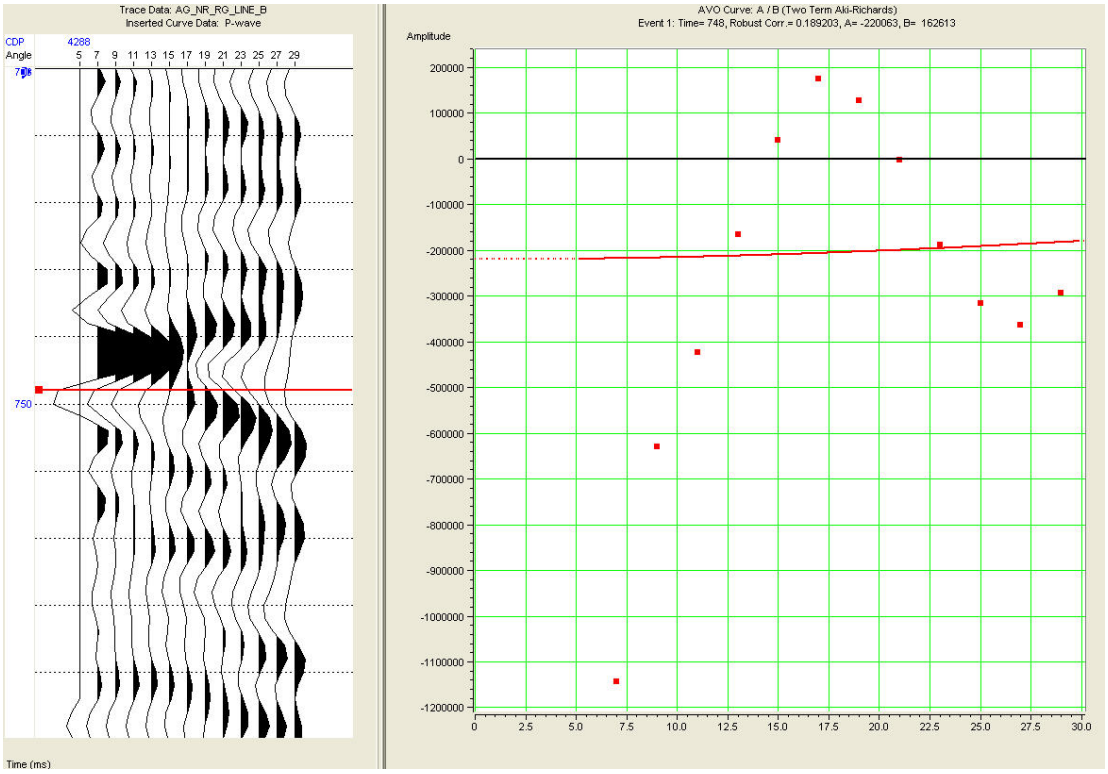

No coherent anomaly at CDP 4288

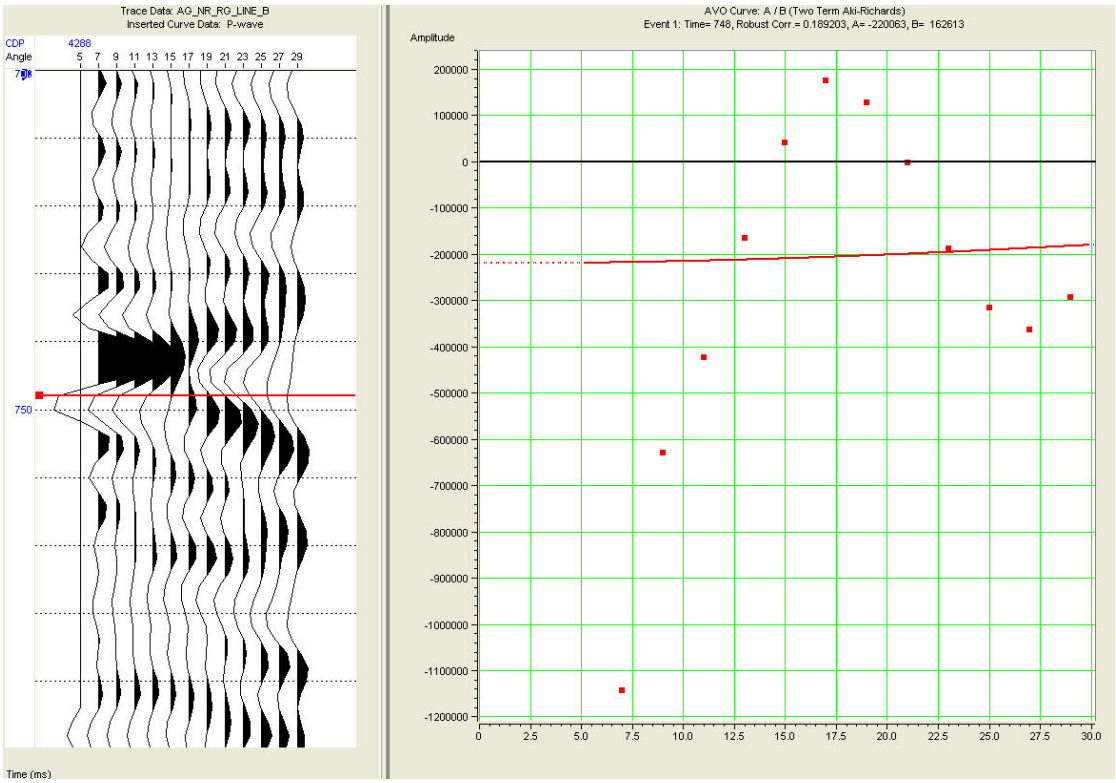

No coherent anomaly at CDP 4289

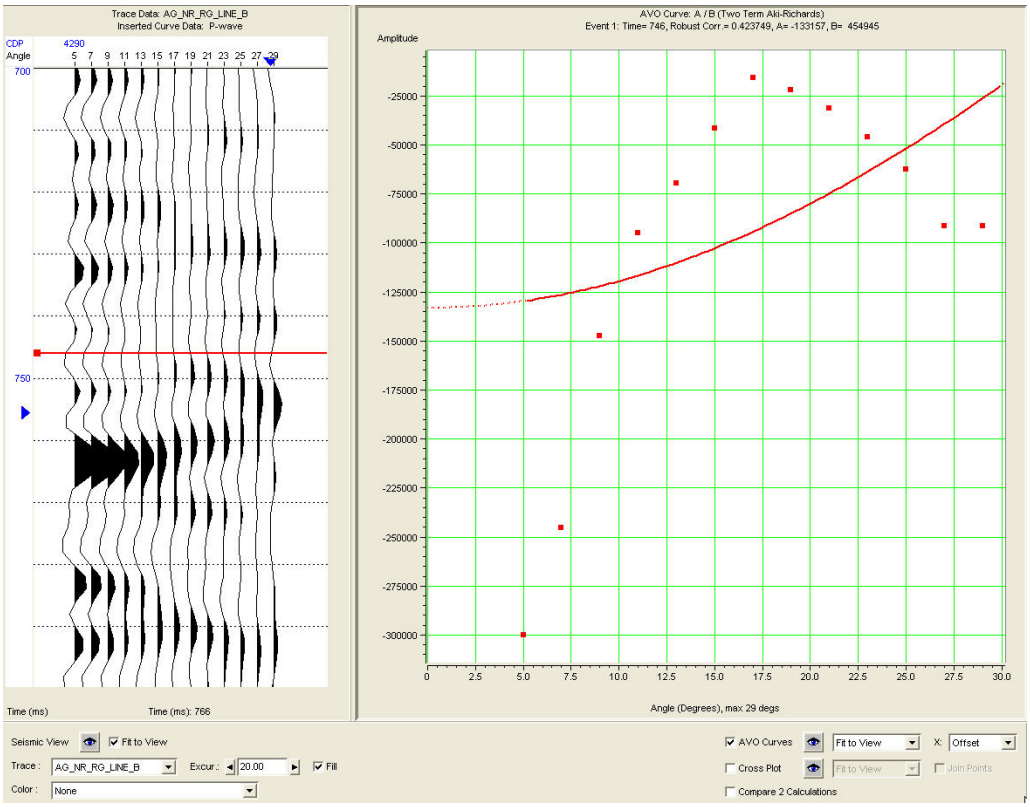

No coherent anomaly at CDP 4290

Gradient Analysis at Top of Utica Reflector between CDPs 4085-4100 over 736-744 ms

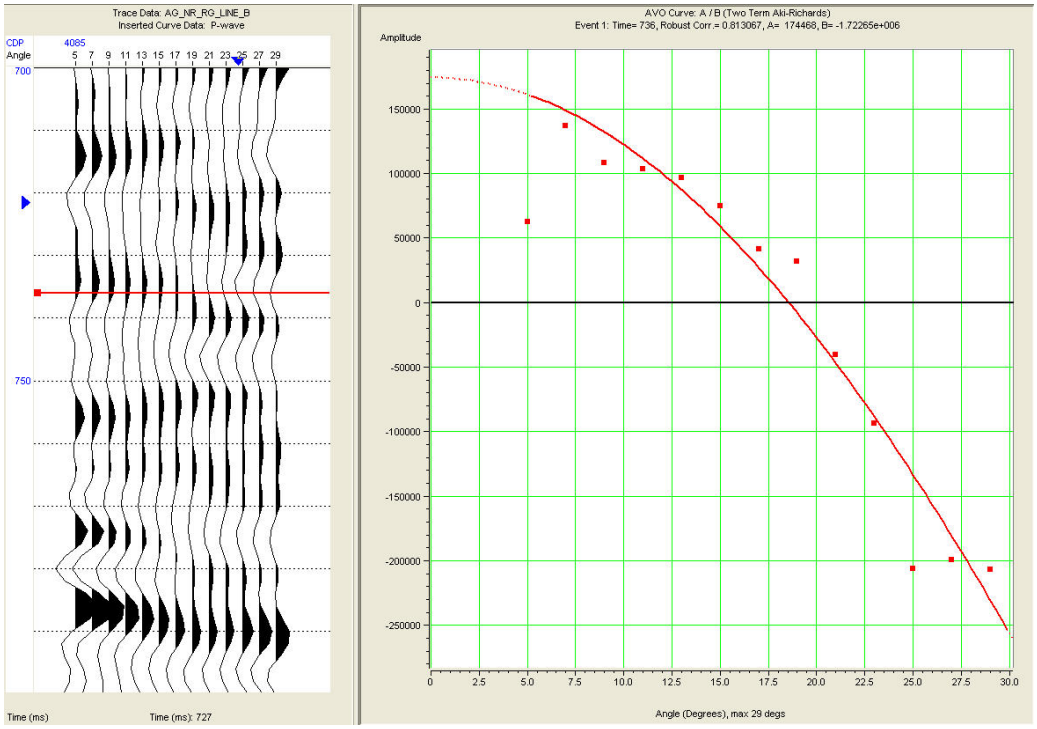

Class IIp anomaly at CDP 4085

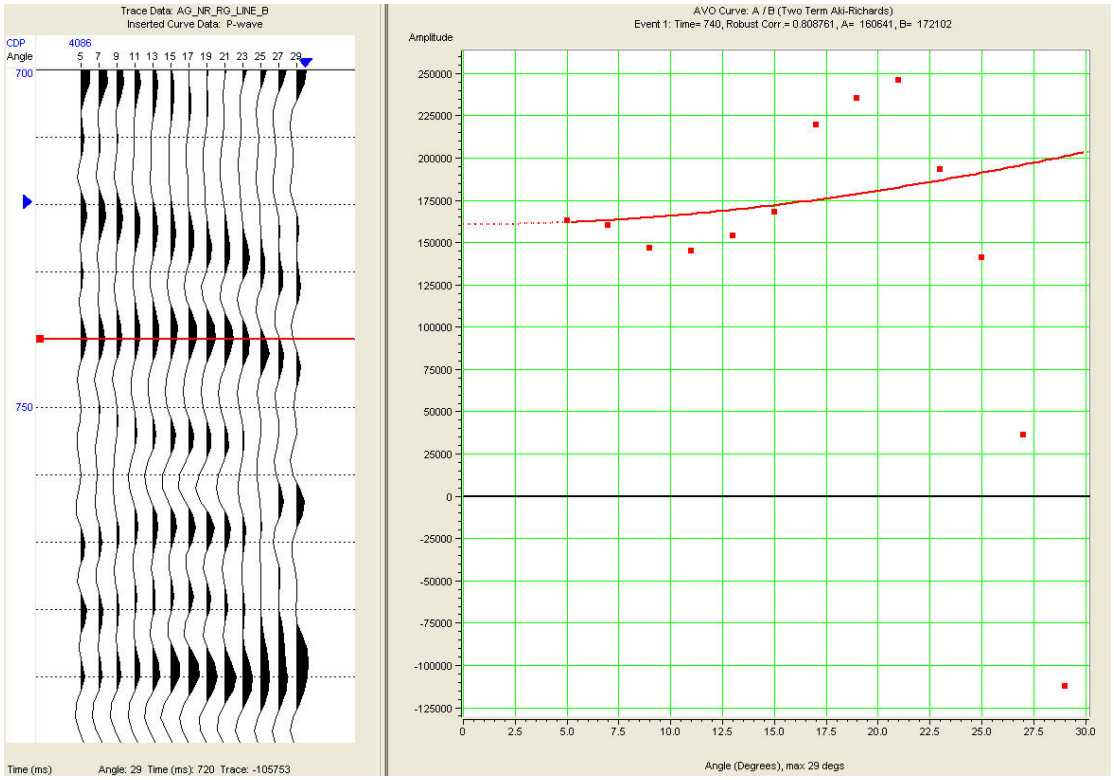

No coherent anomaly at CDP 4086

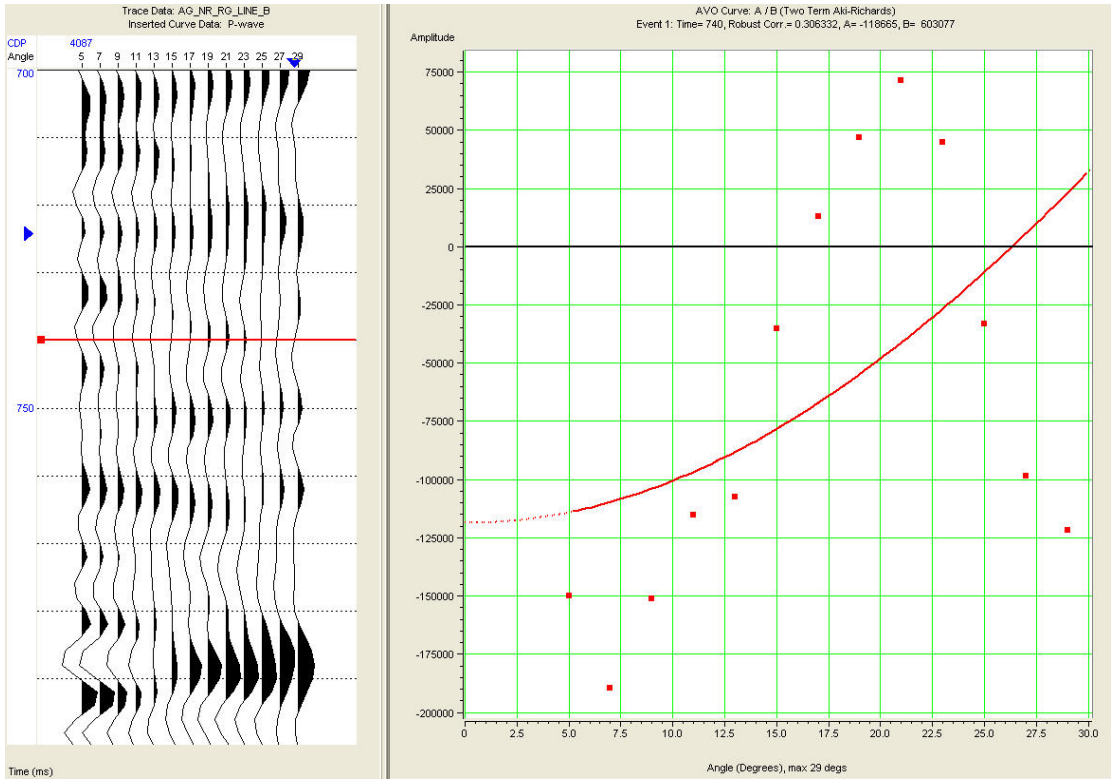

Weak Class IV anomaly at CDP 4087

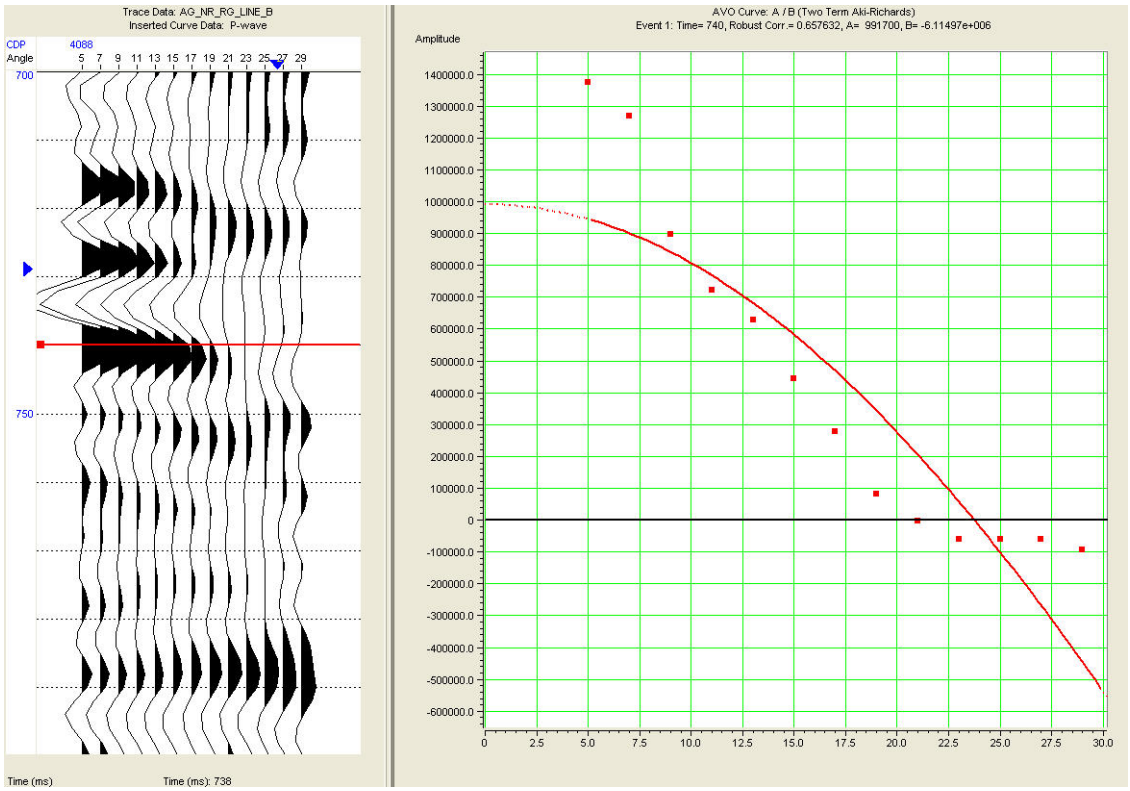

Class I anomaly at CDP 4088

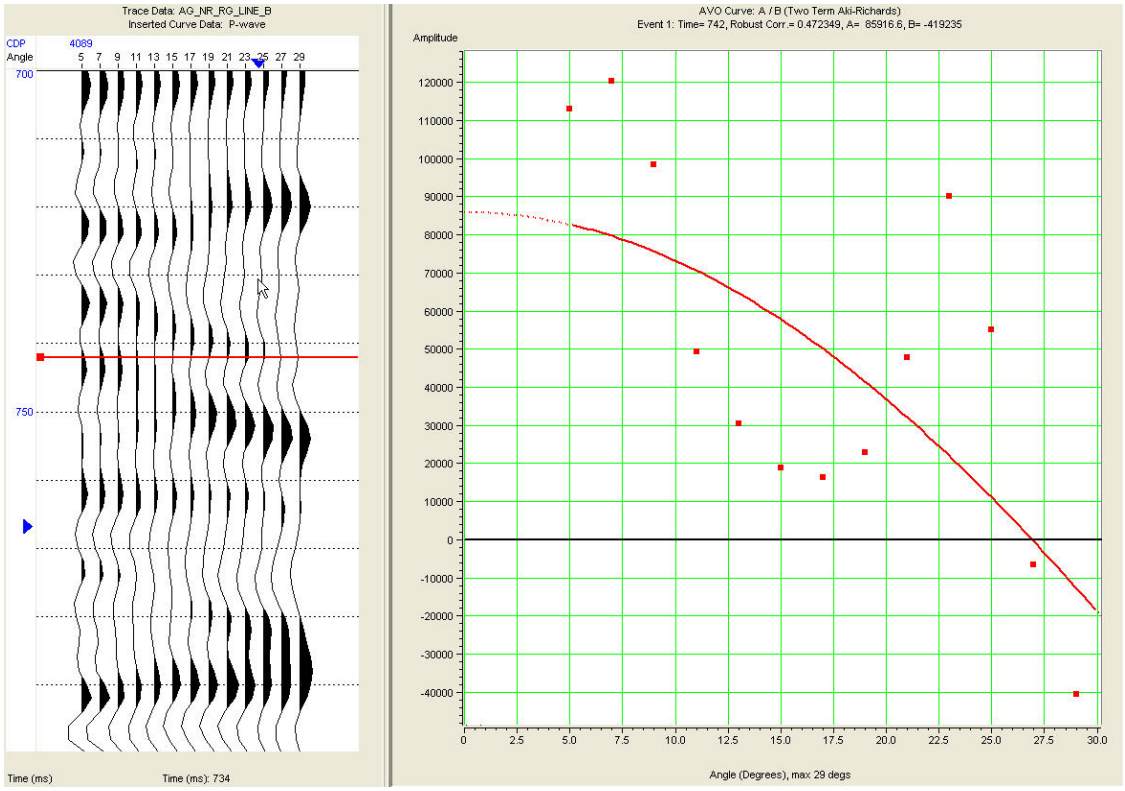

No coherent anomaly at CDP 4089

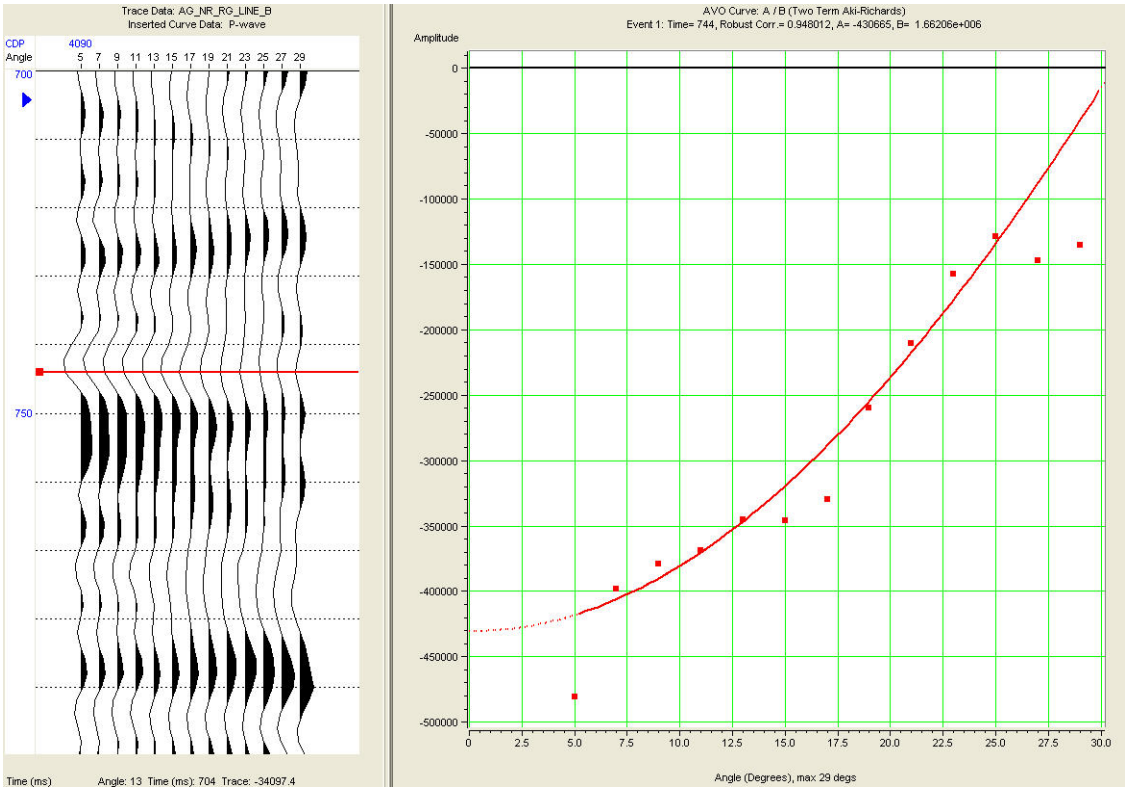

Class IV anomaly at CDP 4090

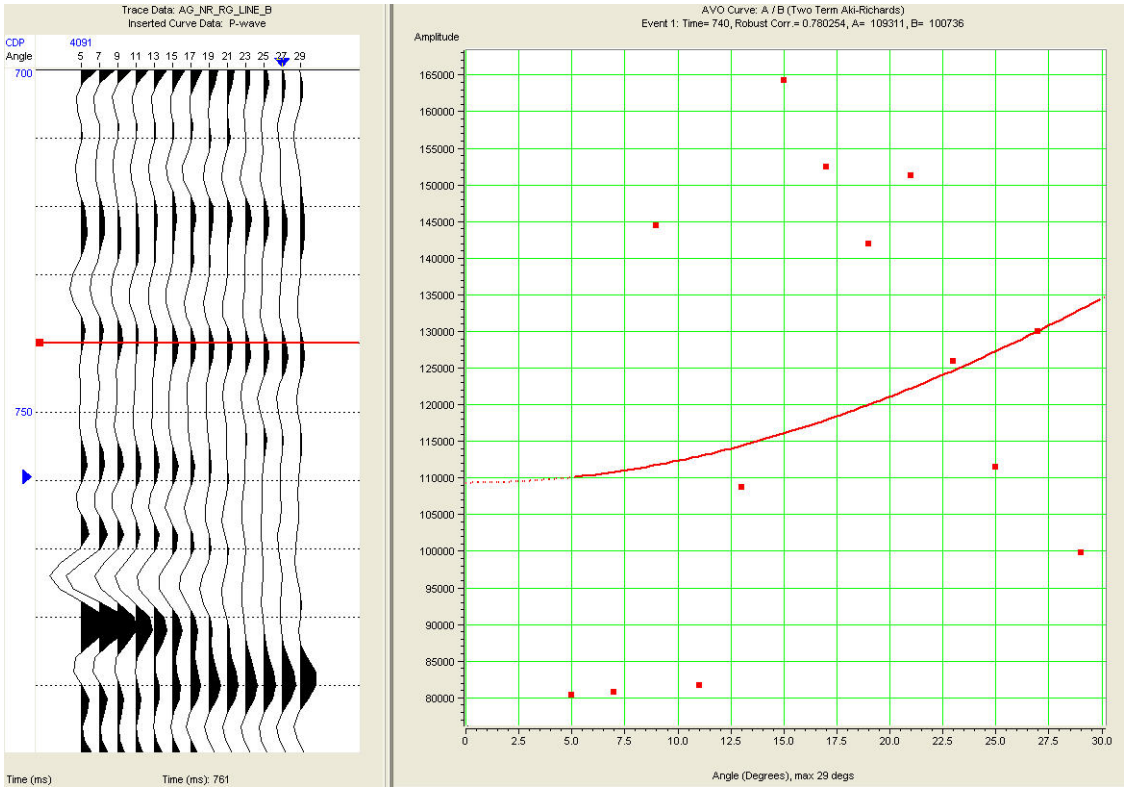

No coherent anomaly at CDP 4091

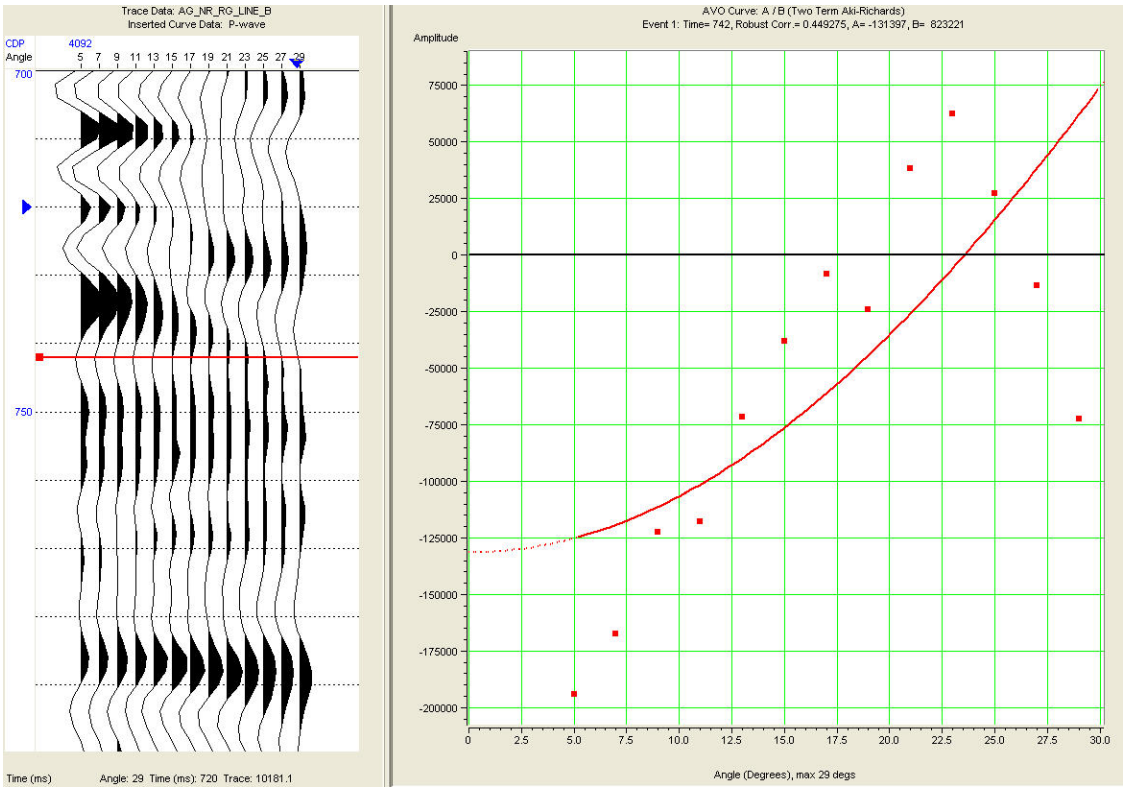

Weak Class IV anomaly at CDP 4092

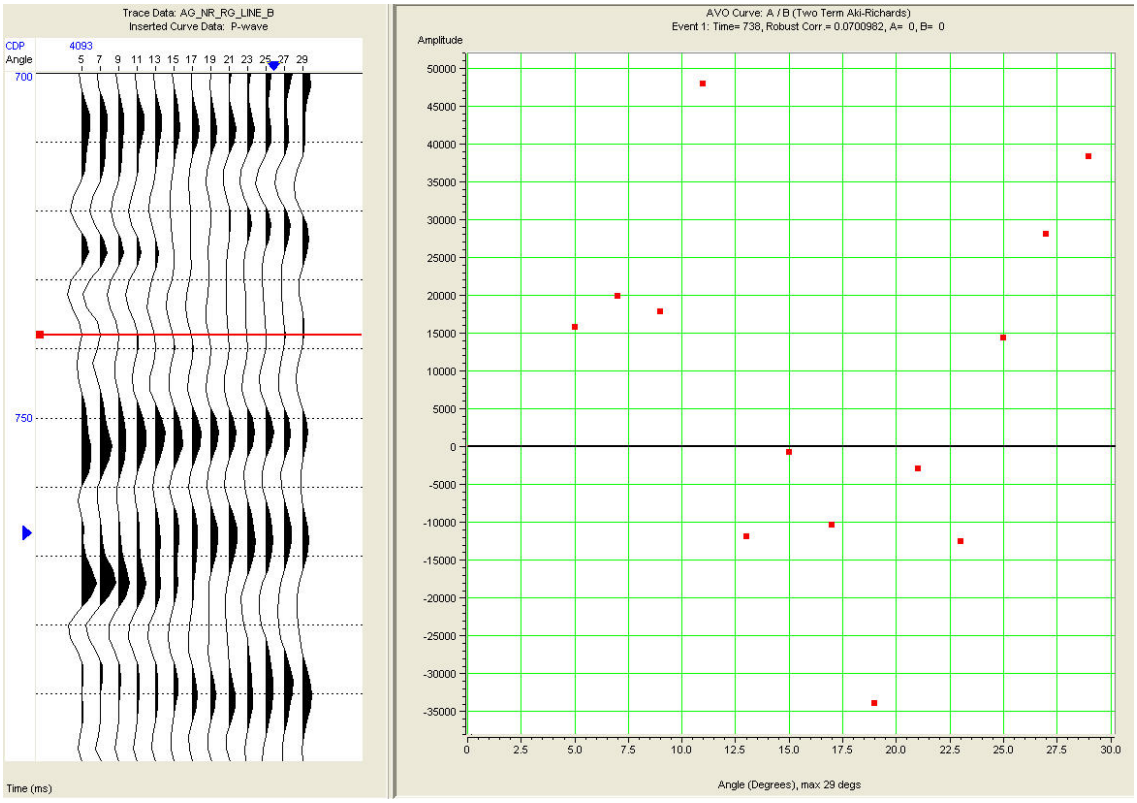

No coherent anomaly at CDP 4093

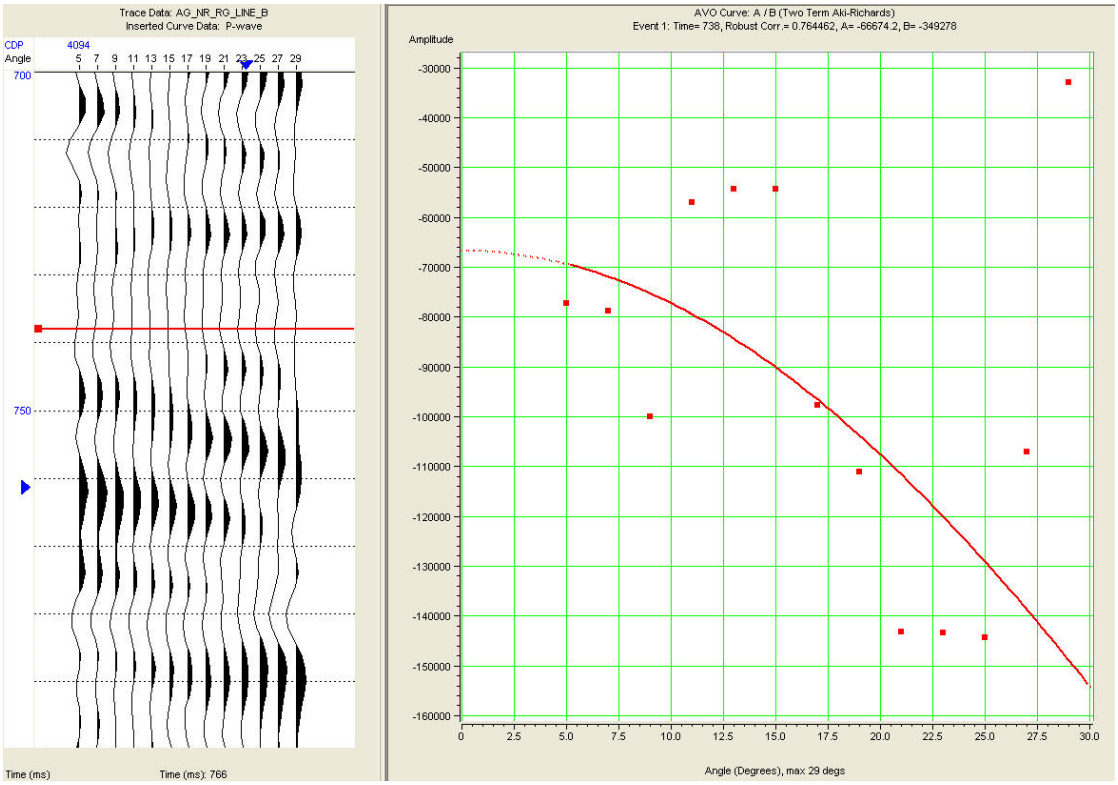

No coherent anomaly at CDP 4094

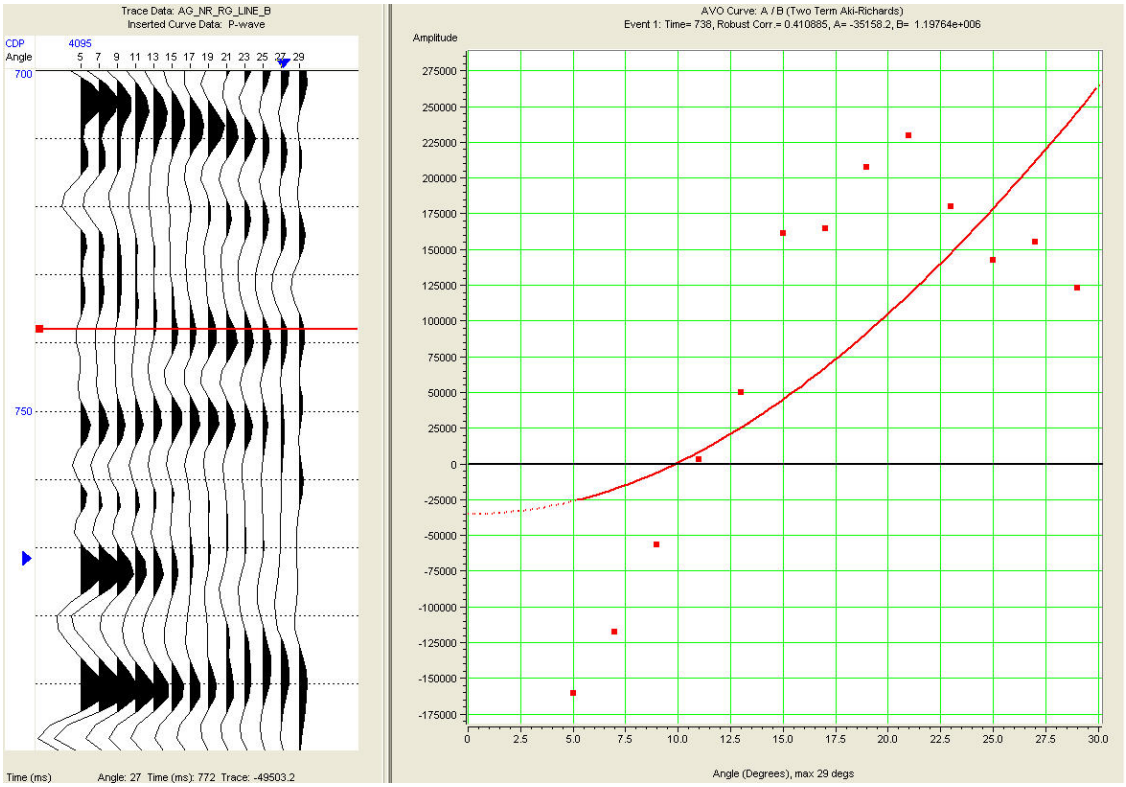

No coherent anomaly at CDP 4095

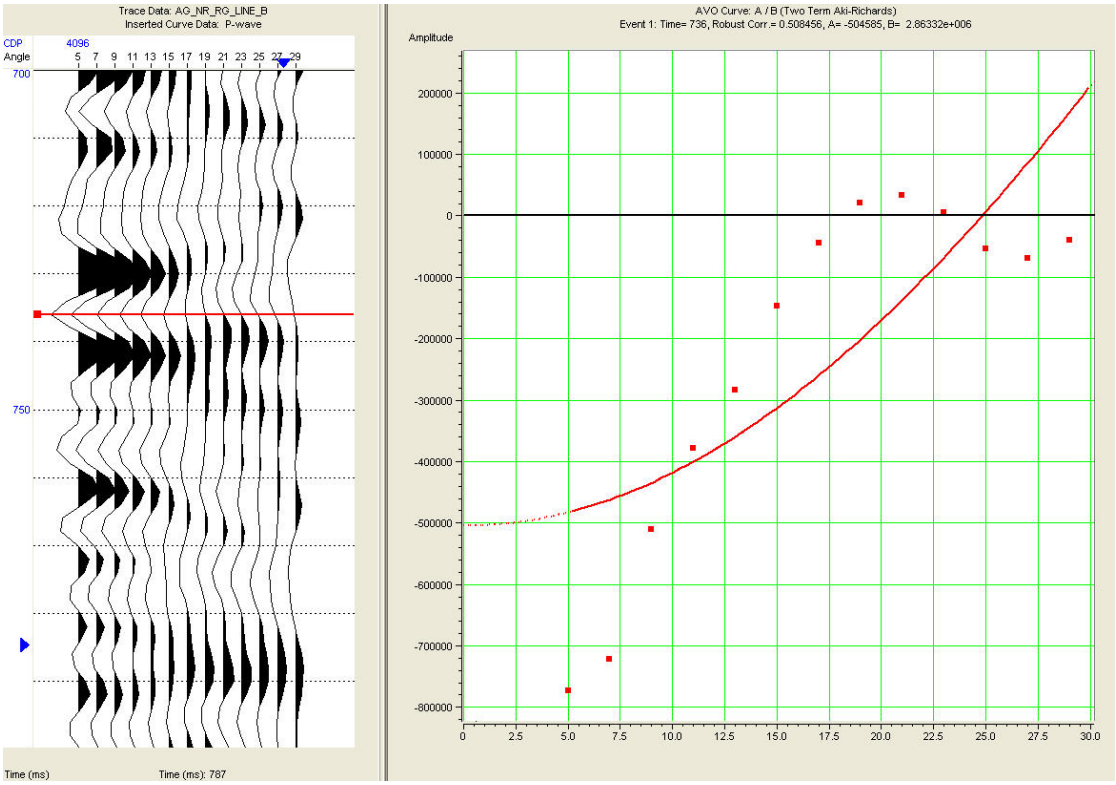

Class IV anomaly at CDP 4096

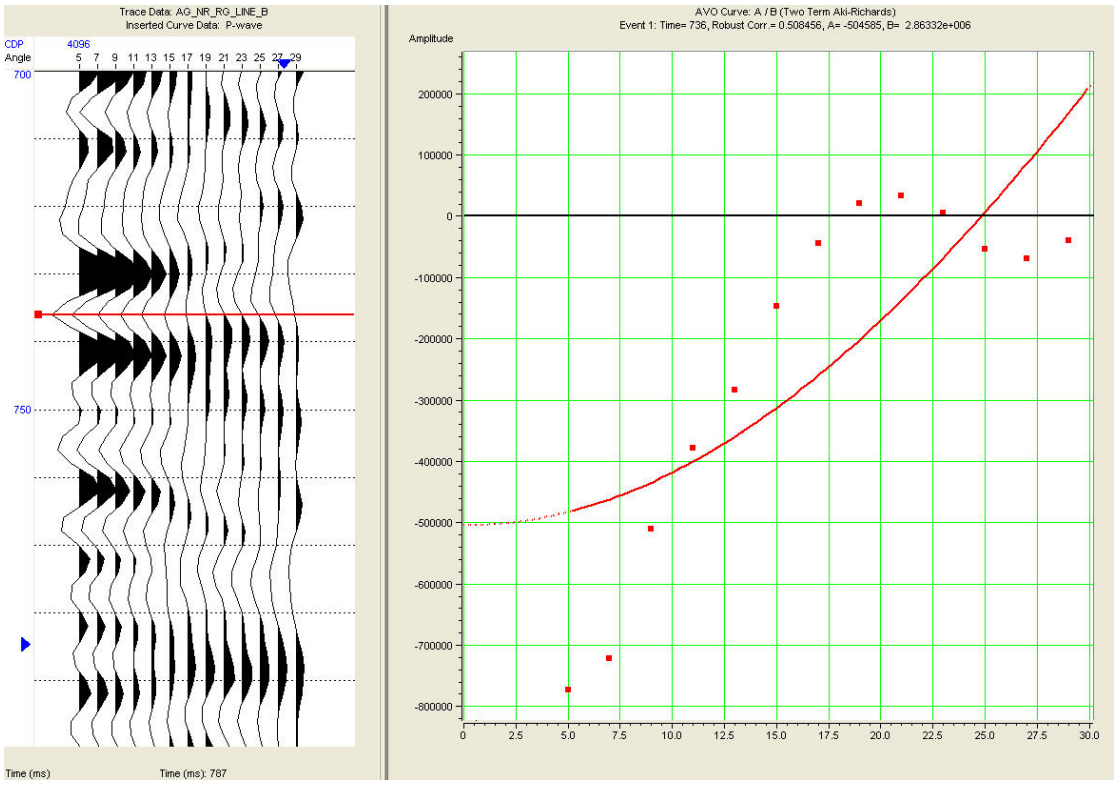

No coherent anomaly at CDP 4097

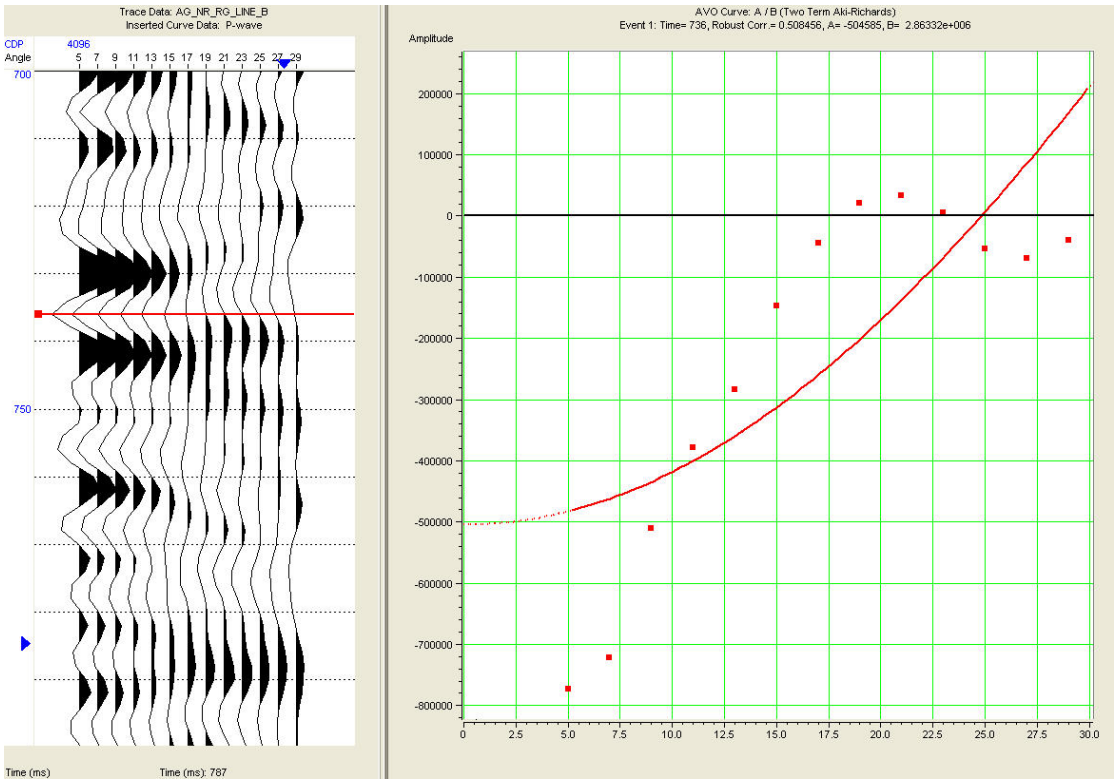

Class IV anomaly at CDP 4098

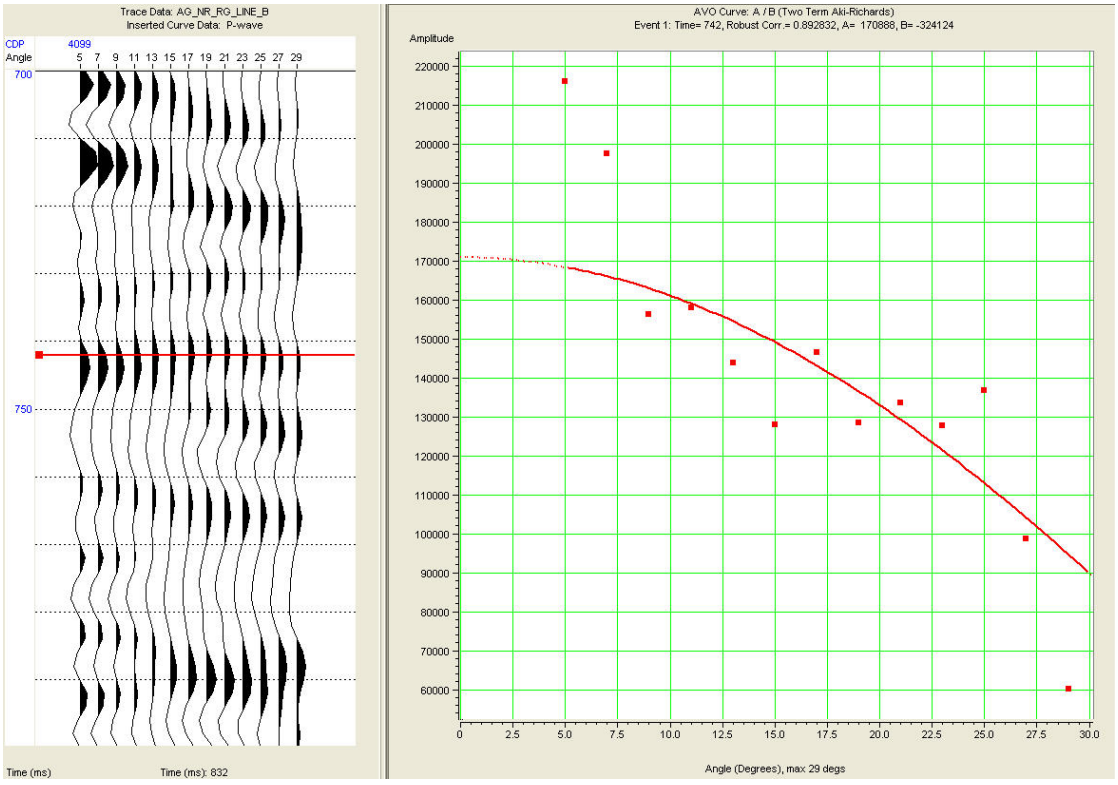

Class I anomaly at CDP 4099

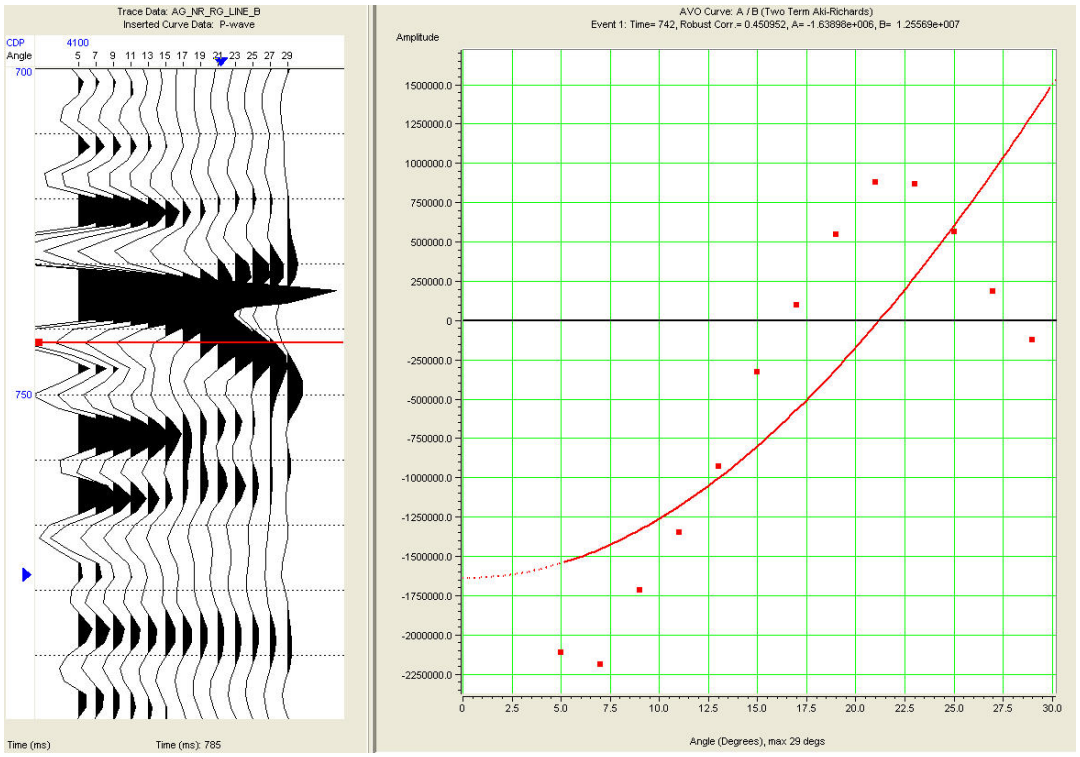

No coherent anomaly at CDP 4100

Gradient Analysis at Bottom of Utica Reflector between CDPs 4131-4175 over 774-782 ms

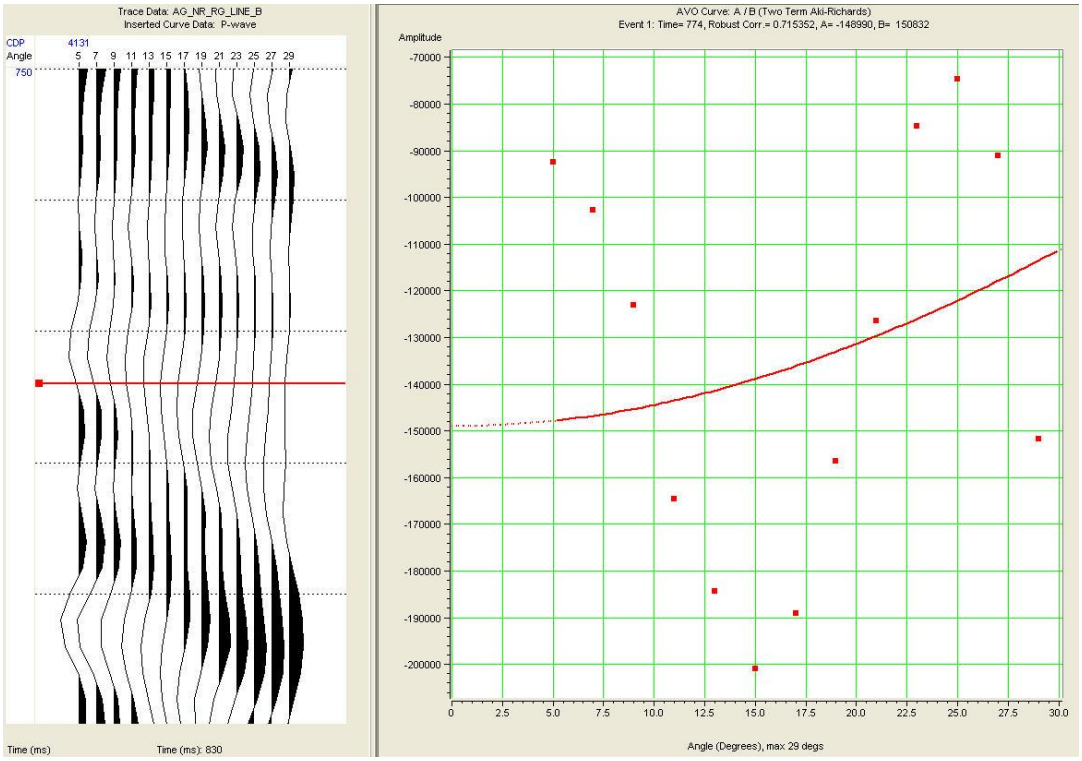

No coherent anomaly at CDP 4131

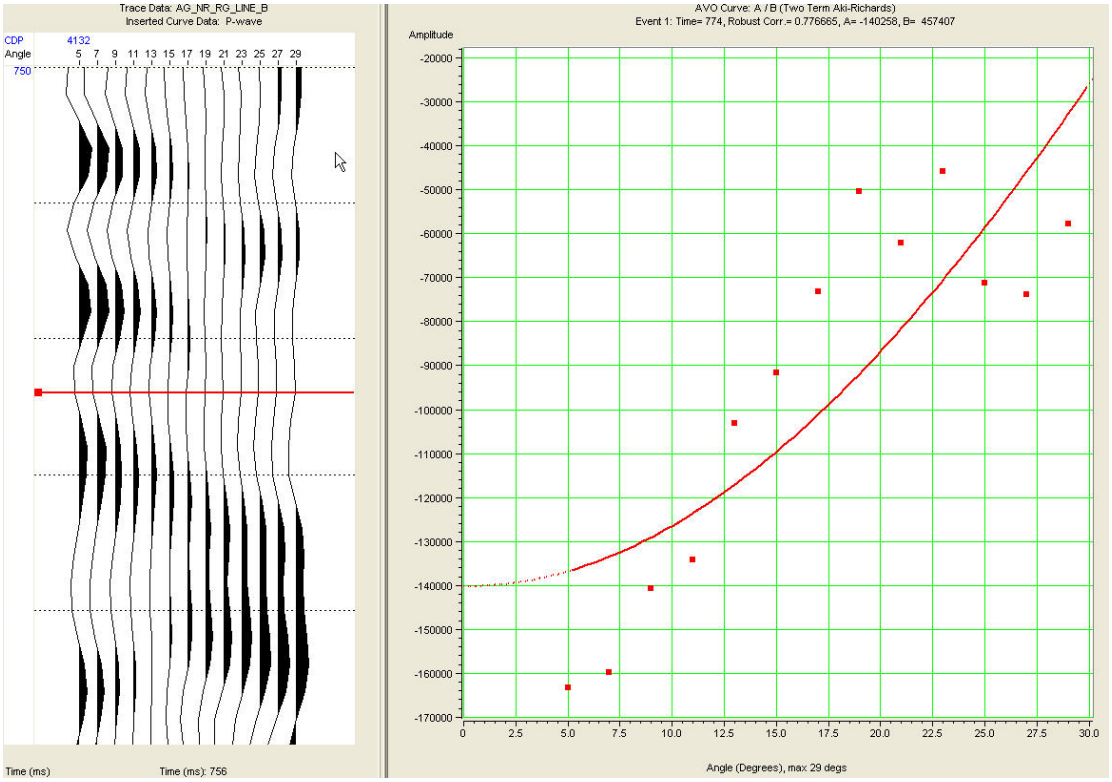

Class IV anomaly at CDP 4132

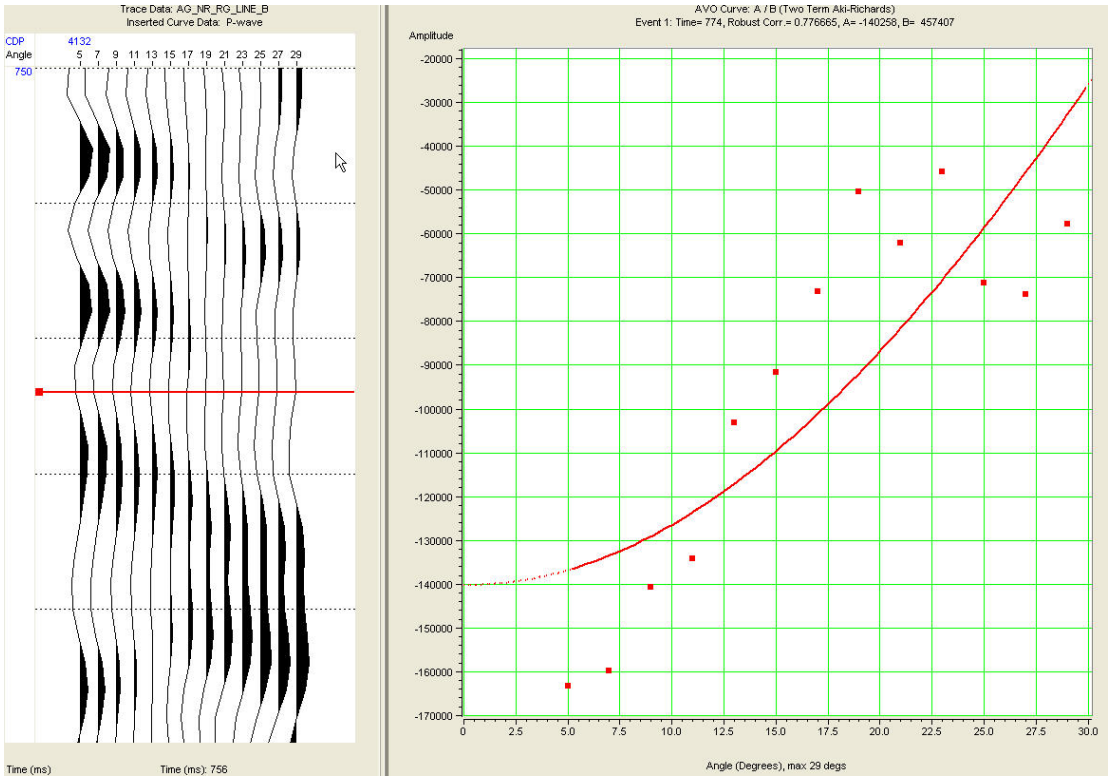

Class IV anomaly at CDP 4133

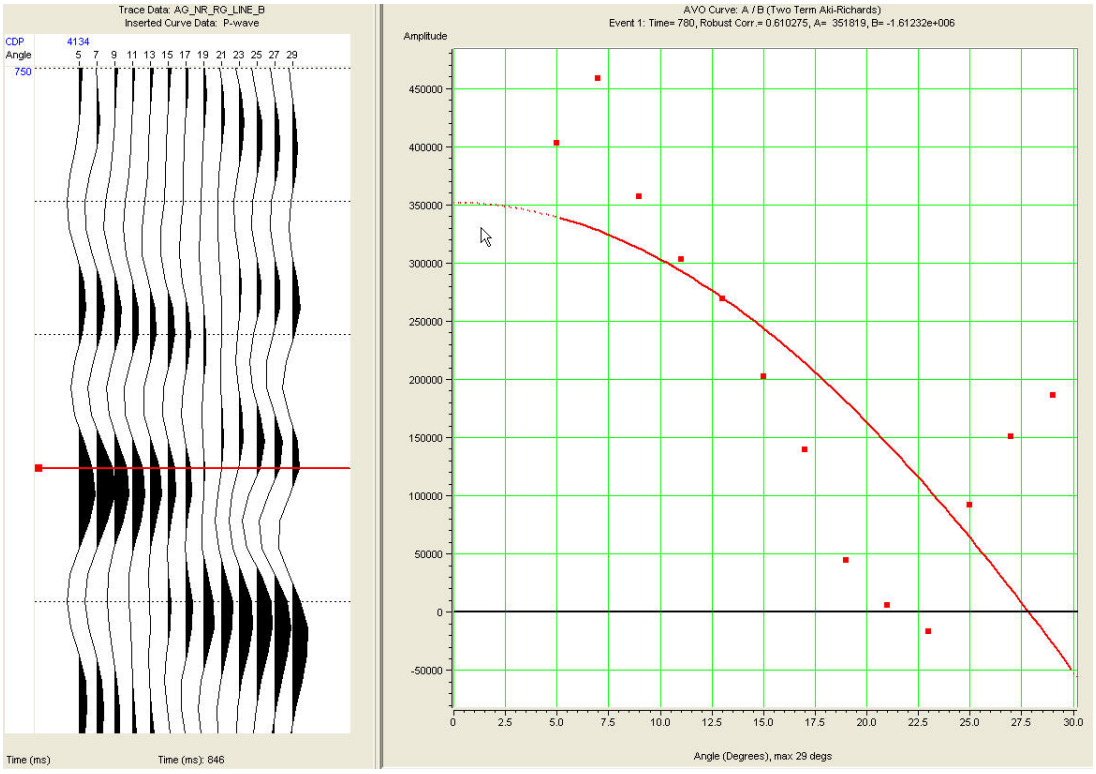

Weak Class I anomaly at CDP 4134

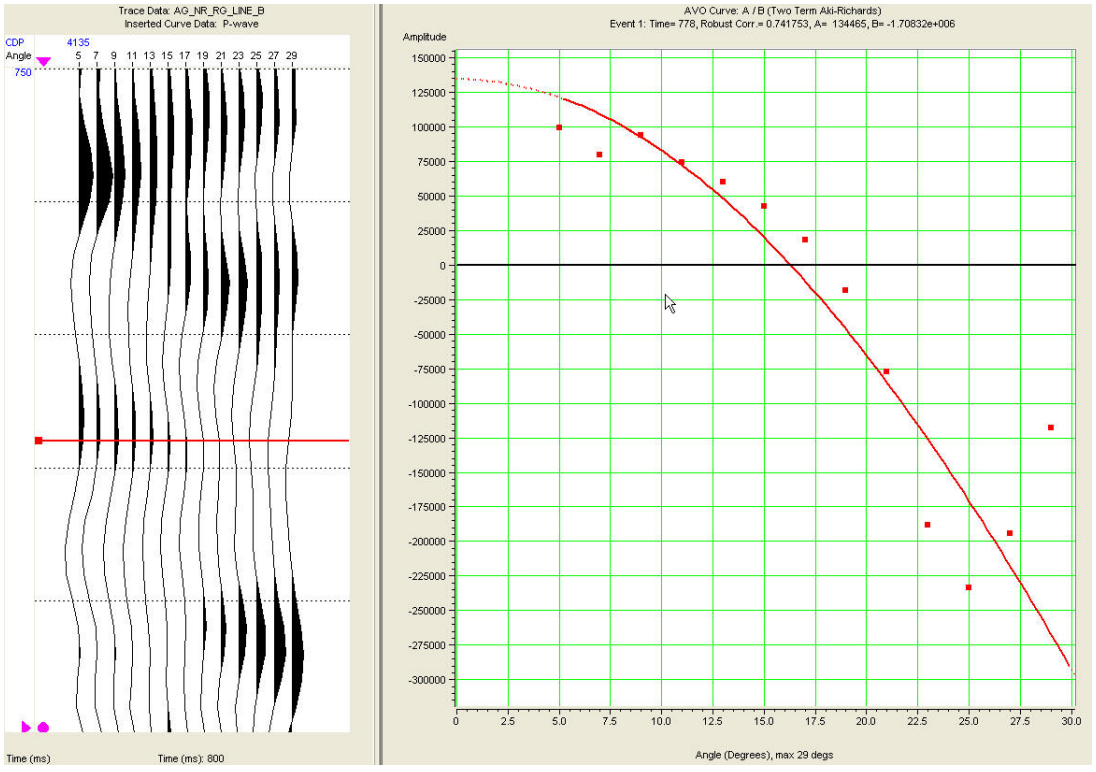

Weak class IIp anomaly at CDP 4135

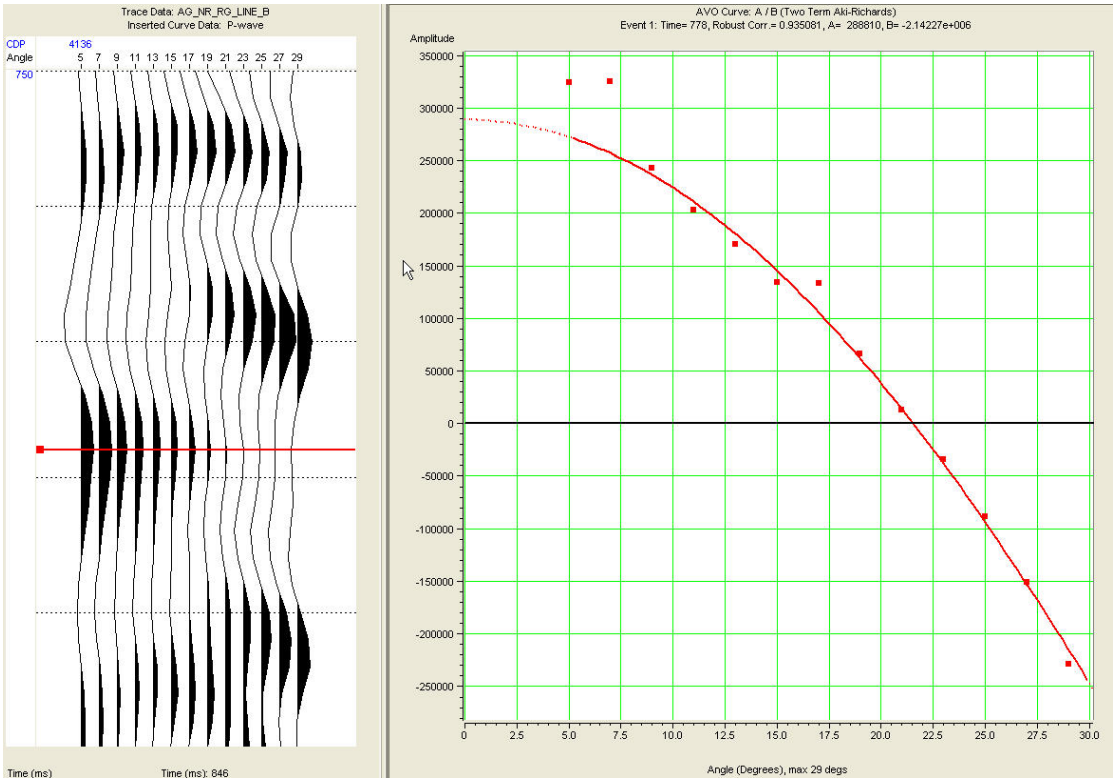

Class I anomaly at CDP 4136

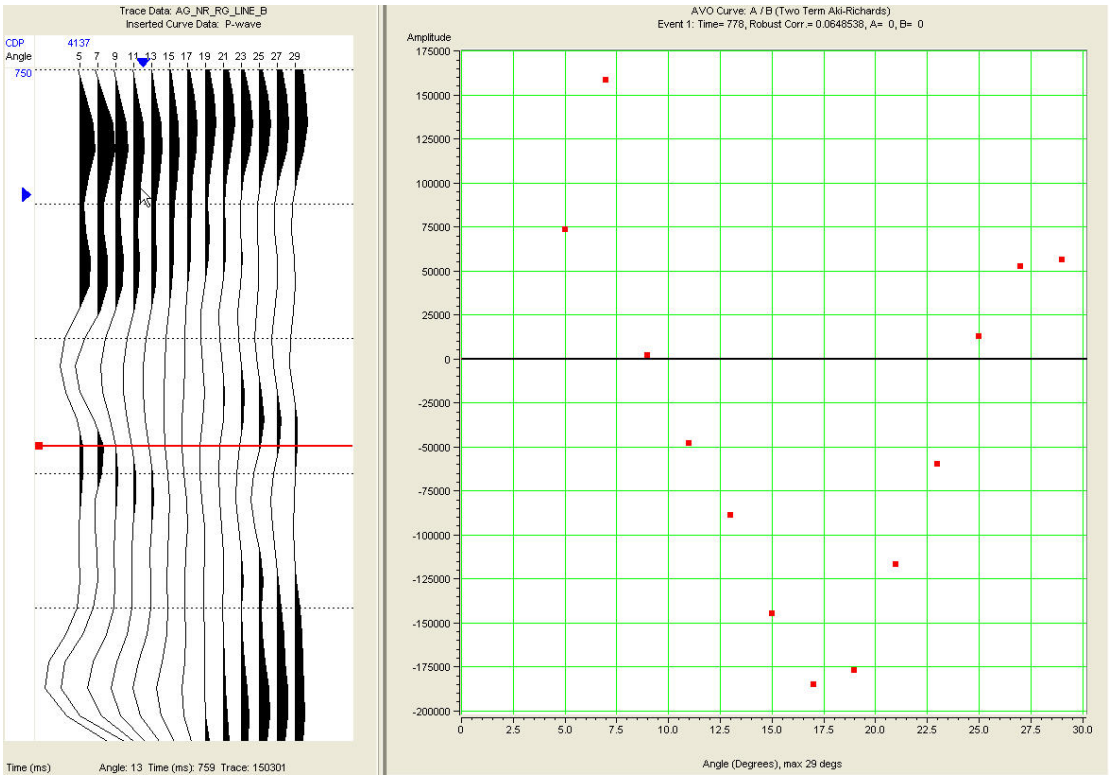

No coherent anomaly at CDP 4137

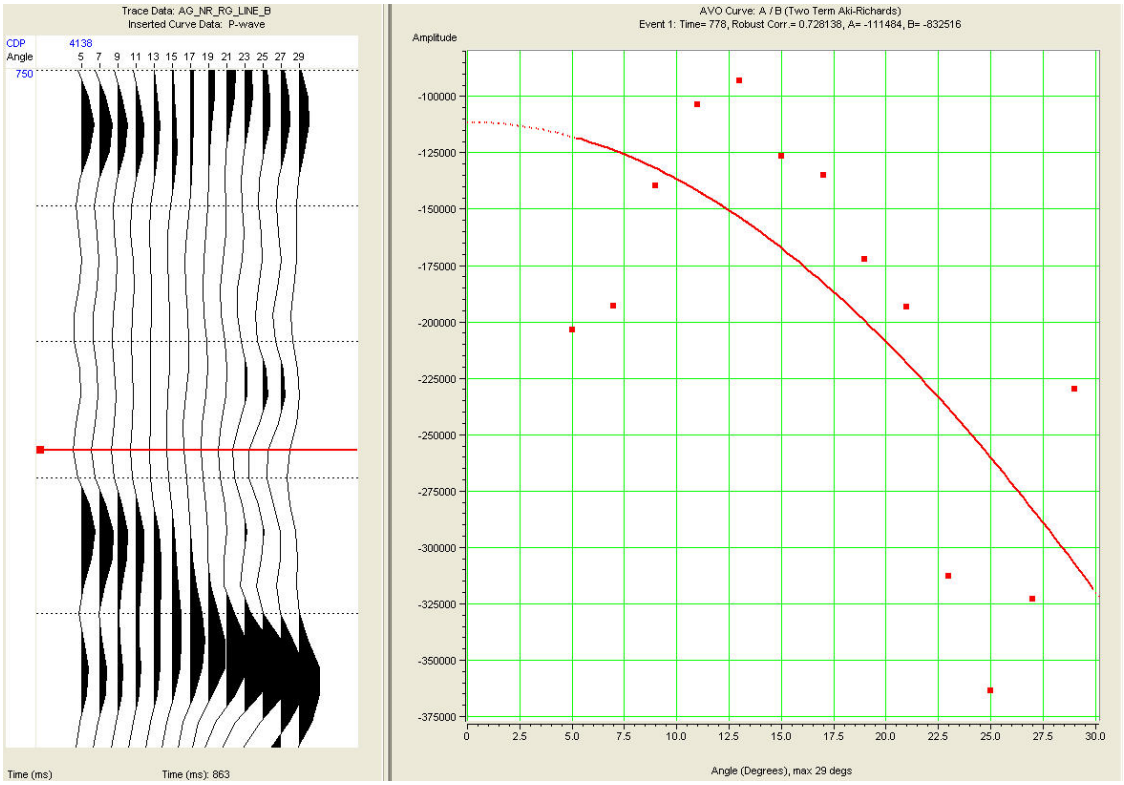

No coherent anomaly at CDP 4138

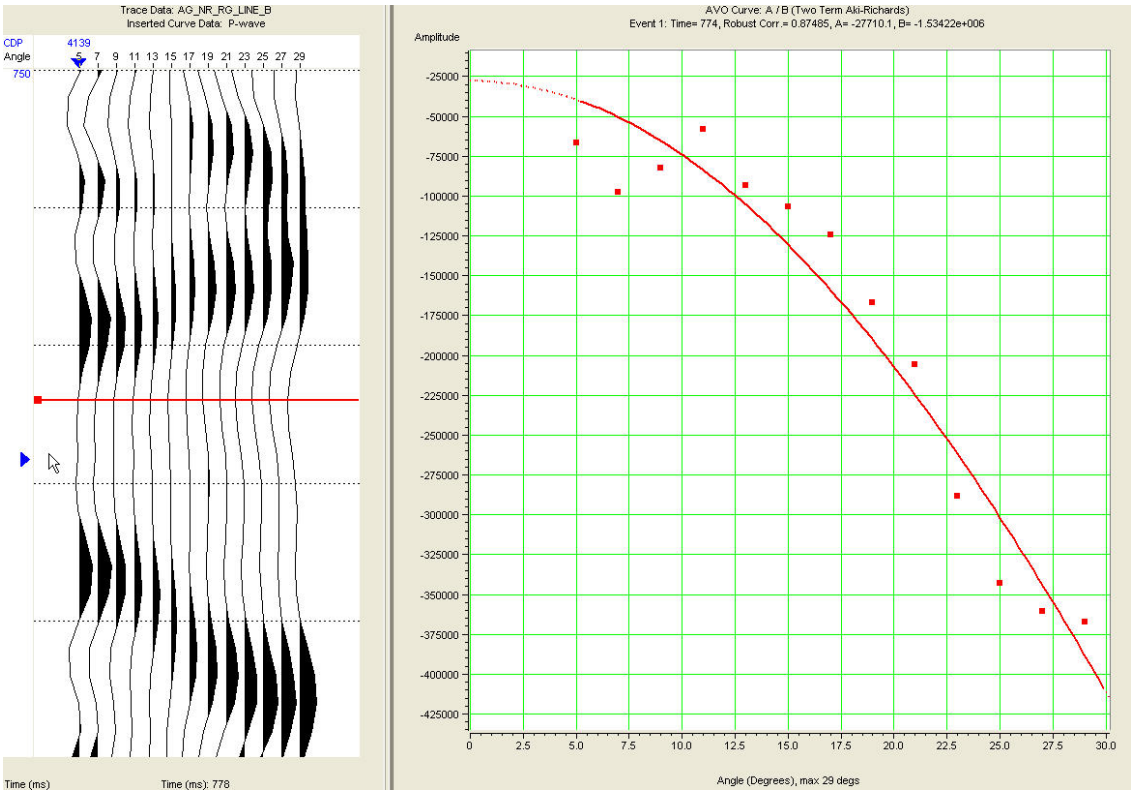

Weak Class III anomaly at CDP 4139

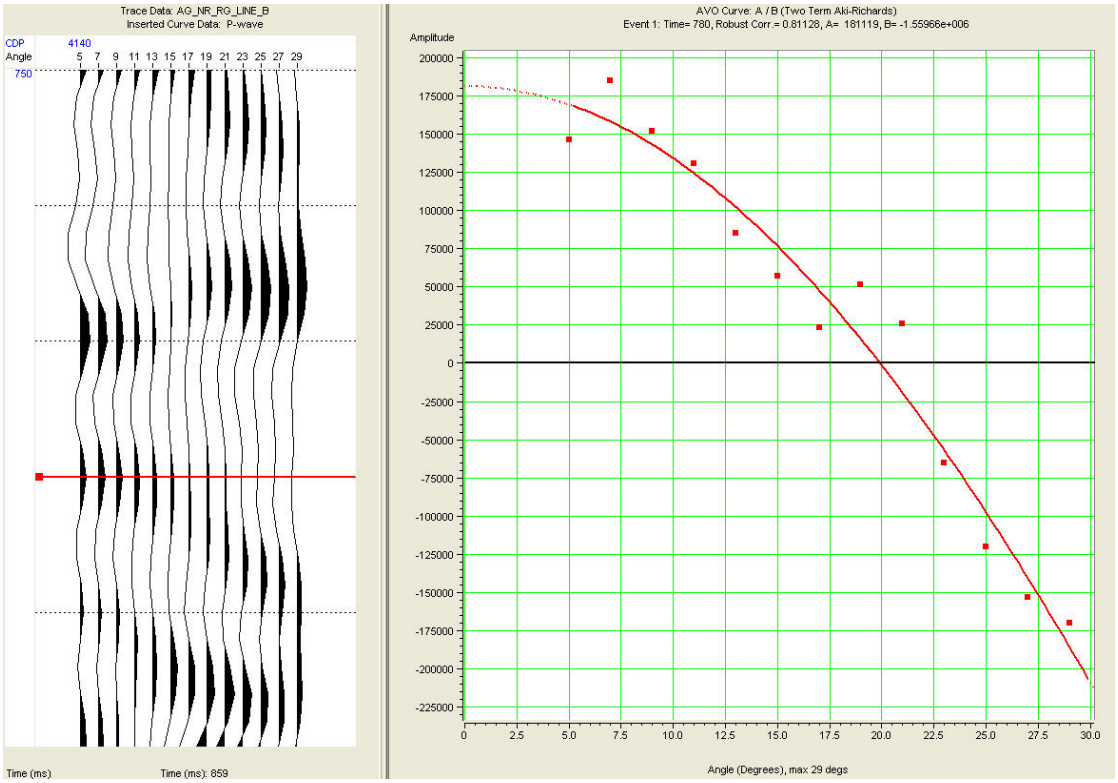

Class I anomaly at CDP 4140

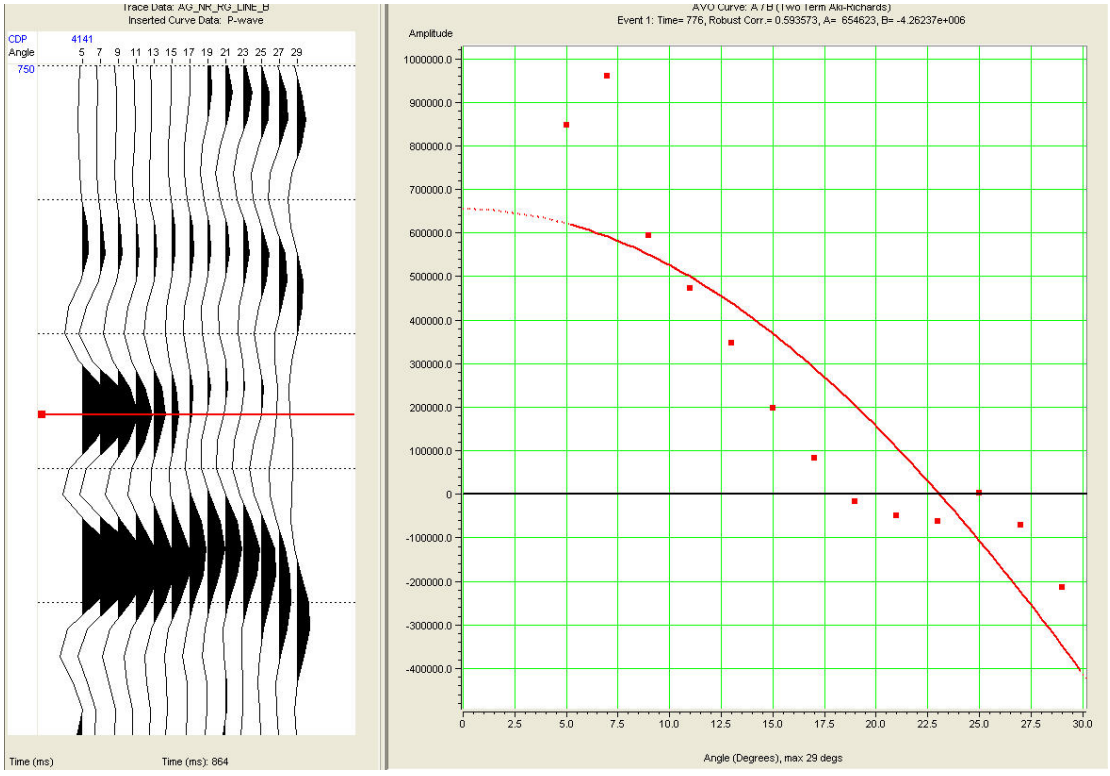

Class I anomaly at CDP 4141

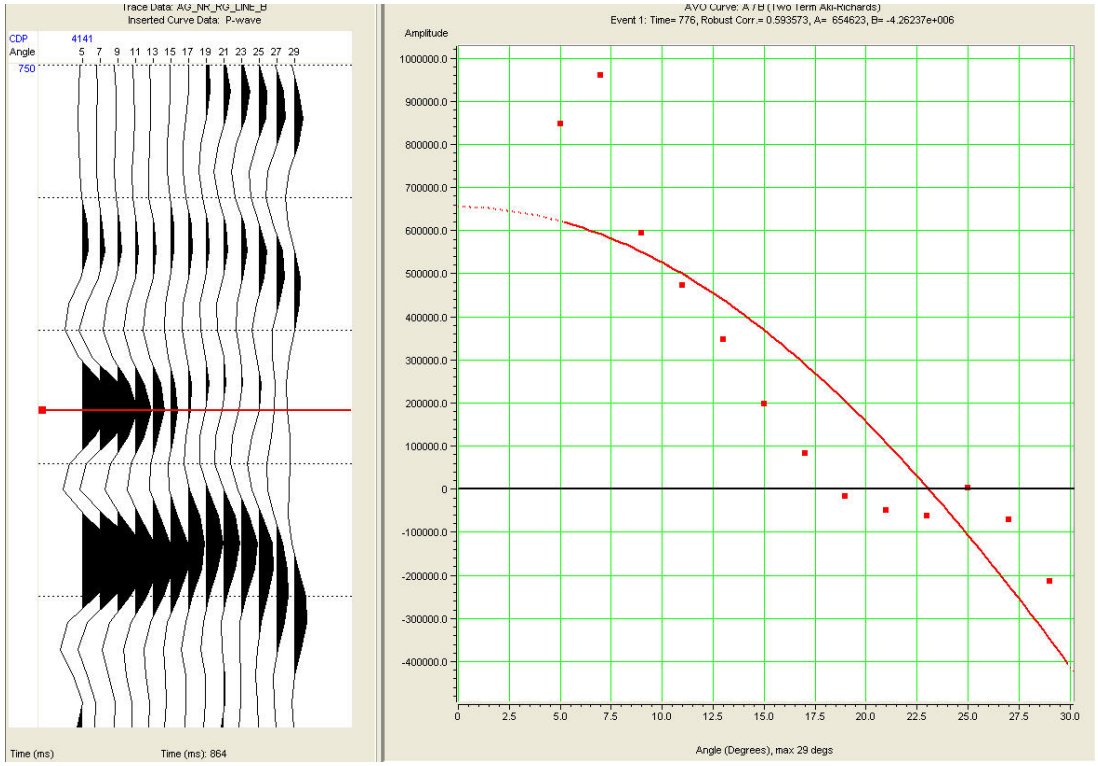

Class I anomaly at CDP 4142

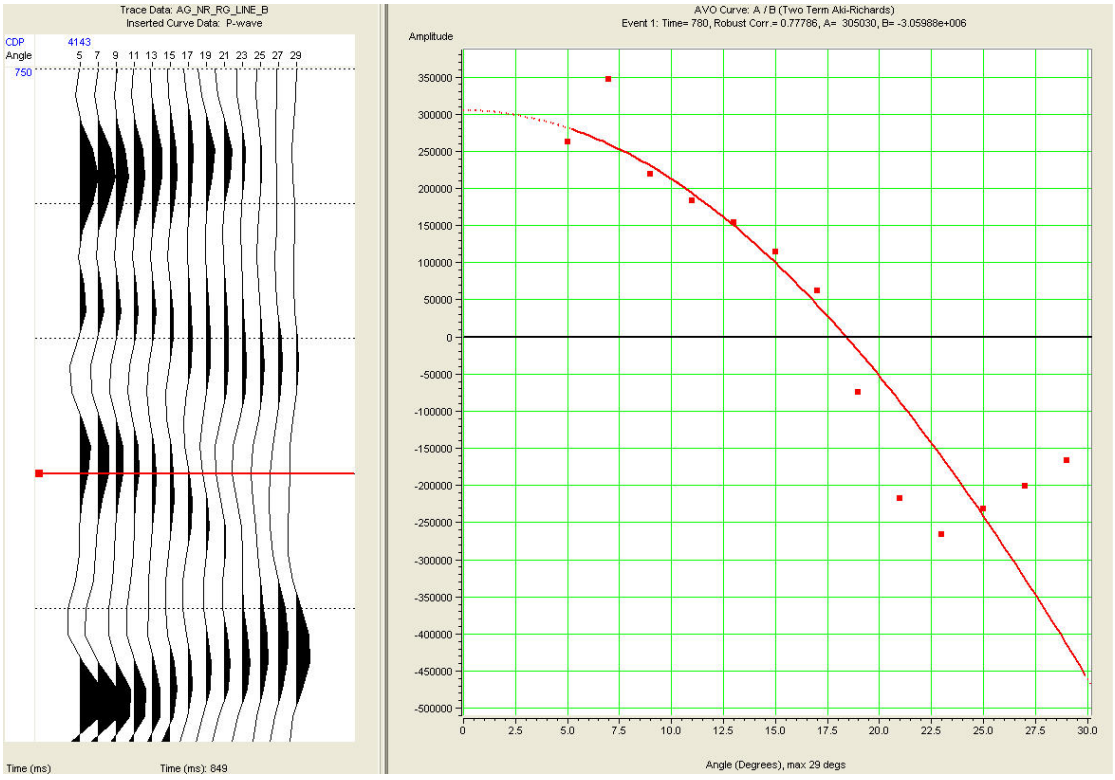

Class I anomaly at CDP 4143

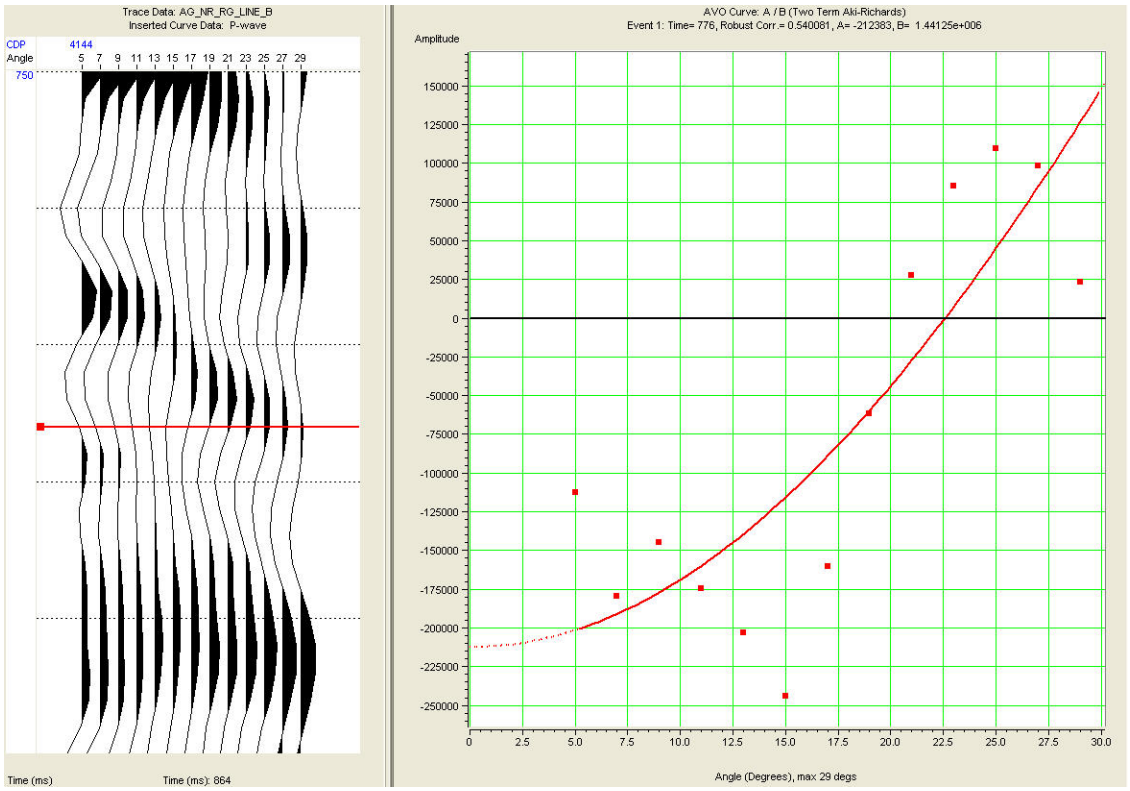

No coherent anomaly at CDP 4144

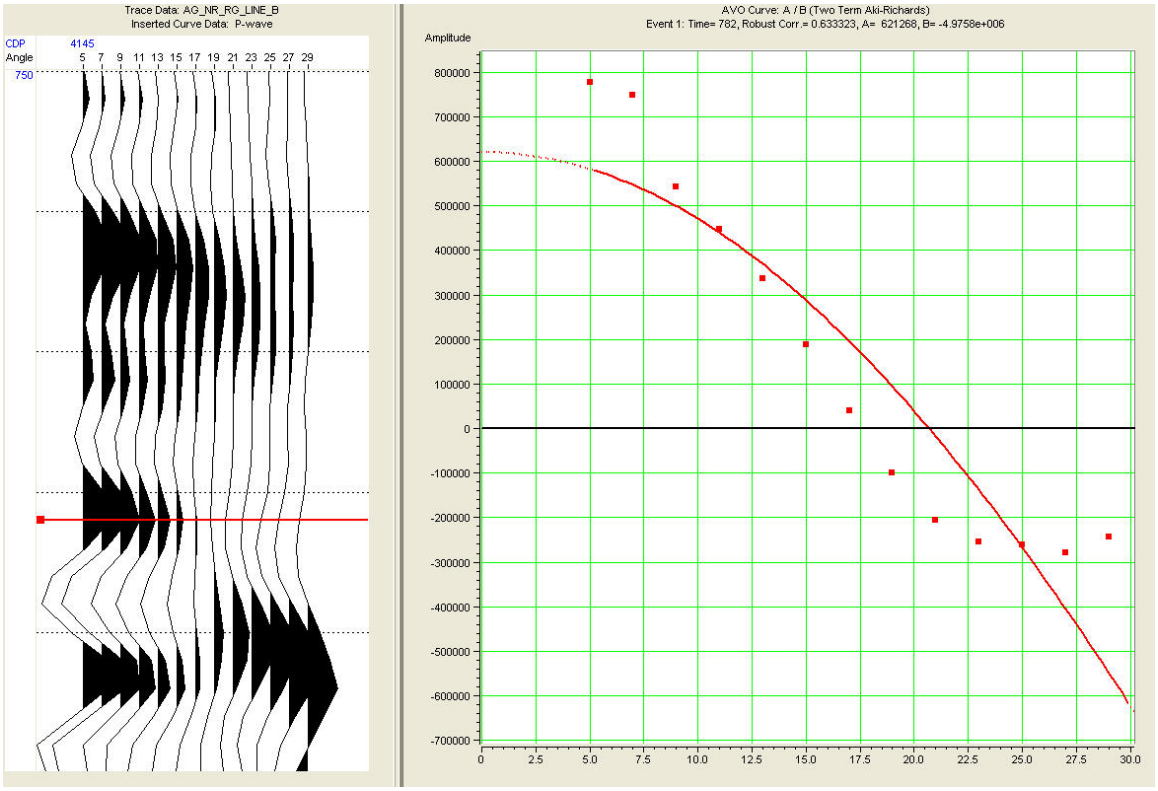

Class I anomaly at CDP 4145

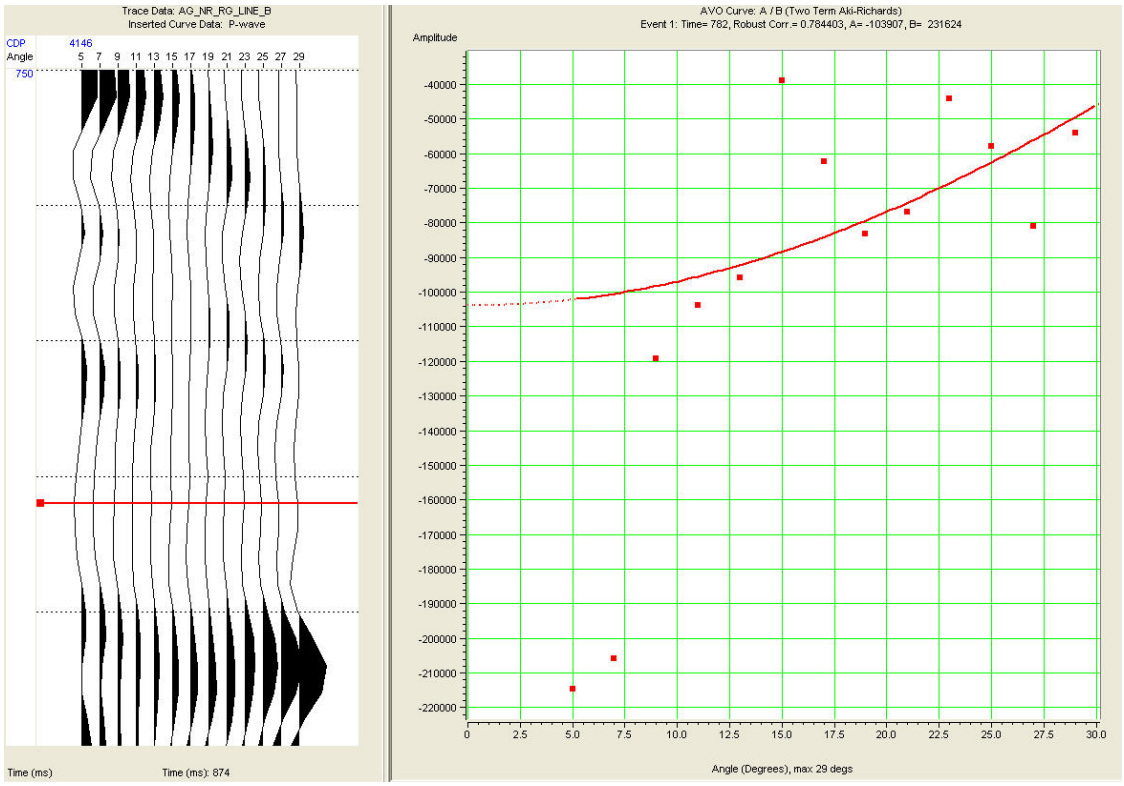

No coherent anomaly at CDP 4146

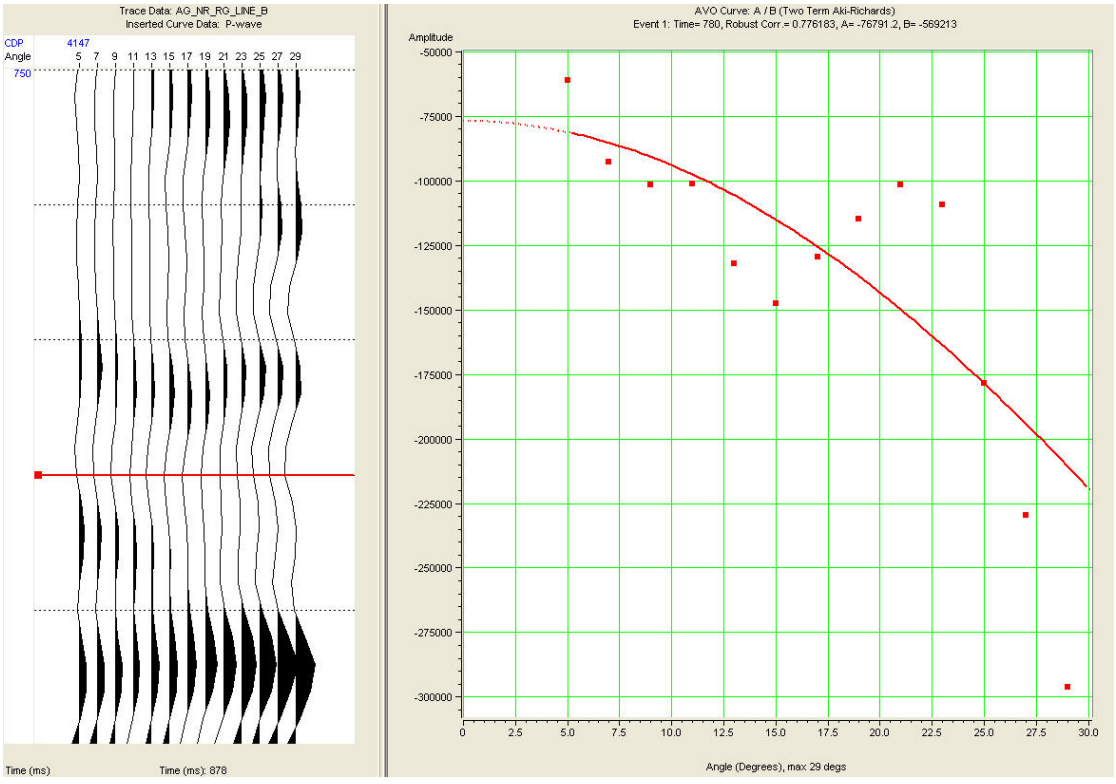

Class III anomaly at CDP 4147

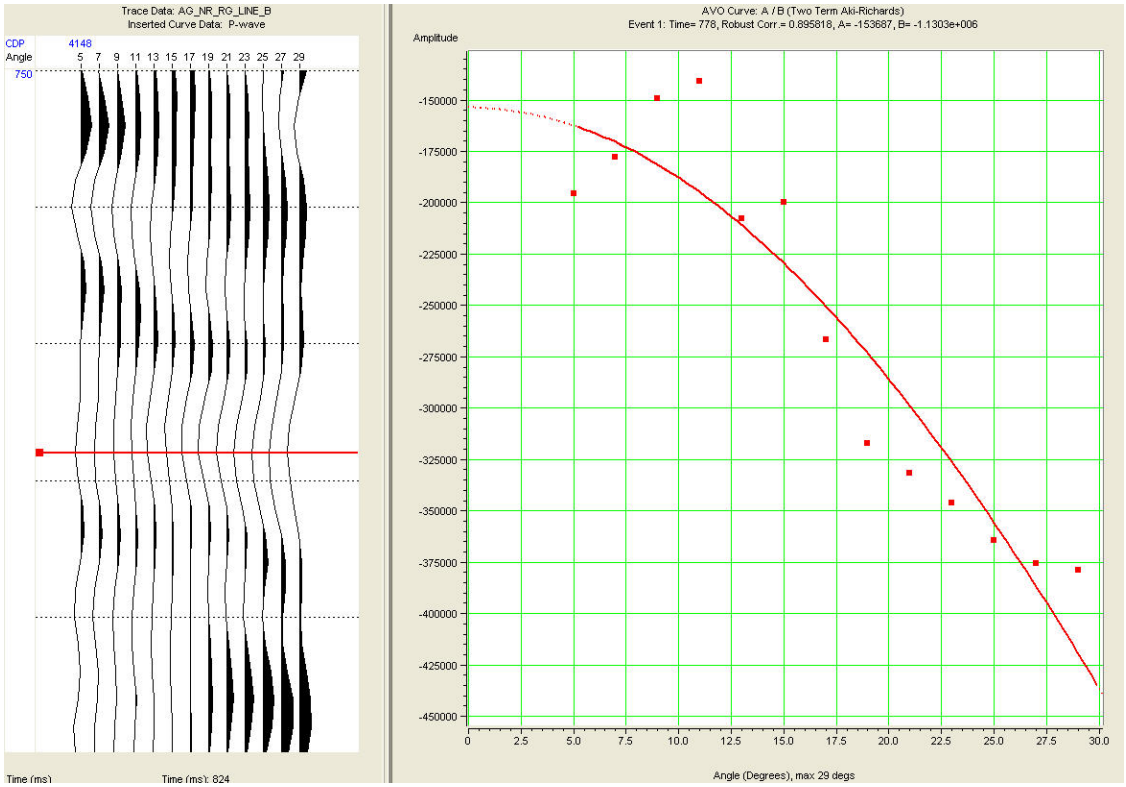

Class III anomaly at CDP 4148

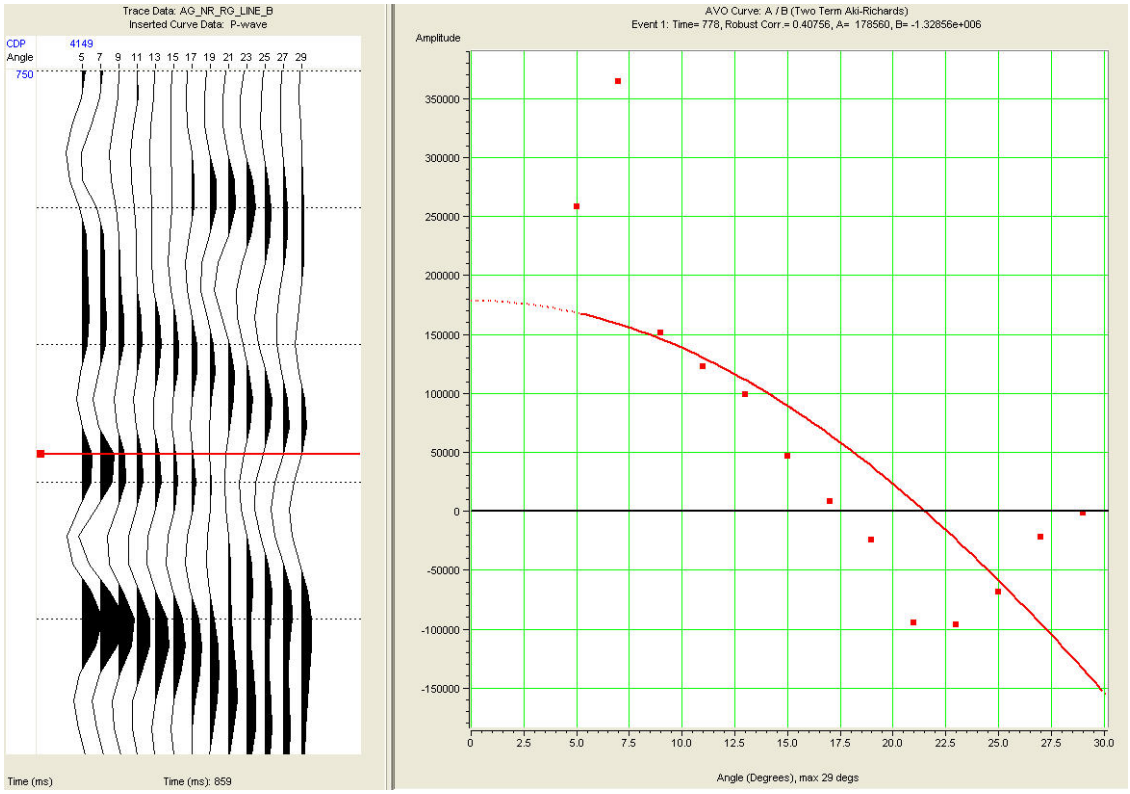

Weak class I anomaly at CDP 4149

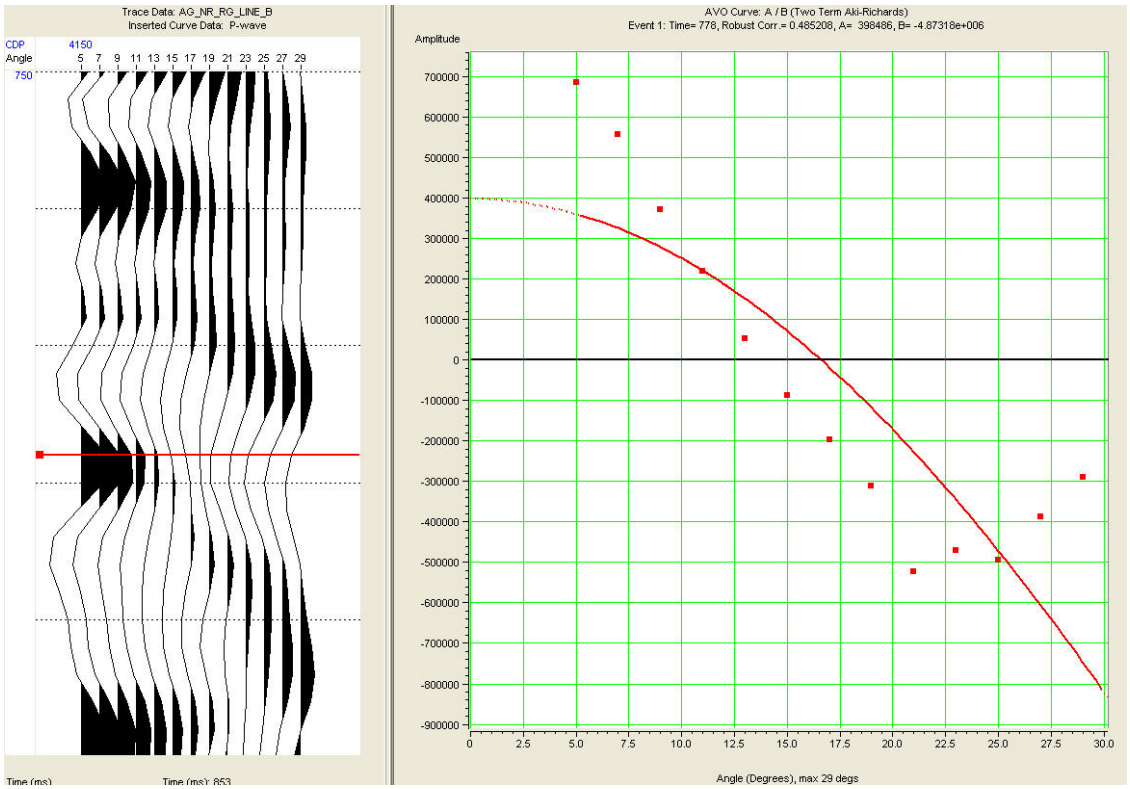

No coherent anomaly at CDP 4150 (low robustness)

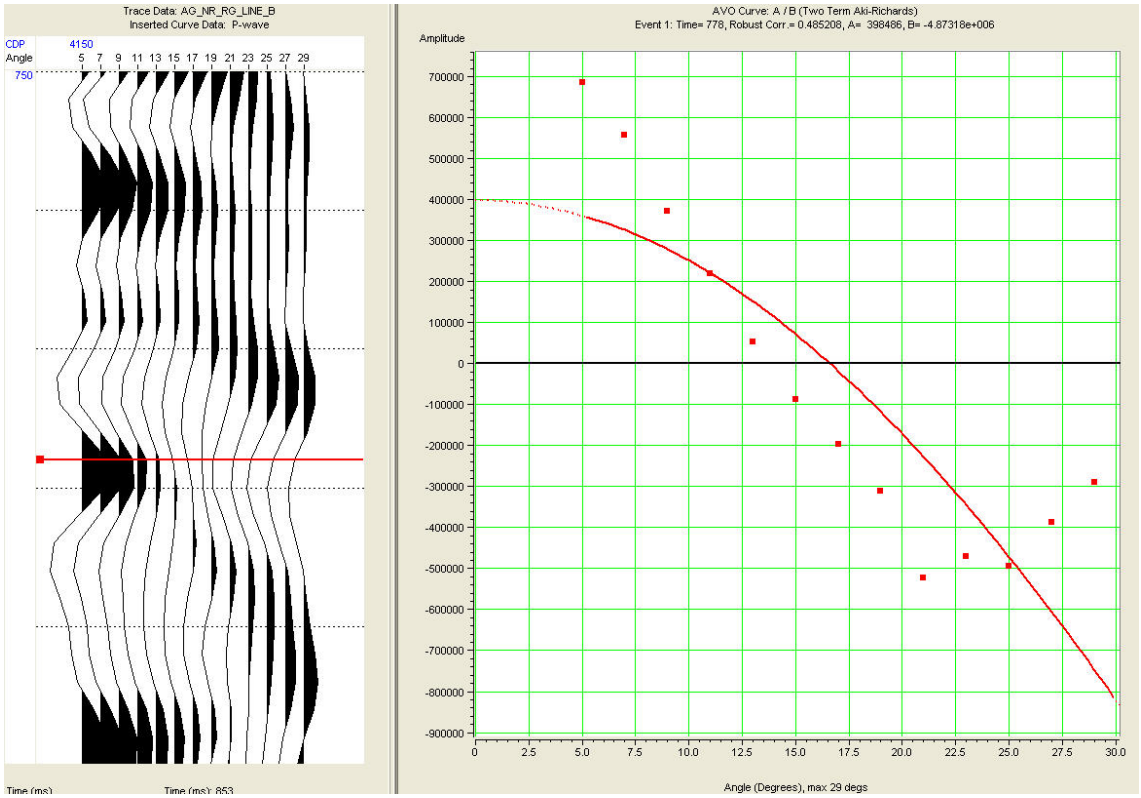

Class I anomaly at CDP 4151

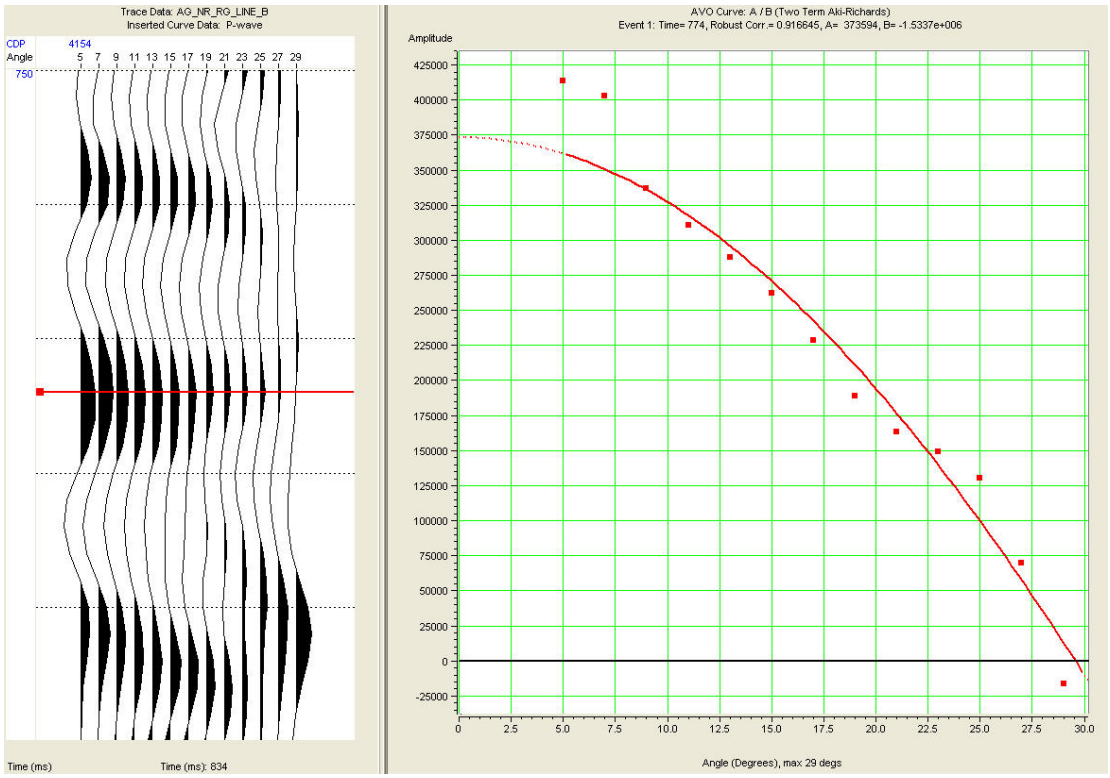

Class I anomaly at CDP 4154

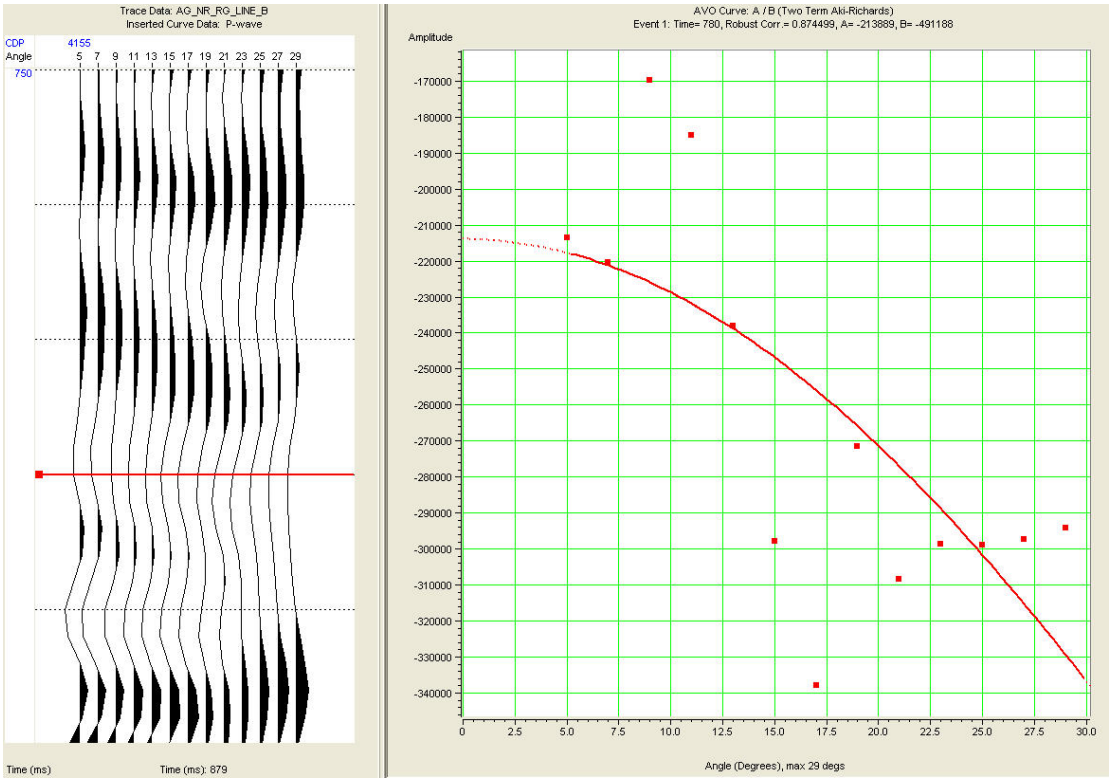

No coherent anomaly at CDP 4155

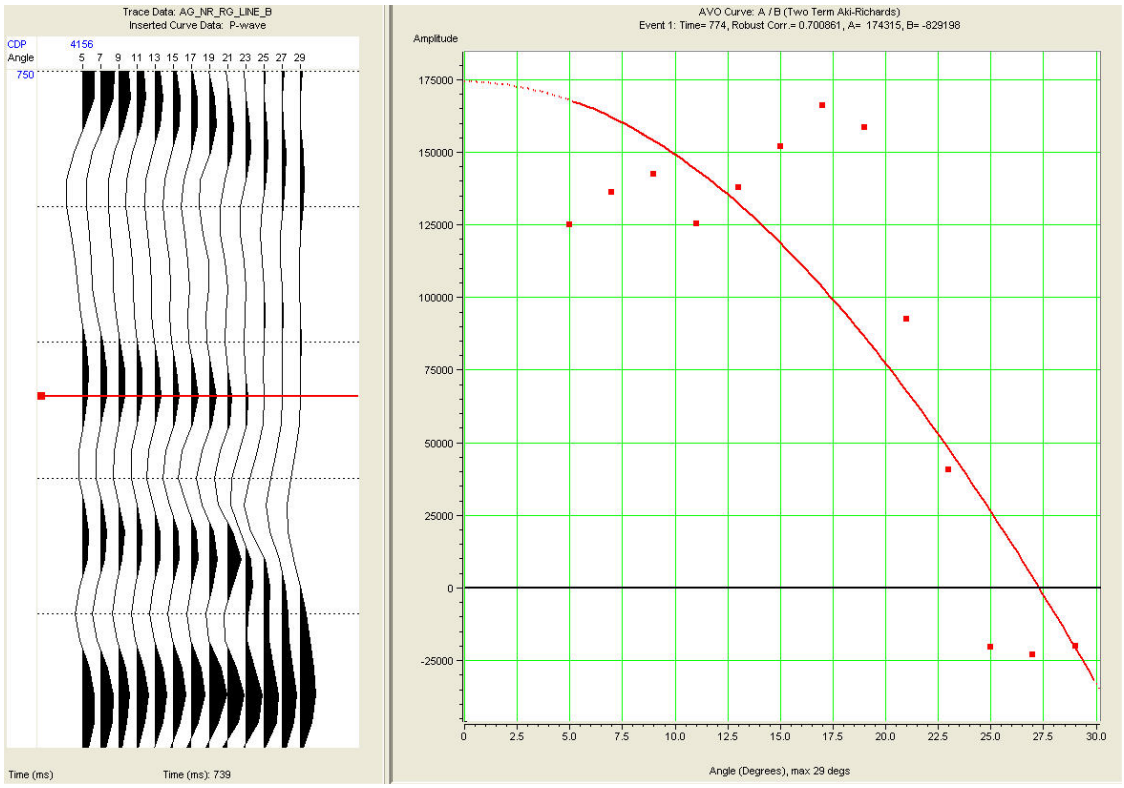

Class I anomaly at CDP 4156

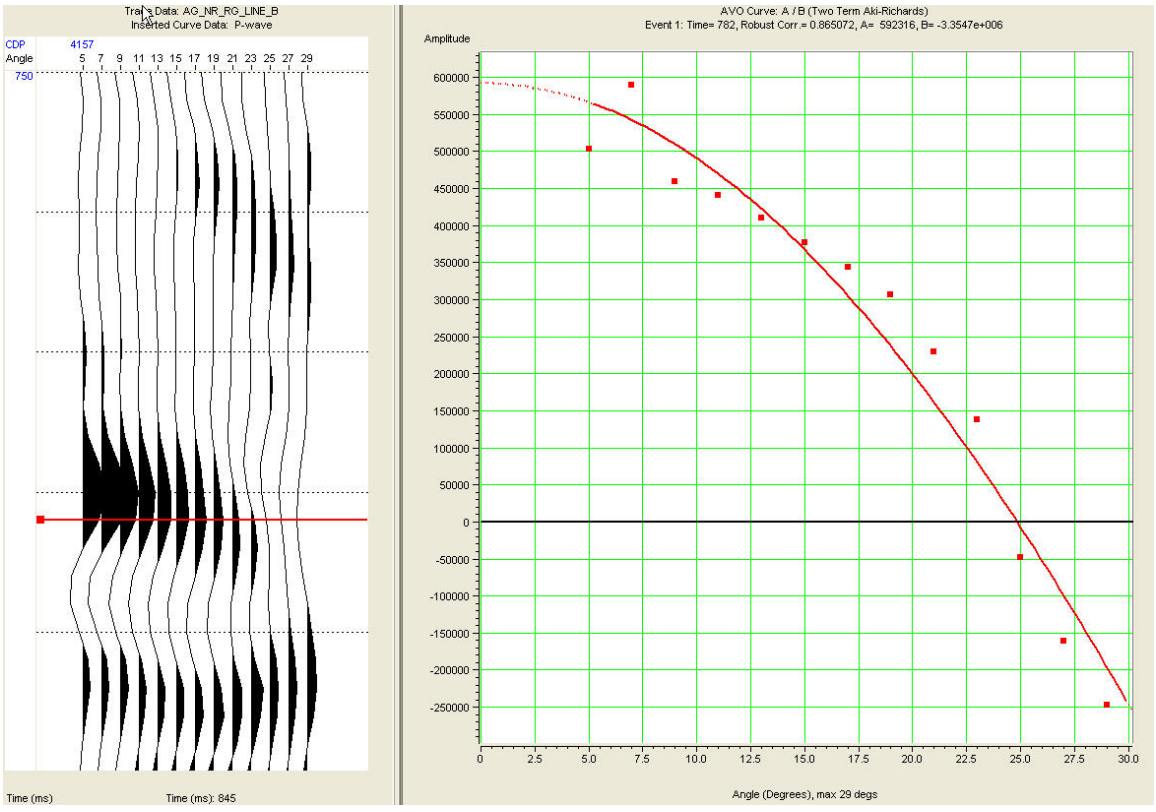

Class I anomaly at CDP 4157

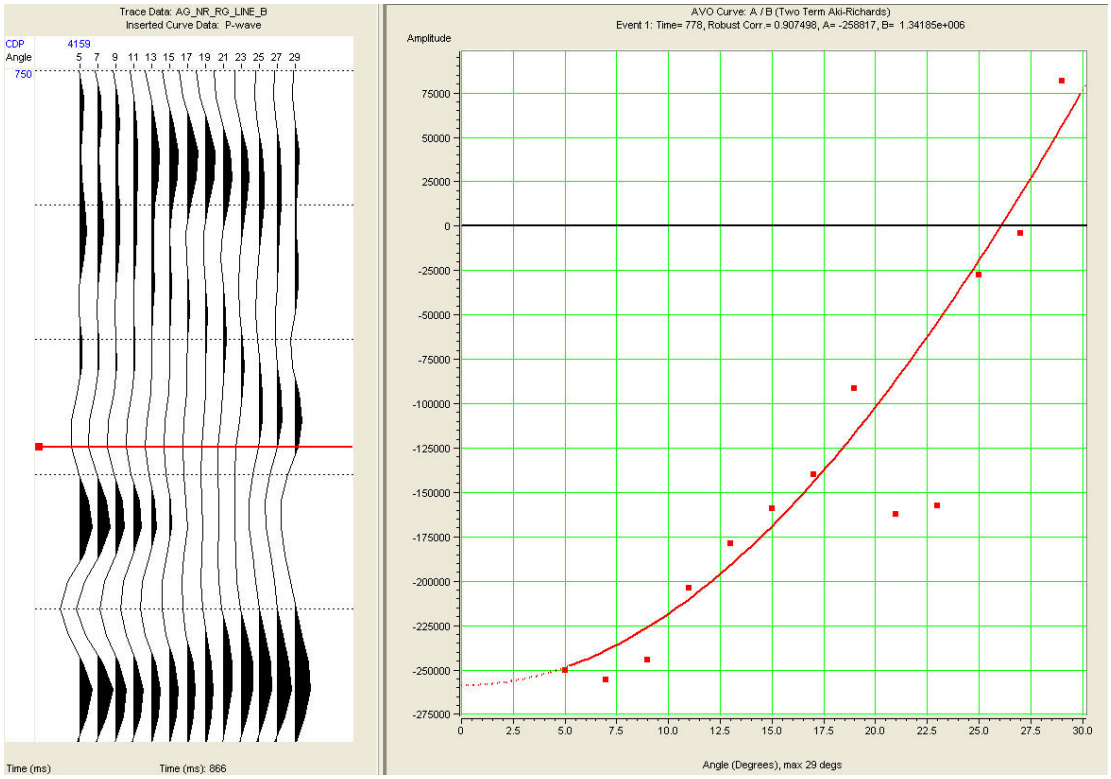

Class IV anomaly at CDP 4159

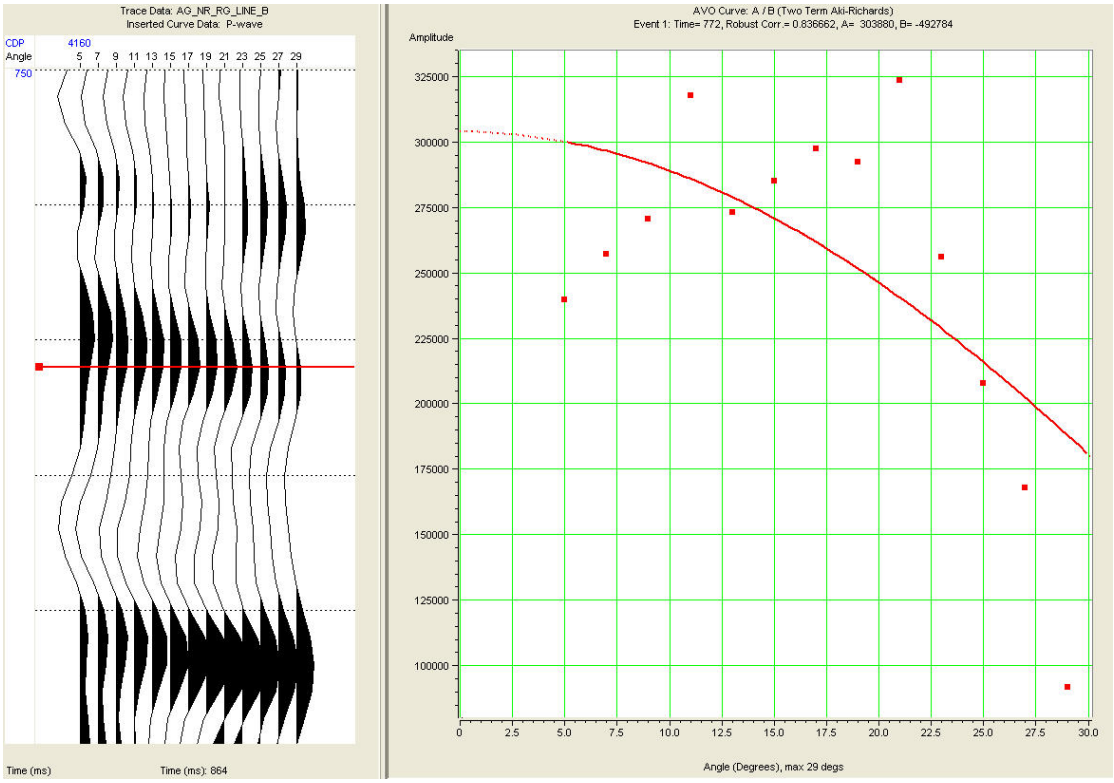

Class I anomaly at CDP 4160

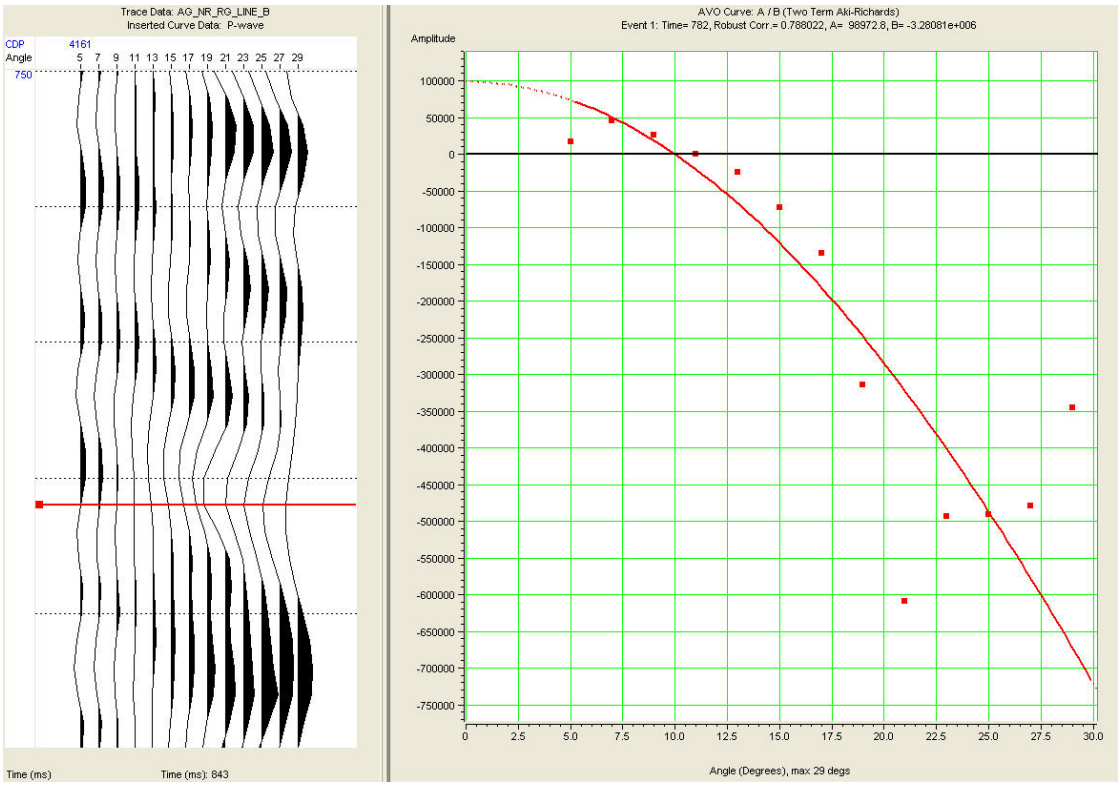

Class IIp anomaly at CDP 4161

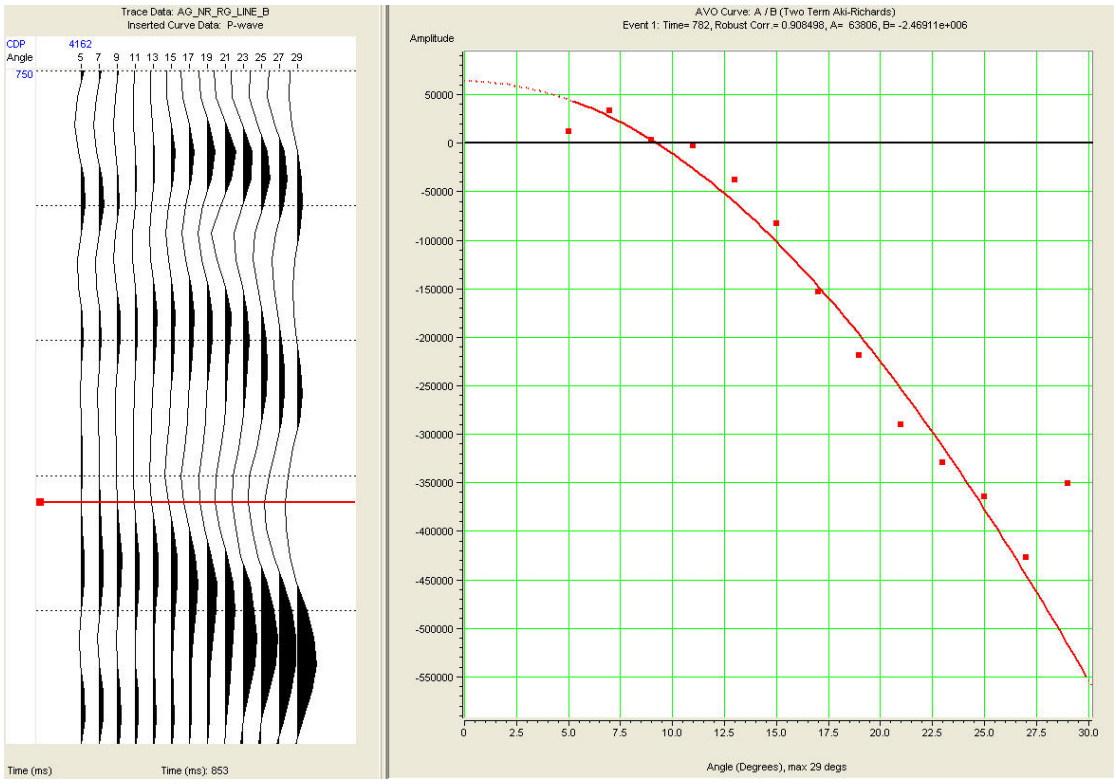

Class IIp anomaly at CDP 4162

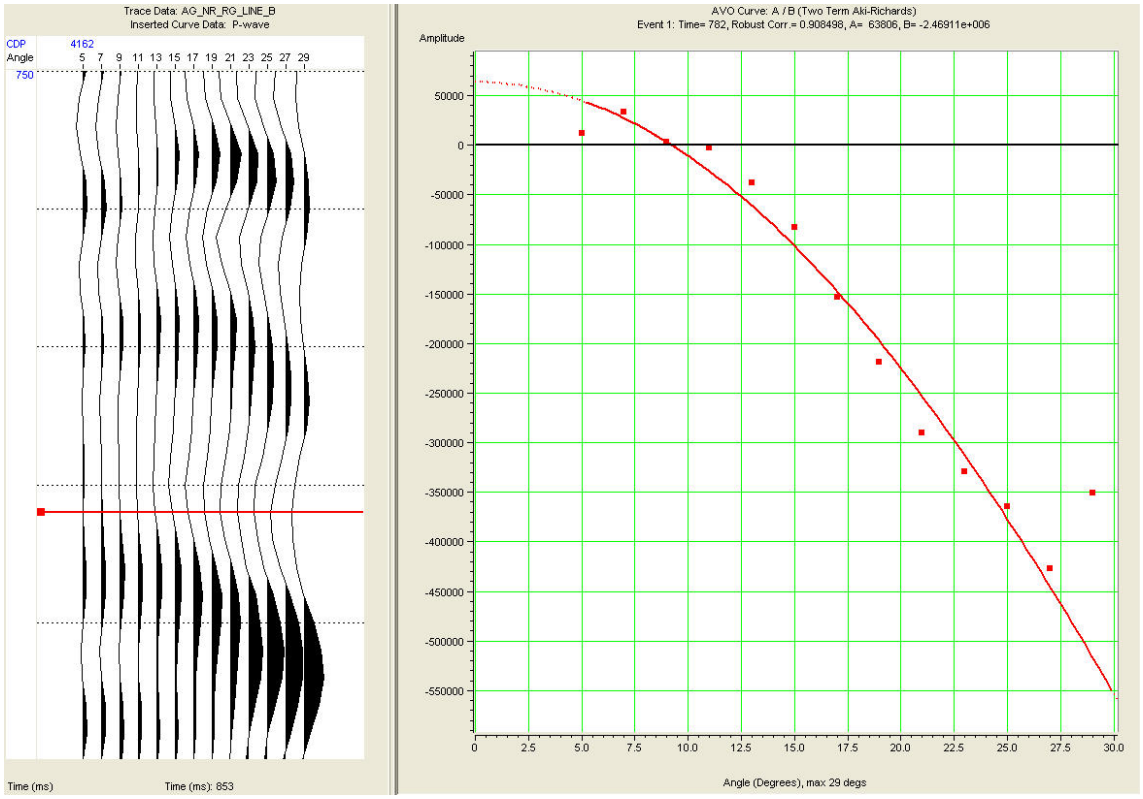

Weak Class IIp anomaly at CDP 4163

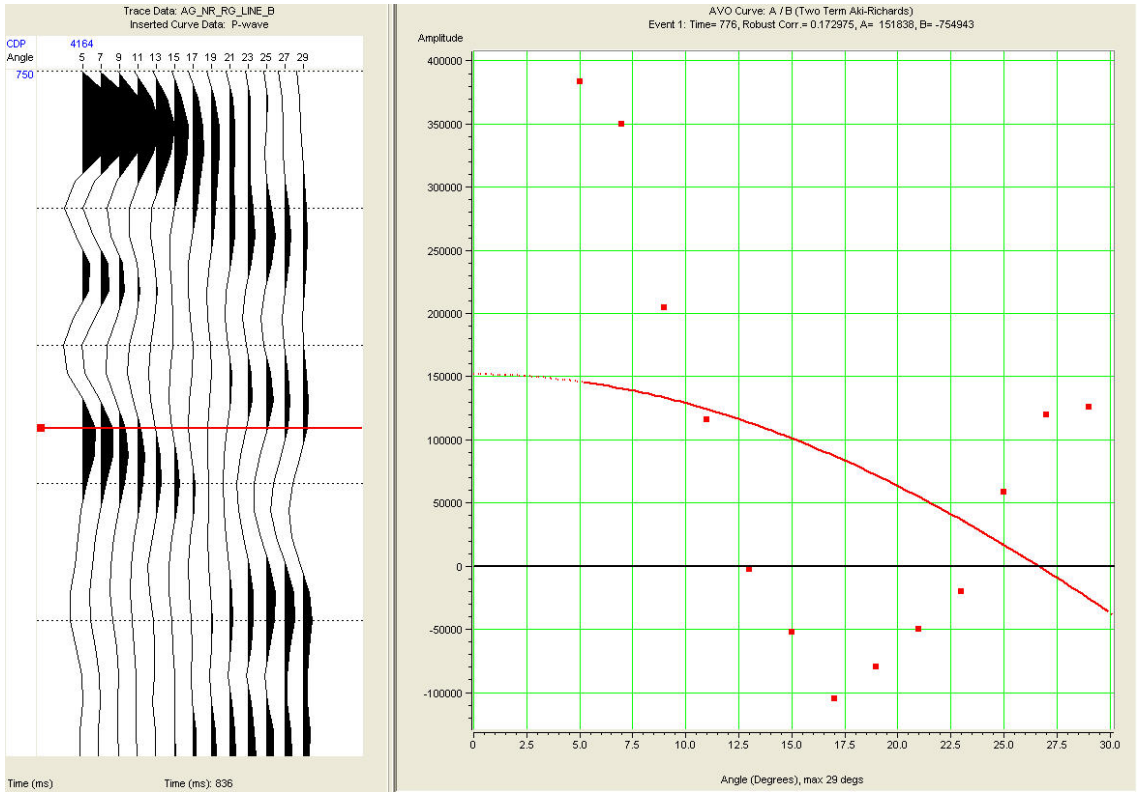

No coherent anomaly at CDP 4164

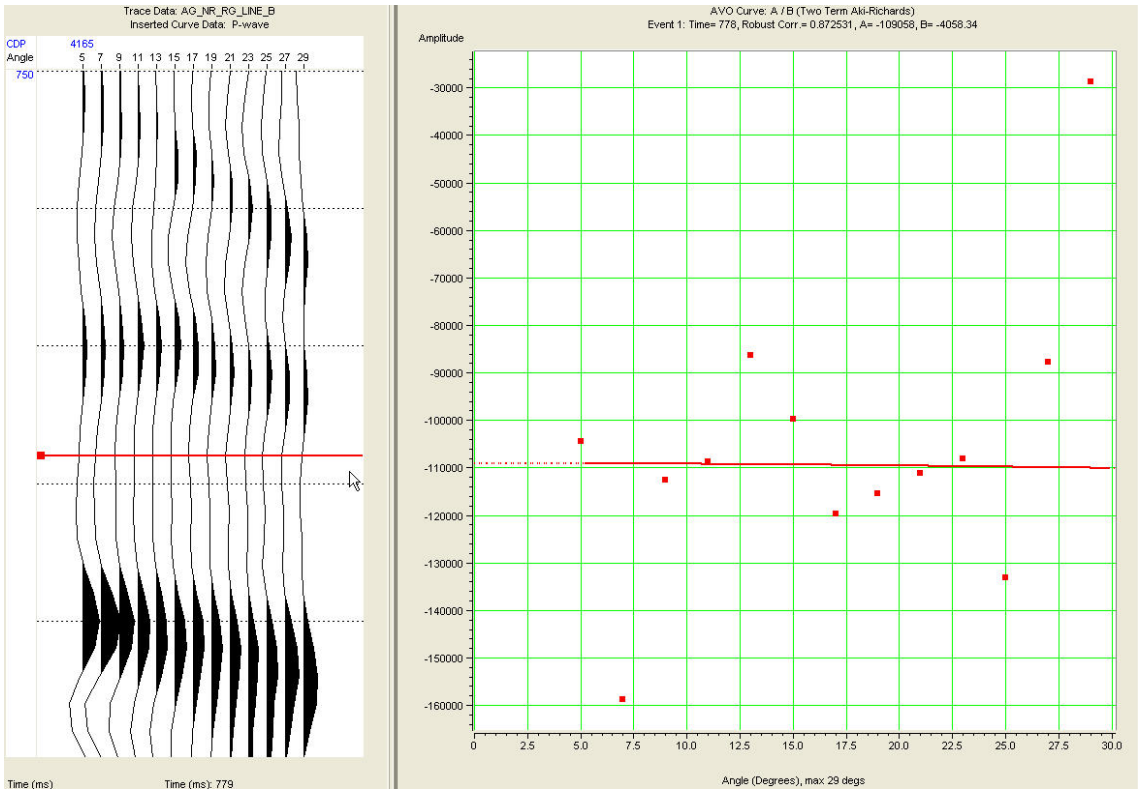

No coherent anomaly at CDP 4165

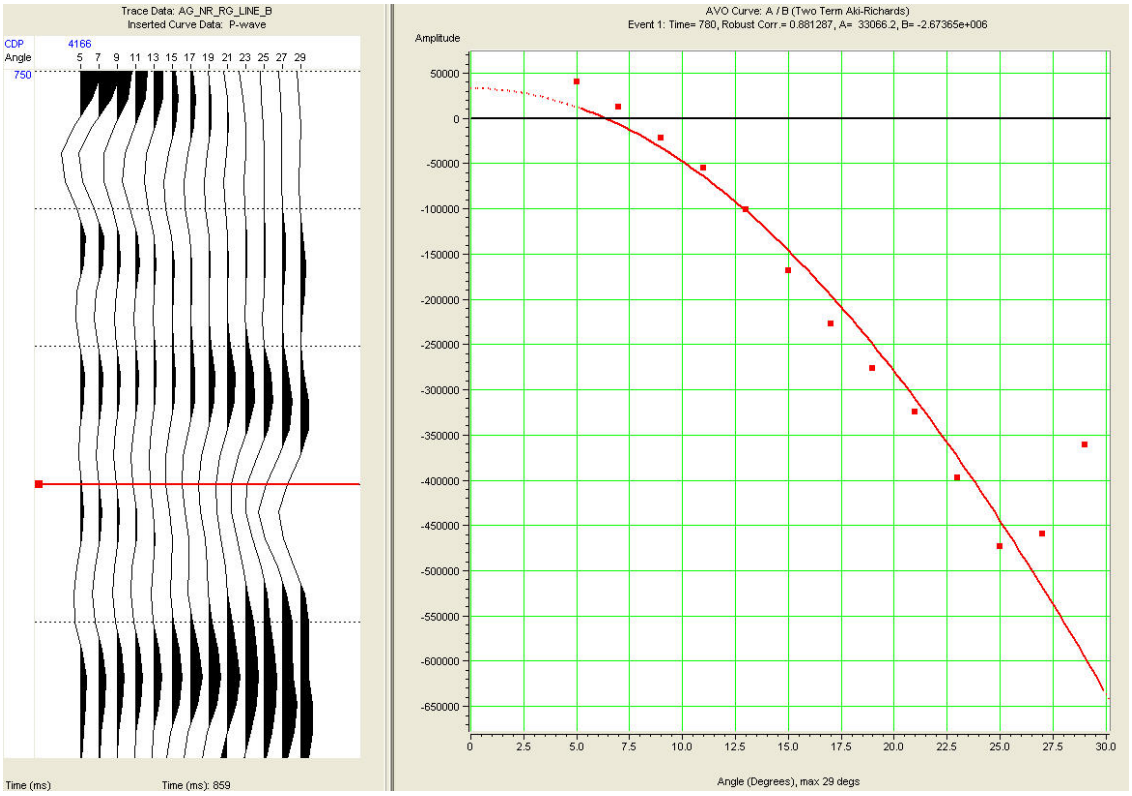

Class IIp anomaly at CDP 4166

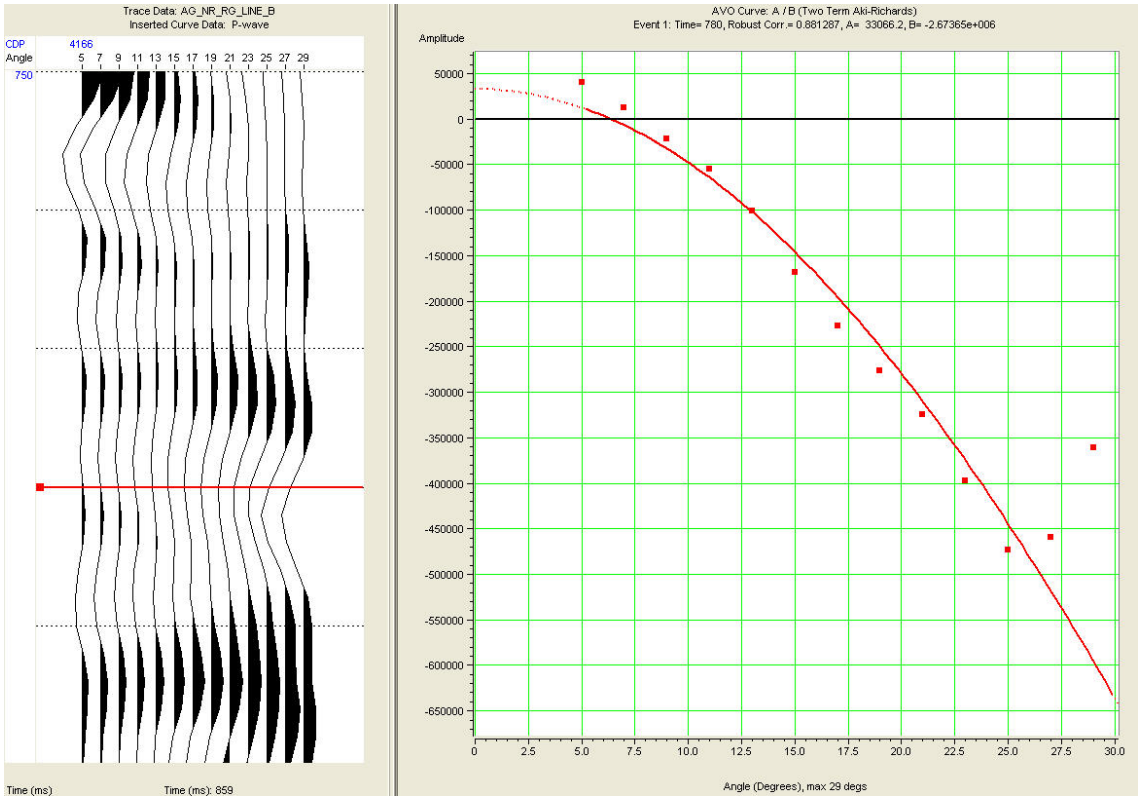

Class III anomaly at CDP 4167

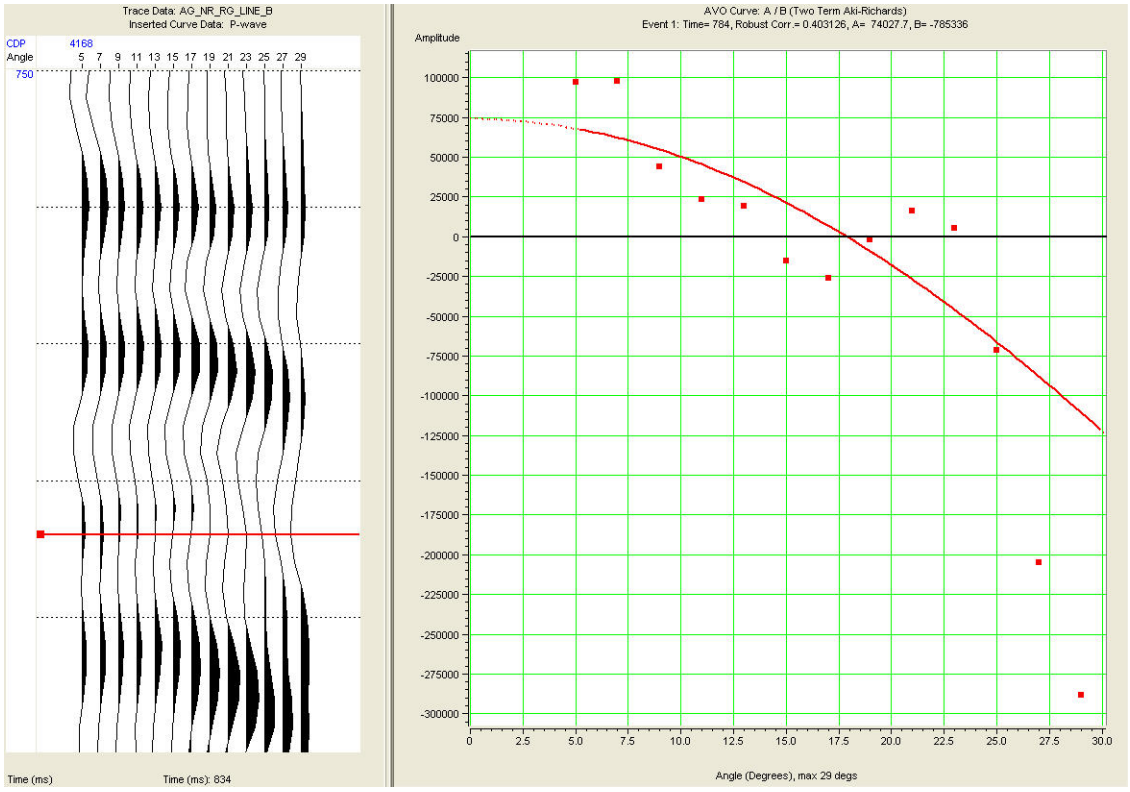

No coherent anomaly at CDP 4168

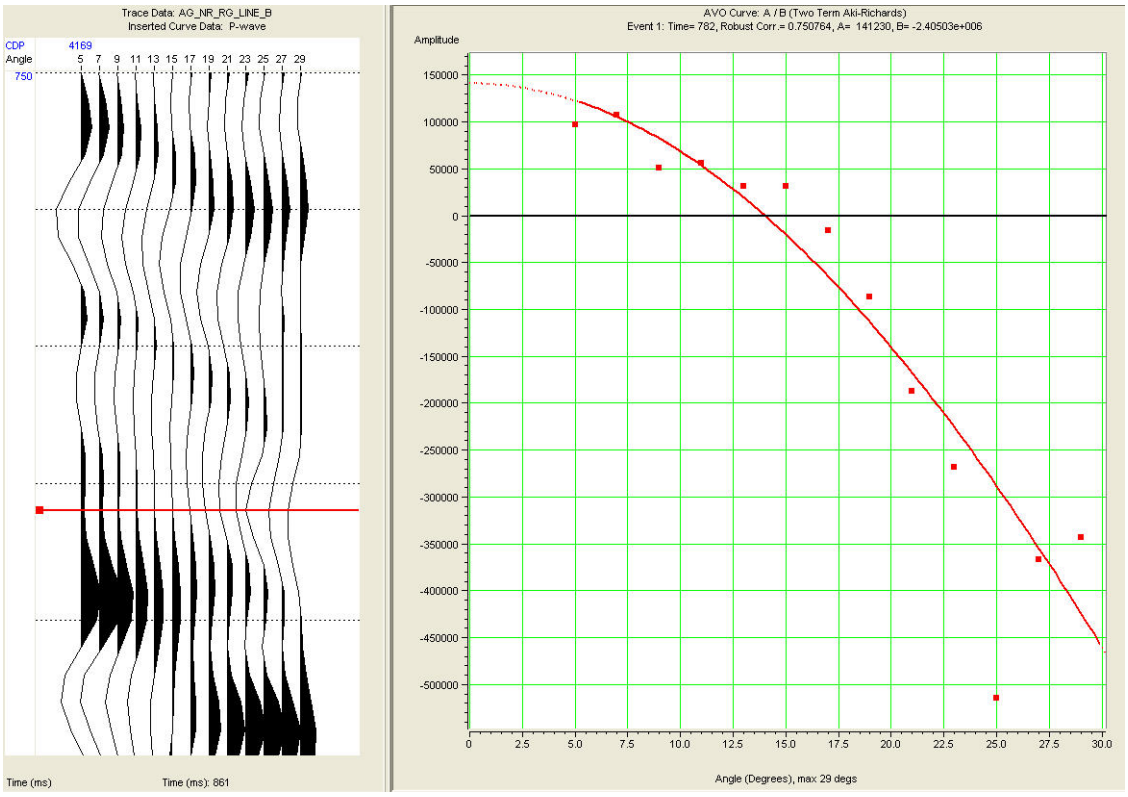

Class IIp anomaly at CDP 4169

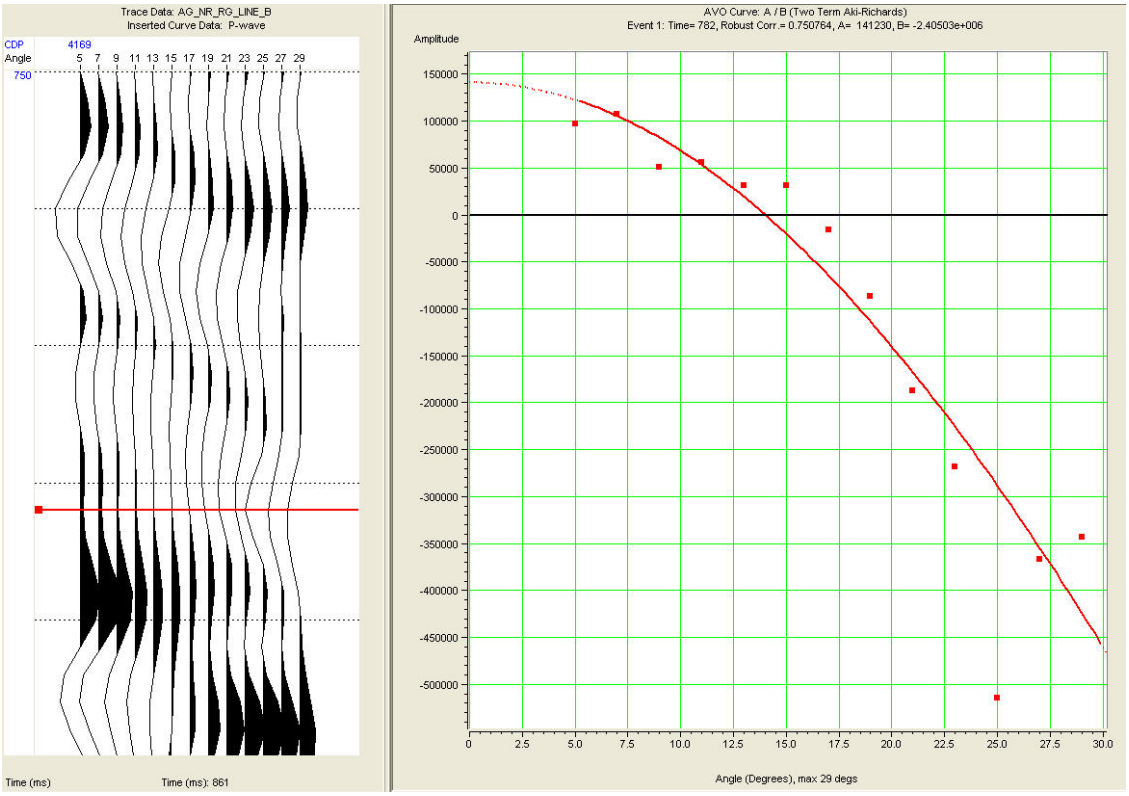

Class IV anomaly at CDP 4170

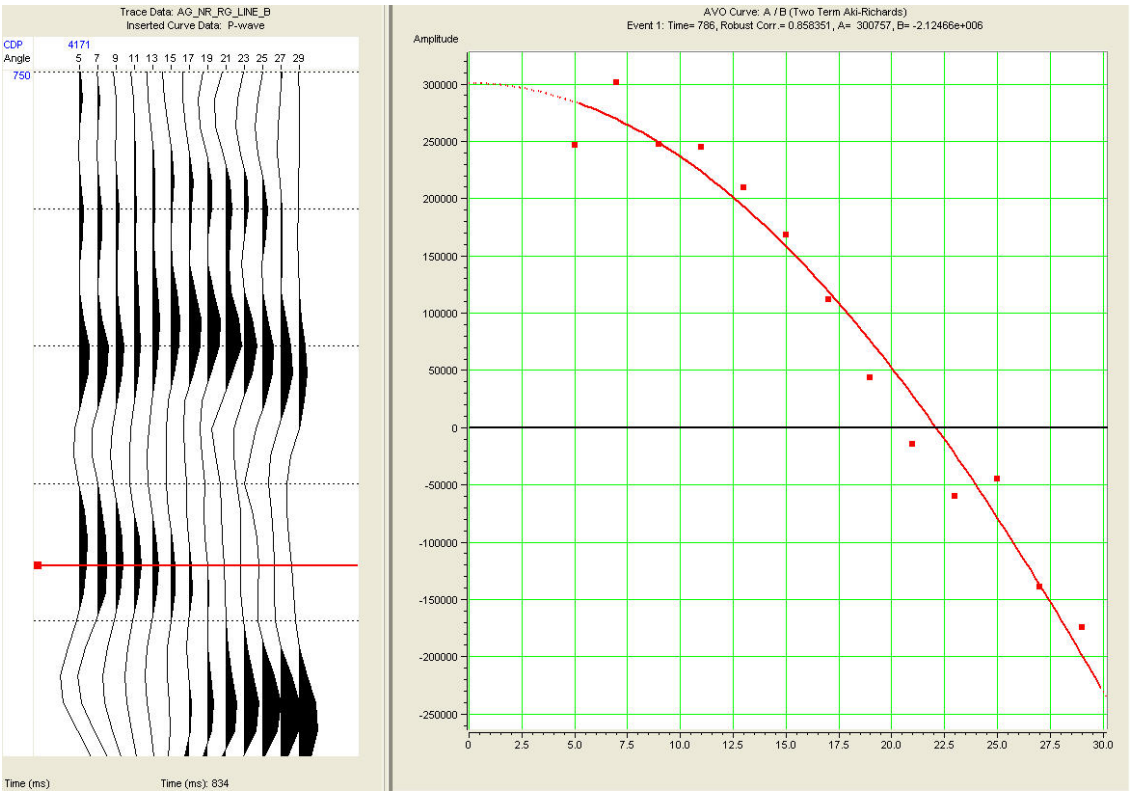

Class I anomaly at CDP 4171

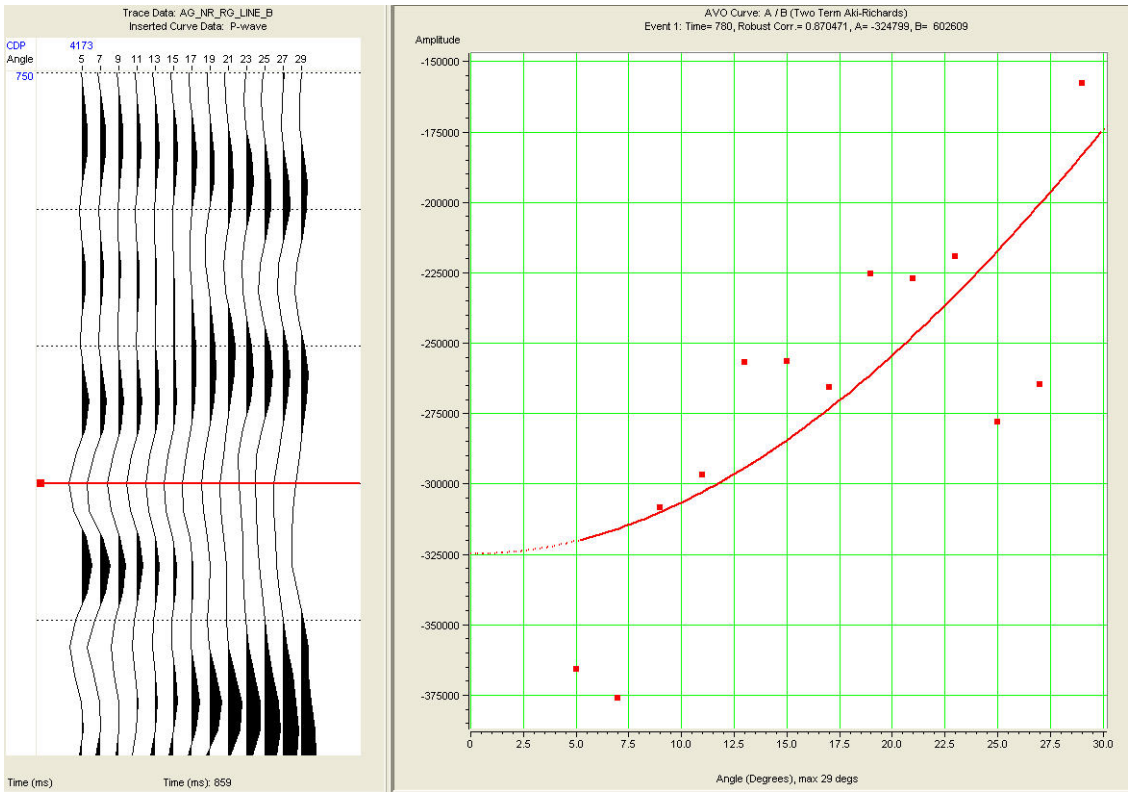

Class IV anomaly at CDP 4173

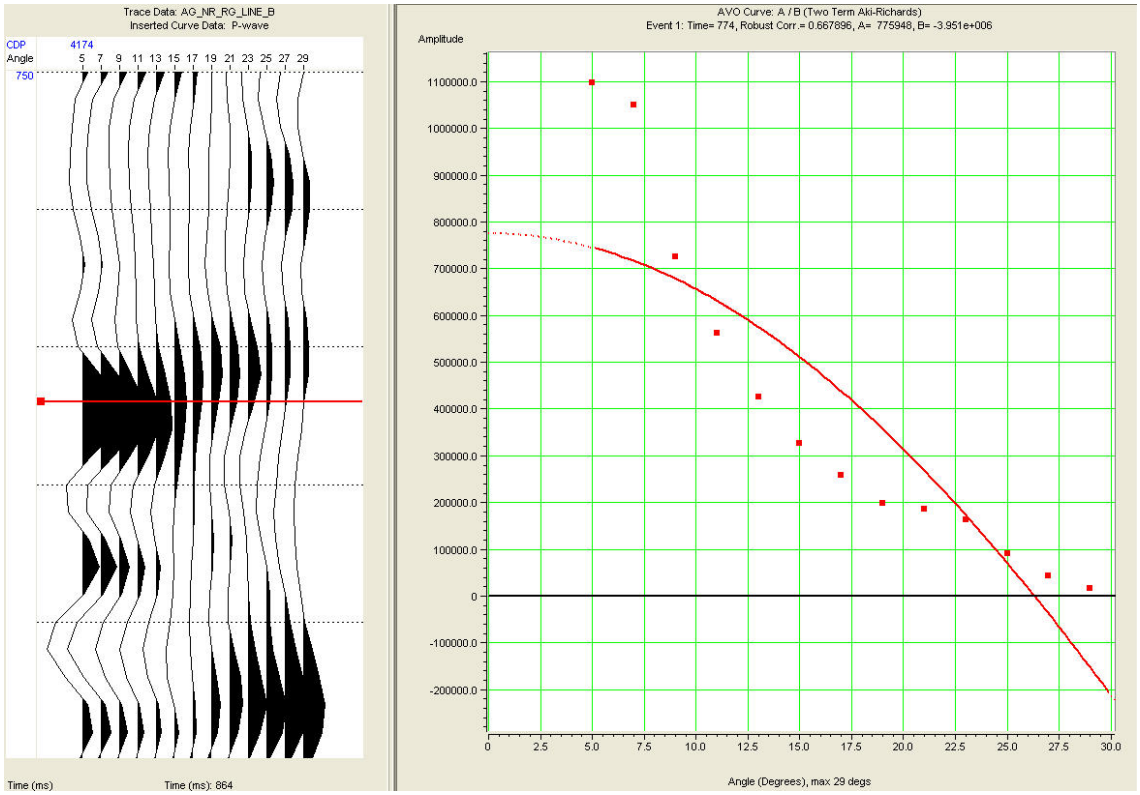

Class IV anomaly at CDP 4174

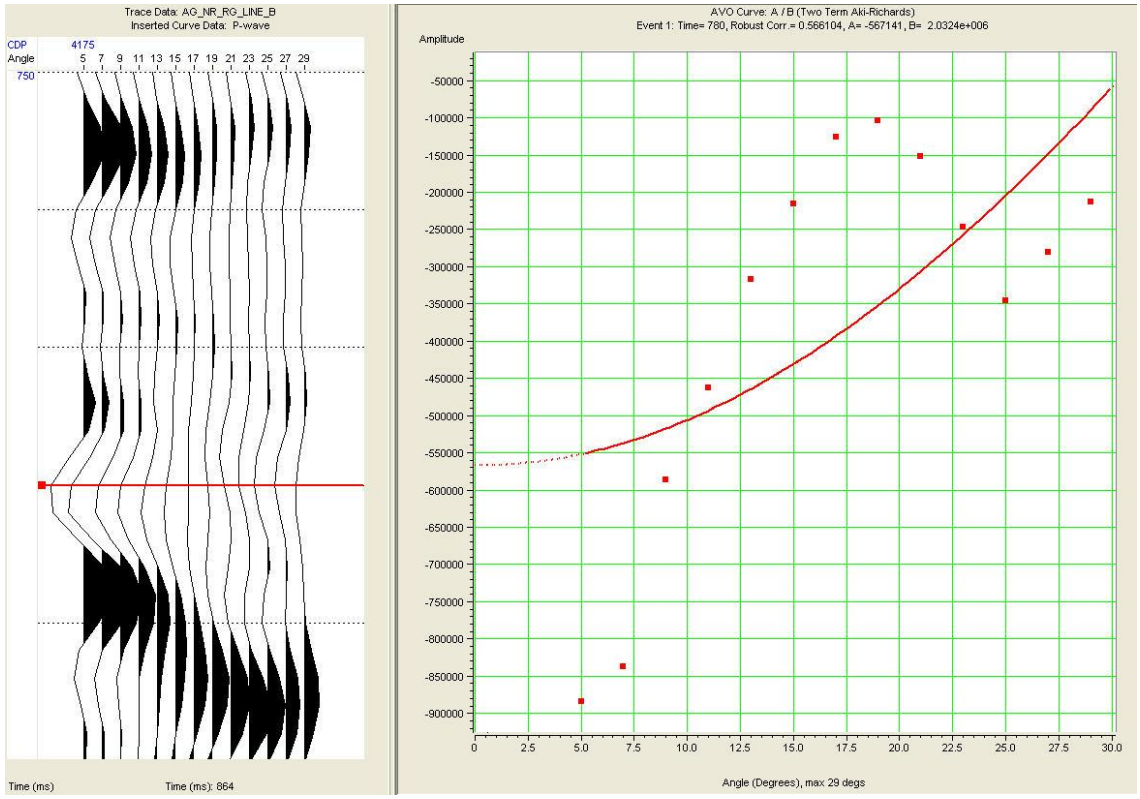

No coherent anomaly at CDP 4175